THE UNIVERSITY
of EDINBURGH

Investigating the Formation and Remodelling of Myelinated Axons *In Vivo*

Jill M Williamson

PhD

The University of Edinburgh

2019

I have read and understood The University of Edinburgh guidelines on plagiarism, and declare that this thesis is the result of my own work, except where indicated by references. This thesis has been submitted to The University of Edinburgh for the degree of Doctor of Philosophy only.

Jill M Williamson

Lay Summary

Neuronal communication is important for nervous system function. In the brain and spinal cord, nerve cells (otherwise known as **neurons**) form many connections with each other to communicate in complex circuits. A neuron sends electrical signals along a long cable-like projection called an **axon**, which triggers the transmission of information to the next neuron(s) in the circuit. Many axons are **myelinated**; this means that they have sheaths of fatty membrane called myelin wrapped around them. Myelin sheaths make axons send electrical signals much faster than unmyelinated axons. Myelin is very important for nervous system function, which is highlighted by the fact that development of myelinated parts of the brain correlates with cognitive development in childhood, and that loss of myelin in diseases such as Multiple Sclerosis can lead to neurological symptoms and permanent disability.

Recent research suggests that modification of myelin throughout life plays an important role in the learning of new skills. It has been proposed that our experiences can shape the myelin in our brains, which will change the speed of electrical signals along axons. This could affect how neurons communicate to one another, and ultimately, lead to changes in cognition. However, a great deal of evidence for the role of myelin in learning comes from brain imaging studies in humans, which can only see very broad changes in myelin-rich parts of the brain. There is a need to study myelin at the microscopic cellular level in order to understand precisely how myelin sheaths can change along axons over time, and how this might affect communication between neurons.

The best way to study how myelin sheaths change along an axon is to image myelinated axons in a living animal at a high magnification (**live imaging**). By imaging the same cells multiple times in a living animal at different ages, we can observe how myelin changes along axons over time. Many studies of myelin biology use rodents, but live imaging myelin in the brains of mice requires complex experimental set-ups, such as a ‘window’ in the skull to image the outer parts of the brain. Larval zebrafish provide a much simpler- and non-invasive alternative method of live imaging myelinated axons in the brain and spinal cord. Larval zebrafish are completely transparent, which means that cells can be easily live imaged repeatedly without any adverse effects. Zebrafish also share many of their genes with mammals, and so

findings from studies of myelin in zebrafish are likely to have some relevance to myelin biology in mammals, such as humans.

During this project, I have live imaged myelinated axons in the zebrafish spinal cord to investigate how myelin changes over time in detail. I found that myelin changes along axons within a specific time period of development, after which myelin sheaths do not change significantly. I described how myelin changes along the axons of different kinds of neurons, predicting that they would show diverse changes in their myelin sheaths. However, I found that that the axons of different kinds of neurons show very similar myelin changes over time.

It has been proposed that brain activity is what shapes myelin in the nervous system. However, it is not known precisely how the electrical activity of neurons affects myelin sheaths themselves. I used genetic tools to stimulate electrical activity in neurons, and then performed live imaging to investigate how this affected myelin sheaths. I found that increasing the electrical activity along axons promotes the growth of myelin sheaths, but only within a specific period during development. After this time period, changing the electrical activity of neurons did not affect myelin sheath development.

Collectively, this research helps us to understand how myelin changes in the nervous system at a cellular level, and how the electrical activity of neurons affects the development of myelin sheaths. Future research will focus on understanding precisely how the cellular changes to myelin that I have described in this project affect neuronal communication and overall cognitive function.

Abstract

Myelin is a crucial component of the vertebrate nervous system, both in facilitating rapid conduction of action potentials and in metabolically supporting axons. Recent research has theorised that myelin sheaths play a more intricate role in nervous system function by regulating circuits in response to experience. The number, length, thickness, and distribution of myelin sheaths along an axon all influence its underlying conduction properties. Thus, establishing or changing particular myelin patterns along axons could refine the precise timing of signals to change circuit outputs. Yet, how the myelin patterns along single axons are established, how myelin is remodelled over time, and how neuronal activity affects these processes, is not yet fully understood. I sought to investigate how myelin is formed, remodelled and maintained over time along individual axons in the larval zebrafish central nervous system.

I first characterised the formation of myelin patterns along two different subtypes of axon in the larval zebrafish spinal cord. Using transgenic tools and confocal microscopy, I performed live imaging of single axons over a period of time during developmental myelination. Reticulospinal (RS) axons are involved in locomotor circuits, and are myelinated in a synaptic vesicle release-dependent manner; whereas, Commissural Primary Ascending (CoPA) axons are involved in sensory processing circuits, and are myelinated in a synaptic vesicle release-independent manner. I hypothesised that myelin patterns along axons are formed in a circuit-dependent fashion, and, therefore, that axons from different circuits would exhibit different myelin patterns. However, I found that both RS and CoPA axons have very similar myelin patterns, in terms of their myelin sheath number, length, myelin coverage, and nodal gap length, and that these patterns are established within a defined time window after the onset of myelination.

I, then, assessed how myelin sheaths are remodelled along RS and CoPA axons over time, and found that myelin sheaths could either grow or shrink in length, or could be fully retracted from the axon itself. I hypothesised that myelin remodelling would occur along axons which use activity-related signals to regulate their myelination, and therefore, that RS axons would exhibit more myelin remodelling than CoPA axons. However, I found that RS and CoPA axons exhibited very similar degrees of myelin remodelling.

Finally, I used a chemogenetic tool and live imaging by confocal microscopy to investigate how increasing activity in individual RS axons affects the dynamics of myelin sheath growth and the formation of myelin patterns. I found that increasing neuronal activity promotes the early growth of myelin sheaths within a critical period; after this period, neuronal activity no longer affects myelin sheath dynamics along RS axons. By promoting this early sheath growth, activity can change the myelin pattern established along individual RS axons.

Collectively, this research begins to elucidate how individual myelinated axons are formed and maintained during nervous system development, and the cellular mechanisms by which neuronal activity may regulate this process.

Acknowledgements

First and absolutely foremost, thanks go to my supervisor David Lyons. It is no exaggeration to say that your stellar mentorship has been a constant inspiration throughout these past 4 years. Thank you for giving me the freedom to explore the things that intrigued my curiosity, and for providing guidance (from the nitty gritty to the very big picture) when I needed it most. I could not have done this without your kindness, patience, and all-round wisdom.

Many thanks also go to the rest of the Lyons lab (members past and present) for all of the help, advice, friendship, cake, and the many burgers at the Southern. Working with you all makes science a genuine pleasure!

I would also like to thank my thesis committee, Professors Catherina Becker, Charles ffrench-Constant, and Tara Spires-Jones, for providing invaluable input and motivation at my annual committee meetings. Thanks are also due to the Tissue Repair PhD programme staff and fellow students for all of the support, excellent discussions and friendship (and of course, the socials!).

I am forever grateful to my comrade-in-arms, Bex – for our shared PhD journeys, for understanding my frustrations, for celebrating my successes with the fishies, for our coffee/writing dates at Café Nero, and for just generally being an absolutely brilliant friend.

To my parents, thank you for always reminding me that as long as I'm happy and trying my best, nothing else matters. Thank you for listening to me and providing perspective when I needed it.

And finally, thanks go to John. I'm not sure I can put into words how grateful I am to have had you by my side throughout it all. I have absolutely no doubt that I could not have done this without your constant love and support. From consoling me with empire biscuits/secret chocolate/Stefano's, to listening to me prattle on about "oligodendrocyte precursor cells", to reminding me that no matter what happens, everything will be ok. Thank you.

Table of Commonly Used Abbreviations

BDNF	brain derived neurotrophic factor
BoNT	botulinum toxin
CiD	circumferential descending
CNS	central nervous system
CoPA	commissural primary ascending
dpf	days post-fertilisation
DRG	dorsal root ganglion
DTI	diffusion tensor imaging
FA	fractional anisotropy
FP-Cntn1a	fluorescent protein-Contactin1a
hpf	hours post-fertilisation
IQR	interquartile range
MBP	myelin basic protein
(m)PFC	(medial) prefrontal cortex
MS	Multiple Sclerosis
OPC	oligodendrocyte precursor cell
PLP	myelin proteolipid protein
PNS	peripheral nervous system
RB	Rohon-Beard
RS	reticulospinal
SCoRe	spectral confocal reflectance microscopy
SD	standard deviation
TeNT	tetanus toxin
TTX	Tetrodotoxin
UAS	Upstream activator sequence

Table of Contents

Chapter 1: Introduction

1.1. Aim of this Thesis

The aim of this thesis is to investigate the dynamics of how myelinated axons form in the central nervous system (CNS), and how myelination is regulated by the activity of these underlying axons. In this introduction, I will discuss the evidence that: myelin is a crucial component of the CNS; that dynamic regulation of myelination may regulate the function of circuits in the nervous system; and that neuronal activity may be a critical signal in the development and regulation of myelinated axons to mediate circuit function.

1.2. The Importance of Myelin

Rapid communication between neurons is crucial for animal survival. When a neuron fires an action potential it is propagated along the axon by voltage-gated Na^+ channels. These channels are opened once the axonal membrane depolarises to the threshold membrane potential, causing Na^+ influx and a sharp depolarisation. This is quickly followed by activation of voltage-gated K^+ channels which allow K^+ efflux to hyperpolarise the membrane back to resting potential. The presence of voltage-gated Na^+ and K^+ channels diffusely along the entire axon ensures that once a single action potential fires it is propagated in a wave down the axon towards the synapse.

Two core strategies have evolved to speed up electrical impulse transmission in the nervous system. The first is to increase axon diameter, as axial resistance of an axon decreases proportionally with increasing fibre diameter. ‘Giant’ axons are found in many different species – including squid, fish, crayfish, and insects – and are often involved in startle or escape responses (Bullock, 1984).

The second strategy is myelination, where specialised plasma membrane is wrapped concentrically around axons and then compacted to form multi-layered sheaths. These lipid-rich myelin sheaths act as electrical insulators by reducing the axon membrane capacitance. Myelinated axons are punctuated by short unmyelinated gaps (usually 1-2 μm in length) between the sheaths known as nodes of Ranvier, where the voltage-gated Na^+ channels are

clustered (along with several other nodal proteins). Myelin sheaths are thought to help localise and maintain these Na^+ channels and other ion channels at discrete positions to facilitate proper conduction (Rasband and Peles, 2016). Action potentials occur only at the exposed axon membrane of the nodes, and so the electrical impulse 'jumps' from node to node along the myelinated axon (Hartline and Colman, 2007) – this is known as saltatory conduction. Myelinated axons therefore conduct impulses much faster than equivalently-sized unmyelinated axons (Waxman, 1980) and allow for fast information processing without drastic increases in nervous system size. Myelin is present in almost all vertebrates (although it is absent from the earliest vertebrates, such as hagfish and lampreys (Bullock et al., 1984)), and was likely a crucial evolutionary step in the emergence of increasingly complex nervous systems within the vertebrate lineage.

1.2.1. *Myelinating Cells*

Myelin sheaths are made by Schwann cells in the peripheral nervous system (PNS) and oligodendrocytes in the CNS. Each myelinating Schwann cell forms just one myelin sheath and is closely associated with its ensheathed axon, whereas oligodendrocytes extend many processes into their surrounding environment and usually form multiple myelin sheaths on several different axons (**Figure 1**). Conduction speeds do not just depend on whether an axon is myelinated; various electrophysiological and mathematical modelling studies have shown that the length and thickness of myelin sheaths along an axon also influences that axon's conduction velocity (reviewed by Waxman, 1980). Myelin sheath number, length, and thickness may be tuned to optimise the speed of signal conduction. In the PNS, axonal expression of neuregulin-1 determines whether an axon becomes myelinated by Schwann cells (Taveggia et al., 2005), and also regulates the thickness of the sheaths formed (Michailov et al., 2004), so that sheath thickness correlates with axon size (Friede and Samorajski, 1967). Schwann cell sheath length is believed to be regulated by the growth of the axons themselves (Hildebrand et al., 1994; Simpson et al., 2013). In the CNS, the number, length, and thickness of

sheaths made by oligodendrocytes can vary significantly. Some spinal cord oligodendrocytes form a single sheath up to 1.5 mm in length (Remahl and Hildebrand, 1990), while oligodendrocytes in the cortex or corpus callosum can form up to 80 sheaths between 20-200 μm in length (Chong et al., 2012; Snaidero and Simons, 2014). CNS myelin sheath length (Murray and Blakemore, 1980) and thickness (Hildebrand and Hahn, 1978) generally increase with the diameter of the axon being myelinated, although sheath length along a single axon of a given diameter can still vary extensively.

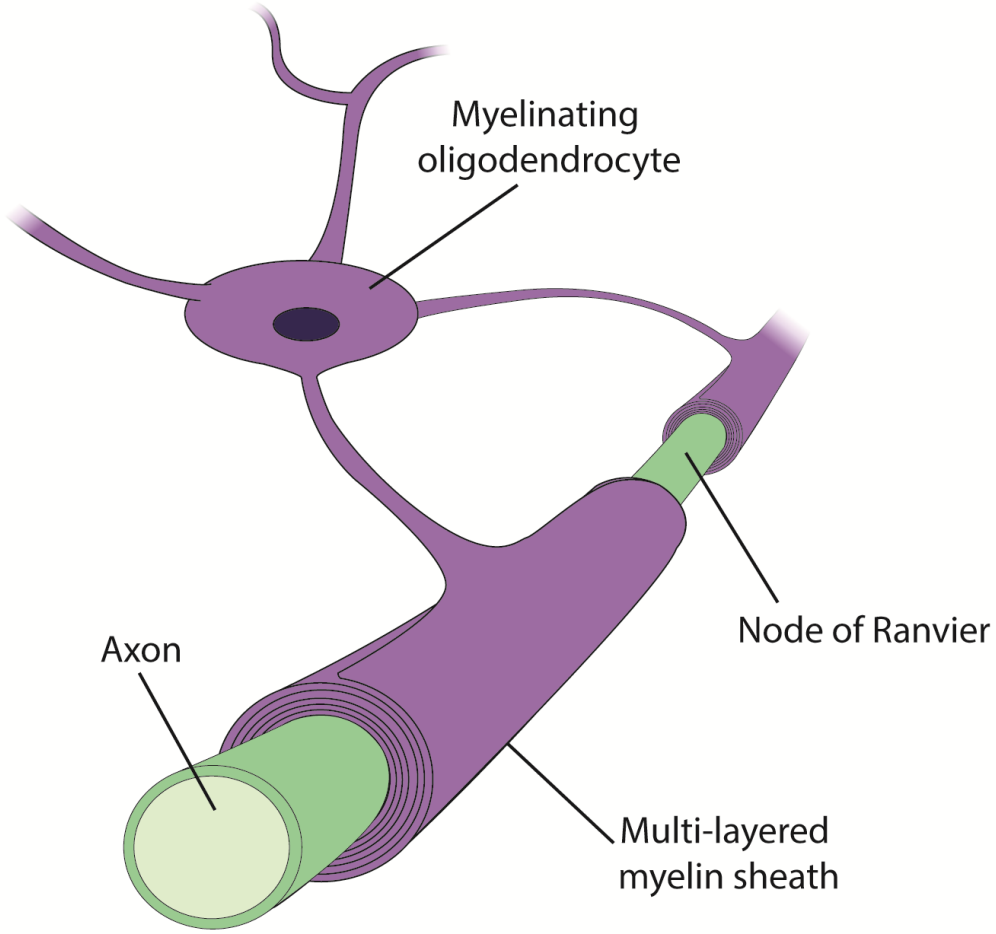

Figure 1 – oligodendrocytes, the myelinating cells of the CNS.

Oligodendrocytes can form multiple myelin sheaths by wrapping membrane concentrically around axons in the CNS. The short gaps between myelin sheaths are known as nodes of Ranvier.

1.2.2. *Additional Roles for Myelin*

Myelin was assumed to be just a static insulator for many years. However, recent research demonstrates that myelinating cells are required for more than just increasing conduction speeds. In the CNS, metabolic coupling between axons and oligodendrocytes is important for maintaining healthy neurons. Axons can uptake lactate from oligodendrocytes to facilitate axonal ATP production (Fünfschilling et al., 2012), and loss of the lactate transporter MCT1 (which is expressed mainly by oligodendrocytes in the CNS) leads to neurodegeneration (Y. Lee et al., 2012). Oligodendrocytes provide essential trophic support, to potentially sustain the required levels of neuronal activity in the circuits being myelinated (Saab et al., 2016). Oligodendrocytes also maintain healthy neuronal function by regulating K^+ homeostasis, presumably after K^+ efflux during action potential firing. Although loss of the inward-rectifying K^+ channel $K_{ir}4.1$ in oligodendroglial cells does not affect oligodendrocyte development or myelination, it does lead to elevated extracellular K^+ levels within the forebrain (Larson et al., 2018). This causes increased seizure susceptibility, impaired recovery of axons after high frequency activity, neurodegeneration, and increased mortality (Larson et al., 2018; Schirmer et al., 2018). It is possible that future research will continue to identify additional functions of myelinating cells in maintaining a healthy functioning nervous system.

1.2.3. *Myelin Dysfunction in the CNS*

Loss or damage to myelin has been documented in numerous conditions. In spinal cord injury, the primary mechanical injury is followed by a secondary injury of excitotoxic damage, apoptosis, and inflammation; this includes oligodendrocyte death and demyelination of surviving axons over the weeks after injury itself (Silva et al., 2014). In the disease Multiple Sclerosis (MS), peripheral immune cells are thought to infiltrate the CNS and trigger oligodendrocyte death and myelin damage in focal lesions throughout both grey and white matter (the evidence for the roles of different immune cells in MS has been reviewed by Baecher-Allan et al., 2018). During immune attacks

(or relapses) patients experience symptoms such as weakness, fatigue, impaired balance and co-ordination, vision deficits or cognitive impairment. A number of drugs targeting immune cells are used to reduce the rate of relapses (summarised by Baecher-Allan et al., 2018).

Demyelination in injury or disease can cause conduction block, but conduction can be restored upon remyelination of affected axons (Smith et al., 1981). These new myelin sheaths are thought to be thinner and shorter than healthy myelin sheaths (Blakemore, 1974; Lasiene et al., 2008; Prineas and Connell, 1979; Totoiu and Keirstead, 2005). As mentioned above, the specific number, length, and thickness of myelin sheaths along an axon is predicted to adjust conduction velocity (Waxman, 1980); the regeneration of thinner, shorter sheaths during remyelination may change the conduction speed of affected neurons (whether this has an impact on overall nervous system function is not clear). In MS, the disease usually transitions to a progressive stage where demyelinated axons degenerate, causing steady accumulation of disability with no recovery. In contrast to the many drugs licensed for use in relapsing-remitting stages of MS, only one drug has been licensed for use in progressive MS. There is some evidence that remyelination may be protective against neurodegeneration (Irvine and Blakemore, 2008; Mei et al., 2016), potentially through the crucial metabolic support provided by oligodendrocytes to axons. Subsequently, several chemical screens have been performed to identify various drugs which promote remyelination in animal models of demyelination (reviewed by Cole et al., 2017). Clinical trials of remyelination-enhancing therapies are ongoing, which may elucidate whether remyelination can prevent neurodegeneration.

Myelin pathologies have also been observed in numerous other conditions. Leukodystrophies are a group of heritable disorders causing progressive cognitive and motor symptoms which are typically fatal in childhood or adolescence (Bonkowsky et al., 2010). Some leukodystrophies have been associated with mutations in key myelin proteins such as myelin proteolipid protein (PLP), suggesting that disruption to myelin formation and maintenance may play a role in at least some cases (Schiffmann and Knaap, 2004).

Oligodendrocyte pathology and demyelination has been observed in amyotrophic lateral sclerosis (ALS) patients. Oligodendrocyte loss occurs in an animal model of ALS and oligodendrocyte-specific deletion of the disease-causing mutation delays both disease onset and death (Kang et al., 2013; Philips et al., 2013). In an animal model of Huntington's disease, expression of mutant huntingtin protein in oligodendrocytes causes demyelination and neurodegeneration (Huang et al., 2015). In Alzheimer's disease, neuroimaging studies have identified white matter abnormalities even during preclinical stages prior to significant neurodegeneration (Nasrabady et al., 2018; Sachdev et al., 2013). Myelin abnormalities are even associated with neuropsychiatric disorders such as schizophrenia (Takahashi et al., 2011). The aetiology of the myelin phenotypes in these disorders remains unclear. It is possible that myelin disruption is a poorly-understood contributor to neurological disease, and may somehow trigger neuronal dysfunction. Alternatively, myelin disruption may be a secondary effect of neuronal pathology. Further research into myelin and myelinating cells is required to fully understand if and how regulation of myelination maintains nervous system health and function.

1.3. Oligodendrocyte Development

1.3.1. *Generation of the Oligodendroglial Lineage*

During embryonic development, specification of the various neural and glial progenitors in the neural tube is established by key transcription factors. The ventral-inducing signal Sonic hedgehog (Shh) is secreted from the floorplate, while the dorsal-inducing bone morphogenic proteins (BMPs) and Wnt proteins are secreted from the roof plate; the opposing gradients of Shh and both BMP and Wnt induce patterning along the dorsoventral axis of the neural tube to create distinct domains which give rise to different progenitors (Rowitch, 2004). In the pMN domain of the ventral neural tube Shh induces the expression of the basic helix-loop-helix transcription factor Olig2 and is required for the generation of pMN domain progeny (Ligon et al., 2006; Lu et al., 2000; Orentas et al., 1999). The pMN domain progenitors first give rise to motor neurons (at E9.5 in rodents), before switching to generating oligodendrocyte progenitor

cells (OPCs) (from E12.5 in rodents; Rowitch, 2004). In rodents there are additional waves of OPC generation from more dorsal regions of the brain and spinal cord (Bergles and Richardson, 2016; Richardson et al., 2006); despite this, the majority of OPCs in the spinal cord are ventrally-derived (Tripathi et al., 2011).

OPCs express transcription factors such as Sox10 and Olig1, as well as proteins NG2 and PDGFRα, which are typically used as identifying markers for OPCs in experimental studies. These cells are highly migratory and proliferative. They respond to numerous attractive and repulsive cues to migrate from the pMN domain and populate the entire CNS (Bergles and Richardson, 2016; Rowitch, 2004). OPCs use vasculature as a scaffold to migrate – this migration requires Wnt-Cxcr4 signalling, and disruption of vasculature development prevents proper OPC dispersal from the ventral progenitor domains (Tsai et al., 2016). As OPCs migrate to their destinations, they explore their surrounding environment via the rapid extension and retraction of filopodium-like processes (Hughes et al., 2013; Kirby et al., 2006). OPCs are a dynamic population of cells – they maintain a constant density and will initiate migration and proliferation if neighbouring OPCs are lost either due to differentiation or cell death (Hughes et al., 2013; Kirby et al., 2006).

OPC differentiation is accompanied by significant transcriptional changes; many transcription factors are either supressed or enhanced to regulate the transition from OPC to oligodendrocyte. An extensive overview of the transcriptional regulation of OPC differentiation is beyond the scope of this thesis introduction; however, the key transcription factors are summarised in **Figure 2**. The transcriptional regulation of OPC differentiation has been comprehensively reviewed elsewhere (Emery and Lu, 2015; Goldman and Kuypers, 2015; Snaidero and Simons, 2017). Interestingly, a surplus of oligodendrocytes are generated in rodents during both early post-natal development and adulthood; as many as half of newly-differentiated oligodendrocytes die without forming myelin sheaths (this is discussed in more detail in section ‘1.4.2 Myelination in Other Mammals’).

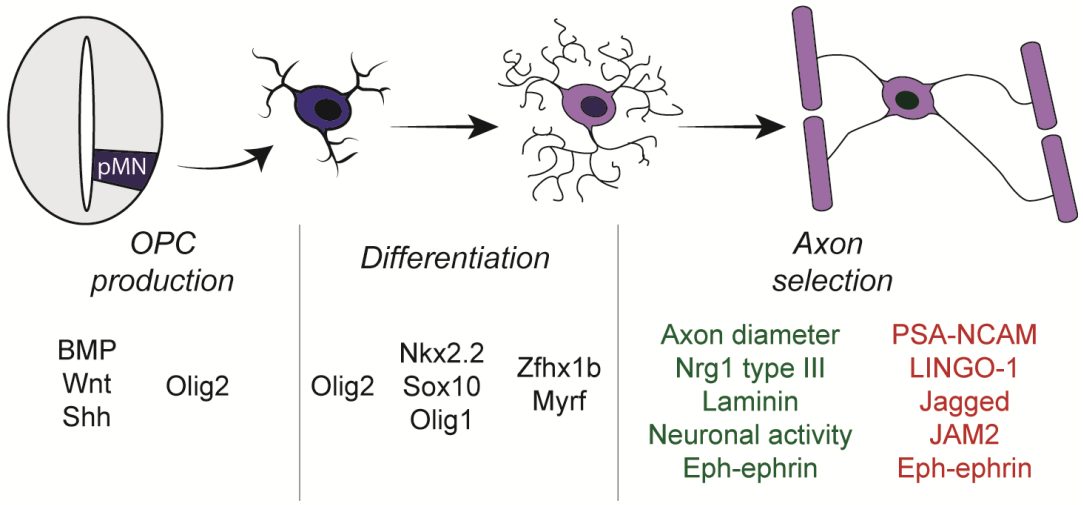

Figure 2 – summary of the known key signals involved in oligodendroglial development.

A brief summary of the signals known to be involved in the production of OPCs from the pMN domain of the spinal cord, the differentiation of OPCs into oligodendrocytes, and the selection of axons for myelination (Black text = transcription factors; green text = attractive signals; red text = repulsive signals).

1.3.2. *Axon Selection*

As an OPC differentiates into an oligodendrocyte, the rapidly extending and retracting filopodia which make contact with their surrounding environment must select the appropriate axons upon which to initiate myelin sheath formation. Physical cues such as axonal diameter can regulate this process. In the PNS, axons over 1 μm diameter are myelinated by Schwann cells (Hildebrand et al., 1993) and experimentally increasing the diameter of normally unmyelinated axons is sufficient to initiate myelination (Voyvodic, 1989). The relationship between axonal diameter and myelination in the CNS is not as clear. The smallest myelinated axons in the CNS range from 0.2-0.8 μm in diameter; but there is considerable overlap in the range of diameters of myelinated versus unmyelinated axons (Hildebrand et al., 1993). Therefore,

axon diameter is not the only signal which regulates target selection for myelination in the CNS.

Molecular signals can also regulate target selection for myelination. In the PNS, axonal expression of Nrg1 type III, which is detected by ErbB2/3 receptor complex in Schwann cells, controls which axons are to be myelinated (Taveggia et al., 2005). It has been suggested that the levels of axonal Nrg1 act as a biochemical indicator of axon diameter to Schwann cells, and thus only axons of diameter > 1 μm express sufficient levels of Nrg1 to initiate myelin sheath formation (Michailov et al., 2004). However, the role of Nrg-ErbB signalling in regulating CNS myelination appears to be more complicated. Some evidence indicates that Nrg-ErbB signalling can influence OPC migration (Ortega et al., 2012) and survival (Fernandez et al., 2000), and loss of Nrg1 reduces the myelination of dorsal root ganglion (DRG) neurons by oligodendrocytes *in vitro* (Taveggia et al., 2008). Inhibiting Nrg1-ErbB signalling, either by expression of a dominant-negative ErbB4 receptor (Roy et al., 2007) or oligodendrocyte-specific knock-out of ErbB3 (Makinodan et al., 2012), reduces myelination *in vivo*. Despite this, Brinkmann et al., 2008 reported that, using numerous different approaches, loss of Nrg1-ErbB signalling in the CNS has no significant effect on CNS myelination *in vivo*. Nrg-ErbB signalling may not be required but is sufficient to influence axonal selection in CNS myelination; there are additional attractive signals which can also regulate this process. Indeed, signals such as laminin-integrin interactions (Taveggia et al., 2010) and neuronal activity have been shown to affect onset of myelination. Different signals may even work together to influence axon selection. For example, oligodendrocytes cultured in the presence of Nrg1 respond to neuronal activity-related signals more than oligodendrocytes cultured without Nrg1 (Lundgaard et al., 2013). The role of neuronal activity will be discussed in greater detail in section ‘1.6 Neuronal Activity can Influence Myelination’.

There are also repulsive cues which influence the selection of axons for myelination. There is evidence to suggest that PSA-NCAM expression in axons prevents myelination. This molecule is initially expressed in all axons

and is down-regulated on axons destined to be myelinated (Charles et al., 2000). Decreasing axonal expression of PSA-NCAM *in vitro* also enhances myelination (Charles et al., 2000). Axonal expression of LRR and Ig domain-containing, Nogo receptor-interacting protein (LINGO-1) inhibits myelination both in DRG neuron-oligodendrocyte co-cultures and *in vivo* in the rodent spinal cord (Lee et al., 2007). Notch-Jagged1 signalling may also inhibit myelination. Jagged1 is primarily expressed on unmyelinated axons, and loss of Notch1 leads to increased myelination throughout the CNS (Givogri et al., 2002). Additionally, some repulsive cues prevent inappropriate myelination of non-axonal targets. JAM2 is a repulsive signal which is expressed on the dendrites and cell bodies of certain neurons to prevent inappropriate myelination of these structures (Redmond et al., 2016).

Some signals may demonstrate both attractive and repulsive effects on axon selection depending on the signalling environment. Ephrins are cell surface ligands which bind to Eph tyrosine kinase receptors. Eph-ephrin interactions are capable of bidirectional signalling, where forward signalling occurs in the Eph-expressing cell and reverse signalling occurs in the ephrin-expressing cell. Neurons and oligodendrocytes express both Eph receptors and ephrin ligands, and so both forward and reverse Eph-ephrin signalling is possible in each cell type. *In vitro* analysis has shown that EphA and EphB forward signalling in oligodendrocytes inhibits myelin membrane formation, while ephrin-B reverse signalling in oligodendrocytes enhances myelination (Linneberg et al., 2015). The specific combination of Eph receptors and ephrin ligands expressed by axons could either attract or repel their selection by oligodendrocytes for myelination (Almeida, 2018).

Hence, unlike the PNS, no single molecular signal has been identified to regulate the selection of axons for myelination in the CNS. Instead, a complex network of attractive and repulsive molecular signals, in conjunction with physical cues of axon diameter, controls the selection of appropriate axons for myelination in the CNS (**Figure 2**). The precise interplay of these various signals, or how they might cross-talk to control myelination throughout life, is still not fully understood.

1.3.3. *Myelin Sheath Formation*

Once an oligodendrocyte has selected an appropriate axon, the oligodendrocyte contact must wrap concentrically around the axon to form the compact, multi-layered structure of the mature myelin sheath. Numerous models for the wrapping process have been proposed, including the 'carpet crawler' (Bunge et al., 1989), the 'liquid croissant' (Sobottka et al., 2011), and the 'ofiomosaic' models (Ioannidou et al., 2012). The most current model was proposed by Snaidero et al. in 2014, whereby the leading edge of the myelin sheet which wraps around the axon is the innermost layer, while the outer layers grow longitudinally along the axon (**Figure 3**). This means that the innermost layer of myelin is shortest, while the outermost layer is the longest; this is in line with previous observations that the number of myelin wraps around an axon can vary along the sheath (Knobler et al., 1974).

The polarised growth of the inner tongue around the axon is driven by turnover of actin filaments at the leading edge (Nawaz et al., 2015). The myelin layers are compacted by myelin basic protein (MBP), which is translated locally in the myelin sheath itself (Colman et al., 1982; Wake et al., 2011), and prevents the diffusion of proteins into the compacted membrane layers (Aggarwal et al., 2011). Improved ultrastructural preservation using high-pressure freezing electron microscopy has revealed that there are uncompacted cytoplasmic channels in growing myelin sheaths which provide cytoplasmic access between the inner tongue and the connecting oligodendrocyte process (Snaidero et al., 2014). These cytoplasmic channels are found in sheaths even in adulthood, and are formed due to actin bundling which counters the compacting forces of MBP to hold channels open in otherwise compact sheaths. 2',3'-cyclic nucleotide 3'-phosphodiesterase (CNP) induces this actin bundling, and so is required for the formation and maintenance of cytoplasmic channels (Snaidero et al., 2017). Loss of CNP leads to fewer cytoplasmic channels (Snaidero et al., 2017) and causes neurodegeneration (Lappe-Siefke et al., 2003).

The neurodegeneration in CNP mutants can be rescued by restoring a normal number of cytoplasmic channels in myelin sheaths via reduced expression of MBP (Snaidero et al., 2017). It is hypothesised that the cytoplasmic channels in myelin sheaths are crucial, not just for oligodendrocytes to provide metabolic support to axons, but also for myelin sheath growth. Snaidero et al., 2014 found that sheaths in the adult rodent CNS have fewer cytoplasmic channels than during active myelination, but that inducible stimulation of the PI3K/AKT/mTOR pathway first increases the number of cytoplasmic channels, and then leads to increased sheath thickness. It is not known whether the reopening of these channels and subsequent radial sheath growth affects the metabolic support or conduction properties of the underlying axon, nor whether these channels reopen in normal physiological conditions in response to signals such as neuronal activity.

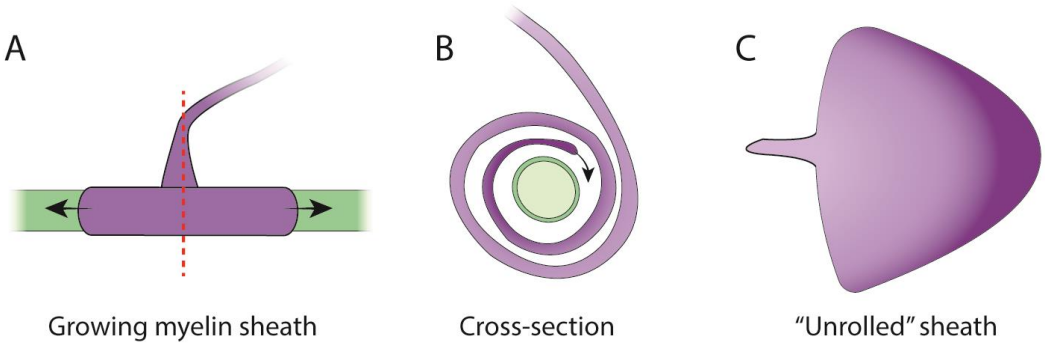

Figure 3 – the most up-to-date model of myelin wrapping in the CNS.

Schematics based on the model proposed by Snaidero et al., 2014. **A)** The outermost layers of the sheath grow longitudinally to increase sheath length, making the outer layers longer than the inner layers during active growth. **B)** A cross-section (shown by the red dotted line in **A**) reveals that a growing zone on the innermost layer (dark purple) of the myelin sheath wraps around the axon (green). **C)** The structure of a growing sheath when unwrapped – the growing zone at the innermost region is shown in dark purple.

1.3.4. *Domains of Myelinated Axons*

Myelin sheaths accelerate the conduction velocity of the underlying axon due to the formation of discrete axonal domains. Each of these axonal domains contain a localised complex network of proteins (**Figure 4**). On a fully myelinated axon, the gaps between myelin sheaths (nodes of Ranvier) are where the action potentials are propagated. These nodes are where voltage-gated Na^+ channels are clustered, as well as various K^+ channels; cell adhesion molecules such as neurofascin isoform 186 (NF-186) and Nr-CAM; and scaffolding proteins such as Ankyrin-G and βIV-spectrin (Rasband and Peles, 2016; Salzer, 2003). The paranodes are the axon-glial contact sites, where the uncompacted ends of the myelin layers form paranodal loops which adhere to the axon via septate-like junctions. Axo-glial adhesion is mediated via the binding of glial neurofascin isoform 155 (NF-155) to axonal Caspr/Contactin-1 complexes. The axonal protein complex is bound to cytoskeletal proteins such as protein 4.1B, αII-, and βII-spectrin (Rasband and Peles, 2016; Salzer, 2003). The juxtaparanode is the region immediately adjacent to the paranode, and is characterised by the clustering of voltage-gated K^+ channels (Kv channels), cell adhesion molecules Caspr2 and Contactin-2, ADAM22, and PDZ-domain proteins PSD-93 and -95 (Rasband and Peles, 2016; Salzer, 2003). The internode is the domain underneath the myelin sheath (the term ‘internode’ is often used synonymously with ‘myelin sheath’; however, internode refers to the domain of the axon itself, whereas myelin sheath refers to the membrane structure *around* the axon which generated by myelinating cells. The term ‘myelin sheath’ will be used throughout this thesis).

Disruption to the organisation of these discrete domains is associated with a number of neurological conditions (discussed by Salzer, 2003). For example, demyelination leads to changes in the expression and distribution of voltage-gated Na^+ channel subtypes, and production of antibodies targeting proteins such as Kv channels leads to neurological symptoms – such as hyperexcitability. Alterations to the expression, localisation, and function of ion channels in axonal domains affect the conduction properties of the axon, and

therefore, accurate formation of these domains is crucial for proper nervous system function.

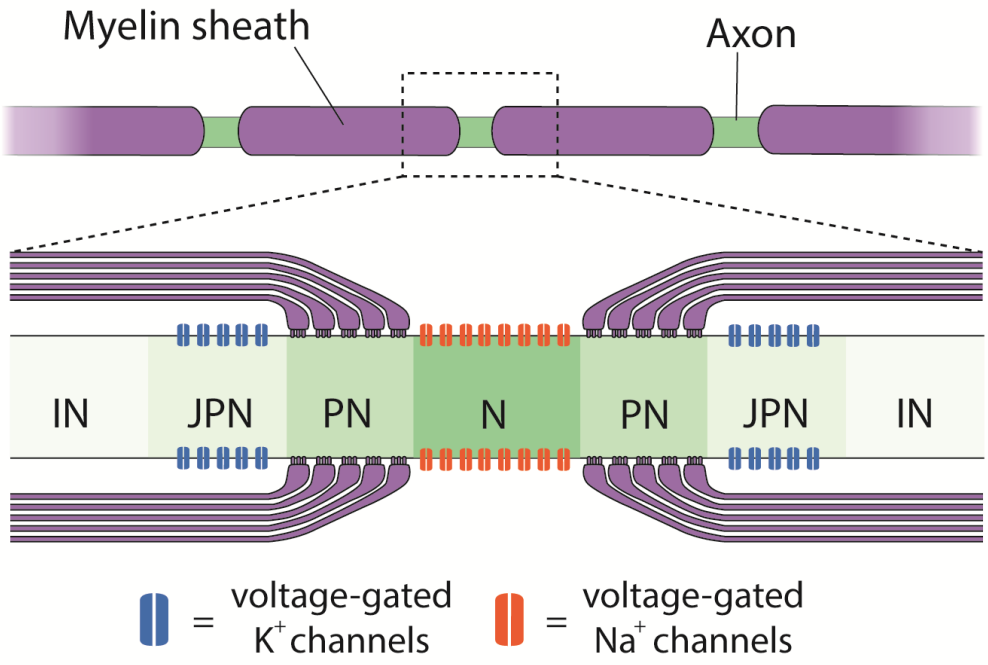

Figure 4 – the different domains of myelinated axons.

Myelination leads to the formation of distinct axonal domains based on protein complex localisation. Zoomed in image shows a longitudinal cross-section through the myelinated axon. Voltage-gated Na^+ channels (orange) are clustered with other proteins at the nodes of Ranvier (N) between myelin sheaths. The paranodal loops of the myelin sheath adhere to the axon at the paranode (PN) via septate-like junctions. Adjacent to the PN is the juxtaparanode (JPN), where voltage-gated K^+ channels (blue) are found. The region under the myelin sheath is the internode (IN).

1.3.5. *Oligodendrocyte Heterogeneity*

There is significant heterogeneity in oligodendroglial cells throughout the CNS. OPCs found in different CNS regions can behave differently to one another. For example, OPCs residing in white matter regions such as the corpus callosum and optic nerve proliferate and differentiate more than OPCs in the cortex or spinal cord grey matter (Rivers et al., 2008; Young et al., 2013). There is evidence to suggest that these differences are intrinsically regulated.

Transplantation of the more proliferative white matter OPCs into grey matter regions does not affect their proliferation, while transplantation of grey matter OPCs into white matter does not increase their proliferative capacity (Viganò et al., 2013). This indicates that extracellular cues alone are not sufficient to regulate the behaviour of OPCs in distinct regions. The myelinating capacity of daughter oligodendrocytes also appears to be intrinsically programmed into OPCs. Rodent OPCs cultured in the presence of synthetic fibres with dimensions similar to axons will differentiate into oligodendrocytes and form myelin sheaths around these fibres (Bechler et al., 2015; S. Lee et al., 2012). In this *in vitro* system, devoid of any neuronal signalling cues, cortex-derived oligodendrocytes make sheaths smaller than those made by spinal cord-derived oligodendrocytes – this is reflective of the myelin sheath lengths observed *in vivo* (Bechler et al., 2015).

The intrinsic differences between different oligodendroglial cells suggests that there may be distinct populations of oligodendrocytes. In recent years, single cell RNA sequencing has become an extremely powerful tool for identifying different cell populations in the CNS based on intercellular transcriptional variation (Zeisel et al., 2015). Marques et al., 2016 identified six distinct populations of myelinating oligodendrocyte in regions throughout the adult rodent CNS. This transcriptional heterogeneity is found in the human CNS as well. Post-mortem single cell RNA sequencing analysis of white matter from healthy individuals or MS patients revealed that there are multiple populations of oligodendrocyte which can be defined by the expression of population-specific markers (Jäkel et al., 2019). Comparison of healthy and MS-afflicted tissue found that there is an altered distribution of oligodendroglial populations in the latter – MS-afflicted tissue had a significantly smaller proportion of OPCs and oligodendrocyte populations 1 and 6, yet a higher proportion of oligodendrocyte populations 2, 3, and 5. These findings suggest that the remyelination of demyelinated lesions in MS does not just require oligodendrocyte production, but also the production of the correct populations of oligodendrocyte. Additionally, this could explain the significant variation in remyelination seen in the disease – for example, it has been observed that

grey matter lesions remyelinate more efficiently than white matter lesions (Albert et al., 2007). However, it is not clear whether these population differences are the consequence or the cause of the disease. It may be that individuals with higher numbers of certain oligodendrocyte populations are more susceptible to developing MS.

Do the different populations of oligodendrocyte represent distinct subtypes, or transient cell states? It is not yet known whether there are transcriptionally distinct subtypes of OPC, possibly defined by developmental origin. Transcriptomic analysis of the white matter and grey matter OPCs known to display behavioural differences and their daughter oligodendrocytes could determine if this is the case. Alternatively, these transcriptionally distinct groups of oligodendrocytes may represent cell states where an oligodendrocyte can transition from one state to another depending on the signals it receives. In support of this, Jäkel et al., 2019 performed “pseudotime” analysis on their transcriptomic data to identify the developmental trajectories predicted by transcriptional similarities between individual cells. This identified that oligodendrocyte population 6 likely represents an early myelinating oligodendrocyte, while oligodendrocyte populations 1 and 5 are more mature oligodendrocytes. Longitudinal analysis of the expression of population-specific markers could confirm whether these identified groups represent transient cell states which can change over time. Regardless of whether they represent states or subtypes, the functional consequences of these distinct populations are not fully understood. One possibility is that certain oligodendrocyte populations respond to certain pro-myelinating signals versus others; this may explain why there are numerous molecular cues which can regulate CNS myelination. Oligodendrocyte diversity could also reflect the variety of circuits which are myelinated; perhaps certain oligodendrocyte populations myelinate specific neuronal subtypes to respond to particular demands of the underlying axons (for example, some axons may require more metabolic support than others, or some axons may use neuronal activity to remodel myelin sheaths more than others). Further research into these distinct oligodendrocyte populations will help to elucidate any functional differences.

1.4. Myelination is a Lifelong Process

1.4.1. *Myelination in Humans*

In humans, myelination take place in a well-characterised spatiotemporal manner, beginning just prior to birth (Brody et al., 1987). Rapid production of oligodendrocytes and extensive myelination occurs during the first few years of life, followed by more gradual myelin formation throughout adolescence (Yakovlev and Lecours, 1967; Yeung et al., 2014).Yet, evidence now indicates that myelination is a lifelong process which continues into adulthood. OPCs are found within the adult human brain, indicating that a source of new oligodendrocytes is present throughout life (Chang et al., 2000). Studies from as early as the mid-twentieth century noted that myelin continues to accumulate beyond the third decade of life in associative areas of the cerebral cortex (Yakovlev and Lecours, 1967). More recently, diffusion tensor imaging (DTI) has been used to measure changes in the myelin-rich white matter regions of the brain over time. DTI measures the diffusion of water molecules in a given tissue; water molecules will exhibit different diffusion properties in different tissue microstructures. The diffusion properties measured by DTI provide a fractional anisotropy (FA) value, which is a ratio of the anisotropy (direction-dependent diffusion) versus isotropy (direction-independent diffusion) of a tissue. Water molecules in white matter tracts (where the tissue consists of long cable-like structures) will diffuse more in a parallel direction than a perpendicular direction, giving a higher FA value than grey matter. Subsequently, DTI can be used to image the white and grey matter regions of the brain, and detect changes in white matter as changes in the FA value over time. Lebel and Beaulieu, 2011 imaged individuals ranging from 5-32 years of age multiple times to observe white matter maturation during childhood, adolescence, and young adulthood. They measured changes in the FA of various tracts as a read-out of white matter maturation. They found that while projection and commissural tracts stopped changing by late adolescence, the association tracts continue to change during young adulthood. However, FA increases both with myelination and increasing axon diameter and density

(Beaulieu, 2002) – thus these observed changes do not necessarily reflect changes in myelination.

Carbon dating analysis has also shed some light regarding the formation of myelin in the human brain throughout life. Yeung et al., 2014 performed carbon dating of both biochemically-purified myelin and oligodendrocyte nuclei from post-mortem tissue of individuals ranging from 0.2-92 years of age. This technique takes advantage of the nuclear bomb tests from the mid-twentieth century which led to a sharp increase in global atmospheric levels of the isotope ^{14}C. When a cell replicates its DNA, this will incorporate ^{14}C into the new DNA strands at levels approximately comparable to atmosphere at the time of S-phase. As ^{14}C levels have been exponentially decreasing at a known rate since the 1960s, the birth-date of a cell (or any carbon-containing molecule) can be determined by comparing the ^{14}C levels of the DNA (or other carbon-based molecules) with the known atmospheric levels (Spalding et al., 2005). Yeung et al. found that the birth date of purified myelin from the corpus callosum is comparable to the time of death even in older adults. This could be due to rapid formation or turnover of myelin sheaths themselves throughout life, or due to the continuous turnover of carbon-containing molecules within stable myelin sheaths. Carbon dating oligodendrocyte nuclei from the frontal cortex showed that new oligodendrocytes are born until the fourth decade of life. There may be regional differences in the rates of lifelong myelination – carbon dating of oligodendrocyte nuclei from the corpus callosum determined that all callosal oligodendrocytes are born during early childhood. Immunohistochemistry of human post-mortem brain tissue also suggests regional variation in the production of oligodendrocytes. Staining for BCAS1 (a novel marker for newly-differentiated oligodendrocytes) revealed very few new oligodendrocytes in white matter tracts beyond the third decade of life. Yet there were several new oligodendrocytes observed in the frontal cortex even in old age (Fard et al., 2017).

Why are there regional differences in lifelong oligodendrocyte production? Such differences may reflect the diversity of circuits which are myelinated in the CNS. Different circuits may have differing demands throughout life. For

example, oligodendrocytes may be produced throughout life in the frontal cortex because cortical axons require increasing metabolic support, whereas as oligodendrocyte production is negligible in the adult corpus callosum because callosal axons do not have such metabolic requirements. Further work is required to understand how myelination throughout life differs between distinct circuits in the CNS.

Nevertheless, the caveats of the carbon dating method in assessing oligodendrocyte production throughout life must be considered (Mount and Monje, 2017). The birth date reflects the time point of S-phase of the OPC, and so this method assumes that all oligodendrocytes are differentiated from recently-divided OPCs. There is evidence that rodent OPCs can differentiate directly into oligodendrocytes without a prior cell division (or at least, OPCs can differentiate a prolonged period of time after their most recent cell division (Hughes et al., 2013)). If OPCs born in childhood differentiate without any further division into oligodendrocytes during adulthood, then the date of oligodendrocyte differentiation cannot be determined by carbon dating. If oligodendrocyte production during adulthood does, indeed, occur in both the frontal cortex and corpus callosum, then the carbon dating results may indicate that OPCs in these distinct areas behave differently. For example, in adulthood, the OPCs of the frontal cortex may always differentiate after cell division, whereas the OPCs of the corpus callosum may differentiate into oligodendrocytes a prolonged period of time after their last cell division. Additionally, this method provides an average birth date of a pool of nuclei, rather than individual nuclei, which could potentially mask variation in birth dates within the oligodendrocyte population (although the authors state that they used mathematical models that should account for this possible source of error) (Yeung et al., 2014). It is possible that the rate of oligodendrocyte production (and subsequent myelination) in the adult human brain may be higher than current carbon dating analysis suggests.

1.4.2. *Myelination in Other Mammals*

Much research has used rodent models to investigate the timescales of oligodendrocyte production and myelination throughout life. In rodents, myelination begins in the ventral spinal cord around birth, and, as in humans, progresses in a stereotyped manner (Baumann and Pham-Dinh, 2001; Foran and Peterson, 1992). Robust myelination is observed throughout the rodent CNS by approximately two months of age (P60), coinciding with young adulthood. During this developmental period, a surplus of oligodendrocytes is generated. These newly-differentiated oligodendrocytes compete for survival factors and many cells die without forming myelin sheaths. In the rat optic nerve, up to 50% of newly-differentiated oligodendrocytes die between P8-P12. This cell death is due to competition for survival factors such as IGFs and PDGF (Barres et al., 1992). Similarly, 20% of newly-differentiated oligodendrocytes in the rat cerebral cortex degenerate between P7-21, while oligodendrocytes that form myelin sheaths show no sign of cell death (Trapp et al., 1997). This extensive oligodendrocyte cell death is mediated by the pro-apoptotic transcription factor TFEB, which is highly expressed in newly-differentiated oligodendrocytes (Sun et al., 2018). Oligodendrocyte-specific loss of TFEB leads to a significant increase in the number of oligodendrocytes due to reduced apoptosis, and precocious myelination in both grey and white matter regions of the CNS as early as P6. Transcriptomic analysis revealed that TFEB promotes expression of PUMA which triggers oligodendrocyte cell death via the Bax-Bak axis (Sun et al., 2018). It remains unknown whether a similar degree of oligodendrocyte overproduction and subsequent cell death occurs during childhood and adolescence in humans.

OPCs continue to proliferate and differentiate into oligodendrocytes beyond P60 in many grey and white matter regions of the rodent CNS (Rivers et al., 2008; Young et al., 2013). More recent studies have used longitudinal live imaging of transgenic mice expressing fluorescent reporters in oligodendrocytes to follow the production of oligodendrocytes at various stages of adulthood (Hill et al., 2018; Hughes et al., 2018). These studies used cranial imaging windows to perform two-photon microscopy of the upper layers

of the somatosensory cortex in anaesthetised animals. Hughes et al., 2018 imaged the cortex of young adult (~P60-120), middle-aged (~P330-420), and old-aged (~P630-720) mice, and found that the oligodendrocyte density of the upper layers almost doubles between young adult and middle age. They also performed repeated imaging in middle-aged transgenic mice with fluorescently-labelled OPCs and oligodendrocytes to follow the fate of differentiating OPCs. By imaging over 50 days, they found that many newly-differentiated oligodendrocytes failed to form myelin sheaths and rapidly underwent cell death – reminiscent of the cell death observed in early myelination. Oligodendrocyte overproduction therefore continues throughout life in rodents.

Hill et al. 2018 imaged the cortex of juvenile (P30), young adult, middle-aged, and old-aged (reaching up to P950) mice, and similarly found that oligodendrocyte numbers increase throughout adulthood, reaching a peak at P630. They also performed the label-free imaging technique Spectral Confocal Reflectance microscopy (SCoRe) which has previously been used to image compact myelin sheaths without the need for any fluorescent protein expression (Schain et al., 2014). SCoRe takes advantage of the reflective properties of myelin sheaths by using multiple confocal lasers and detecting the reflected light in order to visualise compact myelin along axons, even in living tissue. Hill et al., 2018 observed that myelin detected by SCoRe accumulates in the cortex similarly to oligodendrocyte number. Both oligodendrocyte number and myelin levels detected by SCoRe decline from their peak at P630 to P950 – suggesting that death of myelinating oligodendrocytes occurs in old age. Age-related myelin loss will likely have an impact on the conduction of the underlying axons, could significantly disrupt the function of previously-myelinated circuits, and ultimately contribute to age-associated cognitive decline. It is not currently known whether oligodendrocyte number also declines in humans with old age. However, MRI studies have shown that the white matter microstructure (a parameter known to correlate with fluid intelligence (Ritchie et al., 2015)) of various tracts does deteriorate in old age (Cox et al., 2016).

Overall, there is significant evidence that myelination is a protracted process which can span well into adulthood. Why does myelination continue throughout life? Given that myelin sheaths are known to accelerate the conduction of the underlying axon, one possibility is that axons require lifelong tuning of their conduction properties. Adjustments to the conduction of individual axons is likely important in the overall function of circuits, and thus protracted myelination may represent a powerful means by which circuit function can be regulated throughout life. Alternatively, it may be that axons require more metabolic support with age, which could be achieved by increasing the myelin coverage along axons over time.

1.5. Myelin and the Regulation of Circuit Function

Myelination significantly changes the conduction properties of axons and is therefore likely to have a dramatic impact on circuit function. Indeed, myelination correlates with the emergence of various cognitive processes. Numerous MRI studies in children show that white matter volume (which is influenced by myelination) correlates with development of processes such as language acquisition (Pujol et al., 2006), reaction time (Walhovd and Fjell, 2007), information processing speed (Mabbott et al., 2006), working memory, and reading ability (Nagy et al., 2004).

There is considerable variability in the number, length, thickness, and distribution of myelin sheaths along axons in the CNS. For example, myelin sheaths in the spinal cord tend to be longer than sheaths in the corpus callosum (Remahl and Hildebrand, 1990), while sheaths in the cerebral cortex tend to be the shortest on average (Chong et al., 2012). Although sheath length is known to correlate with axon diameter, this may not be the only determinant of sheath length. Murray and Blakemore, 1980 noted that many sheaths in the cat spinal cord are double or half the length predicted by axon diameter alone. Additionally, there are many different patterns of myelination in the CNS. Tomassy et al., 2014 imaged serial sections of the mouse cortex by electron microscopy, and then made reconstructions of single axons to visualise myelinated axon morphology at high resolution. They identified several

different myelin patterns along the axons of pyramidal neurons in the cortex of young adult (P60) mice. Many axons in layers II/III of the visual cortex display intermittent or sparse patterns of myelin where myelin sheaths are separated by stretches of unmyelinated axon much longer than conventional nodes of Ranvier. These intermittent myelin patterns have also been found in deeper layers of the visual cortex imaged by combined lattice light-sheet protein-retention expansion microscopy (Gao et al., 2019). Intermittent myelin patterns may be a feature of specific neural circuits – while layer V/VI axons of the visual cortex are intermittently myelinated (Gao et al., 2019), layer V/VI axons of the somatosensory cortex are continuously myelinated at the same age (Tomassy et al., 2014). Sparsely myelinated axons are also seen in layer I of the somatosensory cortex of middle-aged mice (Hill et al., 2018; Hughes et al., 2018). Repeated imaging demonstrated that new myelin sheaths form on these sparsely myelinated axons in adulthood (Hill et al., 2018); this suggests that sparse myelination reflects axons undergoing very gradual protracted myelination.

What is the functional consequence of this myelin pattern variability in the CNS? Changing the sheath length, thickness, or number will have predictable effects on the conduction velocity of the underlying axon (Waxman, 1980). In the context of circuit function, it is important to not only ensure rapid signal conduction, but also to synchronise the precise timing of signal arrival at synaptic targets. Establishing a particular pattern of myelin along an axon is one such way in which the timing of signals could be fine-tuned to facilitate synchronisation of activity (Pajevic et al., 2014), and therefore different myelin patterns may reflect the different conduction requirements of distinct circuits.

1.5.1. *Myelin is Involved in Signal Synchronisation in the Auditory System*

Sound localisation requires synchronous arrival of input from each ear onto an array of coincidence detector neurons. In birds, nucleus magnocellularis (NM) neurons receive monoaural input from the ipsilateral auditory nerve. The NM neuron has a bifurcating axon; one branch projects to the ipsilateral nucleus laminaris (NL), while the other branch projects to the contralateral NL.

Coincidence detector neurons in each NL receive input from both ears. The slight temporal difference in signal arrival at the NL means that a particular neuron in the coincidence detector array will be stimulated, which allows computation of sound localisation. However, this still requires input from both ears to arrive at the NL with approximate synchrony. The ipsilateral projection of the NM neuron is much shorter than the contralateral projection; this means that the contralateral auditory input to the NL has a much greater distance to travel before reaching the coincidence detector array. To ensure that the contralateral input arrives at the NL to coincide with the ipsilateral input, the contralateral projections of the NM neurons have larger axon diameters and longer myelin sheaths (Seidl et al., 2010). This allows the contralateral projection to conduct at a higher velocity than the ipsilateral projection (Seidl et al., 2014) (**Figure 5A**).

Similar axonal morphologies have been described in mammals. In the mammalian auditory system, bushy cells receive input in the cochlea and then project to the contralateral medial superior olive (MSO) nucleus. Excitatory spherical bushy cells (SBCs) project axons directly to the MSO. Granular bushy cells (GBCs) synapse onto the contralateral medial nucleus of the trapezoid body (MNTB), which sends inhibitory projections to the MSO. GBC-mediated inhibitory input arrives at the MSO before the excitatory SBC input, despite the synaptic delay at the MNTB (Roberts et al., 2013). This is because GBC axons have larger diameter and longer myelin sheaths than SBC axons (Ford et al., 2015). Intriguingly, a subset of GBC neurons exhibit tuning of myelin sheath length independent of axon diameter. GBC axons projecting to the lateral MNTB (which encode low frequency sound) have a larger axon diameter but a shorter myelin sheath length than the GBC axons projecting to the medial MNTB (which encode high frequency sound). These axons also exhibit decreasing myelin sheath length and increasing node diameter along distal regions of the axon close to the presynaptic terminal, which is hypothesised to ensure precise timing of presynaptic depolarisation (Ford et al., 2015) (**Figure 5B**).

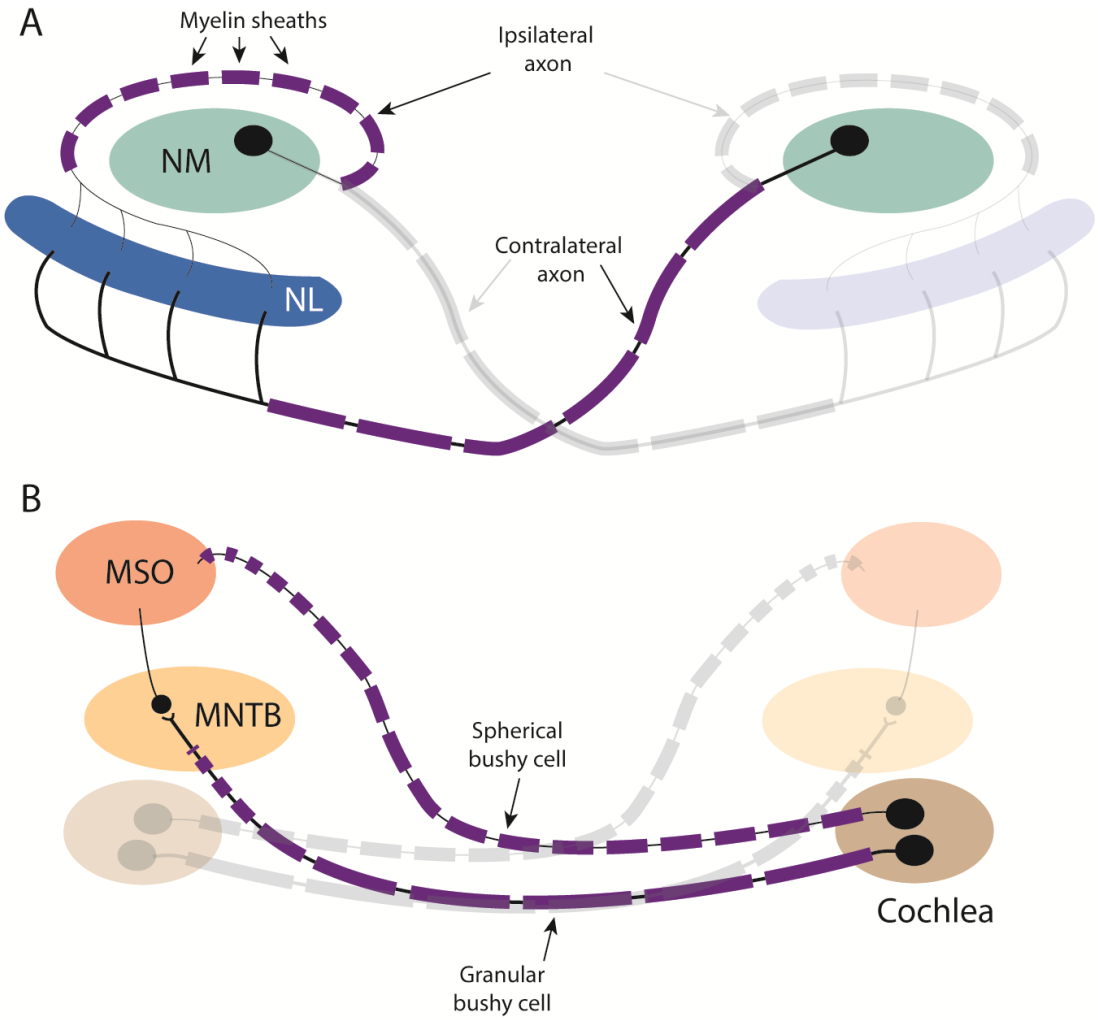

Figure 5 – specific myelin patterns facilitating synchronous activity in the auditory system.

A) A simplified diagram of nuclei in the auditory system of birds. Nucleus magnocellularis (NM) neurons receive auditory input and send impulses along a bifurcating axon; one branch projects to the ipsilateral nucelus laminaris (NL), the other branch projects to the contralateral NL. The contralateral axon has a larger diameter and longer myelin sheaths to increase conduction velocity relative to ipsilateral axon. This means that each NL receives ipsilateral and contralateral auditory inputs at approximately the same time, despite the disparity in the length of the two axons. **B)** A simplified diagram of the nuclei in the mammalian auditory system. Spherical bushy cells (SBCs) project from the cochlea directly to the contralateral medial superior olive (MSO), while Granular bushy cells (GBCs) project to the contralateral medial nucleus of the trapezoid body (MNTB) which then projects onto the MSO. GBC signals arrive at the MSO faster (despite the synaptic

delay) due to increased axon diameter and myelin sheath length along GBCs compared to SBCs. Additionally, both axons have reducing sheath length towards the distal end of the axon which is predicted to ensure precise signal timings.

1.5.2. *Characterising Myelin Patterns along Single Axons In Vivo*

Establishing specific myelin patterns may be crucial in the synchronisation of signals in many other circuits of the CNS. To begin to understand how myelin patterns might regulate circuit function, there is a need to characterise the myelin patterns along single axons within identified circuits and correlate these patterns with known circuit properties. Do certain subtypes of axon exhibit particular myelin patterns? The interplay of the many signals which regulate the selection of axons for myelination (discussed in section '1.3.2 Axon Selection') may play a role in myelin pattern establishment. Certain subtypes of axon may use specific signals to regulate their myelination and myelin pattern formation versus other signals. For example, two neuronal subtypes in the zebrafish spinal cord have been shown to regulate their initial myelination differently. Reticulospinal axons are myelinated in a synaptic vesicle release-dependent manner, whereas CoPA axons are not (Koudelka et al., 2016). In Chapter 3 of this thesis, I will characterise the myelin patterns established along individual axons of different neuron subtypes in the zebrafish spinal cord, and assess whether neuron subtypes from different circuits exhibit different myelin patterns.

1.5.3. *Experience Affects Myelination*

Experience can impact on myelination, particularly during key developmental time windows, and lack of experience can have long-lasting consequences on both myelination and cognitive function. Social experience is one poignant example; Romanian orphans who experienced severe socio-emotional neglect during early childhood have significant alterations to numerous white matter tracts associated with the medial prefrontal cortex (mPFC), as assessed by DTI (Eluvathingal et al., 2006). Numerous social isolation experiments have been performed in rodents to investigate the cellular level effects of social

deprivation. Mice which are socially isolated after weaning display long-lasting cognitive deficits in sociability and working memory (Makinodan et al., 2012). Although isolated mice show no change in the number of oligodendrocytes in the mPFC, there is a significant reduction in both the number and thickness of myelin sheaths that each oligodendrocyte generates. Neither the myelin nor the behavioural phenotypes are rescued by re-socialising the mice, indicating that experience deprivation during juvenile development has sustained effects on cognitive function. The molecular mechanism for these phenotypes may be via Nrg1-ErbB signalling; social isolation leads to reduced expression of Nrg1 type III, while inducible deletion of the Nrg1 receptor ErbB3 from oligodendrocytes replicates the behavioural and myelin phenotypes of socially isolated mice (Makinodan et al., 2012). Given previous research which suggests that Nrg1 is required for oligodendrocytes to respond to neuronal activity (Lundgaard et al., 2013), it is possible that Nrg1 signalling to oligodendrocytes is required for experience-related signals – such as neuronal activity – to influence myelination and regulate circuit function.

Social experience is capable of altering myelin in adulthood, too; social isolation of adult mice leads to thinner myelin sheaths and reduced myelin protein expression in the mPFC (Liu et al., 2012). These effects appear to be circuit-specific, as the myelin phenotypes were not seen in other regions such as the nucleus accumbens, corpus callosum, or cerebellum. Interestingly, resocialisation after isolation in adulthood does reverse both the transcriptional and behavioural phenotypes observed, which contrasts with the lack of change seen when juvenile mice are resocialised. These findings suggest that there is a critical period during development when experience can permanently shape myelination and alter circuit function, whereas changes to myelin and circuit function during adulthood may be more transient or reversible.

Rescuing the myelin phenotype appears to rescue the cognitive deficits caused by social isolation. Mei et al., 2014 performed a large-scale chemical screen for drugs which promote myelination, where they identified clemastine, an anti-muscarinic compound which promotes oligodendrocyte differentiation (Mei et al., 2014). Treating socially isolated adult mice with clemastine

increases the number of mature oligodendrocytes, the number of myelinated axons, and myelin sheath thickness in the PFC compared to vehicle treatments (Liu et al., 2016). Clemastine treatment also increases the social interaction test score of isolated mice so that their sociability is identical to normally-housed mice. Thus, social experience is required to shape the myelin patterns of the PFC, and these myelin patterns may, in turn, affect circuit functional output.

Sensory experience can also influence myelination. Hill et al., 2014 studied survival of oligodendroglial lineage cells in the somatosensory barrel cortex of P10-12 mice in a sensory deprivation paradigm. A sub-population of OPCs was labelled at P6 with YFP by Cre-ER^{T2}-mediated lineage tracing, and then the whiskers from one side were trimmed daily to reduce sensory stimulation from P6-P10/12. The overall number of caspase-3^{+} cells and the number of YFP^{+} caspase-3^{+} cells at P12 was significantly higher in the deprived sensory cortex compared to the spared cortex, indicating that sensory deprivation increased the death of either OPCs, or newly-differentiated oligodendrocytes derived from P6-labelled OPCs. There was no change in the total number of CC1^{+} cells nor the number of caspase-3^{+} CC1^{+} cells, suggesting that despite reduced survival of OPCs or newly-differentiated oligodendrocytes, there was no effect on either the production or survival of myelinating oligodendrocytes. It is possible that a more prolonged period of sensory deprivation would eventually lead to reduced production of myelinating oligodendrocytes and hypomyelination.

Hughes et al., 2018 observed that sensory stimulation increased the production of oligodendrocytes in the somatosensory cortex. They performed longitudinal imaging of fluorescently-labelled oligodendrocytes in the upper sensory cortex of adult mice undergoing a sensory stimulation paradigm. These mice were housed in cages with strings of beads hung inside, so that when the mice moved around the cage their whiskers were stimulated regularly. Hughes et al. imaged a region of the cortex both before and after 3 weeks of sensory stimulation and found that stimulation increased the production of new myelinating oligodendrocytes compared to unstimulated

control mice. This was due to the sensory stimulation itself, as mice housed in the sensory cages, but without any whiskers, did not have elevated numbers of new myelinating oligodendrocytes.

It remains to be seen if myelin phenotypes caused by changing sensory experience alter circuit function and change animal behaviour, as occurs with social experience.

1.5.4. *Myelin may Contribute to Learning*

Learning requires circuit plasticity. The strengthening of synaptic connections through long-term potentiation has long been known to play a vital role in learning and memory (Bliss and Collingridge, 1993). Evidence now suggests that myelination may also be involved in learning processes. In principle, establishing certain patterns of myelin could synchronise signals on a common target; changes to the myelin pattern along axons may facilitate the strengthening of circuits in learning. There is significant evidence that white matter alterations occur with learning. DTI studies have shown that practicing a musical instrument correlates with white matter tract organisation in childhood, adolescence and adulthood (Bengtsson et al., 2005; Steele et al., 2013). Scholz et al., 2009 performed DTI in individuals before and after a period of time spent learning to juggle, and found that individuals who performed this visuo-motor task displayed white matter changes in the intra-parietal sulcus. Similarly, Schlegel et al., 2012 found that individuals who undertook an intensive language course displayed white matter changes in language-associated brain areas. As previously discussed, the measurements obtained from DTI studies are not necessarily caused by changes to myelin. To address whether learning causes changes in myelin, Sampaio-Baptista et al., 2013 performed DTI and immunohistochemistry in rats which were taught a skilled reaching motor task. They found that both the FA measurements and myelination as assessed by MBP staining correlated with the animals' learning rates. This indicates that increased myelination does occur during motor learning.

Is myelination required for learning? To investigate this, McKenzie et al., 2014 conditionally deleted the transcription factor MyRF gene from OPCs in adult mice to prevent any further oligodendrocyte production. These mice were unable to learn a complex running wheel motor task as efficiently as their wild-type littermates. More detailed analysis revealed that when wild-type mice undergo motor learning, this leads to production of newly-differentiated oligodendrocytes in the motor cortex and subcortical white matter just a few hours after training (Xiao et al., 2016).

Collectively, these examples suggest that myelin can regulate the function of circuits to mediate efficient learning; such regulation could explain the gradual formation of myelin which has been observed throughout life.

1.5.5. *How Does Myelin Change? De Novo Myelination versus Myelin Remodelling*

If establishing particular myelin patterns along axons is crucial to circuit function and is involved in learning, then changes to myelin patterns in circuits must occur throughout life. This could be done by producing new myelin sheaths, modifying existing myelin sheaths, or a combination of both strategies.

New myelin sheaths would most likely be produced by newly-differentiated oligodendrocytes. Live imaging in *in vitro* co-cultures (Watkins et al., 2008) and *in vivo* in zebrafish larvae (Czopka et al., 2013) has demonstrated that newly-differentiated oligodendrocytes can only form new myelin sheaths within a restricted time window on the order of hours. Myelin sheath number per oligodendrocyte does not increase beyond this time period (Czopka et al., 2013; Tripathi et al., 2017).

There is significant evidence that new oligodendrocytes are generated throughout adulthood in at least some regions of the human and rodent CNS (see section ‘1.4 Myelination is a Lifelong Process’ above). This suggests that new oligodendrocytes (and subsequently, the addition of new myelin sheaths) are required for learning. Although McKenzie et al., 2014 found that MyRF

knock-out mice exhibit significant motor learning deficits compared to wild-type mice, the knock-outs still show improvement in the complex wheel task over eight days. Therefore, inhibiting *de novo* myelination does not completely prevent learning.

Modification (or remodelling) of existing myelin sheaths could also affect the conduction properties of underlying axons to fine-tune signal timing. This could be done by changing the length or thickness of existing myelin sheaths. Hughes et al., 2018 and Hill et al., 2018 both followed individual myelin sheaths in their cortical live imaging experiments to assess if sheath length is altered over time. They found that, although a small subset of sheaths exhibited changes (both sheath growth and sheath shrinkage were observed), the majority of sheaths showed no discernible change in length over several weeks. Sheath length stability may actually increase with age – Hill et al. found that approximately 80% of sheaths analysed were stable in P60-90 mice, while Hughes et al. found that 99% of sheaths were stable in P365 mice. Sheath length remodelling is unchanged by repeated sensory stimulation of whiskers (Hughes et al., 2018). It is not clear whether more myelin sheaths are remodelled during earlier developmental time windows or in other regions of the CNS, nor whether experience or circuit activity can induce sheath remodelling in other regions or at other developmental stages. It also remains unclear if the sheaths which do remodel in length at middle age belong to a particular subset of dynamic oligodendrocytes. Hill et al. followed individual oligodendrocytes and identified examples of cells which exhibited different behaviours in sheath length changes. One cell showed no sheath length changes, one showed some sheaths which grew, and one showed both sheath growth and sheath shrinkage. Alternatively, sheath length remodelling may only occur along a subset of axons throughout life.

Research in zebrafish larvae also indicates that at least some sheaths are relatively stable in length. Auer et al., 2018 performed repeated imaging of the spinal cords of larvae with fluorescently-labelled oligodendrocytes and myelin sheaths to follow changes in sheath length over time. They found that in the first few days after sheaths are formed, they grow rapidly (although growth rate

was variable between different sheaths). After this initial period of rapid growth, sheaths then become stable in length; however, they are capable of adjusting length when required. For example, as the animal grows (and subsequently, the axons in the spinal cord elongate), myelin sheaths will grow at the same rate to ensure that myelin coverage along the axon is sustained.

Sheath thickness may also be modified over time to influence conduction velocity. The gold-standard technique for measuring myelin sheath thickness is by cross-sectional analysis via transmission electron microscopy of ultra-thin sections (70-80 nm in thickness). Sheath thickness is typically reported as a g-ratio, which is the ratio between the diameter of the axon alone and the diameter of the axon plus the myelin sheath. Transmission electron microscopy can also be used to count the number of membrane wraps in a myelin sheath. Recent technological advancements (for example, high-pressure freezing techniques) have significantly improved the quality of tissue fixation to provide ultra-detailed images of sheath structure (Möbius et al., 2016). However, this technique limits sheath thickness measurement to a single time-point; live imaging techniques are required to properly assess whether myelin sheath thickness can be modified over time. Some techniques are emerging which may allow assessment of sheath thickness dynamics in living animals, such as: third harmonic generation microscopy (Lim et al., 2014) and spectral reflectometry (Kwon et al., 2017).

Nevertheless, there is some electron microscopy evidence that sheath thickness can change over time. Snaidero et al., 2014 investigated how manipulating the PI3K/AKT/mTOR pathway in adult mice affects sheath growth. To do this, they inducibly deleted the PTEN gene in myelinating oligodendrocytes of adult (P100) mice to elevate PIP3 levels (and subsequently stimulate the PI3K/AKT/mTOR pathway). They found that, 30 days after gene deletion, myelin sheaths in the optic nerve had many more cytoplasmic channels than wild-type animals (a feature of growing sheaths in early developmental myelination), but were of similar sheath thickness. When they looked at myelinated optic nerve axons even later (90 days after gene deletion), not only did sheaths in the knock-out animals have many more

cytoplasmic channels, these myelin sheaths contained significantly more wraps of myelin. These results indicate that upregulation of the PI3K/AKT/mTOR pathway in adult myelin sheaths re-initiates the wrapping process to increase sheath thickness. It remains to be seen if this occurs naturally *in vivo* in response to experience and learning.

1.5.6. *Myelin Pattern Remodelling Along Single Axons In Vivo*

Experience (and therefore, circuit activity) may remodel myelin patterns to influence circuit function. Understanding how myelin remodelling might influence circuit function requires characterisation of how myelin is remodelled over time along individual axons within known circuits. Although recent work in rodents suggests that myelin sheaths in the adult somatosensory cortex do not remodel (Hill et al., 2018; Hughes et al., 2018), it remains unknown if myelin remodelling occurs elsewhere or at other time points during development. If myelin is remodelled in response to the activity or demands of an individual circuit, then do axons from different circuits exhibit different types and extents of myelin remodelling? Using the cranial window imaging techniques utilised by both Hill et al., 2018 and Hughes et al., 2018 to investigate these questions is technically challenging. The larval zebrafish is an ideal system to perform non-invasive repeated live imaging of myelin sheaths along single axons *in vivo*. In Chapter 3 of this thesis, I will investigate how and when myelin is remodelled along individual axons of distinct neuron subtypes in the zebrafish spinal cord, and assess whether axons from different circuits exhibit different types and extents of myelin remodelling.

1.6. Neuronal Activity can Influence Myelination

Changes to myelin occur in response to experience, affecting cognitive function and, potentially, mediating learning. What are the signals which cause these changes to myelin? A significant body of research has demonstrated that neuronal activity itself can influence oligodendroglial development and myelination. The first evidence came from studies of visual system development when visual input is altered. The optic nerve is normally

extensively myelinated within the first few weeks of post-natal development. Raising mice in the dark decreases the number of axons which are myelinated during this time period (Gyllensten and Malmfors, 1963), while prematurely opening the eyes of rabbits at P5 accelerates optic nerve myelination (Tauber et al., 1980). Since then, much work has been done to understand the signalling mechanisms connecting neuronal activity to myelination. Here I will first discuss the evidence that manipulating the electrical activity of neurons can impact various aspects of oligodendrocyte development; then, I will discuss various molecular signals proposed to mediate the effects of activity on oligodendroglial cells.

1.6.1. *Electrical Activity of Neurons Affects Numerous Stages of Oligodendroglial Lineage Development*

OPC Proliferation and Differentiation

Barres and Raff, 1993 studied how electrical activity in the optic nerve affects oligodendroglial development by injecting tetrodotoxin (TTX) into the eye of P8 rats. TTX blocks voltage-gated Na^+ channels and thus silences the electrical activity of neurons by preventing action potentials from firing (Narahashi and Scott, 1964). Inhibiting optic nerve electrical activity leads to significantly reduced levels of OPC proliferation, as assessed by BrdU incorporation, which can be reversed by implanting cells which over-express PDGF (Barres and Raff, 1993).

Direct electrical stimulation can enhance OPC proliferation and differentiation *in vivo*. Li et al., 2010 surgically implanted an electrode onto the medullary pyramid of rats in order to electrically stimulate the corticospinal tract and then observe the effects of stimulation on oligodendroglial lineage cells. They found that, after a 10-day stimulation period, the number of proliferating cells was elevated at numerous positions in the spinal cord compared to sham controls (assessed by BrdU incorporation during the stimulation period). Enhanced OPC proliferation and differentiation was confirmed as the number of $BrdU^+$ OPCs and oligodendrocytes was significantly higher in stimulated rats than in shams.

More recent research utilising optogenetics has confirmed that electrical activity in cortical neurons also stimulates OPC proliferation and differentiation (Gibson et al., 2014). In brief, light-sensitive channelrhodopsin cation channels are expressed in neurons of interest *in vivo*, and then exposure of these neurons to a particular wavelength of light opens the light-gated channelrhodopsins, subsequently activating the expressing neuron (Boyden et al., 2005). Channelrhodopsins were expressed in cortical layer V projection neurons of mice with an optical fibre implanted beneath the pial membrane at the premotor cortex, and the expressing neurons were stimulated with blue light for 30 minutes (Gibson et al., 2014). Proliferation was measured by EdU incorporation three hours after stimulation, and showed that OPC proliferation is substantially increased in both the premotor cortex and in the adjacent region of the corpus callosum. Repeated optogenetic stimulation also enhances the differentiation of OPCs into oligodendrocytes. Daily optogenetic stimulation of cortical neurons for seven days leads to a significant increase in the number of EdU^+ oligodendrocytes (new cells generated from recently-proliferating OPCs) four weeks later.

Similar results have been reported using chemogenetics to stimulate neurons in the somatosensory cortex (Mitew et al., 2018). Designer Receptors Exclusively Activated by Designer Drugs (DREADDs) are modified G-protein coupled receptors (GPCRs) with reduced affinity for their endogenous ligand, and high affinity for a synthetic ligand (Alexander et al., 2009). Mitew et al. expressed the DREADD hM3Dq in somatosensory cortical neurons and found that stimulating these neurons by administering the ligand clozapine-N-oxide elevated the levels of OPC proliferation in the corpus callosum, as assessed by EdU incorporation. Stimulation also increased the number of EdU^+ oligodendrocytes in the corpus callosum. Importantly, DREADD stimulation increased OPC proliferation and differentiation in both juvenile (P19) and young adult (P60) mice.

One issue which has not been addressed in these experiments is whether neuronal activity directly influences both OPC proliferation and differentiation. The OPC population appears to be tightly regulated, with OPCs colonising the

CNS uniformly and proliferating in response to disruption of the population (such as OPC death or differentiation (Hughes et al., 2013; Kirby et al., 2006)). It is possible that neuronal activity only directly influences one phenomenon, and that the other is altered indirectly as a consequence. For example, neuronal activity may directly promote the proliferation of OPCs, and this imbalance in the OPC population may drive OPCs to differentiate. Alternatively, neuronal activity may increase OPC differentiation, which, in turn, could lead to proliferation of remaining OPCs to restore the population. Yet, some evidence indicates that neuronal activity can trigger either proliferation or differentiation of OPCs in a frequency-dependent manner. *In vivo* manipulation of neuronal activity in the mouse corpus callosum using an implanted electrode array demonstrated that lower frequencies of activity (5 Hz) promote the differentiation of OPCs into oligodendrocytes, whereas higher frequencies (25 Hz and 300 Hz) promote the proliferation of OPCs (Nagy et al., 2017). It is not yet clear how this relates to physiological firing frequencies in different circuits throughout development, and thus whether physiological neuronal activity influences OPCs in a similar manner.

Myelin Sheath Formation and Growth

Neuronal activity also affects the formation of myelin sheaths by oligodendrocytes. In neuron-oligodendrocyte co-cultures, TTX treatment to silence neuronal activity does not affect the number of mature oligodendrocytes or the number of neurons, but drastically reduces the number of myelin segments identified by MBP staining (Demerens et al., 1996). This has also been confirmed *in vivo*. TTX injection into the right eye of P4 mice followed by analysis of optic nerve myelination at P6 revealed that silencing neuronal activity does not change the number of mature oligodendrocytes expressing MBP. Despite this, it does significantly reduce the number of MBP^+ oligodendrocytes with a myelinating morphology (Demerens et al., 1996). Malone et al., 2013 observed similar results when they electrically stimulated DRG neuron-oligodendrocyte co-cultures. They found that the number of myelin sheaths formed significantly increases with electrical stimulation in a frequency-dependent manner, and that this could be completely blocked by

TTX treatment. Oligodendrocytes will actually preferentially form myelin sheaths on active axons. Chemogenetic stimulation of somatosensory cortical neurons using DREADDs elevates the number of myelinated axons significantly when compared to unstimulated control animals (Mitew et al., 2018). Closer analysis revealed that, in the stimulated animals, there was a 3.4-fold increase in the number of stimulated axons which were myelinated, whereas there was only a 0.3-fold increase in the number of unstimulated axons which were myelinated. They then used Cre-ER^{T2}-mediated lineage tracing to identify oligodendrocytes born during the chemogenetic stimulation period, and found that these new oligodendrocytes make more myelin sheaths on the stimulated axons versus the unstimulated axons. Hence, neuronal activity not only enhances myelination, but can specifically target the formation of new myelin on electrically active circuits.

Can neuronal activity regulate the growth of existing myelin sheaths? The signals which regulate the growth of individual myelin sheaths are still poorly understood. Research has determined that different myelin sheaths made by the same oligodendrocyte can have very different elongation rates, which suggests that local signals can influence myelin sheath growth (Mensch, 2014). Calcium imaging of individual oligodendrocytes in the zebrafish larval spinal cord using genetically-encoded calcium indicators has shown that calcium transients occur in myelin sheaths during early stages of dynamic growth (Baraban et al., 2018; Krasnow et al., 2018). Electrically stimulating the hindbrain to globally increase neuronal activity in the spinal cord increases the number of calcium transients observed in sheaths. Conversely, injecting TTX into the hindbrain to inhibit neuronal activity significantly reduces the number of calcium transients (Krasnow et al., 2018). The frequency of these calcium transients positively correlated with the growth of myelin sheaths in length (Baraban et al., 2018), so that stimulating neuronal activity increases sheath growth, while inhibiting neuronal activity reduces sheath growth (Krasnow et al., 2018). This result highlights the fact that at least some of the calcium transients in growing myelin sheaths are induced by neuronal activity, and suggests that neuronal activity can influence the elongation of myelin sheaths.

It is not clear whether neuronal activity has a global effect on sheath growth, or whether the activity of a single neuron locally regulates the growth of myelin sheaths along its axon. It is possible that myelin patterns are established along individual axons by axonal activity signalling locally to its myelin sheaths to control their growth. Manipulation of activity along individual axons is required to assess whether axonal activity locally influences myelin pattern formation by regulating sheath growth.

Neuronal activity may also regulate sheath thickness. Both optogenetic stimulation of motor cortical neurons (Gibson et al., 2014) and chemogenetic stimulation of somatosensory cortical neurons (Mitew et al., 2018) increases sheath thickness of axons in the corpus callosum. Mitew et al. performed immunogold electron microscopy to identify axons which express the DREADD (and therefore identify the specific population of axons which were stimulated), and found that these stimulated axons had thicker myelin sheaths than neighbouring unstimulated axons. Does neuronal activity stimulate the radial growth of existing myelin sheaths? Or does neuronal activity promote the formation of new myelin sheaths which become thicker than other pre-existing sheaths? Developing imaging techniques to accurately measure sheath thickness dynamics over time will allow the investigation of these two possibilities.

1.6.2. *Neurotransmitter Signalling from Neurons to Oligodendroglia*

How do oligodendroglial lineage cells detect changes in neuronal activity? Action potentials stimulate the synaptic release of neurotransmitters to facilitate neuron-neuron communication within circuits. However, there is significant evidence for neurotransmitter signalling between neurons and oligodendroglial cells as well.

OPCs and Oligodendrocytes Express Neurotransmitter Receptors

Many studies have tested oligodendroglial lineage cells for expression of glutamatergic receptors, both ionotropic (AMPA, kainate, and NMDA receptors) and metabotropic (mGluR1-5). Cultured OPCs isolated from the

rodent optic nerve exhibit inward currents in response to treatment with the excitatory neurotransmitter glutamate, which can be blocked by the AMPA/kainate receptor antagonist CNQX (Barres et al., 1990). OPCs treated with NMDA did not give any current response. Both cerebellar and optic nerve OPCs in culture elicited current responses upon quisqualate (a potent AMPA receptor agonist) and kainate treatment, but not upon NMDA treatment (Wyllie et al., 1991). Oligodendrocytes recorded in corpus callosum slice also exhibit inward currents when exposed to glutamate or kainate, but not when treated with NMDA (Berger et al., 1992). Northern blot analysis showed that purified OPCs and oligodendrocytes express mRNAs for AMPA and kainate receptors (Patneau et al., 1994), which suggests that OPCs and oligodendrocytes detect glutamate via AMPA and kainate receptors, but not NMDA receptors. However, Barres et al. noted that the digestion step in their cell isolation protocol likely damages or removes NMDA receptors, as NMDA receptor-expressing neurons treated with the same digestion also do not respond to NMDA treatment (Barres et al., 1990). Several studies have since shown that OPCs and oligodendrocytes do indeed express active NMDA receptors. Wang et al., 1996 identified OPCs which expressed the NMDA receptor subunit NR1 in a posterior pituitary gland explant culture. These OPCs elicited an inward current upon NMDA administration which could be blocked by MK-801 or Mg^{2+} (known antagonists of NMDA receptors). Both OPCs and oligodendrocytes recorded in rat spinal cord slices responded to glutamate, kainate, or NMDA application (Žiak et al., 1998). Further immunohistochemistry revealed that mature oligodendrocytes in the optic nerve express NMDA receptor subunits (Salter and Fern, 2005). Recordings in both cerebellar and corpus callosum mature oligodendrocytes showed that they respond to NMDA, and these responses were blocked by the NMDA receptor antagonist AP-5 (Káradóttir et al., 2005).

OPCs can exhibit diversity in their responsiveness to neuronal activity. Káradóttir et al., 2008 found that in the P7 rat brain, only half of OPCs express voltage-gated Na^+ channels. These Na^+ channel-expressing OPCs respond to glutamate or NMDA treatment, whereas OPCs which do not express Na^+

channels exhibit very little response to glutamate or NMDA (Káradóttir et al., 2008). More recent research has shown that expression of ionotropic glutamatergic receptors in OPCs can change with age and CNS region. In rodents, after P9 OPCs in the cortex increase their AMPA/kainate receptor density and decrease their NMDA receptor density, whereas OPCs in the corpus callosum show no change in either AMPA or NMDA receptor density (Spitzer et al., 2019). After the onset of myelination (until P330), OPC AMPA receptor density remains fairly consistent while OPC NMDA receptor density decreases in corpus callosum, cortex, and cerebellum. OPCs of the subventricular zone maintain consistent levels of NMDA receptors throughout life, suggesting a functional difference in this specific population of OPCs (Spitzer et al., 2019).

Oligodendroglial lineage cells also express metabotropic glutamate receptors (mGluRs). RT-PCR analysis in rat OPCs and oligodendrocytes identified expression of mGluR3 and mGluR5 (Luyt et al., 2003). Expression of mGluR5 was confirmed by immunocytochemistry, and calcium imaging showed that the group I mGluR agonist DHPG increases the intracellular Ca^{2+} levels of OPCs. Immunocytochemistry of cultured forebrain oligodendrocytes showed expression of mGluR1-5, but expression levels decrease as the cells mature (Deng et al., 2004).

There is also evidence that oligodendroglial lineage cells can respond to neurotransmitters other than glutamate. Both OPCs and oligodendrocytes elicit inward currents in response to GABA treatment which can be prevented by bicuculline treatment (an ionotropic $GABA_A$ receptor antagonist) (von Blankenfeld et al., 1990; Williamson et al., 1998). Similarly, Berger et al., 1992 identified GABA-induced currents in corpus callosum oligodendrocytes. OPCs can also detect adenosine; this reduces OPC proliferation and promotes differentiation into myelinating oligodendrocytes *in vitro* (Stevens et al., 2002). In DRG-OPC co-cultures neuronal stimulation inhibits OPC proliferation and increases myelin formation in an adenosine signalling-dependent manner (Stevens et al., 2002). Whether different neurotransmitters mediate different

developmental processes, or are involved in myelination of distinct circuits or CNS regions, is not yet known.

OPCs Form Neuro-glial Synapses

OPCs form synaptic-like structures with neurons *in vivo*. Glutamatergic neuro-glial synapses were first described by Bergles et al., 2000, who identified labelled OPC processes tightly adjacent to presynaptic boutons by electron microscopy. Electrically stimulating the stratum radiatum in hippocampal slices triggers responses in OPCs which can be blocked by AMPA receptor antagonist CNQX (Bergles et al., 2000). Applying glutamate to the CA3 elicits excitatory post-synaptic currents (EPSCs) in CA1 OPCs which can be blocked by TTX, indicating that the evoked OPC EPSCs are dependent on neuronal activity. The frequency of spontaneous EPSCs in OPCs increases between P4-20, which may represent functional integration of OPCs into hippocampal networks (Mangin et al., 2008). These neuro-glial synapses can even undergo long-term potentiation; theta burst stimulation of Schaeffer collaterals in hippocampal slices induces a calcium-dependent (but NMDA independent) increase in OPC EPSC amplitudes (Ge et al., 2006). Functional GABA-ergic neuro-glial synapses have also been described in the hippocampus (Lin and Bergles, 2004).

Glutamatergic neuro-glial communication is downregulated with oligodendroglial lineage progression. Although pre-myelinating and mature oligodendrocytes are still responsive to glutamate, they exhibit fewer spontaneous EPSCs than OPCs (Kukley et al., 2010). Both neuronal stimulation and glutamate uncaging experiments also trigger smaller AMPA-mediated EPSCs in pre-myelinating and mature oligodendrocytes than in OPCs (De Biase et al., 2010; Kukley et al., 2010).

Neuro-glial synaptic connections are hypothesised to form along the axon rather than at the traditional presynaptic terminal. Both Kukley et al. 2007 and Ziskin et al. 2007 identified activity-dependent responses in OPCs within the rodent corpus callosum (a white matter tract devoid of neuronal soma or synaptic terminals). Both studies analysed the OPC responses in corpus

callosum slices, finding that electrical stimulation of callosal axons induces currents within OPCs which can be blocked by pharmacological inhibition of AMPA receptors. Callosal OPCs in TTX-treated cultures also exhibit miniature EPSCs when synaptic vesicle release is stimulated in callosal axons either by ruthenium red (Kukley et al., 2007) or by α-latrotoxin (Ziskin et al., 2007). Transmission electron microscopy identified distinct synaptic structures between labelled OPCs and callosal axons, such as: pools of vesicles at the axonal membrane adjacent to the OPC process (Kukley et al., 2007); immunogold labelling for vesicular glutamate transporter 1 in the axon (vGLUT1, a presynaptic protein); and the presence of electron-dense material at the OPC post-synaptic membrane (Ziskin et al., 2007). Measuring the conduction velocities of axons which produce current responses in OPCs showed that these axons are unmyelinated (Ziskin et al., 2007). Axon-OPC synapses may play a role in the early stages of myelination, where neuronal activity in unmyelinated axons can signal to OPCs, possibly to regulate differentiation into mature oligodendrocytes and the formation of myelin sheaths.

Blocking Vesicular Release of Neurotransmitters Inhibits Myelination

Inhibiting neurotransmitter signalling via the blockade of neurotransmitter release can impact myelination. This is typically done using clostridial neurotoxins, which encompasses tetanus toxin (TeNT) and seven distinct types of Botulinum toxin (BoNT). These toxins inhibit the release of neurotransmitters via proteolytic cleavage of SNARE proteins required for synaptic vesicle exocytosis.

Wake et al., 2011 used *in vitro* DRG-OPC co-cultures to investigate how inhibiting synaptic vesicle release affects the initiation of myelination. They found that pre-treating the DRG neurons with either BoNT-A or TeNT prior to the addition of OPCs led to significant reduction in the number of myelin segments formed on DRG axons. Ca^{2+} imaging analysis showed that Ca^{2+} transients in OPCs are reduced when synaptic vesicle release is inhibited by BoNT-A. The local translation of MBP protein in the processes of OPCs is also

reduced in co-cultures containing BoNT-A-treated neurons, suggesting that synaptic vesicle release promotes this local translation, and therefore, the initiation of myelin sheath formation. This is believed to be glutamate-mediated, as AMPA and NMDA receptor inhibition reduces OPC Ca^{2+} transients, and NMDA receptor or group I mGluR inhibition reduces the local translation of MBP protein. AMPA receptor inhibition does not affect local translation of MBP protein; which raises the intriguing possibility that different types of glutamate receptor regulate different stages of oligodendrocyte development and myelination.

Neurotransmitter release outside of axo-glial synapses may also regulate myelination. In a similar DRG-OPC co-culture system, Wake et al., 2015 found there was no evidence for synaptic communication between the axons and OPCs, yet BoNT-A treatment still inhibits myelin sheath formation. Electrical stimulation of the neurons failed to elicit any current responses in recorded OPCs. Transmission electron microscopy analysis of these cultures revealed that although OPCs form close contacts with axons, these connections lack the hallmarks of synapses. It is possible that neurotransmitter signalling occurs extrasynaptically to promote myelination.

Regardless of whether synaptic vesicle release occurs at neuro-glial synapses or extrasynaptically, it is clear that these neurotoxins can also inhibit myelination *in vivo*. Global manipulations of synaptic vesicle release in larval zebrafish can be done by microinjection of TeNT mRNA into the 1-cell stage egg; this mRNA will be translated to produce TeNT protein throughout the entire animal, and effectively silences synaptic transmission in the CNS for at least the first four days of development (Mensch et al., 2015). Spinal cord neurons in these animals develop normally. Despite this, there is an approximately 40% reduction in the number of myelinated axons in the spinal cord compared to unsilenced animals. Further investigation revealed that this is due to a combination of effects: firstly, a 10% reduction in the number of oligodendrocytes in the spinal cord; and secondly, a 30% reduction in the number of sheaths made per individual oligodendrocyte. Timelapse analysis found that the reduction in oligodendrocyte number may be due to reduced

generation of OPCs from the pMN domain rather than reduced proliferation of the OPC population, as there are fewer OPCs, but OPC proliferation is unchanged in TeNT-expressing animals. The reduction in the number of sheaths made per oligodendrocyte could be due to reduced initial formation of myelin sheaths, or increased retraction of sheaths from axons. Timelapse analysis confirmed that the number of sheath retractions is also unchanged, indicating that global inhibition of neurotransmitter release reduces the initial formation of myelin sheaths. Crucially, TeNT exerts this effect in an oligodendrocyte-independent manner. Oligodendrocytes transplanted from control animals into TeNT-expressing animals also form fewer sheaths than in full control conditions, whereas TeNT-expressing oligodendrocytes transplanted into control animals generate a normal number of sheaths (Mensch et al., 2015).

Similar results were reported by Hines et al., 2015, who generated transgenic zebrafish larvae expressing TeNT in all neurons and found that axons expressing TeNT are significantly less myelinated compared to control axons. This TeNT expression also leads to oligodendrocytes making fewer myelin sheaths. Unlike the findings from Mensch et al., 2015, this is due to an increase in the retraction of nascent myelin sheaths. This discrepancy in findings can be explained by the different definitions of a 'myelin sheath' used in each study. When analysing sheath retractions, Mensch et al. defined myelin sheaths as oligodendrocyte contacts on an axon which were greater than 5 μm in length, whereas Hines et al. included contacts shorter than 5 μm in their retraction analysis. One explanation might be that synaptic vesicle enhances the stabilisation of short oligodendrocyte contacts (< 5 μm), but once these contacts exceed 5 μm in length, synaptic vesicle does not affect sheath retraction.

Both Hines et al., 2015 and Mensch et al., 2015 globally inhibited synaptic vesicle release. It remains unknown if the vesicular release from a single axon locally regulates the stabilisation of its myelin sheaths. Additionally, it is not clear whether synaptic vesicle release affects the growth of myelin sheaths after initial formation. Global increases in activity promote sheath growth

(Krasnow et al., 2018), but whether this is mediated via neurotransmitter signalling is not known. Although myelinating oligodendrocytes do express neurotransmitter receptors, their responsiveness to neurotransmitter signalling is significantly lower than in OPCs (De Biase et al., 2010; Kukley et al., 2010). Manipulation of synaptic vesicle release along individual axons, coupled with longitudinal analysis of their myelin sheaths, could determine whether local neurotransmitter signalling regulates sheath fate, and whether neurotransmitter signalling continues to regulate sheath growth.

Does synaptic vesicle release regulate the myelination of all axons? To investigate this, Koudelka et al., 2016 expressed TeNT in two different neuronal subtypes and assessed how this affected their myelination during the first week of development. They found that expressing TeNT in individual reticulospinal axons significantly inhibits their myelination (fewer and shorter myelin sheaths), whereas the myelination of individual commissural primary ascending (CoPA) axons expressing TeNT is completely unaffected. Why might some neurons regulate their myelination in a synaptic vesicle-dependent manner, while others do not? Both reticulospinal and CoPA neurons have axons of approximately similar calibre, are myelinated within the same time period (Koudelka et al., 2016), and are both glutamatergic (Higashijima et al., 2004). One possibility is that only certain circuits require their myelination to be regulated by neuronal activity. Additional signals may be required to facilitate activity-dependent myelination, and thus selective expression of these additional signals in certain circuits could restrict activity-mediated regulation of myelination to where it is necessary. Comparison of the transcriptomes between reticulospinal and CoPA neurons might reveal the presence of molecular signal(s) which facilitate activity-dependent myelination in reticulospinal axons.

Function of Neurotransmitter Signalling?

How exactly does neurotransmitter signalling affect the development of oligodendroglial cells and myelination? Given the significant evidence that oligodendroglial cells can detect and respond to glutamate, numerous studies

have disrupted either AMPA or NMDA receptors specifically in OPCs or oligodendrocytes to understand receptor function in more detail. Kougioumtzidou et al., 2017 confirmed that OPCs express the AMPA receptor sub-units GluA2-4 before deleting each sub-unit from OPCs using Cre-Lox technology. They found that deleting just GluA2 or 3 alone had no significant impact on OPC survival, proliferation, or differentiation into myelinating oligodendrocytes. However, deleting both sub-units led to reduced AMPA-mediated currents induced by kainate application, a reduced frequency of spontaneous EPSCs in OPCs, and a reduced number of oligodendrocytes in the corpus callosum during early myelination (which recovers to normal levels by P21). Deleting GluA2, 3 and 4 from oligodendroglial cells induced a slightly more severe phenotype; this significantly reduced kainate-evoked AMPA currents in OPCs and slightly reduced the number of oligodendrocytes in the corpus callosum in adulthood. The reduction in oligodendrocyte number was due to oligodendrocyte apoptosis, suggesting that AMPA signalling promotes the survival of newly-generated oligodendrocytes. The number and length of myelin sheaths generated by surviving oligodendrocytes was unchanged in the triple knock-out animals (Kougioumtzidou et al., 2017).

More recent work has shown that modification of AMPA current properties in OPCs can affect OPC proliferation and differentiation. Chen et al., 2018 virally over-expressed various mutated forms of AMPA receptor GluA2 sub-unit in OPCs to manipulate AMPA current properties, and observed the subsequent effects on oligodendroglial cell development. They found that increasing Ca^{2+} permeability (GluA2 Ca^{2+} permeable mutant) or reducing pore function of AMPA receptors (GluA2 pore-dead mutant) increases OPC proliferation. Additionally, over-expressing either of these mutated GluA2 sub-units or over-expressing the GluA2 cytoplasmic tail (which should downregulate the trafficking of AMPA receptors to the plasma membrane) reduce the differentiation of transfected OPCs into oligodendrocytes (Chen et al., 2018). This indicates that impairing AMPA signalling in OPCs leads to reduced oligodendrocyte production and increased self-renewal. Why does overexpression of functionally-disrupting AMPA subunits affect OPC

proliferation and differentiation, but deletion of AMPA receptor subunits from OPCs does not? It may be that other signals controlling OPC population dynamics compensate when AMPA receptor signalling is completely lost. Such compensatory changes have been observed in experimentally-generated mutants, but do not occur when genes are simply knocked down (Rossi et al., 2015). Checking for transcriptional changes in AMPA receptor-deficient OPCs could determine if loss of AMPA receptor signalling triggers compensatory upregulation of other signalling pathways to keep the OPC population stable.

OPCs also express NMDA receptors; however, loss of NMDA receptors in OPCs also does not significantly alter oligodendroglial cell development. Conditional deletion of the NR1 sub-unit of NMDA receptors from OPCs has no effect on OPC proliferation or survival, differentiation, oligodendrocyte survival, or myelination as assessed by electron microscopy (De Biase et al., 2011). Saab et al., 2016 did note that conditional deletion of NR1 subunit leads to a slight delay in the myelination of the optic nerve, which recovers by P70. Again, it is possible that deletion of NMDA signalling in oligodendrocytes is compensated by upregulation of other receptors or signalling pathways. NMDA signalling does appear to play a role in the metabolic support provided by oligodendrocytes to axons. Saab et al., 2016 found that conditional deletion of NR1 sub-unit from oligodendrocytes reduces expression of the glucose transporter GLUT1 in myelin sheaths and reduces recovery of axons after being challenged with high-frequency stimulation. These conditional knock-out animals also displayed signs of neurodegeneration later in adulthood (Saab et al., 2016). NMDA signalling may be required for oligodendrocytes to detect the activity levels (and therefore, the energetic demands) of the underlying axon and to subsequently supply metabolites to maintain neuronal health. Although NMDA receptor signalling is not required for initial myelination, it may be important for any *de novo* myelination or myelin remodelling which occurs in response to experience or circuit activity. Such myelin changes may not regulate conduction times in circuits, but instead may reflect the changing metabolic demands of circuits with learning.

Other neurotransmitters may also regulate the oligodendrocyte population. Hamilton et al., 2016 found that inhibiting GABA signalling in rodent brain slices (by applying the GABA receptor antagonist GABAzine) significantly increases the number of oligodendrocytes, the number of myelinated axons, and leads to shorter myelin sheaths. This suggests that endogenous GABA signalling can influence oligodendrogenesis and myelination. It is important to consider that Hamilton et al.'s results could be due to a global increase in neuronal activity; suppressing GABA signalling will reduce overall inhibition and subsequently increase neuronal activity, promoting the release of other activity-related signals which then influence myelination. Cell type-specific manipulation of GABA signalling in oligodendroglial cells is required to determine whether GABA directly or indirectly regulates oligodendrogenesis and myelination.

1.6.3. *BDNF Signalling to Oligodendroglial Lineage Cells*

It is important to consider that molecular signals other than neurotransmitters may also be released from active axons and influence oligodendroglial development. For example, neuronal activity can stimulate the production of brain-derived neurotrophic factor (BDNF). Reducing neuronal activity in the visual cortex of adult rats either by rearing in darkness or by intraocular injection of TTX reduces levels of both BDNF mRNA and TrkB (the BDNF receptor) mRNA in the cortex, without affecting transcription of other growth factors such as NGF (Castrén et al., 1992). The SNARE proteins VAMP2 and SNAP-25 which are required for neurotransmitter release are also required for release of BDNF (Shimojo et al., 2015). Subsequently, experiments demonstrating that neurotoxins (such as BoNT-B and TeNT) which proteolytically cleave VAMP2 or SNAP-25 reduces myelination actually inhibit both neurotransmitter and BDNF signalling. Hence, BDNF is another candidate molecule which could affect myelination in an activity-dependent manner.

Furthermore, there is evidence that BDNF can influence oligodendroglial cell development. Oligodendrocytes express the BDNF receptor TrkB (Vondran et

al., 2010), and treating oligodendrocytes with BDNF *in vitro* activates TrkB, MAPK and Akt (Veer et al., 2009). Mice with global haploinsufficiency of BDNF have fewer OPCs and reduced myelin protein expression in the basal forebrain (Vondran et al., 2010). Oligodendrocyte-specific loss of BDNF signalling via deletion of TrkB significantly reduces myelination during early development; however, this phenotype recovers by adulthood (Wong et al., 2013), suggesting that BDNF signalling is not absolutely necessary for proper myelination.

Recent research suggests that the stimulation of OPC proliferation seen in previous optogenetic experiments occurs via release of BDNF. Geraghty et al., 2019 used the same optogenetic method as Gibson et al., 2014 to stimulate pyramidal neurons in the motor cortex, but tested this technique in mice with deficient BDNF signalling. They found that by either preventing activity-mediated BDNF release, or deleting TrkB receptor expression from oligodendroglial cells, the enhancement of OPC proliferation and increased sheath thickness normally seen with optogenetic stimulation is also prevented. Thus, BDNF plays a critical role in activity-mediated regulation of the oligodendroglial population. It is possible that BDNF and neurotransmitter signalling work together to regulate myelination. Lundgaard et al., 2013 found that myelination in DRG-oligodendrocyte co-cultures is unaffected by NMDA receptor inhibition (via MK-801 treatment) in the absence of BDNF, but NMDA receptor inhibition in the presence of BDNF led to significant impairment of myelination. BDNF may therefore be required to initiate an activity-dependent programme of myelination in oligodendrocytes. It is important to note that these experiments relied solely on pharmacological manipulations, and so it is not clear whether the myelination phenotype is due to a direct effect on oligodendrocytes, or an indirect effect through neurons. Genetic manipulations are required to determine the specific cellular mechanisms by which BDNF and NMDA receptor signalling interact to regulate myelination.

1.6.4. *Other Activity-related Signals*

Some evidence suggests that other signals from active axons may also play a role in regulating myelination. The growth of gliomas (brain tumours which are thought to derive from OPCs and neural precursor cells) is enhanced by optogenetic stimulation of neuronal activity (Venkatesh et al., 2015), similar to the proliferative effects of optogenetic stimulation on OPCs (Gibson et al., 2014). Glioma growth is stimulated by neuroligin-3, which is secreted by active neurons. The effects of secreted neuroligin-3 on proliferation of non-cancerous OPCs remains to be investigated.

Activity-mediated myelination may actually be regulated by complex interactions between multiple molecular signals. As previously discussed, there is conflicting evidence for axonal expression of Nrg1 regulating myelination in the CNS (see section '1.3.2 Axon Selection'). Socially isolated animals have reduced Nrg1 expression, hypomyelination and behavioural deficits; oligodendrocyte-specific deletion of the Nrg1 receptor ErbB3 replicates both the myelin and behavioural phenotypes seen in isolated animals (Makinodan et al., 2012). Nrg1 may not be required for basal myelination, but may be important for regulating myelination in response to experience or neuronal activity. In support of this, Lundgaard et al., 2013 found that, like BDNF, adding Nrg1 to OPC-DRG neuron co-cultures appears to induce a switch to activity-mediated myelination. It is not clear whether certain neurons or circuits use BDNF versus Nrg1 to control their myelination in response to activity, or whether both signals are required for activity to shape myelination. More in-depth characterisation and manipulation of expression of these activity-related factors in different neuronal subtypes could clarify whether distinct circuits use different signals for activity-mediated myelination.

1.6.5. *How Does Neuronal Activity Affect Myelin Pattern Formation and Remodelling along Single Axons In Vivo?*

Research has shown that experience and learning can shape circuit myelination in the CNS, which may influence the function of these circuits. Changes to myelin are thought to occur in a neuronal activity-dependent

manner. Manipulating the activity of large populations of neurons, or global changes to activity-related molecular signals, can affect OPC proliferation, differentiation, and myelin sheath formation and growth. New evidence proposes that active axons are actually preferentially myelinated over neighbouring inactive axons (Mitew et al., 2018), suggesting that neuronal activity may control myelination in a local axon-specific manner. However, it is not known how the activity of an individual axon relates to its myelination. The activity of a single axon may locally regulate the formation and growth of its myelin sheaths to ultimately control formation of its own myelin pattern. In order to understand how neuronal activity and activity-related signals affect overall circuit myelination and function, there is a need to investigate the role of these signals at the level of individual axons. By manipulating and following a single axon, one can characterise how local neuronal activity affects myelin sheath growth and myelin pattern formation within a single circuit over time. Performing such longitudinal experiments in rodent models is technically challenging, whereas the larval zebrafish is an ideal model system for undertaking such investigations in a non-invasive manner. In Chapter 4, I will investigate how manipulating the activity of individual reticulospinal neurons in the zebrafish spinal cord affects the growth dynamics of individual myelin sheaths, and the formation of myelin patterns.

1.7. Zebrafish as a Model to Investigate Myelinated Axon Biology

1.7.1. *Advantages of the Zebrafish Model*

The zebrafish initially gained popularity as a vertebrate model organism for its use in large-scale genetic screens to identify novel genes involved in developmental processes. Two seminal forward genetic screens collectively generated ~1800 different mutant lines in hundreds of different genes with many phenotypes affecting early development, CNS, heart, skin, fin, liver, and pigment pattering developmental processes (Driever et al., 1996; Haffter et al., 1996). Larval zebrafish are an ideal vertebrate model organism for such large-scale studies due to their rapid development (progressing from fertilisation to a motile larvae in a matter of days), and the ability to generate large numbers

of animals in a short space of time (an adult female can lay over 200 eggs in a single mating session). The zebrafish continues to be a useful model for genetic studies of vertebrate biology, particularly given that they have a highly conserved vertebrate genome in both sequence and function, with homologues for many human genes (Barbazuk et al., 2000; Postlethwait et al., 2000). In fact, one such forward genetic screen identified 13 mutations in 10 genes involved in the development of myelinated axons (Pogoda et al., 2006).

Zebrafish are widely used beyond genetic screens, particularly for live imaging of cellular and subcellular biological processes. Larval zebrafish are ideal for such studies because they are optically transparent for the first few weeks of life. This transparency allows for live imaging of fluorescently-labelled cells or tissues of interest at cellular and subcellular resolution; several studies have employed zebrafish on this basis to define the dynamics of myelination (Almeida et al., 2018, 2011; Baraban et al., 2018; Czopka et al., 2013; Koudelka et al., 2016; Mensch et al., 2015). Mutant lines which disrupt pigment cell development can further increase the transparency of larvae, such as the *nacre* line, which lacks melanophores – this line carries a mutation in a transcription factor necessary for melanophore development (Lister et al., 1999). Zebrafish are also highly amenable to transgenic manipulation. Transposon systems such as the Tol2kit (Kwan et al., 2007) facilitate simple and efficient generation of transgenic lines to express transcriptional activators (such as Gal4 or KalTA4), fluorescent proteins, or any other protein in cells or tissues of interest. There is currently a number of established transgenic lines expressing fluorescent reporters or transcriptional activators in various types of neurons and at numerous stages of oligodendroglial development. The lines used in this thesis are summarised in **Table 1** in Chapter 2.

1.7.2. *Myelination in Zebrafish*

By 24 hours post-fertilisation (hpf), the zebrafish embryo has identifiable organs and tissues (for example, head, eyes, brain, tail, muscles) and exhibits rudimentary motor function (Kimmel, 1989). By 3 days post-fertilisation (dpf), the spinal cord contains axons of many different neuronal subtypes, including

the reticulospinal neurons of the hindbrain (Mendelson, 1986a, 1986b), and many well-characterised spinal neurons (Bernhardt et al., 1990). The axons of many of these identified neuron subtypes are myelinated at larval stages of development (**Figure 6**). OPCs are produced by progenitors of the pMN domain of the ventral spinal cord starting at 36 hpf, and migrate to colonise the CNS (Kirby et al., 2006; Park et al., 2004). These OPCs begin to differentiate into oligodendrocytes from 2-3 dpf, with a rapid increase in both oligodendrocyte number and extensive myelination of the CNS within the first two weeks (Brösamle and Halpern, 2002; Buckley et al., 2010; Czopka et al., 2013). Both OPCs and oligodendrocytes express homologues of many proteins involved in oligodendroglial development and myelination in the mammalian CNS, such as Sox10, Olig2, Nkx2.2a, DM20, and MBP (Brösamle and Halpern, 2002; Kucenas et al., 2008; Park et al., 2002; Schweitzer et al., 2006).

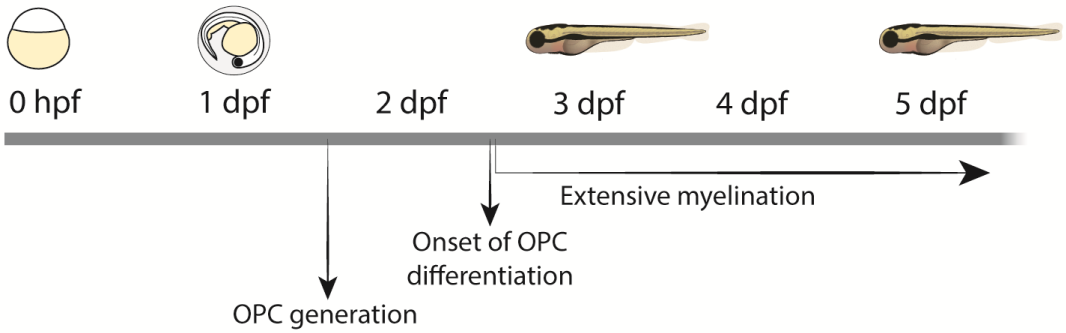

Figure 6 – onset of myelination in the larval zebrafish.

A summary of the first 5 days of development in the larval zebrafish, with key developmental stages during myelination highlighted. By 5 days post-fertilisation (dpf) many axons in the spinal cord are well myelinated.

It is important to consider molecular differences which have arisen through evolution. One particular molecular difference between zebrafish and mammalian myelination is the expression of the adhesion immunoglobulin P0. In zebrafish and other teleosts, P0 is primarily expressed by oligodendrocytes and is a major CNS myelin component (Brösamle and Halpern, 2002;

Waehneldt et al., 1986). In mammals, P0 is expressed exclusively by Schwann cells in the PNS; instead mammals express PLP and its isoform DM20 in CNS myelin (Waehneldt et al., 1986). Zebrafish have numerous homologues of DM20 due to a genome duplication in the teleost lineage, and the closest homologue DMα2 is expressed by oligodendrocytes (Schweitzer et al., 2006). However, teleost DM20 homologues lack PLP-specific sequences found in mammals (Yoshida and Colman, 1996). It has been suggested that the evolution of PLP has replaced P0 in mammalian CNS myelin (Yoshida and Colman, 1996).

Despite this biochemical difference between mammalian and zebrafish myelin, there are numerous examples of biological processes and signals regulating myelination which have been conserved between the two evolutionary branches. OPCs in both species exhibit similar highly explorative behaviours (Hughes et al., 2013; Kirby et al., 2006). Both zebrafish and rodent oligodendrocytes have a limited time period to initiate the formation of new myelin sheaths (Czopka et al., 2013; Watkins et al., 2008). Neuronal activity and synaptic vesicle release has been shown to affect myelination in both zebrafish and mammals (see section '1.6 Neuronal Activity can Influence Myelination'). Additionally, several genes identified in a zebrafish genetic screen to discover novel regulators of myelination also regulate mammalian myelination (Lyons et al., 2005; Monk et al., 2011; Monk and Talbot, 2009; Pogoda et al., 2006). Therefore any novel biological mechanisms uncovered from studies of zebrafish myelination are likely to be conserved in other vertebrates, and will be of both interest and relevance to mammalian myelin biology.

Collectively, this makes the larval zebrafish an ideal model system to study the cellular and subcellular processes of myelination. In this thesis, I will use larval zebrafish to perform longitudinal analysis of individual myelinated axon development. The specific aims of my thesis are:

1. To characterise the establishment of myelin patterns and myelin sheath remodelling along individual axons (Chapter 3).

2. To assess whether different subtypes of axon exhibit different myelin patterns, or different extents or types of myelin remodelling (Chapter 3).
3. To manipulate neuronal activity of individual axons and observe how this affects myelin pattern establishment and specific dynamics of myelin sheath growth along axons (Chapter 4).

Chapter 2: Methods

2.1. Zebrafish Husbandry and Transgenic Lines Used

All of the adult zebrafish used in this project were maintained in a 14-10 hour light-dark cycle, and housed according to UK Home Office regulations in the CBS zebrafish facility, Queen's Medical Research Institute, University of Edinburgh. Zebrafish larvae were maintained in E3 embryo medium in a 28.5 ^{0} C incubator with a 14-10 hour light-dark cycle. Zebrafish were maintained under the project licence 70/8436. To obtain animals for experiments, one adult male and one or two adult female fish of appropriate transgenic lines were placed in a pair-mating tank with a divider the afternoon before mating. The divider was removed in the morning just prior to peak mating time, and the fertilised eggs were collected from the pair mating tank after one to three hours of mating. **Table 1** lists the transgenic zebrafish lines which were used in this thesis (where 'Tg' = 'transgenic').

Table 1 - transgenic lines used in this thesis.

Line	Origin	Use
Tg(RS:KalTA4)	Dr. Isaac Bianco, UCL (unpublished)	Express transgenes under Upstream Activator Sequences (UAS:transgenes) mainly in reticulospinal neurons (and occasionally additional neurons).
Tg(HuC:Gal4)	Mensch et al. 2015	Express UAS:transgenes in post-mitotic neurons.
Tg(UAS:TRPV1-tagRFPt)	Generated for this thesis	Express the fusion protein of cation channel TRPV1 with tagRFPt in Gal4/KalTA4+ cells. Used to activate single neurons via the application of TRPV1 agonist capsaicin.
Tg(UAS:GFP-Contactin1a)	Generated for this thesis	Express the fusion protein of Contactin1a with eGFP, which labels unmyelinated axon space, in Gal4/KalTA4+ cells. Used to follow the myelination status of single axons.

Tg(mbp:eGFP)	Almeida et al. 2011	Express eGFP in myelinating cells. Used to quantify the number of myelinating oligodendrocytes in the dorsal spinal cord.
Tg(mbp:nls-eGFP)	Karttunen et al., 2017	Express nucleus-localised eGFP in myelinating cells. Used to quantify the number of myelinating oligodendrocytes in the ventral spinal cord.
Tg(mbp:eGFP-CAAX)	Almeida et al. 2011	Express a membrane-tethered eGFP in myelinating cells. Used to visualise myelinating cells and their myelin sheaths.
Tg(mbp:TRPV1-tagRFPt)	Generated for this thesis	Express TRPV1-tagRFPt in myelinating cells. Used to ablate myelinating cells via the application of TRPV1 agonist capsaicin.

The recipe for E3 embryo medium is as follows:

50x HEPES buffer stock (500 ml)

95.58 g HEPES

500 ml ddH_2O

50x E3 stock solution (1L)

14.61 g NaCl (250 mM)

0.63 g KCl (8.5 mM)

1.83 g $CaCl_2$ (16.5 mM)

4.07 g $MgSO_4$ (16.5 mM)

Make up to 1 L with ddH_2O

10 mM HEPES buffered E3 Embryo medium (2L)

1920 ml ddH_2O

40 ml 50x HEPES

40 ml 50x E2 medium

Adjust to pH 7.2 with 5 M NaOH

2.2. Plasmids Used and Generated

The plasmid DNA constructs used in this thesis are summarised in **Table 2**.

To generate UAS:tagRFPt-Contactin1a plasmid, the entry vectors p5E-10xUAS, pME-tagRFPt-Contactin1a, p3E-polyA, and pdestTol2pA2 were recombined by an LR reaction (LR clonase II, Thermo Fisher Scientific) using the multisite Gateway system (Kwan et al. 2007).

To generate UAS:TRPV1-tagRFPt plasmid, I first generated a pME-TRPV1-tagRFPt entry vector plasmid. To do this, TRPV1-tagRFPt sequence was amplified by PCR from the (islet1:GAL4VP16,4xUAS:TRPV1-RFPT) plasmid used by Chen et al. 2016, using the following primers:

attB1_TRPV1_fwd:

5'GGGGACAAGTTTGTACAAAAAAGCAGGCTGCCACCATGGAACAACGGGC 3');

attB2_TRPV1_rev:

5'GGGGACCACTTTGTACAAGAAAGCTGGGTTTAATTGTACAGCTCGTCCATGC 3').

This PCR fragment was then inserted into the backbone pDONR221 by a BP reaction (BP Clonase II, Thermo Fisher Scientific). The entry vectors p5E-10xUAS, pME-TRPV1-tagRFPt, p3E-polyA, and pdestTol2pA2 were recombined by an LR reaction to make the final plasmid.

To generate mRNA from pCS2+ Tol2 Transposase: the plasmid was linearised by NotI restriction enzyme digestion (New England Biolabs); the linearised plasmid was purified using the Qiaquick gel extraction kit (Qiagen); mRNA was

transcribed from the linearised plasmid using the mMessage mMachine SP6 transcription kit (Thermo Fisher Scientific); and transcribed mRNA was purified using the RNEasy mini kit (Qiagen).

Table 2 – plasmid constructs used in this thesis.

Plasmid	Origin	Use
UAS:GFP	Dr. Sigrid Koudelka, unpublished	To label individual neurons in Gal4-expressing larvae.
UAS:GFP-Contactin1a	Koudelka et al. 2016	To follow the myelination status of single axons.
mbp:eGFP-CAAX	Almeida et al. 2011	To label individual myelinating oligodendrocytes and their myelin sheaths.
pCS2+ Tol2 Transposase	Kwan et al. 2007	To transcribe tol2 transposase mRNA *in vitro*.
UAS:axon-GCaMP7	Dr. Rafael Almeida, unpublished	To image Ca^{2+} activity in reticulospinal axons.
UAS:tagRFPt-Contactin1a	Generated for this thesis	To follow the myelination status of single axons.
UAS:TRPV1-tagRFPt	Generated for this thesis	To activate or ablate single neurons via the application of TRPV1 agonist capsaicin.

2.3. Generating Transgenic Lines

Stable transgenic lines were generated by injecting 1-2 nl of 10-15 ng/µl plasmid DNA with 25 ng/µl tol2 transposase mRNA into wild-type eggs (see section '2.5 DNA Microinjection'). Where possible, the injected larvae were screened for mosaic transgene expression (expression in a few random cells), and transgene-positive larvae were raised to adulthood (F0 generation). Only some F0s will contain transgenic insertions within the germline; therefore, F0s were outcrossed and their progeny (F1 generation) screened for full expression of the transgene. Transgene-positive F1 larvae were raised to

adulthood, outcrossed, and their transgenic-positive progeny (F2 generation) raised to adulthood. Experiments were carried out using F2 and subsequent generations.

2.4. Mounting Larvae on Glass Slides for Live Imaging

For all live imaging experiments, except for calcium imaging (see section '2.8 Calcium Imaging and Analysis') and counting dorsal oligodendrocyte numbers, larvae were anaesthetised in 168 µg/mL MS222 tricaine (Sigma-Aldrich) in E3 embryo medium. Each larvae was then gently positioned laterally on glass coverslips in 1.4% low melting-point agarose in E3 embryo medium using fine forceps (Williamson et al., 2019). A well of MS222 tricaine in E3 embryo medium was made on a glass slide using silicon grease, and the coverslip mounted onto the well with immobilised larva(e) facing down into the medium.

2.5. DNA Microinjection

Fertilised 1-4 cell-stage eggs were injected with 0.5-2 nl of DNA injection solution (plasmid DNA at 5-10 ng/µl, with 25 ng/µl tol2 transposase mRNA to facilitate transgenesis) (Williamson et al., 2019). Microinjections were performed using a glass microinjection needle fitted to a Pneumatic Picopump PV830 (World Precision Instruments Ltd, Hertfordshire, UK) and a Micromanipulator M3301R (World Precision Instruments Ltd, Hertfordshire, UK). For mosaic labelling of single cells, injected larvae were screened at 2-4 dpf for expression in cells of interest (for example, single reticulospinal or CoPA neurons). This was done by first anaesthetising in 168 µg/mL MS222 tricaine in E3 embryo medium, and then mounting larvae laterally on glass coverslips in 1.4% low melting-point agarose in E3 embryo medium as described in section 2.4 'Mounting Larvae on Glass Slides for Live Imaging', finally, screening for fluorescence using an epifluorescence microscope.

2.6. Image Acquisition

Mounted larvae were imaged using a 20x dry lens on a Zeiss LSM880 Airyscan confocal microscope in super-resolution mode. Z-stack images were acquired at optimal z-depth, spanning the entire portion of spinal cord being analysed.

For time-course experiments, larvae were carefully removed from agarose after image acquisition using microknives, and placed in fresh E3 embryo medium to recover from anaesthetic (this was confirmed by return of locomotor activity).

For live imaging axons in Chapter 3, three overlapping images were acquired at each time point covering a stretch of axon approximately 400-600 µm in length. For reticulospinal axons (which project caudally from the hindbrain down the spinal cord), the first image began at somite 1, and the subsequent images were acquired in a caudal direction along the axon (reaching approximately somite 4-5). For CoPA axons (which project rostrally from the spinal cord to the brain), the first image began at the cell body of the CoPA neuron, and the subsequent images were acquired in a rostral direction along the axon. For live imaging axons and ventral oligodendrocyte number in Chapter 4, a single image was acquired at each time point covering a stretch of axon approximately 150-250 µm in length at somite 7.

For quantification of dorsal oligodendrocyte number, larvae were anaesthetised in MS222 tricaine and arrayed into a 96-well plate at a density of 1-3 larvae in 300 µl E3 embryo medium per well. This 96-well plate was placed in the Vertebrate Automated Screening Technology BioImager system (Union Biometrica), which automated the positioning of larvae and image acquisition using a Zeiss spinning disk confocal microscope (VAST-SDCM - Early et al. 2018).

2.7. Capsaicin Treatment

Capsaicin (Sigma-Aldrich) was prepared as a 5 mM primary stock in 100% DMSO and stored at -80 ^{0} C. Capsaicin treatments of 1-10 µM in 1% DMSO in E3 embryo medium were bath-applied to zebrafish larvae for either one or four hours per day depending on the experiment (specific durations stated in Chapter 4). For acute treatment experiments, capsaicin was applied once at 3 dpf. For time-course experiments, capsaicin was applied daily from 3-7 dpf, and the media was replaced with fresh E3 embryo medium three times after each treatment.

2.8. Calcium Imaging and Analysis

Larvae were paralysed in 1.5 mg/ml mivacurium chloride (Abcam) in E3 embryo medium and positioned laterally on glass coverslips in 1.5% low melting-point agarose. A window of agarose, stretching from approximately somite 15-27, was then carefully removed using microknives. Immobilised larvae were mounted onto glass slides as described in section '2.4 Mounting Larvae on Glass Slides for Live Imaging', with 1.5 mg/ml mivacurium chloride in E3 embryo medium in the silicon grease well.

Mounted larvae were imaged using a 20x dry lens on a Zeiss LSM880 Airyscan confocal microscope. For each larva, a high-resolution image of TRPV1-tagRFPt and axon-GCaMP7 in the expressing reticulospinal axon(s) of interest was acquired within the exposed region of the tail (somite 15-27). Then, a three to five minute timelapse movie (pre-treatment) of axon-GCaMP7 fluorescence only was acquired at approximately one frame per second. Next, the medium was removed from the silicon grease well and replaced with either vehicle (1% DMSO) or capsaicin (1 µM Csn, 1% DMSO) in 1.5 mg/ml mivacurium chloride in E3 embryo medium. A second timelapse movie was acquired (post-treatment) 15 minutes after treatment application.

Both the pre-treatment and post-treatment timelapse movies were then analysed using Fiji ImageJ software. For analysis, a background region of interest (ROI) was defined, and the average grey value of this region for each frame of the movie tabled. A clearly-defined collateral branching from the main reticulospinal axon was defined as an ROI, and the average grey value of this region for each frame of the movie was tabled. Background was subtracted from the collateral grey values to generate a FT value for each frame. The pre-treatment movie was considered a measure of baseline neuronal activity, and so the average FT grey value of the pre-treatment movie was used as a baseline value (F0). The change in fluorescence was calculated for each frame of the post-treatment movie using the following equation:

$$\text{Change in fluorescence} = {}^{(FT - F0)} / {}_{F0}$$

2.9. Preparation of Samples for Transmission Electron Microscopy – Chemical Fixation

The following protocol for chemical fixation and preparation of zebrafish larvae for electron microscopy was established by Czopka & Lyons, 2011.

Primary fixation: Larvae were terminally anaesthetised in MS222 tricaine in E3 embryo medium, and transferred to 1.5 ml Eppendorf tubes (up to five larvae/tube). Primary fixative (2% glutaraldehyde + 4% paraformaldehyde, 0.1 M sodium cacodylate buffer, pH 7.4) was applied to terminally anaesthetised larvae. Samples were microwaved to aid with fixation as follows: one minute at 100 W, one minute off (x2); 20 seconds at 450 W, 20 seconds off (x5). Samples were kept in an ice bath during microwave steps to prevent overheating. Samples were left in primary fixative for at least a further two hours at room temperature, before rinsing in 0.1 M sodium cacodylate buffer (3x 10 minute washes at room temperature).

Secondary fixation: Secondary fixative (2% Osmium tetroxide, 0.1 M sodium cacodylate, 0.1 M imidazole, pH 7.5) was applied to samples, which were then microwaved to aid with fixation as follows: one minute at 100 W, one minute off (x2); 20 seconds at 450 W, 20 seconds off (x5). Samples were kept in an ice bath during microwave steps to prevent overheating. Samples were left in secondary fixative for at least a further one hour at room temperature, before rinsing with distilled water (3x 10 minute washes at room temperature). Ideally, secondary fixative was left overnight, or until larvae were uniformly stained a dark brown colour.

En bloc stain: Saturated uranyl acetate (~8% w/v in water) was applied to samples, which were then microwaved as follows: one minute at 450 W, one minute off, one minute at 450 W.

Dehydration: 50% EM-grade ethanol in distilled water was applied to samples, which were then microwaved as follows: 45 seconds at 250 W, 10 minutes off at room temperature. This was repeated with 70% and 95% ethanol. 100% ethanol was added to samples and microwaved as follows: one minute at 250

W, one minute off, one minute at 250 W, 10 minutes off at room temperature. This 100% ethanol incubation step was repeated with fresh ethanol. 100% acetone was then applied to samples and microwaved as follows: one minute at 250 W, one minute off, one minute at 250 W, 10 minutes off at room temperature. This 100% acetone incubation step was repeated a further three times.

Embedding in EMBED resin: EMBED resin was made using the Embed-812 kit (Electron Microscopy Sciences). A 1:1 solution of EMBED:acetone was applied to samples and left overnight at room temperature. 100% EMBED was applied to samples and left for at least six hours at room temperature in the fume hood. Then, the larvae were transferred in 100% EMBED into wells of silicon embedding moulds, oriented appropriately using fine forceps so that each larva lay in the middle of the mould parallel to the surface. Moulds were baked in an oven at 65 ^{0} C for 48-72 hours, until resin had fully polymerised.

Sectioning: EM blocks were carefully trimmed by hand using razor blades until approximately somite 14 (just anterior of the cloaca, located at the gap between the ventral fins). Semi-thin transverse sections through the larvae were cut using a glass knife on a Reichert Jung Ultracut microtome (Leica) until the cloaca was reached and the block face was uniformly smooth. Then, ultra-thin silver sections (thickness approximately 70-80 nm) were cut using a Diatome diamond knife. Sections were flattened using chloroform, and then carefully transferred from the diamond knife water boat to hexagonal copper electron microscopy grids (200 Mesh Grids, Agar Scientific) using a perfect loop.

Section staining: Each copper grid was stained with 1:1 saturated uranyl acetate:EM-grade ethanol for five minutes, followed by a wash with 50% ethanol for one minute, and blotted dry on Whatman filter paper. Then, each grid was stained with Sato's lead stain for five minutes, followed by a wash with pure water for one minute, and blotted dry on Whatman filter paper.

Sato's lead stain recipe:

0.2 g lead citrate

0.15 g lead nitrate

0.15 g lead acetate

1 g sodium citrate

48.2 ml boiled and cooled pure water (filtered through Millipore filter)

1.8 ml 5M NaOH prepared from boiled and cooled pure water

Lead citrate was heated on a hot plate in a fume hood until it changed colour from white to pale grey. The lead citrate was combined with all other ingredients in a beaker and stirred continuously until dissolved. Stain solution was aliquoted into syringes and stored at 4 ^{0} C until required.

Imaging of stained sections: Stained grids were imaged at the King's Buildings EM facility, University of Edinburgh, on a Jeol JEM-1400 Plus electron microscope at 12,000x magnification.

2.10. Preparation of Samples for Transmission Electron Microscopy – High Pressure Freezing

The following protocol was adapted from a previously published protocol for high-pressure freezing by Möbius et al. 2010.

High-pressure freezing: Larvae were terminally anaesthetised with MS222 tricaine in E3 embryo medium, and then transferred to cryoprotectant solution (20% BSA in E3 embryo medium). Using microknives, each larva was dissected to remove the head and tail tip, leaving a section of the larvae trunk from approximately somite 2-20. The dissected larva trunk was transferred to a HPM100 3 mm specimen carrier (Leica) with enough cryoprotectant to fill the specimen carrier. Another specimen carrier was 'sandwiched' on top, using plastic cassettes to hold the specimen carriers in place. This was, then, immediately frozen using the Leica EM HPM100 high-pressure freezer.

Freeze substitution: Specimen carriers were removed from the high-pressure freezer, but kept in liquid nitrogen to prevent defrosting of samples. Specimen carriers were transferred to a freeze-substitution solution (0.1% tannic acid, 2% osmium tetroxide, 0.1% TAAB EM Stain 336) at liquid nitrogen temperature, and transferred to the Leica EM AFS2 freeze substitution system. Samples were incubated in freeze-substitution solution for 72 hours at -90 ^{0} C, warmed to -20 ^{0} C for one hour, and then warmed to 20 ^{0} C. Once at room temperature, samples were removed from specimen carriers and transferred to 100% acetone solution.

After freeze-substitution, samples were embedded in EMBED resin and sectioned as per the chemical fixation protocol above.

Section staining: Copper grids were stained using 25% TAAB EM stain 336 for 45 minutes, followed by a wash with pure water, and blotted dry on Whatman filter paper.

Stained sections were imaged as per the chemical fixation protocol above.

2.11. Image Analysis

Sheath and axon length measurements: Confocal fluorescence images were analysed using Fiji/ImageJ. The length of sheaths and axons were traced using the 'segmented line' tool, and their length measured using the 'measure' function.

For axons labelled with FP-Cntn1a reporter, a myelin sheath was measured if there was a gap in FP-Cntn1a fluorescence which spanned the entire diameter of the axon. For Chapter 3, all sheaths along axons were measured twice, and the average of these two measurements was taken as the actual value. The duplicate measurements were always within 1 µm of each other, confirming the precision of these measurements.

Oligodendrocyte number measurements: For total dorsal oligodendrocyte number, the images acquired by the VAST-SDCM system were processed using a concatenating and stitching script written by Dr. Jason Early, and

analysed using an automated counting macro for Fiji/ImageJ (with manual adjustments) also written by Dr. Jason Early (Early et al., 2018). For local ventral oligodendrocyte number, images were analysed using the Cell Counter plug-in for Fiji/ImageJ.

Electron microscopy measurements: Electron microscopy images were analysed using Fiji/ImageJ. G-ratios were analysed by first tracing the outline of the axon using the 'polygon' tool, and its area measured using the 'measure' function. Then the outline of the myelin sheath was traced using the 'polygon' tool, and its area measured using the 'measure' function. The radii of the axon and the myelin sheath were calculated from the area measurements by solving the equation for circular area:

$$\text{Area} = \pi.r^2$$

Then, sheath thickness was measured as a g-ratio as follows:

$$\text{g-ratio} = \frac{\text{axon diameter}}{\text{myelin sheath diameter}}$$

2.12. Statistical Analysis

Statistical analysis was performed using Microsoft Excel 2013 and GraphPad Prism software. Graphs were generated using GraphPad Prism software, and the n used represents the number of larvae, unless otherwise stated.

D'Agostino & Pearson omnibus normality tests were performed where possible, to determine whether the data was distributed normally. For experiments where all data were normally distributed, the data averages are described in the text as means, and the error bars in associated graphs denote mean and standard deviation (SD) (as noted in figure legends). For experiments containing not normally distributed data, the data averages are described in the text as medians, and the error bars in associated graphs denote median and interquartile range (IQR) (as noted in figure legends).

Statistical tests were chosen based on experimental design and the normality distribution of the data (parametric tests for normally distributed data, non-

parametric tests for not normally distributed data where possible), and are described in appropriate figure legends. When testing for statistical significance using the null hypothesis, * = $p < 0.05$, ** = $p < 0.01$, and *** = $p < 0.001$.

Chapter 3: Characterising the Remodelling of Myelinated Axons over Time

3.1. Introduction

In Chapter 1, I discussed the evidence that changes to myelin occur in response to experience, and that such changes may, in turn, impact circuit function (see section '1.5 Myelin and the Regulation of Circuit Function'). I also discussed the fact that there is significant heterogeneity in the myelin patterns (the number, length, thickness, and distribution of sheaths) along individual axons throughout the CNS. Given that these myelination parameters can alter the underlying conduction properties of the axon, it is possible that specific myelin patterns are established to optimise circuit function. Moreover, axons belonging to particular circuits may develop particular myelin patterns based on circuit function. However, it is not clear how or when myelin patterns are established along individual axons, or whether these patterns are susceptible to remodelling over time.

Characterisation of myelin pattern establishment along individual axons requires longitudinal analysis of single myelinated axons *in vivo*. Recent live imaging studies in rodents have demonstrated that longitudinal analysis of myelin is possible in the mammalian CNS. Combining cranial imaging windows with repeated two-photon microscopy allowed researchers to follow both *de novo* myelination and myelin remodelling over time (Hill et al., 2018; Hughes et al., 2018). However, these experiments limited analysis to a very specific region of the CNS, as only the upper 400 μm of the somatosensory cortex could be imaged. The authors did not identify specific subtypes of neurons to assess if, indeed, neuronal subtypes exhibit differences in myelination and myelin remodelling. These experiments are also technically very challenging to perform.

The larval zebrafish is a powerful complementary model system for live imaging myelin patterns and myelin remodelling over time *in vivo* (see section '1.7 Zebrafish as a Model to Investigate Myelinated Axon Biology'). Their small size and optical transparency, coupled with the suite of transgenic fluorescent reporters available, allows for individual axons and their myelin to be followed over prolonged periods of time. In a study by Auer et al., 2018, the myelin

patterns along various different axons in the spinal cord were imaged by live confocal microscopy, and showed that myelin sheath length can vary significantly both along and between axons. This variability may be a characteristic of particular neuron subtypes, or sheath length variability may change with time and therefore reflect the developmental stages of the axons analysed. The authors also followed individual fluorescently-labelled myelin sheaths in the larval zebrafish spinal cord by confocal microscopy for up to two weeks to measure their growth dynamics (Auer et al., 2018). It was determined that myelin sheaths grow in a stereotypical fashion, where sheaths undergo variable but rapid growth for the first three days after sheath formation, and then remain stable (thereafter growing only at the approximate rate of overall body elongation). However, it is not clear whether this phenomenon is consistent across axons of different neuronal subtypes, or, for example, if myelin is remodelled in certain circuits more than others.

In order to understand myelin pattern establishment and remodelling in the context of circuit function, myelination must be assessed along axons of identified neuronal subtypes within characterised circuits over time. By 3 dpf (the approximate time of myelination onset in the zebrafish CNS), the larval zebrafish spinal cord contains axons of numerous neuron subtypes classified based on cellular morphology, position, and timing of axogenesis (Bernhardt et al., 1990; Hale et al., 2001; Mendelson, 1986b, 1986a). These subtypes include motor neurons, sensory neurons, reticulospinal neurons, and various interneurons. The axons of several of these known neuron subtypes are myelinated from 3 dpf onwards (such as reticulospinal neurons, commissural primary ascending (CoPA) interneurons, and circumferential descending (CiD) interneurons), whilst other axons are not myelinated (such as commissural bifurcating longitudinal (CoBL) interneurons, circumferential ascending (CiA) interneurons, and Rohon-Beard (RB) sensory neurons (Mensch, 2014)). Therefore, the larval zebrafish spinal cord contains several identified subtypes of myelinated axon which can be analysed to determine how myelin pattern establishment and myelin remodelling occurs along specific axons in different circuits.

Interestingly, different myelinated axon subtypes appear to use different mechanisms to regulate their initial myelination. Koudelka et al., 2016 expressed tetanus neurotoxin (TeNT – to inhibit synaptic vesicle release) in individual reticulospinal and CoPA axons, and then followed the myelination of these axons over several days. They found that while synaptic vesicle release was successfully inhibited in both subtypes, only the myelination of reticulospinal axons was reduced by TeNT expression. Reticulospinal and CoPA neurons exhibit many similarities, including their time of birth and myelination, axon diameter, and neurotransmitter (Higashijima et al., 2004; Koudelka et al., 2016), yet seem to have different mechanisms by which they regulate their myelination. It is possible that this is due to differing requirements of the specific circuits in which these two neuron subtypes are found. For example, the myelination of reticulospinal neuron-containing circuits may be shaped by neuronal activity in order to optimise circuit function; whereas the myelination of CoPA interneuron-containing circuits may be shaped by some other developmental signal. Subsequently, these two axon subtypes may establish different myelin patterns and exhibit different types or extents of myelin remodelling during myelinated axon development. Here, I will discuss what is known about the circuitry of these two neuronal subtypes in the zebrafish CNS.

3.1.1. Reticulospinal Neurons and their Circuitry

Reticulospinal neurons are found in the mid- and hindbrain of the zebrafish, projecting their axons caudally along the spinal cord. In teleosts, these neurons are responsible for relaying locomotor control from the brain to the spinal cord by synapsing onto motor neurons and other spinal interneurons to give rise to locomotor behaviour. There are approximately 150 reticulospinal neurons which are arrange in bilaterally symmetrical pairs (**Figure 7**). The different subtypes of reticulospinal neurons are typically classified based on their time of birth and axogenesis, cell body position in the brain, dendritic and axon morphology, and known circuit function (Gahtan and O'Malley, 2003; Kimmel et al., 1982; Metcalfe et al., 1986). Most reticulospinal neurons are born within the first 24 hours of life (Mendelson, 1986a). This is then followed by two waves

of axogenesis; the first “primary wave” occurring between 20-24 hours post-fertilisation (hpf), and the “secondary wave” occurring between 30-34 hpf (Mendelson, 1986b).

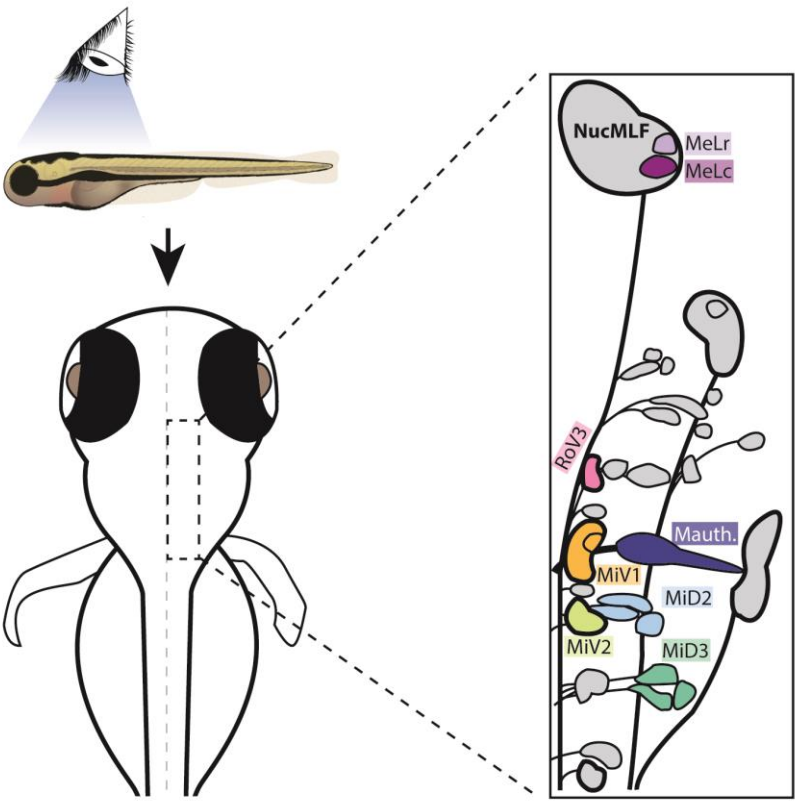

Figure 7 – the different subtypes of reticulospinal neurons found in the zebrafish midbrain and hindbrain.

Reticulospinal neurons can be identified based on the morphology and positioning of their cell bodies. The inset shows a schematic of the different subtypes of reticulospinal cells. The bold shapes represent clusters of cells rather than individual soma. RS subtypes known to regulate certain behaviours are coloured and named. Mauthner, MiD2cm (within the MiD2 cluster) and MiD3cm (within the MiD3 cluster) regulate escape responses. MeLr and MeLc in the nucleus of the medial longitudinal fasciculus (nucMLF) are involved in prey capture behaviour. RoV3, MiV1 and MiV2 are involved in direction changes during optomotor response. Figure drawn using information from Orger et al., 2008.

Among the first born reticulospinal neurons are the Mauthner cells (the largest diameter axons in the zebrafish) and their segmental homologue cells, MiD2cm and MiD3cm (collectively known as the M-series) (Mendelson, 1986a), which mediate rapid escape response behaviours in fish. Escape responses can be evoked by visual, tactile, and auditory sensory stimuli, suggesting that these reticulospinal neurons receive inputs from multiple sensory systems (Eaton et al., 1977). Indeed, the Mauthner cell dendrites are known to receive inputs from auditory, lateral line, vestibular, visual, and somatosensory systems (Faber et al., 1989). Mauthner cells project axons to the contralateral spinal cord and grow small unbranched collaterals, which synapse onto motor neurons and other interneurons along the whole length of the spinal cord (Fetcho and Faber, 1988; Jontes et al., 2000). MiD2cm and MiD3cm also project their axons to the contralateral spinal cord, but have more complexly branching collaterals, which project bilaterally to the ventral spinal cord (MiD2cm) and ipsilaterally to the dorsal spinal cord (MiD3cm) (Gahtan and Malley, 2003). Although the post-synaptic targets of these collaterals are not fully known, it is hypothesised that MiD2/3cm also synapse onto motor neurons and interneurons to mediate the escape response (Gahtan and O'Malley, 2003). Activation of a Mauthner or homologue cell stimulates motor neurons contralateral to the stimulus, as well as inhibiting the contralateral M-series – this causes contralateral muscle contraction and thus the fish turns away from the threatening stimulus (known as the "C-bend"). It is likely that having multiple cells capable of initiating escape responses serves to ensure that escape is still possible should one cell fail. However, the different cells also exhibit variances in their responses to sensory stimuli. Calcium imaging shows that all cells in the M-series can respond to tactile stimulus of the head, whereas only the Mauthner cell is activated by tactile stimulus of the tail (O'Malley et al., 1996). This was confirmed by ablation experiments, where ablation of all cells in the M-series eliminates both head- and tail-elicited escape responses; whereas ablation of just the Mauthner only eliminates tail-elicited escape responses (Liu and Fetcho, 1999). Therefore, the segmental

homologues of the M-series may form overlapping but distinct circuits which converge on the same behavioural output.

The Mauthner axon is the first to be myelinated in the zebrafish spinal cord with myelination beginning at 60 hpf (Almeida et al., 2011), closely followed by the larger diameter reticulospinal axons such as MiD2cm and MiD3cm. Myelination between 2 to 4 dpf significantly increases the conduction velocity along Mauthner axon (Dr. Daumantė Šuminaitė and Dr. Jenea Bin, unpublished). Interestingly, the latency of the escape response does not significantly change between 2-4 dpf, but other kinematics of the escape response (such as maximum velocity, duration of initial contraction, and displacement in the first 105 msec) do change (Eaton et al., 1977). Synaptogenesis and post-synaptic neuron development may underlie these changes. However, myelination may also influence emergence of circuit function in more complex ways than simply reducing response latency.

The circuitry of other subtypes of reticulospinal neurons are less characterised. Gahtan et al., 2002 found that tactile stimulus of the head induces activity in the majority of identified reticulospinal neurons (not just the M-series), suggesting that other reticulospinal subtypes also receive sensory input and contribute to escape response behaviour. However, it has been noted that this result may be an artefact of the experimental set-up, where the larval zebrafish were completely immobilised in agar. Global activity of all reticulospinal neurons may, therefore, be due to physical struggling during attempts to perform normal swimming behaviour (Fetcho et al., 2008). This would indicate that many reticulospinal neuron subtypes are involved in normal swimming.

A number of other reticulospinal subtypes have been shown to play a role in particular locomotor behaviours. The MeLr and MeLc neurons are required for prey capture behaviour; these cells reside within the nucleus of the medial longitudinal fasciculus (nucMLF), with dendrites projecting into the ventral tectum (a structure which is also required for prey capture) (Gahtan et al., 2005). Bilateral ablation of MeLr and MeLc ameliorates prey capture behaviour but does not affect other motor behaviours, while ablation of other random

reticulospinal neurons does not affect prey capture (Gahtan et al., 2005). Meanwhile, calcium imaging of the entire reticulospinal population has identified cells involved in visually-guided swimming. Orger et al., 2008 exposed fish to directional gratings which can induce forward swimming or change in swimming direction to match that of the gratings (known as the optomotor response). Various nucMLF cells are activated during forward swimming, whereas the ipsilateral RoV3, MiV1 and MiV2 cells are active during changes in direction, and laser ablation of the RoV3/MiV1/MiV2 group prevents corresponding changes in direction (Orger et al., 2008).

Reticulospinal neurons are believed to be myelinated in an activity-dependent manner. Inhibiting synaptic vesicle release via expression of TeNT in individual reticulospinal neurons inhibits their myelination by reducing both the number and length of myelin sheaths formed along the axon (Koudelka et al., 2016). Given that reticulospinal neurons are specifically involved in locomotor circuits, and that the myelin patterns of circuits are hypothesised to be shaped by experience (and therefore influenced by signals relating to neuronal activity), it is possible that reticulospinal neurons establish a specific myelin pattern along their axons to optimise circuit function. Additionally, if myelin remodelling in response to neuronal activity is important for the establishment of myelin patterns, then sheaths along reticulospinal axons should exhibit remodelling.

3.1.2. CoPA Interneurons and their Circuitry

CoPA interneurons are born in the zebrafish spinal cord at approximately 17-18 hpf (Bernhardt et al., 1990). Their cell bodies are located in the dorsal spinal cord and they typically extend two dendrites – one rostrally and one caudally along the dorsal tract of the spinal cord (Bernhardt et al., 1990; Hale et al., 2001). Approximately one CoPA interneuron is found in each hemi-segment of the spinal cord, and each cell projects an axon to the ventral tract where it crosses to the contralateral side, and then projects back up to the dorsal tract (**Figure 8)**.

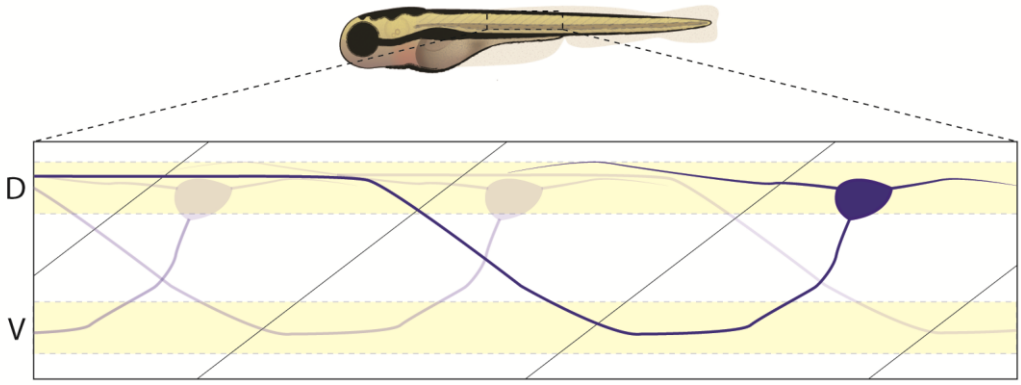

Figure 8 – CoPA interneurons in the zebrafish spinal cord.

CoPA interneurons are found along the entire spinal cord. Their cell bodies are located in the dorsal (D) tract, and project an axon to the ventral (V) tract which then ascends back up to the dorsal tract, proceeding rostrally towards the brain.

CoPA interneurons receive excitatory input from RB sensory neurons (Pietri et al., 2009), which have extensive neurite arborisations that span the surface of the animal to detect sensory stimuli. Synapses between RB and CoPA cells have been observed as early as 25 hpf (coinciding with the emergence of touch-elicited behaviour). This suggest that CoPA interneurons are an important part of sensory relay circuitry mediating locomotor responses to sensory stimuli (Easley-Neal et al., 2013). However, RB sensory neurons are believed to be a transient population which undergo programmed cell death during the first few days of life (Svoboda et al., 2001; Williams et al., 2000). Therefore, CoPA interneurons may receive excitatory inputs from other cells as well. Branching collaterals emerge along the length of the CoPA axon (Mensch, 2014), but the post-synaptic targets of these collaterals are not yet fully known. One study suggests that CoPA interneurons send signals to the rostral spinal cord and synapse onto descending interneurons to mediate touch-elicited locomotor behaviour (Pietri et al., 2009).

Depolarising glycinergic inputs to CoPA interneurons have been reported (at larval stages glycine depolarises due to the high intracellular levels of Cl^- (Knogler and Drapeau, 2014; Pietri et al., 2009). Knogler and Drapeau, 2014

found that contralateral sensory stimulation elicited a rapid glutamatergic input in CoPA cells (inducing suprathreshold depolarisation and action potential firing), closely followed by a prolonged glycinergic input. It is hypothesised that this prolonged glycinergic signalling prevents CoPA cells from firing multiple action potentials in response to glutamatergic inputs. However, the source of this glycinergic input is not yet known. CoPA interneurons also receive inhibitory input. GABAergic cerebrospinal fluid contacting-neurons (CSF-cNs) synapse onto CoPA interneurons and motor neurons; this inhibition is required to maintain a balanced posture during swimming (Hubbard et al., 2016).

Thus, it seems that CoPA interneurons play a crucial role in the transfer and processing of sensory information. CoPA neurons are believed to be in different circuits from reticulospinal neurons; if myelin patterns are tuned to the function of individual circuits, then CoPA axons should exhibit different myelin patterns to reticulospinal axons. Additionally, CoPA axon myelination seems to be independent of neuronal activity, as TeNT-expressing CoPA axons have a normal sheath number and sheath length (Koudelka et al., 2016). If CoPA neurons do not use activity to shape their myelination, then they may exhibit less myelin remodelling than the sheaths along reticulospinal axons.

3.1.3. Aims for this Chapter

Reticulospinal and CoPA neurons play key roles in motor and sensory circuits respectively. These two subtypes of axon are amongst the first to be myelinated in the zebrafish spinal cord, and research has shown that these two different subtypes use diverse signals to regulate their initial myelination. In this chapter, I aim to investigate: how myelin patterns form along individual reticulospinal and CoPA axons in the zebrafish spinal cord; how these myelinated axons are remodelled after initial myelin sheath formation; and whether these two subtypes of axon exhibit any differences in myelin patterns and sheath remodelling. I hypothesise that reticulospinal axons will exhibit different myelin patterns compared to CoPA axons, and that reticulospinal axons will exhibit a greater degree of myelin remodelling after initial myelin sheath formation. To test this hypothesis, I performed live imaging of single

reticulospinal and CoPA axons using fluorescent reporters to assess myelination at the single axon level. I live imaged single axons at multiple time points, and then characterised the myelin patterns for both subtypes, focusing on parameters of sheath number, sheath length, axon diameter, and unmyelinated gap length. I also assessed the remodelling of individual myelin sheaths, and how this correlates with various parameters of myelinated axon development. Finally, I performed a time-course analysis by electron microscopy in collaboration with Dr. Jenea Bin to assess how sheath thickness changes over the same time period.

3.2. Results

3.2.1. Live Imaging of Reticulospinal and CoPA Axons after Initial Myelination

In order to visualise myelination along single axons, single-cell stage zebrafish eggs were injected with reporter-encoding plasmid DNA to facilitate mosaic transgenesis. Tg(HuC:Gal4) eggs were injected with 5 pg 10xUAS:eGFP and 5 pg of 10xUAS:tagRFPt-Contactin1a plasmids. Gal4 is a yeast transcriptional activator which controls gene expression by binding to specific target sequences called Upstream Activator Sequences (UAS), thereby activating the expression of downstream genes (Scheer and Campos-Ortega, 1999). The transgenic line Tg(HuC:Gal4) expresses Gal4 under the control of the HuC promotor, and thus, in the majority of post-mitotic neurons (Mensch et al., 2015). This means that some neurons where transgenesis of the injected plasmids occurs will express the genes of interest. Cytoplasmic expression of eGFP labelled the morphology of entire cells and visualised the axons and branching collaterals. The fusion protein tagRFPt-Contactin1a (hereafter denoted as RFP-Cntn1a) is a fluorescently-tagged version of one of the zebrafish homologs for Contactin1. This axonal membrane-bound protein is involved in axo-glial adhesion at paranodes and is also localised to nodes of Ranvier in the CNS (Rasband and Peles, 2016; Salzer, 2003). Zebrafish have two homologues for Contactin1, Contactin1a and Contactin1b. Both are expressed in the zebrafish CNS, with Contactin1b expression beginning later than Contactin1a (Gimnopoulos et al., 2002; Haenisch et al., 2005). It has been

shown that FP-Cntn1a fusion proteins can be used as a reporter of myelination along single axons; first FP-Cntn1a is expressed along the entire unmyelinated axon, but once an oligodendrocyte forms contacts with the axon, this extrudes the FP-Cntn1a reporter from these contact sites (Koudelka et al., 2016). The gaps in FP-Cntn1a along an axon indicate the location of myelin sheaths, while the regions of FP-Cntn1a expression denote unmyelinated axon or nodes of Ranvier. By expressing both eGFP and RFP-Cntn1a in single axons, both axon morphology and myelin patterns along reticulospinal and CoPA axons can be visualised.

Injected larvae were screened to identify animals where isolated reticulospinal (RS) or CoPA axons were labelled, with the two subtypes identified based on the morphology of their axons in the spinal cord, as described in section '3.1 Introduction'. Only one cell was imaged and analysed per animal. For RS axons, the Mauthner cells were excluded from imaging and analysis because these axons are myelinated in a non-traditional fashion. Along Mauthner axons, instead of distinct sheaths being separated by nodes of Ranvier, neighbouring sheaths overlap with one another and nodes are localised to the short collaterals.

Myelination in the zebrafish spinal cord begins at approximately 2-3 days post-fertilisation (dpf), and RS and CoPA axons are extensively myelinated within the first few days of myelination. Therefore, the axon of each identified cell was imaged by confocal microscopy at 5, 7, and 9 dpf, to assess how myelinated axons change after this initial period of sheath formation (**Figure 9A**). Note that, in experiments where all data are normally distributed, the data averages are described as means with standard deviation (SD) error bars; for experiments containing not normally distributed data, the data averages are described as medians with interquartile range (IQR) error bars. Almost all of the axons analysed had significant coverage of myelin along their axons from 5 dpf onwards (the median % axon myelinated of RS axons was 93.4% at 5 dpf, 97.4% at 7 dpf, and 97.2% at 9 dpf; the median % axon myelinated of CoPA axons was 89.3% at 5 dpf, 94.3% at 7 dpf, and 97.3% at 9 dpf; **Figure 9C-E**). Approximately similar lengths of axon were analysed for the two

subtypes (median total length of RS axon analysed was 540.5 µm, median total length of CoPA axon analysed was 574.2 µm; **Figure 9F**).

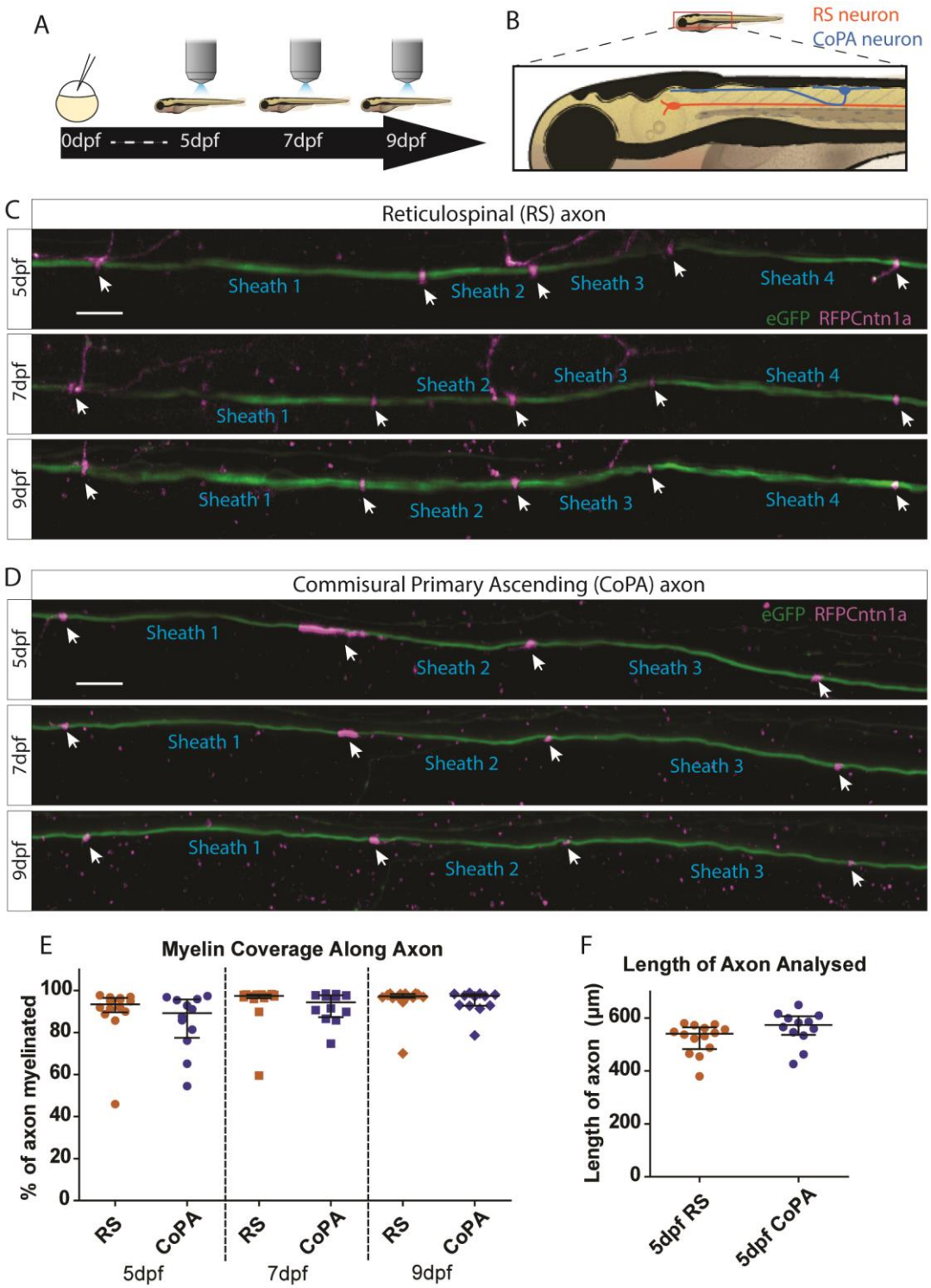

Figure 9 - live imaging myelinated axon development over time in the zebrafish spinal cord.

A) Experimental timeline; fertilised eggs were injected with plasmids to mosaically label single neurons in the spinal cord with fluorescent reporters of myelination. The axons of identified reticulospinal (RS) and CoPA neurons were imaged at 5, 7, and 9 dpf. **B)** Schematic highlighting the positions of RS and CoPA neurons and their axons. RS soma are located in the hindbrain and project axons caudally along the ventral spinal cord. CoPA soma are located at each somite of the spinal cord, and project ascending axons rostrally towards the brain. **C)** An example RS axon imaged at 5, 7, and 9 dpf, with myelin sheaths labelled. White arrows = unmyelinated axon labelled with RFP-Cntn1a. **D)** An example CoPA axon imaged at 5, 7, and 9 dpf, with myelin sheaths labelled. **E)** Quantification of the myelin coverage along RS and CoPA axons at 5, 7, and 9 dpf. The median % axon myelinated of RS axons was 93.4% (IQR = 89.6-96.5) at 5 dpf, 97.4% (IQR = 96.3-98.1) at 7 dpf, and 97.2% (IQR = 96.6-98.4) at 9 dpf. The median % axon myelinated of CoPA axons was 89.3% (IQR = 77.5-95.8) at 5 dpf, 94.3% (IQR = 87.3-97.7) at 7 dpf, and 97.3% (IQR = 92.7-98.3) at 9 dpf. **F)** Quantification of the length of axon analysed (total axon length from three overlapping confocal images). The median total length of RS axon analysed was 540.5 µm (IQR = 482.2-565.1), and the median total length of CoPA axon analysed was 574.2 µm (IQR = 536.7-606.6). RS n = 14, CoPA n = 12. Scale bars = 10 µm.

3.2.2. Changes in Sheath Number over Time

First, the number of myelin sheaths along RS and CoPA axons between 5 and 9 dpf was quantified to see if this significantly changed after the initial period of sheath formation. The mean number of sheaths along RS axons (normalised to axon length analysed) was 2.6 sheaths/100 µm axon at 5 dpf, 2.5 sheaths/100 µm axon at 7 dpf, and 2.5 sheaths/100 µm axon at 9 dpf, with no statistically significant change in sheath number during this time period (Repeated Measures ANOVA, p = 0.572; **Figure 10C**). For CoPA axons, the median number of sheaths/100 µm axon was 2.5 at 5 dpf, 2.4 at 7 dpf, and 2.4 at 9 dpf, and again there was no significant change in sheath number over time (Friedman test, p = 0.779, **Figure 10F**).

By imaging the same region of axon at each time point, individual myelin sheaths could be followed over time (**Figure 10C-D**). This allowed assessment of whether new sheaths were added or existing sheaths were retracted between 5 to 9 dpf (**Figure 10A-B**). While both phenomena occasionally occurred, the majority of axons showed no such changes in sheath number over time. Only five sheaths were added 5-7 dpf across the 26 axons analysed (an increase of total sheath number of 2.29%); 7-9 dpf, only one sheath was added (an increase of 0.29%). Sheath addition was limited to longer unmyelinated portions of the axon, as new sheaths were never added into the short nodal gaps between existing sheaths. Between 5 to 7 dpf, 12 sheaths were retracted (3.43% of total sheaths), while only two sheaths were retracted 7-9 dpf (0.58% of total sheaths). All of the sheaths which were retracted were of short length; of the 14 sheaths which were retracted, 13 were under 10 µm in length; the final sheath was 10.6 µm in length. On both RS and CoPA axons, there was no significant change in the degree of sheath addition or retraction throughout the time period analysed (**Figure 10D-E, G-H**, Wilcoxon signed rank tests, see **Figure 10** legend for statistics).

Based on these results, I concluded that the vast majority of sheaths along RS and CoPA axons are made during early myelination (3-5 dpf), and that, thereafter, sheath number remains relatively stable. However, it is possible to remove sheaths as shown by the occasional incidence of sheath retractions. Sheath retractions have been described in numerous other studies, such as in timelapse imaging of single oligodendrocytes undergoing myelination in the zebrafish spinal cord (Hines et al., 2015; Mensch et al., 2015). Interestingly, Hines et al. 2015 noted that all of the sheath retractions they observed were of sheaths under 10 µm in length, similar to my findings along RS and CoPA axons. This raised the intriguing hypothesis that sheath fate can be predicted based on length. To investigate this, the sheaths were binned by length and the percentage which were either retracted or maintained was calculated. Between 5 to 7 dpf, 75% of sheaths under 5 µm long were retracted, while only 20% of sheaths between 5-10 µm long and 5.3% of sheaths between 10-15 µm long were retracted (**Figure 10I**). Between 7 to 9 dpf, 25% of sheaths under

5 µm long, 16.3% of sheaths between 5-10 µm long, and 0% of sheaths between 10-15 µm long were retracted (**Figure 10J**). This suggests that there is a correlation between sheath length and fate.

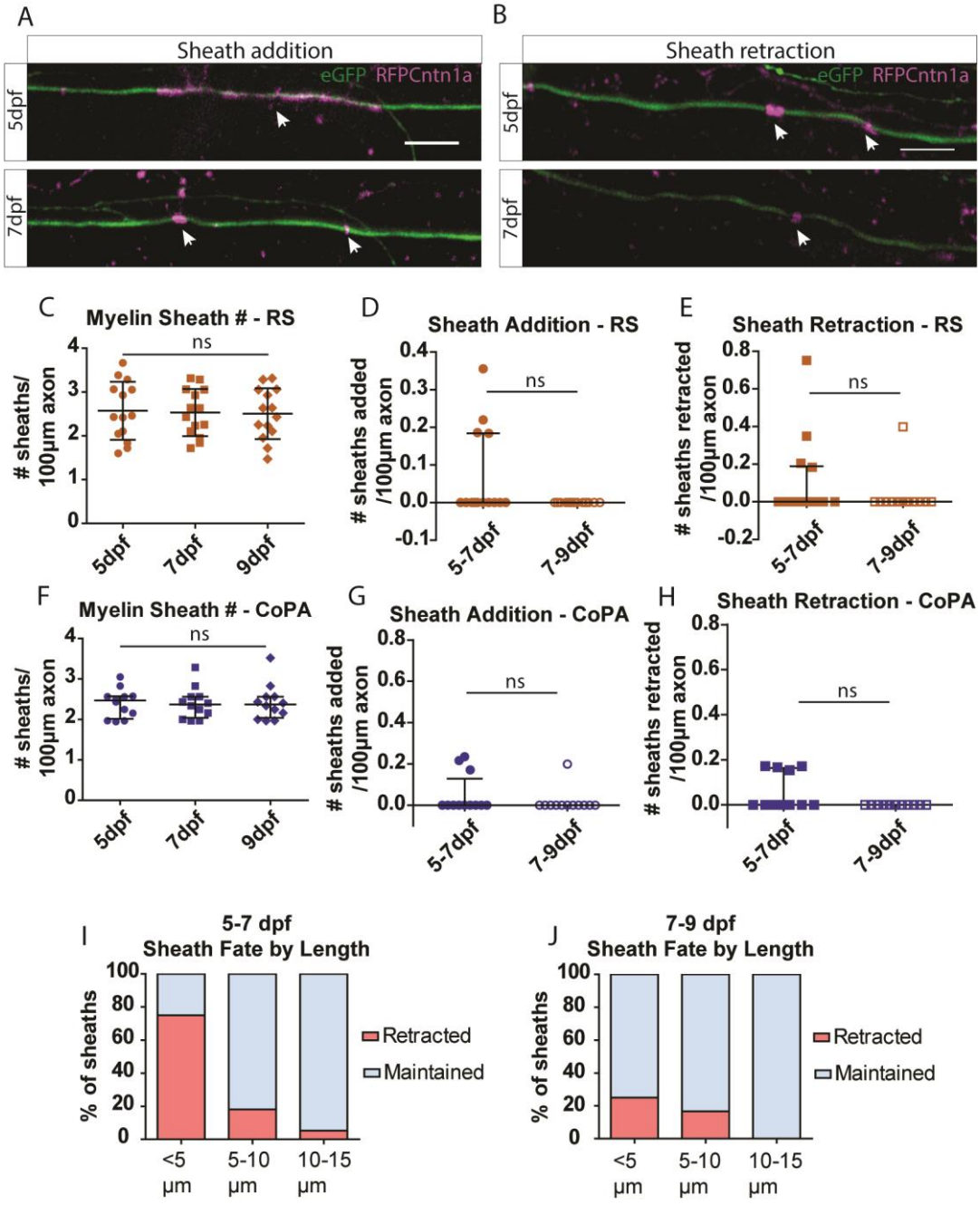

Figure 10 – sheath number along RS and CoPA axons over time.

A) An example of a new sheath being added to an axon; white arrows = unmyelinated axon labelled with tagRFPt-Cntn1a. **B)** An example of a sheath being retracted from an axon. **C)** The number of sheaths along RS axons over time. The

mean number of sheaths/100 µm axon was 2.6 (SD = 0.7) at 5 dpf, 2.5 (SD = 0.5) at 7 dpf, and 2.5 (SD = 0.6) at 9 dpf. There was no statistically significant change in sheath number over time (Repeated Measures ANOVA, p = 0.572, n = 14). **D)** Quantification of sheath addition along RS axons over time. The median number of sheaths added/100 µm axon 5-7 dpf was 0 (IQR = 0-0.18); the median number of sheaths added/100 µm axon 7-9 dpf was 0 (IQR = 0-0). There was no statistically significant change in sheath addition with time (Wilcoxon signed rank test, p = 0.125, n = 14). **E)** Quantification of sheath retraction along RS axons over time. The median number of sheaths retracted/100 µm axon 5-7 dpf was 0 (IQR = 0-0.19); the median number of sheaths retracted/100 µm axon 7-9 dpf was 0 (IQR = 0-0). There was no statistically significant change in sheath retraction with time (Wilcoxon signed rank test, p = 0.375, n = 14). **F)** The number of sheaths along CoPA axons over time. The median number of sheaths/100 µm axon was 2.5 (IQR = 2.0-2.6) at 5 dpf, 2.4 (IQR = 2.0-2.6) at 7 dpf, and 2.4 (IQR = 2.0-2.6) at 9 dpf. There was no statistically significant change in sheath number over time (Friedman test, p = 0.779, n = 12). **G)** Quantification of sheath addition along CoPA axons over time. The median number of sheaths added/100 µm axon 5-7 dpf was 0 (IQR = 0-0.13); the median number of sheaths added/100 µm axon 7-9 dpf 0 (IQR = 0-0). There was no statistically significant change in sheath addition with time (Wilcoxon signed rank test, p = 0.250, n = 12). **H)** Quantification of sheath retraction along CoPA axons over time. The median number of sheaths retracted/100 µm axon 5-7 dpf was 0 (IQR = 0-0.16); the median number of sheaths retracted/100 µm axon 7-9 dpf 0 (IQR = 0-0). There was no statistically significant reduction in sheath retraction with time (Wilcoxon signed rank test, p = 0.125, n = 12). **I)** The 5-7 dpf fate of myelin sheaths at different bins of sheath length. For sheaths < 5 µm in length at 5 dpf, 75% of sheaths were retracted, 25% of sheaths were maintained 5-7 dpf (# sheaths = 12). For sheaths 5-10 µm in length at 5 dpf, 18.2% of sheaths were retracted, 81.8% of sheaths were maintained 5-7 dpf (# sheaths = 11). For sheaths 10-15 µm in length at 5 dpf, 5.3% of sheaths were retracted, 94.7% of sheaths were maintained 5-7 dpf (# sheaths = 19). **J)** The 7-9 dpf fate of myelin sheaths at different bins of sheath length. For sheaths < 5 µm in length at 7 dpf, 25% of sheaths were retracted, 75% of sheaths were maintained 7-9 dpf (# sheaths = 4). For sheaths 5-10 µm in length at 7 dpf, 16.7% of sheaths were retracted, 83.3% of sheaths were maintained 7-9 dpf (# sheaths = 6). For sheaths 10-15 µm in length

at 7 dpf, 0% of sheaths were retracted, 100% of sheaths were maintained 7-9 dpf (# sheaths = 10). Scale bars = 10 µm.

3.2.3. Sheath Length and Sheath Length Variability over Time

Next, the length of myelin sheaths along RS and CoPA axons was quantified at 5, 7, and 9 dpf. The mean sheath length for each axon analysed was plotted over time (**Figure 11A-B**). The mean sheath length for RS axons significantly increased from 36.7 µm at 5 dpf to 39.8 µm at 7 dpf, but did not change significantly at 9 dpf when it was 39.9 µm (Repeated Measures ANOVA, $p = 0.0003$, Tukey's Multiple Comparisons test, **Figure 11A**). For CoPA axons, the mean sheath length also increased from 36.0 µm at 5 dpf to 39.9 µm at 7 dpf, and then did not change at 9 dpf when it was 40.5 µm (Repeated Measures ANOVA, $p < 0.0001$, Tukey's Multiple Comparisons test, **Figure 11B**).

Previous studies have shown that there can be significant variation in the length of sheaths along a given axon (Auer et al., 2018; Ibrahim et al., 1995; Murray and Blakemore, 1980); whether this variability is transient or maintained over time is not yet known. The sheaths along an axon may be remodelled in length over time, so that they all become a similar length to evenly space out the nodes of Ranvier. Both RS and CoPA axons exhibited significant variation in sheath length along axons at 5 dpf, with sheaths along a single axon often ranging from < 5 µm to > 60 µm (**Figure 11E, G**). At 9 dpf, these axons still have considerable variability in sheath length (**Figure 11F, H**). To quantify this variability, the standard deviation (SD) of sheath length measurements for each axon was taken at 5, 7, and 9 dpf (**Figure 11C-D**). The variability of sheath length along RS axons did not change between 5 and 9 dpf (median sheath length variability was 15.2 at 5 dpf, 14.4 at 7 dpf, and 13.5 at 9 dpf; Friedman test, $p = 0.257$). CoPA axons also showed no change in sheath length variability over time (mean sheath length variability was 17.1 at 5 dpf, 17.0 at 7 dpf, and 17.1 at 9 dpf; Repeated Measures ANOVA, $p = 0.951$).

Based on these results, I concluded that sheath length variability along axons is maintained after initial sheath formation, and as with myelin sheath number, that very little myelin length remodelling takes place after axons are completely myelinated.

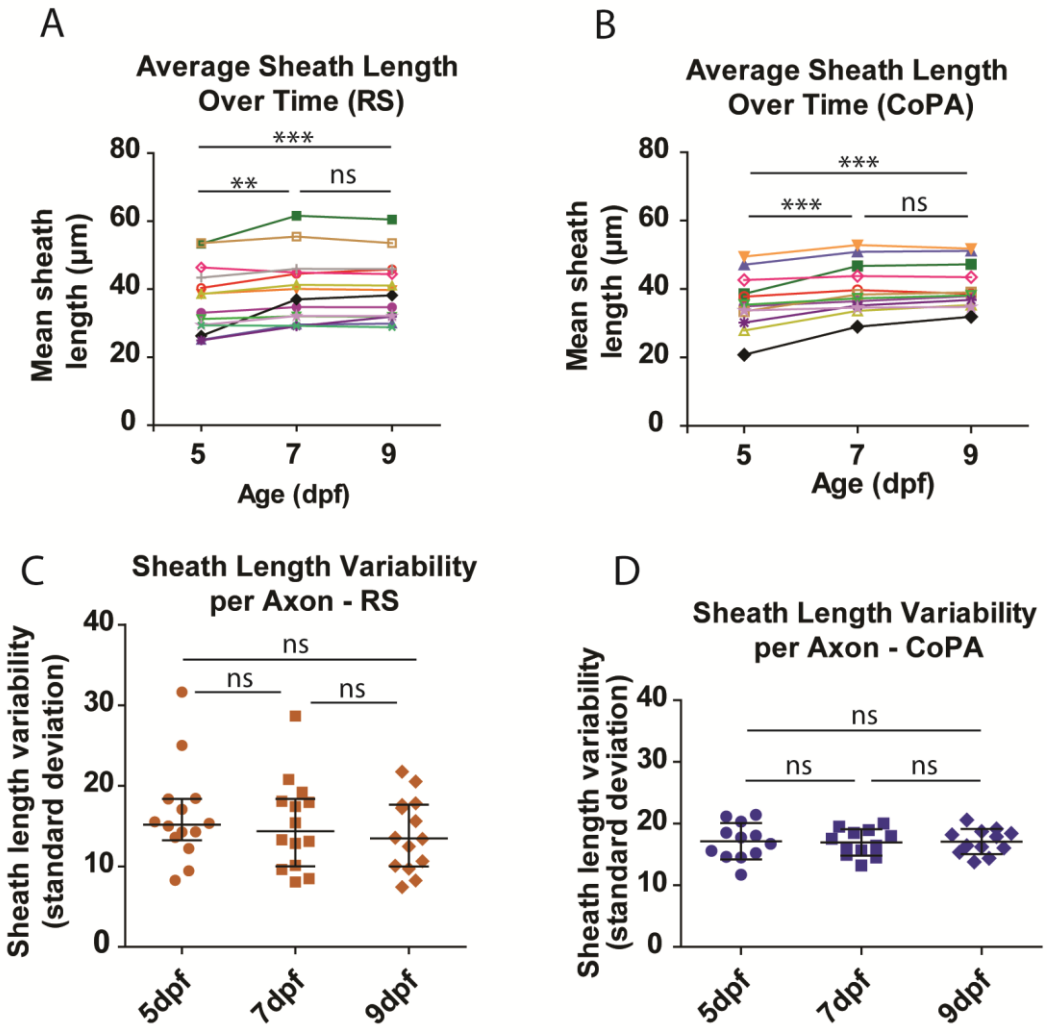

Figure 11 – sheath lengths along RS and CoPA axons over time (continued on next page).

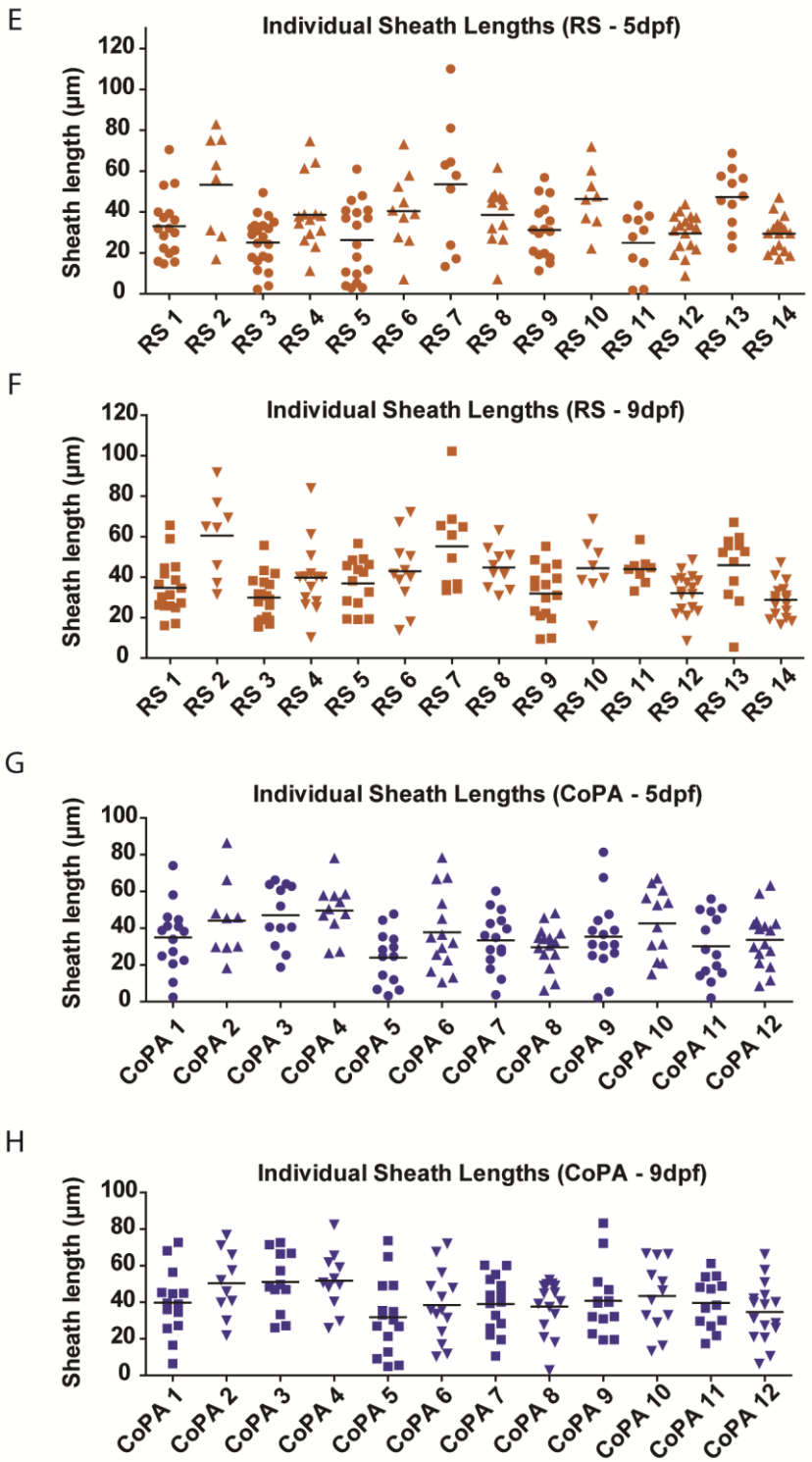

Figure 11 (continued).

A) The mean sheath length of each RS axon at 5, 7, and 9 dpf. The overall mean sheath length was 36.7 µm (SD = 9.8) at 5 dpf, 39.8 µm (SD = 10.0) at 7 dpf, and 39.9 µm (SD = 9.4) at 9 dpf. There was a statistically significant change in mean

sheath length over time (Repeated Measures ANOVA, p = 0.0003; Tukey's Multiple Comparisons test: 5 dpf vs 7 dpf p = **, 5 dpf vs 9 dpf p = ***, 7 dpf vs 9 dpf p = ns). RS n = 14. **B)** The mean sheath length of each CoPA axon at 5, 7, and 9 dpf. The overall mean sheath length was 36.0 µm (SD = 8.0) at 5 dpf, 39.9 µm (SD = 7.3) at 7 dpf, and 40.5 µm (SD = 6.5) at 9 dpf. There was a statistically significant change in mean sheath length over time (Repeated Measures ANOVA, p < 0.0001; Tukey's Multiple Comparisons test: 5 dpf vs 7 dpf p = ***, 5 dpf vs 9 dpf p = ***, 7 dpf vs 9 dpf p = ns). CoPA n = 12**. C)** Quantification of sheath length variability along individual RS axons. Sheath length variability was assessed as the standard deviation of sheath lengths along each axon. The median sheath length variability was 15.2 (IQR = 13.3-18.4) at 5 dpf, 14.4 (IQR = 10.0-18.4) at 7 dpf, and 13.5 (IQR = 10.0-17.7) at 9 dpf. There was no statistically significant change in sheath length variability over time (Friedman test, p = 0.257). RS n = 14. **D)** Quantification of sheath length variability along individual CoPA axons. The mean sheath length variability was 17.1 (SD = 3.0) at 5 dpf, 17.0 (SD = 2.1) at 7 dpf, and 17.1 (SD = 2.0) at 9 dpf. There was no statistically significant change in sheath length variability over time (Repeated Measures ANOVA, p = 0.951). CoPA n = 12. **E)** The 5 dpf lengths of individual sheaths along each RS axon analysed (each data point = a single myelin sheath; the black line = mean sheath length). **F)** The 9 dpf lengths of individual sheaths along each RS axon analysed. **G)** The 5 dpf lengths of individual sheaths along each CoPA axon analysed. **H)** The 9 dpf lengths of individual sheaths along each CoPA axon analysed.

3.2.4. Changes in Axon Diameter over Time

Myelin sheath length was variable between axons as well as along axons, with mean sheath length ranging from between 20-50 µm for both RS and CoPA axons (**Figure 11A-B**). It has been shown that, on average, sheath length correlates with the diameter of the underlying axon (Ibrahim et al., 1995; Murray and Blakemore, 1980). Therefore, the diameter of RS and CoPA axons was measured in order to assess whether sheath length correlates with axon diameter. Firstly, the area and length of a stretch of axon was measured, then the diameter was calculated by dividing area by length (**Figure 12A**). This was

measured for three different regions of each axon, and then the mean of these measurements was taken as the final axon diameter measurement.

The mean RS axon diameter increased from 1.1 µm at 5 dpf to 1.2 µm at 7 dpf, but showed no significant change thereafter, being 1.2 µm at 9 dpf (Repeated Measures ANOVA, $p < 0.0001$, Tukey's Multiple Comparisons test, **Figure 12B**). CoPA axons showed no change in mean axon diameter during the period analysed, being 0.8 µm at 5 dpf, 0.8 µm at 7 dpf, and 0.8 µm at 9 dpf (Repeated Measures ANOVA, $p = 0.105$, **Figure 12F**). This is concurrent with previous characterisation of axon diameter growth of these axon subtypes (Mensch, 2014).

Next, the axon diameter was plotted against mean sheath length at each age to determine if the variability in mean sheath length can be explained by axon diameter. However, there was no significant correlation between axon diameter and mean sheath length at any age for both RS and CoPA axons (**Figure 12C-E, G-I**, Pearson's correlation test; see **Figure 12** legend for statistics). The variability in sheath length between axons is, thus, not due to variation in axon diameter.

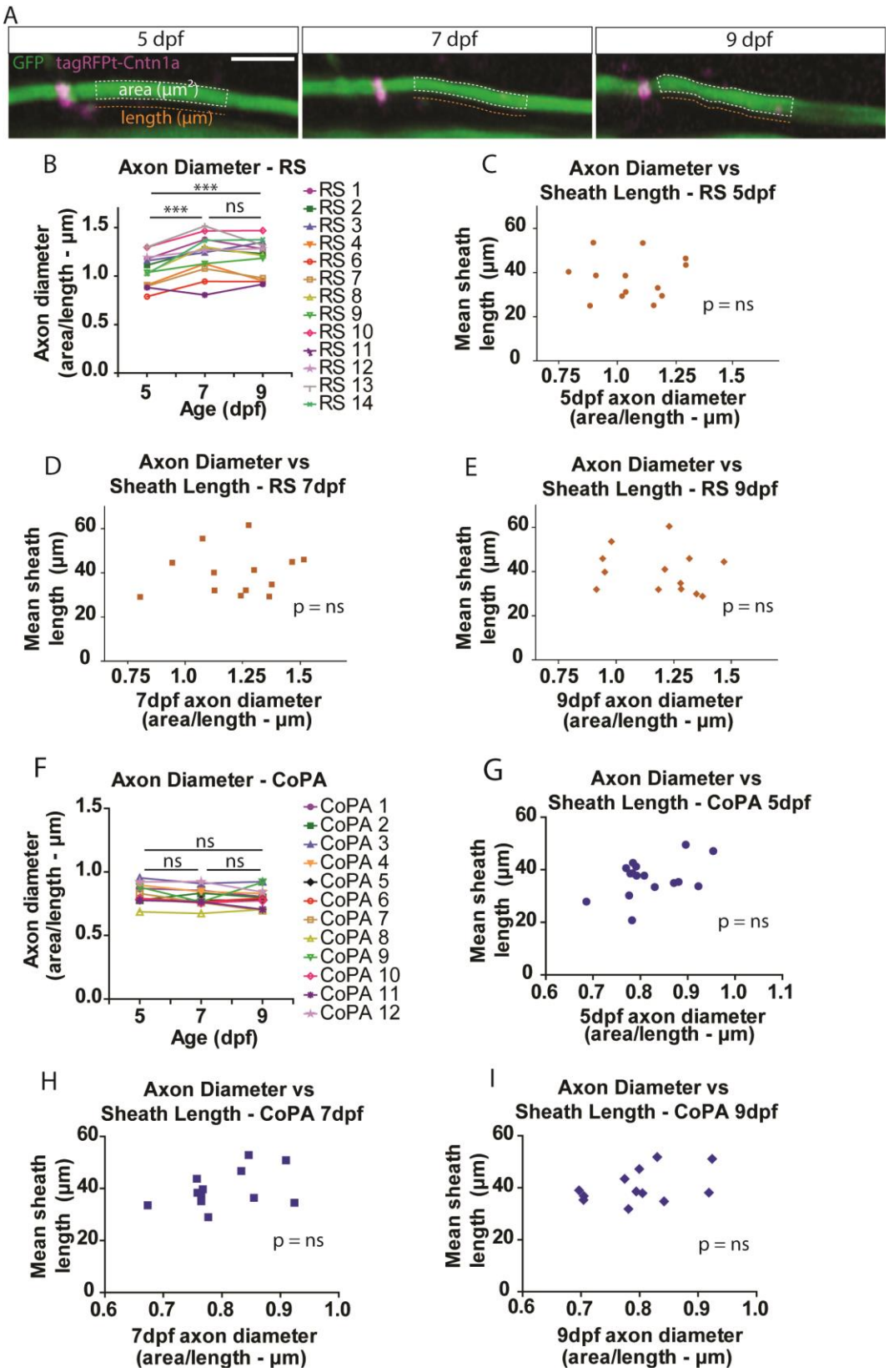

Figure 12 - axon diameter of RS and CoPA axons over time.

A) Example images showing measurement of axon diameter over time. The area of a region of an axon was divided by the length to calculate diameter. **B)** Quantification of axon diameter of each RS axon at 5, 7, and 9 dpf. The mean axon diameter was 1.1 µm (SD = 0.2) at 5 dpf, 1.2 µm (SD = 0.2) at 7 dpf, and 1.2 µm (SD = 0.2) at 9 dpf. There was a statistically significant increase in axon diameter over time (Repeated Measures ANOVA, $p < 0.0001$; Tukey's Multiple Comparison's test: 5 dpf vs 7 dpf p = ***, 5 dpf vs 9 dpf p =***, 7 dpf vs 9 dpf p = ns). RS n = 13. **C)** Axon diameter plotted against mean sheath length for RS axons at 5 dpf. There was no statistically significant correlation between axon diameter and sheath length (Pearson's correlation test, $p = 0.917$). **D)** Axon diameter plotted against mean sheath length for RS axons at 7 dpf. There was no statistically significant correlation between axon diameter and sheath length (Pearson's correlation test, $p = 0.689$). **E)** Axon diameter plotted against mean sheath length for RS axons at 9 dpf. There was no statistically significant correlation between axon diameter and sheath length (Pearson's correlation test, $p = 0.544$). **F)** Quantification of axon diameter of each CoPA axon at 5, 7, and 9 dpf. The mean axon diameter was 0.8 µm (SD = 0.08) at 5 dpf, 0.8 µm (SD = 0.07) at 7 dpf, and 0.8 µm (SD = 0.08) at 9 dpf. There was no statistically significant change in axon diameter over time (Repeated Measures ANOVA, $p = 0.105$). CoPA n = 12. **G)** Axon diameter plotted against mean sheath length for CoPA axons at 5 dpf. There was no statistically significant correlation between axon diameter and sheath length (Pearson's correlation test, $p = 0.088$). **H)** Axon diameter plotted against mean sheath length for CoPA axons at 7 dpf. There was no statistically significant correlation between axon diameter and sheath length (Pearson's correlation test, $p = 0.181$). **I)** Axon diameter plotted against mean sheath length for CoPA axons at 9 dpf. There was no statistically significant correlation between axon diameter and sheath length (Pearson's correlation test, $p = 0.180$). Scale bar = 5 µm.

3.2.5. Unmyelinated Gap Length and Gap Length Variability over Time

The next step in my investigation was to examine the length of unmyelinated gaps between sheaths along RS and CoPA axons between 5 and 9 dpf. These gaps included both long stretches of unmyelinated axon and the smaller gaps, which likely represent nodes of Ranvier. For seven RS axons (RS 1, 2, 5, 6, 9, 11, and 14), not all unmyelinated gaps were included in this analysis as some

gaps could not be accurately measured at 9 dpf due to limitations in image resolution. Instead, only the gaps which could be accurately measured at all ages were analysed and plotted in **Figure 13**.

The unmyelinated gap length decreased over time along both RS and CoPA axons. For RS axons, the median gap length was 2.3 µm at 5 dpf, 1.0 µm at 7 dpf, and 1.0 at 9 dpf (Friedman test, $p < 0.0001$; Dunn's Multiple Comparisons test, **Figure 13A**). For CoPA axons, the median gap length was 4.4 µm at 5 dpf, 1.4 µm at 7 dpf, and 1.1 at 9 dpf (Friedman test, $p < 0.0001$; Dunn's Multiple Comparisons test, **Figure 13C**).

As with myelin sheath length, there was noteworthy variability in the length of unmyelinated gaps along RS and CoPA axons at 5 dpf (**Figure 13E-F**). Unmyelinated gap length variability was quantified as the standard deviation (SD) of unmyelinated gap length measurements for each axon at 5, 7, and 9 dpf. Gap length variability significantly declines over time. For RS axons, the median gap length variability was 2.7 at 5 dpf, 0.3 at 7 dpf, and 0.2 at 9 dpf (Friedman test, $p = 0.009$; Dunn's Multiple Comparisons test, **Figure 13B**). For CoPA axons, the median gap length variability was 5.0 at 5 dpf, 1.2 at 7 dpf, and 0.5 at 9 dpf (Friedman test, $p < 0.0001$; Dunn's Multiple Comparisons test, **Figure 13D**). By 9 dpf, the majority of unmyelinated gaps were under 2 µm long and likely represented maturing nodes of Ranvier (**Figure 13G-H**).

Therefore, the length of unmyelinated gaps between sheaths along both RS and CoPA axons becomes significantly less variable as they shorten into mature nodes of Ranvier with myelinated axon development. However, some axons still had large unmyelinated gaps at 9 dpf; for example, RS 11 was only 70% myelinated and still had gaps up to 60 µm in length (**Figure 13G**). These axons may be sparsely myelinated, as have previously been described in the rodent cortex (Gao et al., 2019; Hill et al., 2018; Tomassy et al., 2014) and the zebrafish spinal cord (Auer et al., 2018). It is possible that these axons are simply myelinating at a slower rate than other axons; following these axons beyond 9 dpf may reveal that they eventually become fully myelinated with shorter nodes of Ranvier between their sheaths.

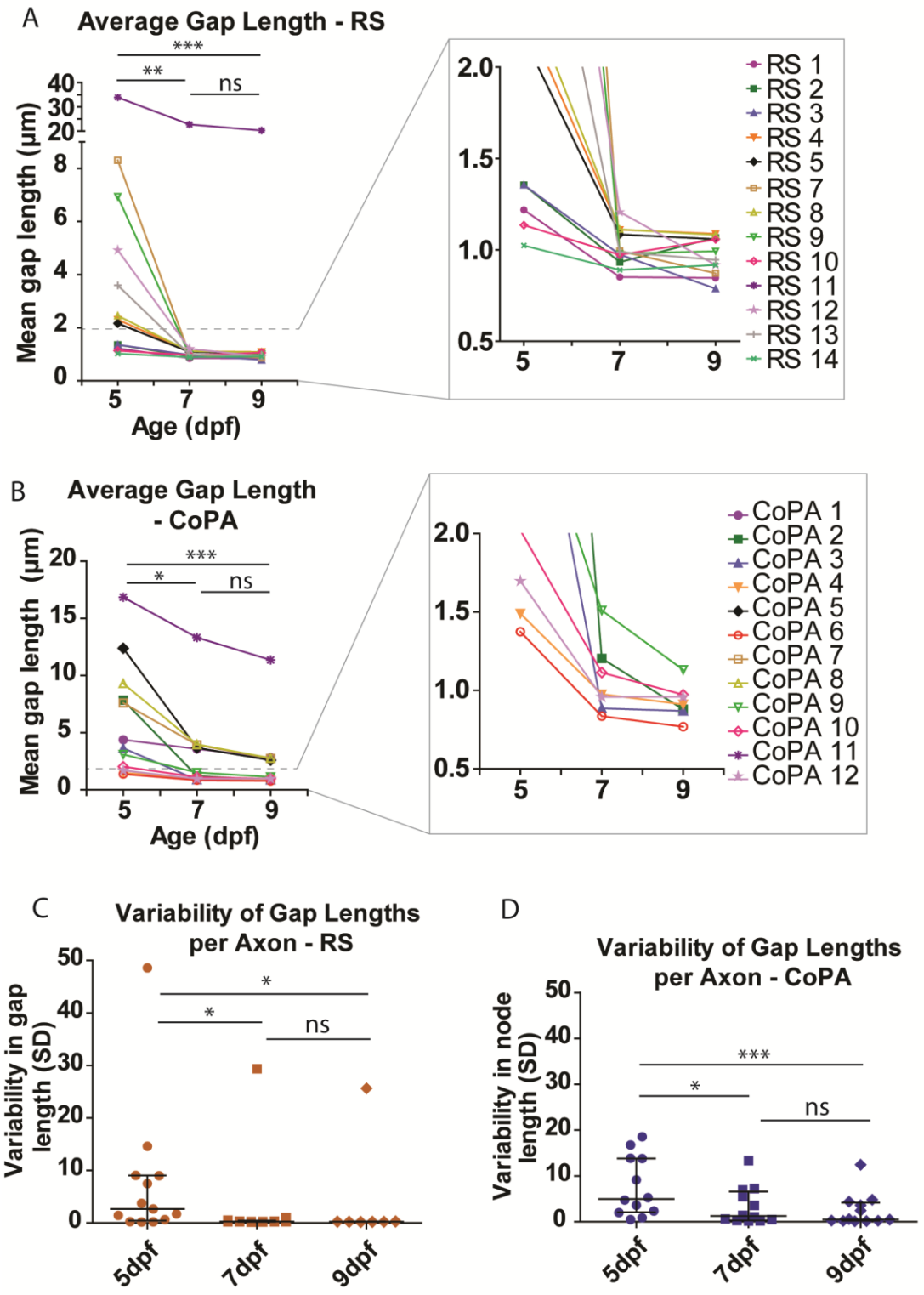

Figure 13 – unmyelinated gap lengths along RS and CoPA axons over time (continued on next page).

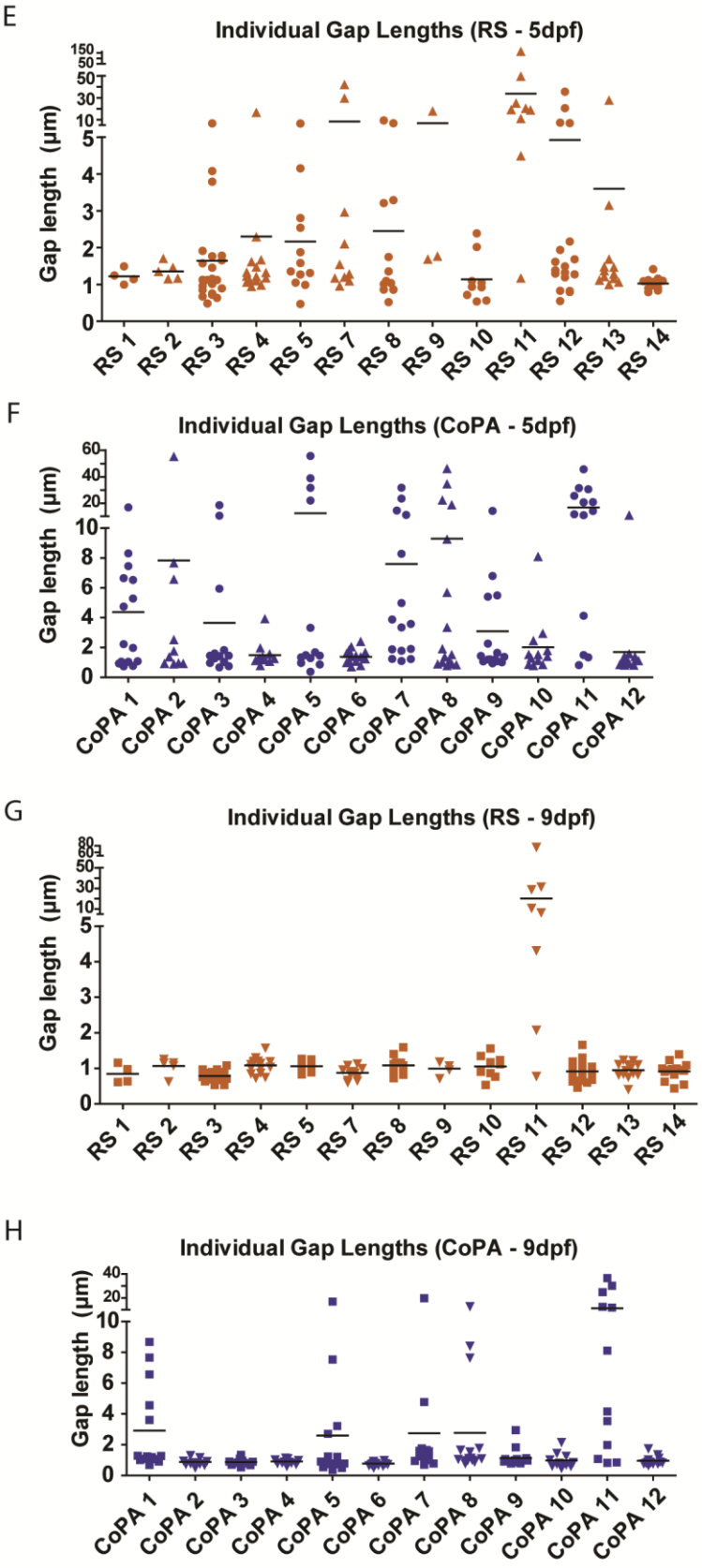

Figure 13 (continued).

A) The mean unmyelinated gap length of each RS axon at 5, 7, and 9 dpf. The overall median unmyelinated gap length was 2.3 µm (IQR = 1.3-5.9) at 5 dpf, 1.0 µm (IQR = 1.0-1.1) at 7 dpf, and 1.0 (IQR = 0.9-1.1) at 9 dpf. There was a statistically significant reduction in unmyelinated gap length over time (Friedman test, $p < 0.0001$; Dunn's Multiple Comparisons test: 5 dpf vs 7 dpf p = **, 5 dpf vs 9 dpf p = ***, 7 dpf vs 9 dpf p = ns). RS n = 13. **B)** The mean unmyelinated gap length of each CoPA axon at 5, 7, and 9 dpf. The overall median unmyelinated gap length was 4.4 µm (IQR = 1.8-8.9) at 5 dpf, 1.4 µm (IQR = 1.0-3.9) at 7 dpf, and 1.1 µm (IQR = 0.9-2.8) at 9 dpf. There was a statistically significant reduction in unmyelinated gap length over time (Friedman test, $p < 0.0001$; Dunn's Multiple Comparisons test: 5 dpf vs 7 dpf p = *, 5 dpf vs 9 dpf p = ***, 7 dpf vs 9 dpf p = ns). CoPA n = 12. **C)** Quantification of unmyelinated gap length variability along individual RS axons. Unmyelinated gap length variability was assessed as the standard deviation of unmyelinated gap lengths along each axon. The median unmyelinated gap length variability was 2.7 (IQR = 0.4-9.0) at 5 dpf, 0.3 (IQR = 0.2-0.5) at 7 dpf, and 0.2 (IQR = 0.2-0.3) at 9 dpf. There was a statistically significant reduction in unmyelinated gap length variability over time (Friedman test, $p = 0.009$; Dunn's Multiple Comparisons test: 5 dpf vs 7 dpf p = *, 5 dpf vs 9 dpf p = *, 7 dpf vs 9 dpf p = ns). RS n = 13. **D)** Quantification of unmyelinated gap length variability along individual CoPA axons. The median unmyelinated gap length variability was 4.9 (IQR = 2.1-13.8) at 5 dpf, 1.2 (IQR = 0.3-6.6) at 7 dpf, and 0.5 (IQR = 0.2-4.2) at 9 dpf. There was a statistically significant reduction in unmyelinated gap length variability over time (Friedman test, $p < 0.0001$; Dunn's Multiple Comparisons test: 5 dpf vs 7 dpf p = *, 5 dpf vs 9 dpf p = ***, 7 dpf vs 9 dpf p = ns). CoPA n = 12. **E)** The 5 dpf lengths of individual unmyelinated gaps along each RS axon analysed. Only the unmyelinated gaps which could be accurately measured at all time points are plotted. Each data point = a single unmyelinated gap between two sheaths. **F)** The 5 dpf lengths of individual unmyelinated gaps along each CoPA axon analysed. **G)** The 9 dpf lengths of individual unmyelinated gaps along each RS axon analysed. **H)** The 9 dpf lengths of individual unmyelinated gaps along each CoPA axon analysed.

3.2.6. Comparison of the Myelin Patterns between RS and CoPA Axons

I hypothesised that RS and CoPA axons would exhibit different myelination patterns. To test this, the various parameters described in sections '3.2.2', '3.2.3', and '3.2.5' were compared between the two axon subtypes. The comparisons (performed using Two-Way ANOVAs) are summarised in **Table 3**. Overall, there were no differences in the myelin patterns between RS and CoPA axons.

Table 3 – comparison of the myelin pattern parameters between RS and CoPA axons.

Parameter tested	**Any significant differences between RS and CoPA?** ***(Two-Way ANOVA p values)***
Myelin sheath number	No significant differences (p = 0.509)
Sheath addition	No significant differences (p = 0.987)
Sheath retraction	No significant differences (p = 0.303)
Myelin sheath length	No significant differences (p = 0.619)
Myelin sheath length variability	No significant differences (p = 0.246)
Unmyelinated gap length	No significant differences (p = 0.896)
Unmyelinated gap length variability	No significant differences (p = 0.902)

Based on these results, I concluded that, although RS and CoPA neurons use different signals to regulate their initial myelination, the myelin patterns established along their axons are very similar.

3.2.7. Remodelling of Single Myelin Sheaths over Time

After characterising the myelin patterns along RS and CoPA axons, I then investigated how individual myelin sheaths along these axons remodel during

the time period imaged. I have already characterised the retraction of individual sheaths along RS and CoPA axons (**Figure 10**). By following the same sheaths from 5 to 9 dpf, I was also able to assess how individual myelin sheaths change in length, either by growth or shrinkage (**Figure 14A-B**).

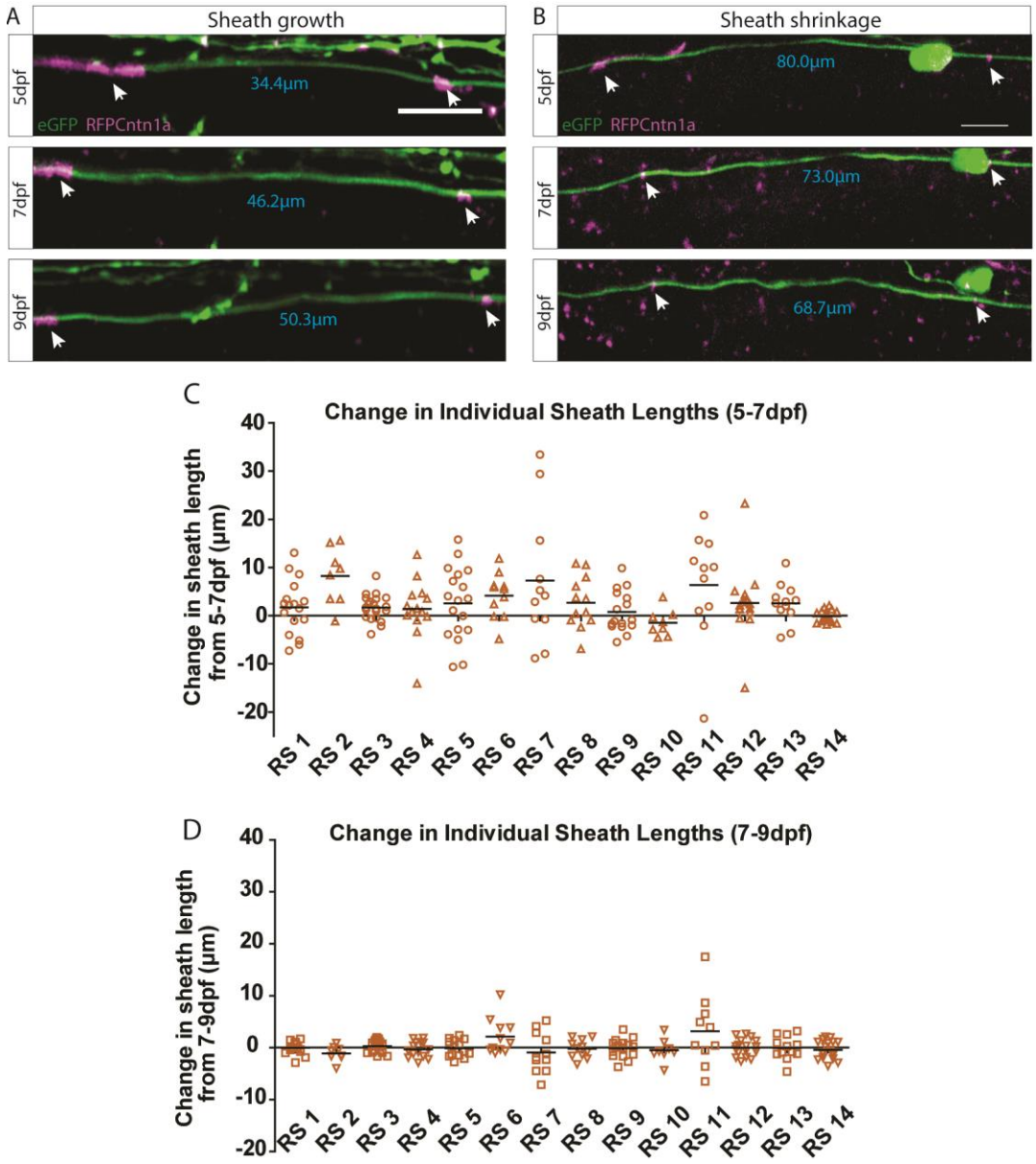

Figure 14 – changes in sheath length along RS and CoPA axons over time (continued on next page).

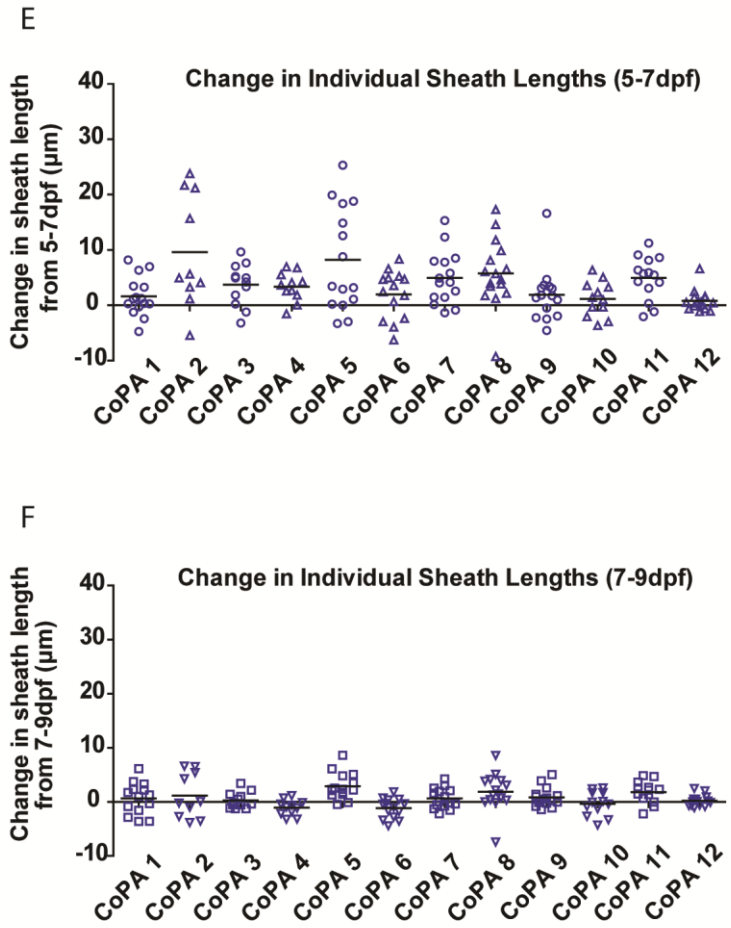

Figure 14 (continued).

A) An example of a single sheath growing in length 5-9 dpf. White arrows = unmyelinated adjacent to myelin sheath, blue text = length of myelin sheath at each age. **B)** An example of a single sheath shrinking in length 5-9 dpf. **C)** The change in length 5-7 dpf of individual sheaths along each RS axon analysed (each data point = a single myelin sheath). **D)** The change in length 7-9 dpf of individual sheaths along each RS axon analysed. **E)** The change in length 5-7 dpf of individual sheaths along each CoPA axon analysed. **F)** The change in length 7-9 dpf of individual sheaths along each CoPA axon analysed. Scale bars = 10 µm.

For both RS and CoPA axons, individual axons had both growing and shrinking sheaths along their length (**Figure 14C-F**). However, the degree of change in sheath length seems to decline with time. Quantifying the total sheath growth per RS axon (normalised to length of axon analysed) showed that median sheath growth declines from 9.0 µm/100 µm axon 5-7 dpf, to 1.8 µm/100 µm

axon 7-9 dpf (Wilcoxon signed rank test, p = 0.0006, **Figure 15A**). Sheath shrinkage along RS axons does not significantly change (but trends towards a decrease over time), with mean shrinkage per axon being -3.0 µm/100 µm axon 5-7 dpf, and -2.1 µm/100 µm axon 7-9 dpf (paired t-test, p = 0.082, **Figure 15B**). This means that the median overall change in sheath length per RS axon (summation of sheath growth and shrinkage values) is 7.0 µm/100 µm axon 5-7 dpf, and significantly declines to -0.4 µm/100 µm axon 7-9 dpf (Wilcoxon signed rank test, p = 0.0004, **Figure 15C**). Similar changes occur along CoPA axons. Median sheath growth per CoPA axon declines over time from 8.0 µm/100 µm axon 5-7 dpf to 2.8 µm/100 µm axon 7-9 dpf (Wilcoxon signed rank test, p = 0.0005, **Figure 15D**), while mean sheath shrinkage per axon remains unchanged from -1.2 µm/100 µm axon 5-7 dpf to -1.4 µm/100 µm axon 7-9 dpf (paired t-test, p = 0.457, **Figure 15E**). This means that the mean overall change in sheath length per CoPA axon reduces from 10.1 µm/100 µm axon 5-7 dpf to 1.7 µm/100 µm axon 7-9 dpf (paired t-test, p = 0.0005, **Figure 15F**).

I hypothesised that, given that RS and CoPA axons use different signals to regulate their myelination, the two axon subtypes would exhibit differences in the extent of myelin sheath remodelling that occurs. However, comparison of sheath growth, sheath shrinkage, and overall sheath length change between RS and CoPA axons by Two-Way ANOVAs showed few significant differences in the extent of myelin remodelling 5-9 dpf, as summarised in **Table 4**.

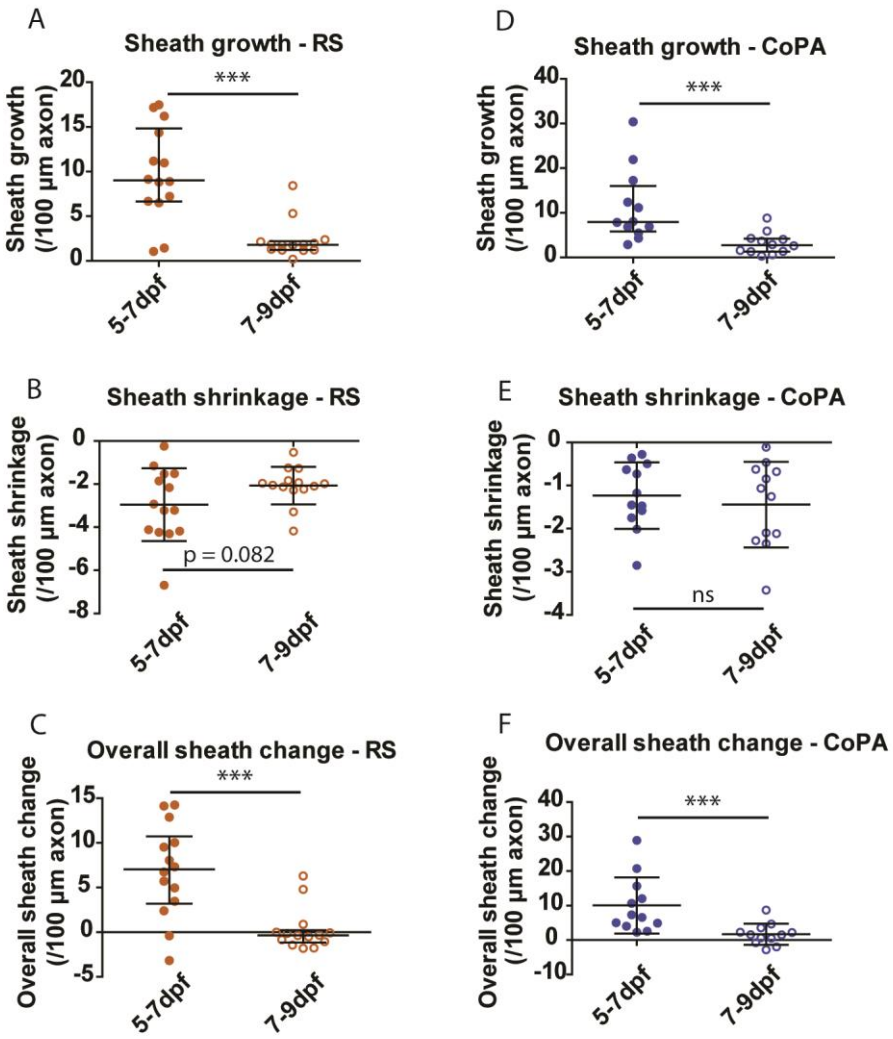

Figure 15 – total changes in sheath length along RS and CoPA axons over time.

A) Quantification of the total sheath growth along RS axons 5-9 dpf, normalised to length of axon analysed. The median total sheath growth was 9.0 µm/100 µm axon (IQR = 6.6-14.8) 5-7 dpf, and 1.8 µm/100 µm axon (IQR = 1.2-2.2) 7-9 dpf. There was a statistically significant reduction in sheath growth over time (Wilcoxon signed rank test, p = 0.0006, n = 14). **B)** Quantification of the total sheath shrinkage along RS axons 5-9 dpf, normalised to length of axon analysed. The mean total sheath shrinkage was -3.0 µm/100 µm axon (SD = 1.7) 5-7 dpf, and -2.1 µm/100 µm axon (SD = 0.9) 7-9 dpf. There was no statistically significant change in sheath shrinkage over time (paired t-test, p = 0.082, n = 14). **C)** Quantification of the overall change in sheath length along RS axons from 5-9 dpf, normalised to length of axon analysed. The median overall change in sheath length was 7.0 µm/100 µm axon

(IQR = 3.2-10.7) 5-7 dpf, and -0.4 µm/100 µm axon (IQR = -1.2-0.2) 7-9 dpf. There was a statistically significant reduction in overall change in sheath length over time (Wilcoxon signed rank test, p = 0.0004, n = 14). **D)** Quantification of the total sheath growth along CoPA axons 5-9 dpf, normalised to length of axon analysed. The median total sheath growth was 8.0 µm/100 µm axon (IQR = 5.8-16.0) 5-7 dpf, and 2.8 µm/100 µm axon (IQR = 1.3-4.2) 7-9 dpf. There was a statistically significant reduction in sheath growth over time (Wilcoxon signed rank test, p = 0.0005, n = 12). **E)** Quantification of the total sheath shrinkage along CoPA axons 5-9 dpf, normalised to length of axon analysed. The mean total sheath shrinkage was -1.2 µm/100 µm axon (SD = 0.8) 5-7 dpf, and -1.4 µm/100 µm axon (SD = 1.0) 7-9 dpf. There was no statistically significant change in sheath shrinkage over time (paired t-test, p = 0.457, n = 12). **F)** Quantification of the overall change in sheath length along CoPA axons from 5-9 dpf, normalised to length of axon analysed. The mean overall change in sheath length was 10.1 µm/100 µm axon (SD = 8.1) 5-7 dpf, and 1.7 µm/100 µm axon (SD = 3.1) 7-9 dpf. There was a statistically significant reduction in overall change in sheath length over time (paired t-test, p = 0.0005, n = 12).

Table 4 – comparison of the myelin remodelling parameters between RS and CoPA axons.

Parameter tested	**Any significant differences between RS and CoPA?** ***(Two-Way ANOVA p values)***
Sheath growth	No significant differences (p = 0.497)
Sheath shrinkage	Significant difference between subtypes (p = 0.003). *Sidak's Multiple Comparisons test identifies significant difference (p = ***) between RS 5-7 dpf and CoPA 5-7 dpf.*
Overall change in sheath length	No significant differences (p = 0.303)

Based on these results, I concluded that myelin sheath remodelling can occur in the form of growth and shrinkage, and that both RS and CoPA axons exhibit

remarkably similar degrees of sheath remodelling (with the exception of sheath shrinkage 5-7 dpf). Additionally, sheath growth remodelling significantly decreases on both RS and CoPA axons after 7 dpf, whereas sheath shrinkage does not significantly change over time.

3.2.8. Correlation of Myelin Remodelling with Stage of Myelination

The degree of myelin sheath growth significantly declines after 7 dpf on both RS and CoPA axons. This suggests that sheath growth is regulated by some factor which also changes over this time period. It is possible that such myelin remodelling only occurs at certain stages of myelination. To investigate this, I plotted the sheath remodelling values (growth and shrinkage) against the percentage of axon myelinated (as a read-out of stage of myelination – **Figure 16**). There was an inverse correlation between sheath growth and percentage of axon myelinated both between 5 to 7 dpf and 7 to 9 dpf, and this was the case for both RS and CoPA axons (Spearman's correlation tests, see **Figure 16** legend for statistics). However, there was no significant correlation between sheath shrinkage and percentage of axon myelinated at any stage on either RS or CoPA axons (Spearman's correlation tests, see **Figure 16** legend for statistics).

Based on these results, I concluded that both RS and CoPA axons which are more myelinated will, in turn, exhibit less myelin sheath growth, suggesting that myelin sheath growth can only occur when there is empty space in which to grow. Additionally, myelin sheath growth and shrinkage may be independently regulated, as the sheath shrinkage observed at these stages is unaffected by the amount of unmyelinated axonal space available.

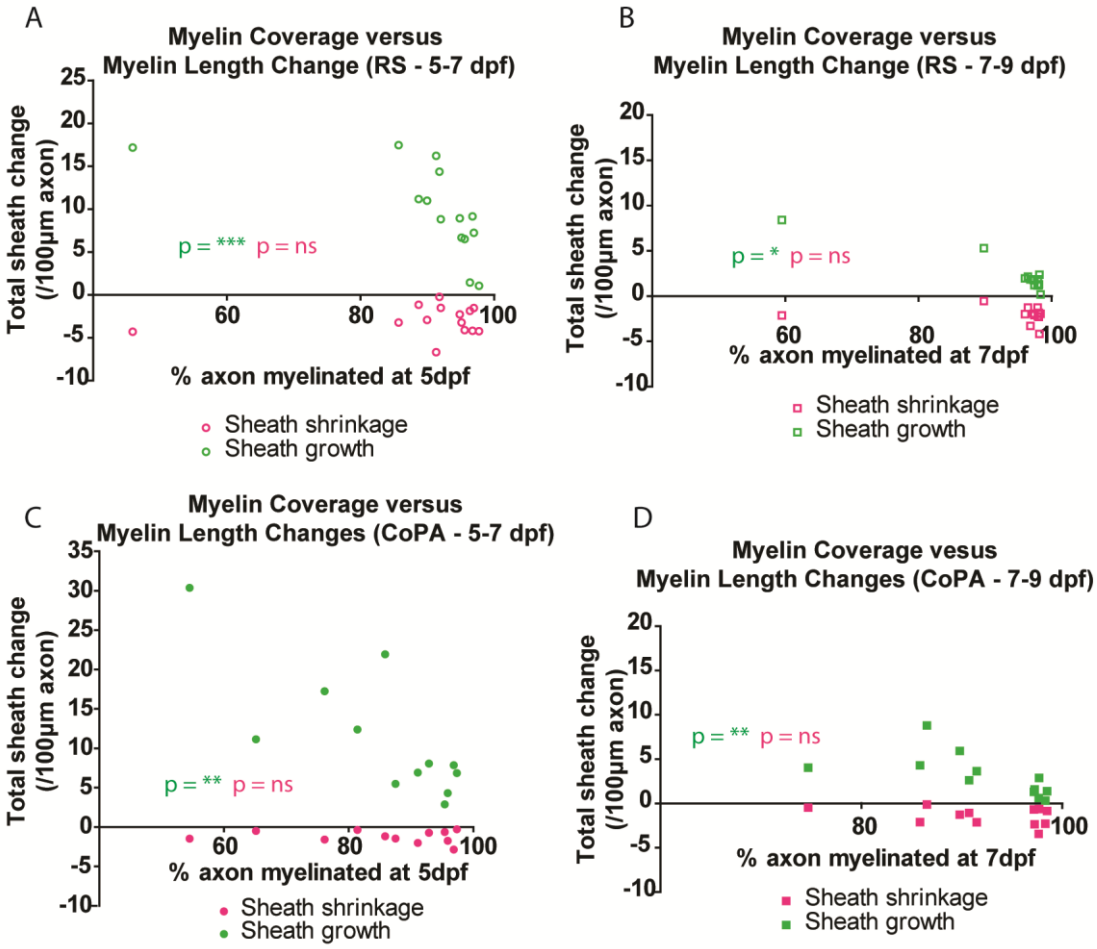

Figure 16 - correlations between changes in sheath length and myelin coverage along RS and CoPA axons.

A) The RS axon 5-7 dpf sheath growth (green data points) and sheath shrinkage (magenta data points) measurements plotted against % of axon myelinated at 5 dpf. There was a significant inverse correlation between sheath growth and % axon myelinated (Spearman's correlation test, p = 0.0001, r = -0.851, n = 14). There was no statistically significant correlation between sheath shrinkage and % axon myelinated (Spearman's correlation test, p = 0.982, n = 14). **B)** The RS axon 7-9 dpf sheath growth and sheath shrinkage measurements plotted against % of axon myelinated at 7 dpf. There was a significant inverse correlation between sheath growth and % axon myelinated (Spearman's correlation test, p = 0.019, r = -0.618, n = 14). There was no statistically significant correlation between sheath shrinkage and % axon myelinated (Spearman's correlation test, p = 0.409, n = 14). **C)** The CoPA axon 5-7 dpf sheath growth and sheath shrinkage measurements plotted against % of axon myelinated at 5 dpf. There was a significant inverse correlation

between sheath growth and % axon myelinated (Spearman's correlation test, p = 0.006, r = -0.741, n = 12). There was no statistically significant correlation between sheath shrinkage and % axon myelinated (Spearman's correlation test, p = 0.812, n = 12). **D)** The CoPA axon 7-9 dpf sheath growth and sheath shrinkage measurements plotted against % of axon myelinated at 7 dpf. There was a significant inverse correlation between sheath growth and % of axon myelinated (Spearman's correlation test, p = 0.003, r = -0.783, n = 12). There was no statistically significant correlation between sheath shrinkage and % axon myelinated (Spearman's correlation test, p = 0.265, n = 12).

3.2.9. Correlation of Myelin Remodelling with Axon Growth

Recent research has shown that individual myelin sheaths continue to grow after initial myelination at the rate of overall body growth (Auer et al., 2018). It is hypothesised that this is to ensure that the myelin coverage along axons in functioning circuits remains consistent as the animal, and in turn the axons, grow in size. For example, the RS axons involved in escape response behaviour are myelinated very early in development, but escape response behaviour must be maintained through to adulthood (when the animal has grown in size many-fold). If these myelin sheaths did not respond to growth in axon length then the relative myelin pattern along the axon would change. Altering the relative myelin pattern could adjust the conduction speed along the axon, which might affect circuit function and behaviour.

To investigate how axon growth affects myelin remodelling along RS and CoPA axons, I plotted the overall change in myelin sheath length, myelin growth, and shrinkage values against change in axon length (**Figure 17**). To calculate the change in axon length over time, I measured the distance between the first and last collateral branch along the region of axon imaged. Assuming that the position of these branching collaterals on the axon is fixed, any change in the distance between these collaterals over time should reflect change in the length of this region of axon. For CoPA axons, change in axon length could only be calculated for seven out of the twelve cells; this was

because the branching location of collaterals could not be determined for five CoPA axons (CoPA 3, 4, 5, 9, and 11).

The overall change in sheath length correlated with changes in axon length along RS axons both between 5 to 7 dpf and between 7 to 9 dpf (**Figure 17A-B**, Pearson's and Spearman's correlation tests, see **Figure 17** legend for statistics). When broken down into sheath growth and sheath shrinkage, sheath growth significantly correlated with change in axon length 5-7 dpf but not 7-9 dpf (**Figure 17C-D**, Pearson's correlation tests, see **Figure 17** legend for statistics), while sheath shrinkage did not correlate with change in axon length at either time point (**Figure 17C-D**, Pearson's and Spearman's correlation tests, see **Figure 17** legend for statistics). The lack of correlation between sheath growth or shrinkage and change in axon length 7-9 dpf (**Figure 17D**) appeared to be contradictory to the correlation between overall change in sheath length and change in axon length (**Figure 17B**). However, the correlation between sheath shrinkage and change in axon length may be underpowered ($p = 0.074$, suggesting that it may approach significant with increased sample size).

For CoPA axons, the overall change in sheath length did not correlate with change in axon length between 5-7 dpf, but did become significant between 7 to 9 dpf (**Figure 17E-F**, Pearson's correlation tests, see **Figure 17** legend for statistics). When broken down into sheath growth and sheath shrinkage, sheath growth did not significantly correlate with change in axon length 5-7 dpf, but did significantly correlate 7-9 dpf (**Figure 17G-H**, Pearson's and Spearman's correlation tests, see **Figure 17** legend for statistics). However, the lack of correlation in both overall change in sheath length and sheath growth with change in axon length may be underpowered due to the reduced sample size, as there appeared to be a trend in both cases. Sheath shrinkage did not correlate with change in axon length at either time point (**Figure 17G-H**, Pearson's and Spearman's correlation test, see **Figure 17** legend for statistics).

Based on these results, I concluded that sheath growth can correlate with change in axon length for both RS and CoPA axons, but that sheath shrinkage does not correlate with change in axon length. This provides further evidence that sheath growth and sheath shrinkage are independently regulated types of myelin sheath remodelling.

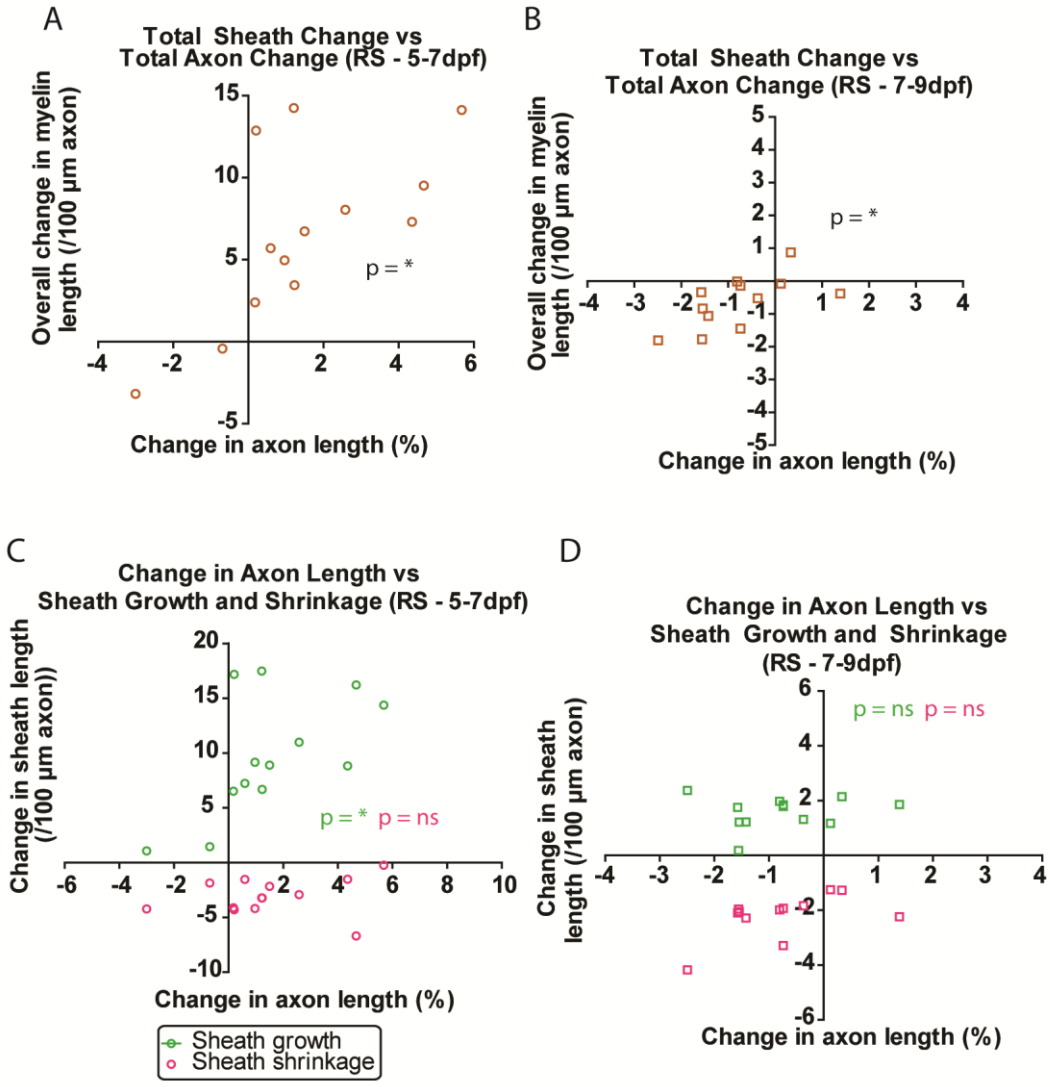

Figure 17 – correlations between changes in sheath length and changes in axon length (continued on next page).

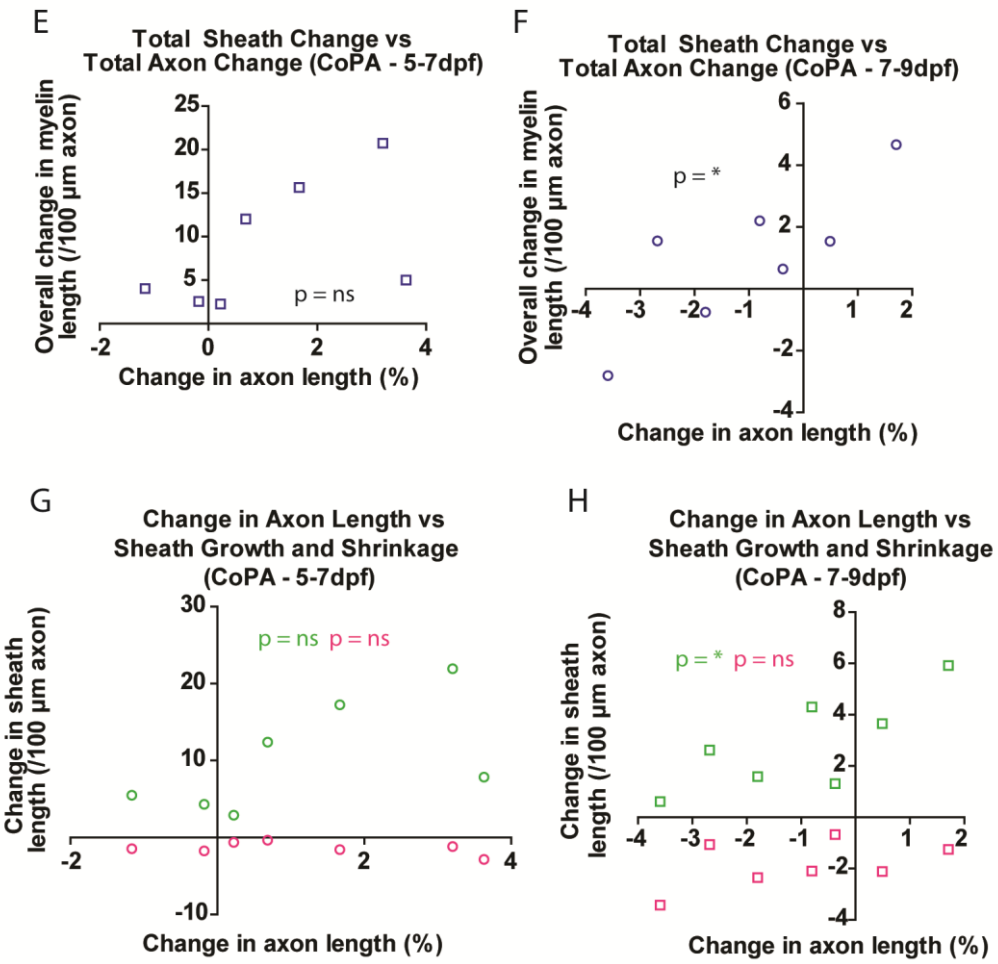

Figure 17 (continued).

A) The total change in sheath length along RS axons 5-7 dpf plotted against the total change in axon length 5-7 dpf. There was a statistically significant correlation between the two measurements (Pearson's correlation test, p = 0.012, r = 0.673, n = 14). **B)** The total change in sheath length along RS axons 7-9 dpf plotted against the total change in axon length 7-9 dpf. There was a statistically significant correlation between the two measurements (Spearman's correlation test, p = 0.042, r = 0.594, n = 14). **C)** The sheath growth and shrinkage along RS axons 5-7 dpf plotted against the total change in axon length 5-7 dpf. There was a statistically significant correlation between sheath growth and change in axon length (Pearson's correlation test, p = 0.031, r = 0.598, n = 14); there was no significant correlation between sheath shrinkage and change in axon length (Pearson's correlation test, p = 0.497, n = 14). **D)** The sheath growth and shrinkage along RS axons 7-9 dpf plotted against the total change in axon length 7-9 dpf. There was no significant correlation between sheath growth and change in axon length

(Spearman's correlation test, p = 0.697, n = 14); there was no significant correlation between sheath shrinkage and change in axon length (Pearson's correlation test, p = 0.074, n = 14). **E)** The total change in sheath length along CoPA axons 5-7 dpf plotted against the total change in axon length 5-7 dpf. There was no significant correlation between the two measurements (Pearson's correlation test, p = 0.202, n = 12). **F)** The total change in sheath length along CoPA axons 7-9 dpf plotted against the total change in axon length 7-9 dpf. There was a statistically significant correlation between the two measurements (Pearson's correlation test, p = 0.026, r = 0.815, n = 12). **G)** The sheath growth and shrinkage along CoPA axons 5-7 dpf plotted against the total change in axon length 5-7 dpf. There was no significant correlation between sheath growth and change in axon length (Spearman's correlation test, p = 0.139, n = 12); there was no significant correlation between sheath shrinkage and change in axon length (Pearson's correlation test, p = 0.318, n = 12). **H)** The sheath growth and shrinkage along CoPA axons 7-9 dpf plotted against the total change in axon length 7-9 dpf. There was a statistically significant correlation between sheath growth and change in axon length (Pearson's correlation test, p = 0.040, r = 0.776, n = 12); there was no significant correlation between sheath shrinkage and change in axon length (Spearman's correlation test, p = 0.383, n = 12).

3.2.10. Remodelling of Nodal Gaps over Time

The length of nodes of Ranvier is another parameter which can be adjusted to modify conduction properties of an axon. In the rodent cortex, nodes identified by Na^+ channel and Caspr expression can vary in length by almost nine-fold, and computational modelling indicates that subtle changes to node length could have a significant impact on conduction speeds (Arancibia-Cárcamo et al., 2017). Changing node length could either adjust the density of Na^+ channels, or allow for increased number of Na^+ channels per node. However, whether node length changes over time remains unknown.

Node length may be controlled by the length of the flanking myelin sheaths. Myelin sheaths along both RS and CoPA axons show limited changes in length after 7 dpf; however, even subtle changes in sheath length could have profound effects on node length. Hence, it is possible that node lengths also

change over time, and that these changes continue after the predominance of sheath length remodelling has ceased.

The reporter RFP-Cntn1a does not specifically label mature nodes, but rather all of the unmyelinated gaps between sheaths. Thus, it is not possible to definitively analyse mature node lengths in this data set. However, the long unmyelinated gaps, which presumably do not reflect nodes of Ranvier, can be eliminated from the data set by analysing only the short unmyelinated gaps (Cntn1a-labelled gaps which were < 5 µm in length). These gaps were termed 'nodal gaps' (**Figure 18A**).

To determine if nodal gaps are adjusted along RS and CoPA axons, the mean change in nodal gap length was calculated per axon 5-7 dpf and 7-9 dpf. Only axons where all of the nodal gaps along the axon could be accurately measured were included in the analysis. For RS axons the overall mean change in nodal gap length was -0.39 µm 5-7 dpf, which significantly declined to -0.09 µm 7-9 dpf (paired t-test, $p = 0.003$, **Figure 18B**). For CoPA axons, the overall mean change in nodal gap length was -0.43 µm 5-7 dpf, and also significantly declined to -0.11 µm 7-9 dpf (paired t-test, $p = 0.037$, **Figure 18C**). Therefore, nodal gaps reduce in length during myelin pattern establishment, but the degree of node refinement significantly declines after 7 dpf along both RS and CoPA axons.

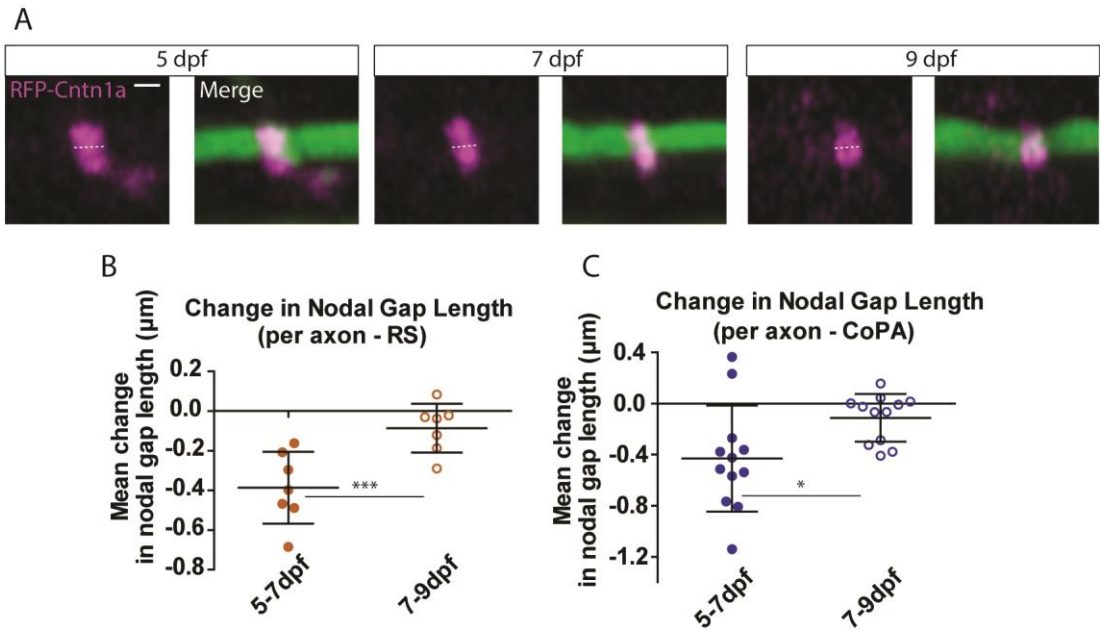

Figure 18 – changes in nodal gap length along RS and CoPA axons.

A) Images of a single nodal gap between two sheaths at 5 dpf, 7 dpf, and 9 dpf. White dotted line = the length of the nodal gap. Nodal gaps were defined as unmyelinated gaps < 5 µm in length. **B)** The mean change in nodal gap length per RS axon over time. Only axons where all nodal gaps along the axon could be confidently measured were included in the analysis. The overall mean change in nodal gap length was -0.39 µm (SD = 0.18) 5-7 dpf, and -0.09 µm (SD = 0.12) 7-9 dpf. There was a statistically significant change in mean change in nodal gap length over time (paired t-test, p = 0.003, n = 7). **C)** The mean change in nodal gap length per CoPA axon over time. The overall mean change in nodal gap length was -0.43 µm (SD = 0.42) 5-7 dpf, and -0.11 µm (SD = 0.19) 7-9 dpf. There was a statistically significant change in mean nodal gap length over time (paired t-test, p = 0.037, n = 12). Scale bar = 1 µm.

Although both RS and CoPA axons showed similar extents of myelin sheath remodelling, it is possible that they differ in the extent of refinement of nodes of Ranvier. To investigate this, the change in nodal gap length was compared between RS and CoPA axons by Two-Way ANOVA. There was no significant difference between the two cell types (Two-Way ANOVA, p = 0.710).

Based on these results, I concluded that nodal gap length refinement declines significantly after 7 dpf along both RS and CoPA axons, and that these two axon subtypes showed no differences in the extent of nodal gap refinement that occurs.

3.2.11. Time-Course Measurement of Sheath Thickness by Electron Microscopy

By live imaging myelinated RS and CoPA axons, I was able to assess the number and length of myelin sheaths along the axon. Sheath thickness is another important parameter which contributes to myelin patterns, and which could be remodelled over time. The current gold-standard method of measuring sheath thickness is by imaging cross-sections of myelinated axons via transmission electron microscopy, which provides nanometre scale resolution. Such resolution is required to detect differences in sheath thickness, which may only be a few layers of lipid membrane thick. The extent and timing of sheath thickness remodelling can be inferred performing by electron microscopy analysis at various ages.

Electron microscopy was used to investigate how myelin sheath thickness changes during the same time period in which live imaging of myelinated axon development was performed (5-9 dpf). Dr. Jenea Bin performed the chemical fixation, dehydration, and embedding of 5, 7, and 9 dpf larval zebrafish, and then both myself and Dr. Bin performed sectioning, staining, and imaging of these prepared samples. When sectioning the embedded larvae, a distinct point of the spinal cord was selected to ensure that samples were comparable – this was the middle region of the trunk, where the ventral fins are divided by the cloaca (**Figure 19A**). In a cross section of the zebrafish spinal cord (**Figure 19A**), the axonal tracts are located on the lateral sides with the cell bodies of neurons located in the centre. There are two tracts of large-diameter axons which are myelinated in each hemispinal cord. These are: the ventral tract, where the predominance of myelinated axons will be of reticulospinal neurons, including the very large-diameter Mauthner axon (**Figure 19C**); and the dorsal tract, which includes the dorsal portion of axons from CoPA cells originating

caudal to the site of sectioning (**Figure 19B**). The dorsal and ventral tracts are separated by much smaller-diameter axons and processes, the majority of which are not myelinated. The occasional myelinated axon can be found in between the dorsal and ventral tracts, which likely represents myelinated axons (like CoPA axons) which cross from ventral to dorsal, or vice versa.

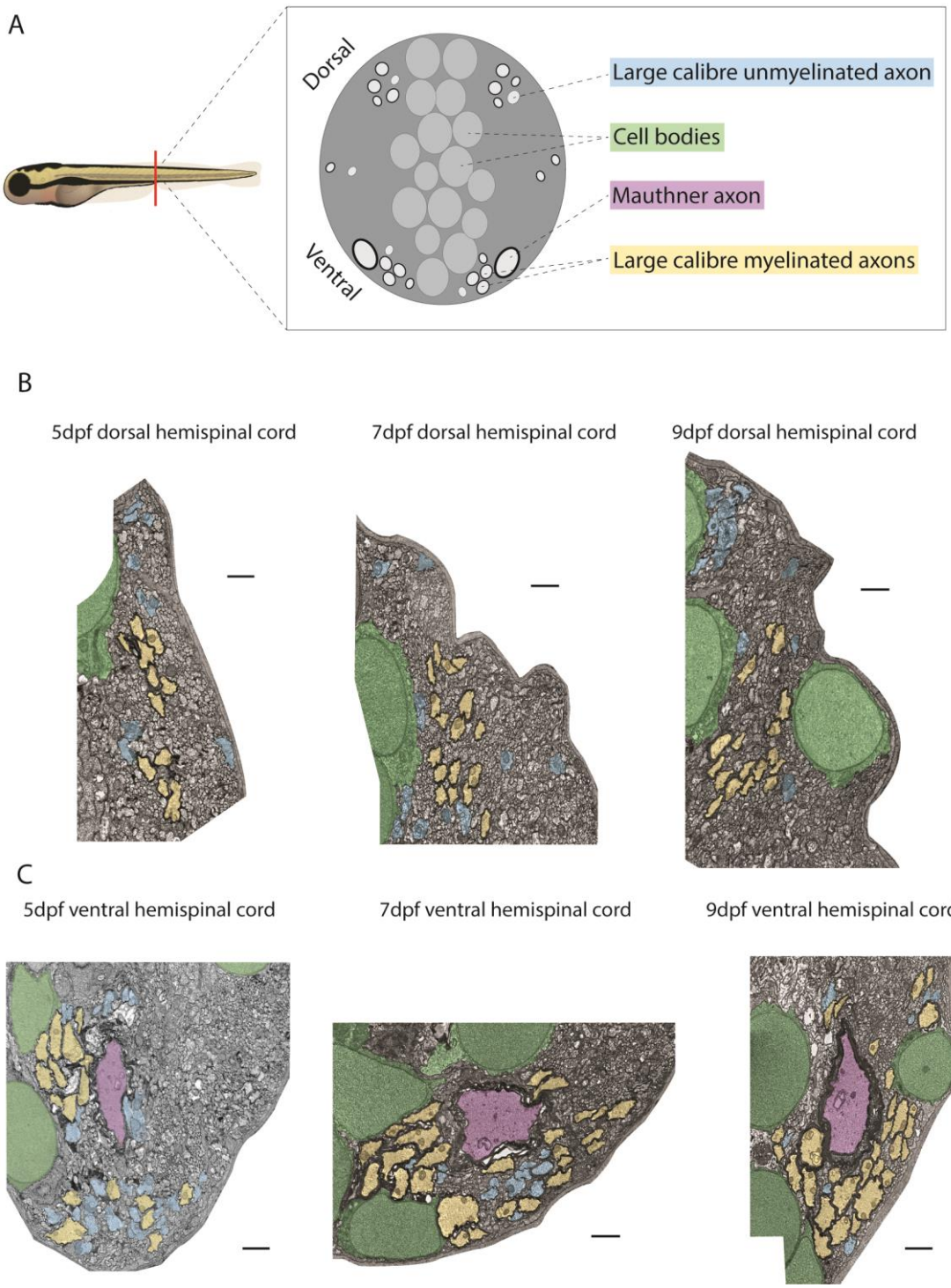

Figure 19 – assessing myelin sheath thickness in the zebrafish spinal cord over time by transmission electron microscopy.

A) A schematic highlighting the location of sections cut for transmission electron microscopy. Transverse sections were cut at the cloaca (approximately somite 15 – red line). Inset: a schematic of a transverse section of the larval zebrafish spinal

cord, with labels colour coded to match pseudo-colouring of features in images below. **B)** Example images of the dorsal spinal cord at 5 dpf, 7 dpf and 9 dpf; myelinated axons are highlighted in yellow, unmyelinated large diameter axons are highlighted in blue. **C)** Example images of the ventral spinal cord at 5 dpf, 7 dpf and 9 dpf. The largest axon (Mauthner) is highlighted in purple. Scale bars = 1 µm.

3.2.12. Sheath Thickness Change in the Dorsal and Ventral Tracts

The number and g-ratios of all myelinated axons in the dorsal or ventral tract were measured at 5, 7, and 9 dpf. The mean number of myelinated axons in the dorsal tract did not significantly change between different ages, being 13.7 at 5 dpf, 19.8 at 7 dpf, and 17.2 at 9 dpf (One-Way ANOVA, p = 0.110, **Figure 20A**). However, it did significantly increase between 5-7 dpf in the ventral tract, being 16.0 at 5 dpf, 26.8 at 7 dpf, and 26.6 at 9 dpf (One-Way ANOVA, p = 0.009, Tukey's Multiple Comparisons test, **Figure 20B**).

The g-ratio of a myelinated axon is the axon diameter divided by the myelin sheath diameter. However, the quality of larval zebrafish spinal cord tissue preservation is not as high as it is for standard rodent electron microscopy; axons in the zebrafish spinal cord rarely retain a circular shape which makes it difficult to decide which diameter to measure. Instead, the area of the axon and the area of the axon plus myelin sheath were measured and the diameters calculated assuming the axons should have a circular shape (where area = $\pi.r^2$). Using these calculations, the g-ratios of all myelinated axons in the dorsal and ventral spinal cord were plotted against axon diameter (**Figure 20C-D**). It has already been well-established that myelin sheath thickness correlates with the diameter of the axon (Hildebrand and Hahn, 1978). In accordance with this, there was a highly-significant correlation between axon diameter and g-ratio at all ages for both dorsal and ventral tract myelinated axons (**Figure 20C-D**, Pearson's correlation tests, see **Figure 20** legend for statistics).

To assess how sheath thickness changes over time, the same population of axons needs to be analysed at each age; for example, if sheaths on axons myelinated before 5 dpf increase in thickness between 5-7 dpf, but there are

also thin sheaths formed on previously unmyelinated axons between 5-7 dpf, then the average change in g-ratio of all myelinated axons will be negligible. Thus, to compare g-ratios between the different ages, only the g-ratios of the ten largest-diameter axons (excluding Mauthner) in each animal were selected, to ensure that the same population of axons was analysed at each age. The mean dorsal tract g-ratio per animal did not change between different ages, being 0.81 at 5 dpf, 0.82 at 7 dpf, and 0.82 at 9 dpf (One-Way ANOVA, $p = 0.705$, **Figure 20E**). The mean ventral tract g-ratio per animal also did not significantly change between different ages, being 0.82 at 5 dpf, 0.85 at 7 dpf, and 0.83 at 9 dpf (One-Way ANOVA, $p = 0.121$, **Figure 20F**).

It is possible for a change in sheath thickness over time to be undetected by g-ratio analysis if the axon diameter also increased over time. To address this, the diameters of the ten largest-diameter axons in the dorsal and ventral tracts were analysed 5-9 dpf. However, there was no significant difference in the overall mean axon diameter between different ages in the dorsal tract, being 636.0 nm at 5 dpf, 691.4 nm at 7 dpf, and 650.5 nm at 9 dpf (One-Way ANOVA, $p = 0.626$, **Figure 20G**); nor in the ventral tract, being 702.7 nm at 5 dpf, 868.1 nm at 7 dpf, and 817.2 nm at 9 dpf (One-Way ANOVA, $p = 0.138$, **Figure 20H**).

There may be small but significant changes in sheath thickness over the time period analysed, but this data set is too underpowered to detect them. For example, a power calculation shows that the comparison of g-ratio of ventral myelinated axons at 5 and 7 dpf (**Figure 20F**) has only 30% power with five samples per group. A sample size of 16 per group would be required to reach 80% power.

Based on this data, I concluded that there were no large changes in sheath thickness 5-9 dpf in the zebrafish spinal cord. However, it is not possible to conclude whether or not myelin sheaths exhibit smaller changes in sheath thickness between 5-9 dpf.

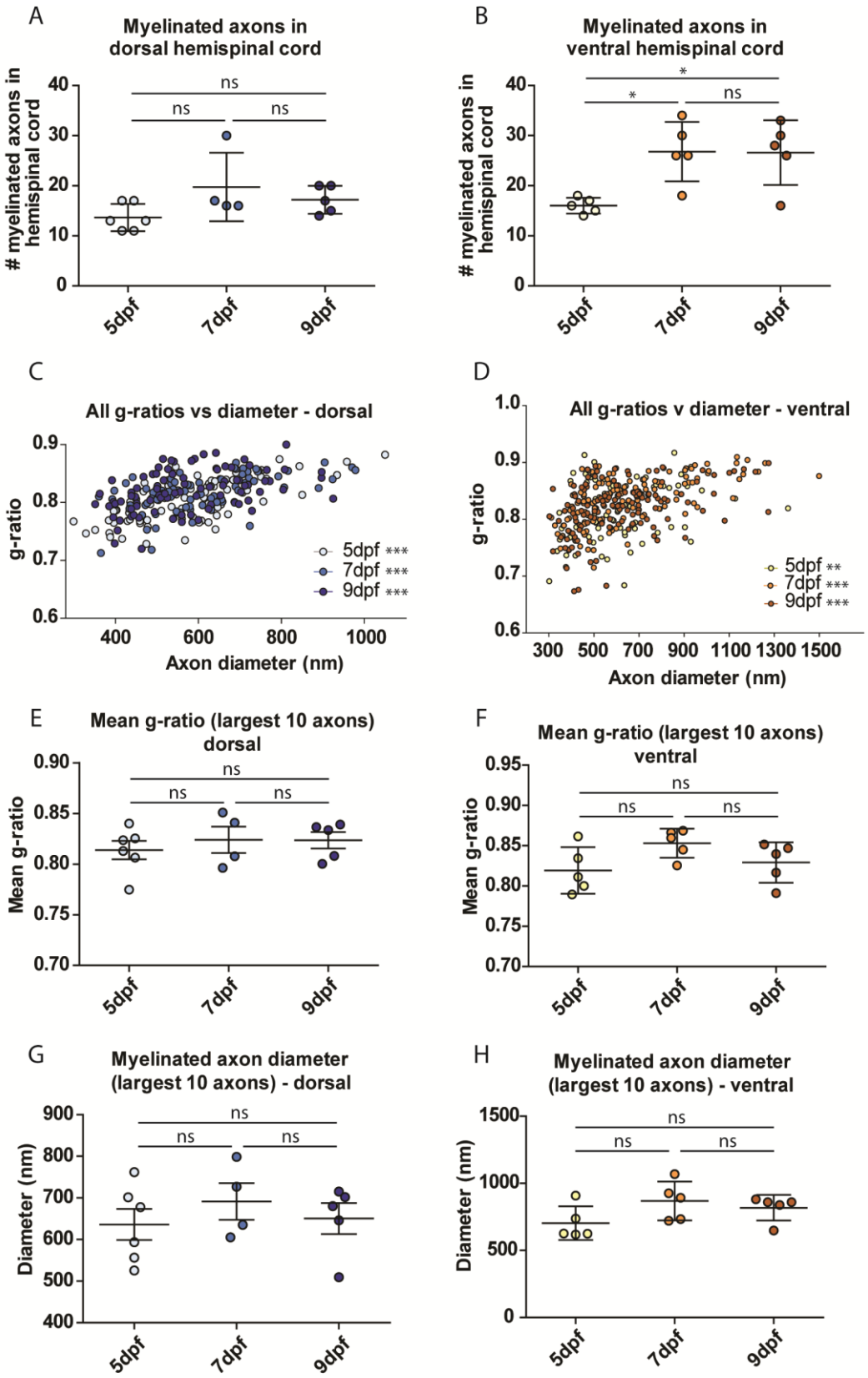

Figure 20 – sheath thickness on myelinated axons in the dorsal and ventral spinal cord.

A) The number of myelinated axons in a dorsal hemispinal cord at 5 dpf, 7 dpf, and 9 dpf. The mean number of myelinated axons was 13.7 (SD = 2.7) at 5 dpf, 19.8 (SD = 6.9) at 7 dpf, and 17.2 (SD = 2.8) at 9 dpf. There was no statistically significant change in the number of myelinated axons with age (One-way ANOVA, p = 0.110, 5 dpf n = 6, 7 dpf n = 4, 9 dpf n = 5). **B)** The number of myelinated axons (excluding Mauthner) in a ventral hemispinal cord at 5 dpf, 7 dpf, and 9 dpf. The mean number of myelinated axons was 16.0 (SD = 1.6) at 5 dpf, 26.8 (SD = 5.9) at 7 dpf, and 26.6 (SD = 6.5) at 9 dpf. There was a statistically significant increase in the number of myelinated axons with age (One-way ANOVA, p = 0.009; Tukey's Multiple Comparisons test: 5 dpf vs 7 dpf p = *, 5 dpf vs 9 dpf p = *, 7 dpf vs 9 dpf p = ns. 5 dpf n = 5, 7 dpf n = 5, 9 dpf n = 5). **C)** The g-ratios of all dorsal myelinated axons plotted against axon diameter. There was a statistically significant correlation between g-ratio and axon diameter at all ages (Pearson's correlation test; 5 dpf p < 0.0001, r = 0.681, n = 82 axons; 7 dpf p < 0.0001, r = 0.552, n = 79 axons; 9 dpf p < 0.0001, r = 0.418, n = 86 axons). **D)** The g-ratios of all ventral myelinated axons plotted against axon diameter. There was a statistically significant correlation between g-ratio and axon diameter at all ages (Pearson's correlation test; 5 dpf p = 0.006, r = 0.303, n = 80 axons; 7 dpf p < 0.0001, r = 0.576, n = 132 axons; 9 dpf p < 0.0001, r = 0.409, n = 128 axons). **E)** The mean g-ratio of the 10 largest dorsal myelinated axons per animal at 5 dpf, 7 dpf, and 9 dpf. The overall mean g-ratio was 0.81 (SD = 0.02) at 5 dpf, 0.82 (SD = 0.03) at 7 dpf, and 0.82 (SD = 0.02) at 9 dpf. There was no statistically significant change in g-ratio with age (One-way ANOVA, p = 0.705, 5 dpf n = 5, 7 dpf n = 5, 9d pf n = 5). **F)** The mean g-ratio of the 10 largest ventral myelinated axons per animal at 5 dpf, 7 dpf, and 9 dpf. The overall mean g-ratio was 0.82 (SD = 0.03) at 5 dpf, 0.85 (SD = 0.02) at 7 dpf, and 0.83 (SD = 0.03) at 9 dpf. There was no statistically significant change in g-ratio with age (One-way ANOVA, p = 0.121, 5 dpf n = 5, 7 dpf n = 5, 9 dpf n = 5). **G)** The mean diameter of the 10 largest dorsal myelinated axons per animal at 5 dpf, 7 dpf, and 9 dpf. The overall mean myelinated axon diameter was 636.0 nm (SD = 91.8) at 5 dpf, 691.4 nm (SD = 88.2) at 7 dpf, and 650.5 nm (SD = 83.2) at 9 dpf. There was no statistically significant change in myelinated axon diameter with age (One-way ANOVA, p = 0.626, 5 pf n = 5, 7 dpf n = 5, 9 dpf n = 5). **H)** The mean diameter of the 10 largest ventral myelinated axons per animal at 5 dpf, 7 dpf, and 9 dpf. The overall mean myelinated axon diameter was 702.7 nm (SD = 125.4) at 5 dpf, 868.1 nm (SD = 144.8) at 7 dpf, and 817.2 nm (SD = 95.7) at 9 dpf. There was no

statistically significant change in myelinated axon diameter with age (One-way ANOVA, p = 0.138, 5 dpf n = 5, 7 dpf n = 5, 9 dpf n = 5).

3.2.13. Improving the Quality of Zebrafish Electron Microscopy Using High-Pressure Freezing Techniques

As discussed in section '3.2.11 Time-Course Measurement of Sheath Thickness by Electron Microscopy', the quality of zebrafish larval tissue fixed using conventional chemical fixation techniques is generally much poorer than typically seen in rodent tissue. The shapes of axon and myelin sheath cross sections are often distorted, making any measurement of axon diameters and g-ratios challenging to perform. One method in which sheath thickness could be measured would be to count the number of myelin wraps contained within a sheath. However, the quality of chemically fixed larval zebrafish spinal cord tissue is rarely good enough to distinguish the individual wraps in myelin sheaths. There is a need to improve the quality of zebrafish electron microscopy to facilitate more accurate and reliable quantification of myelin sheath ultrastructure.

High-pressure freezing fixation has been described to vastly improve the quality of tissue ultrastructural preservation, in both rodents and zebrafish, for electron microscopy (Möbius et al., 2016, 2010). This technique relies on the extremely rapid freezing of tissue to liquid nitrogen temperature under high pressure, followed by osmium fixation and dehydration whilst frozen, before warming up to room temperature for embedding and sectioning as per normal electron microscopy protocols (Möbius et al., 2010). I decided to test whether high-pressure freezing could improve the quality of zebrafish larvae spinal cord tissue preservation to allow for more accurate quantification of myelin sheath thickness.

In collaboration with Dr. Joanna Brown, I performed preliminary tests of a high-pressure freezing protocol using 5 dpf zebrafish larvae. The successfully processed larvae were imaged using the same transmission electron microscope, and are shown in comparison to equivalent chemically-fixed larva

tissue in **Figure 21**. The shapes of axonal structures were vastly different using high-pressure freezing, appearing to retain a more circular shape. Additionally, the contrast and clarity of membranes was significantly improved using high-pressure freezing. For example, a high magnification image of the Mauthner axon showed that individual wraps of membrane could be seen in tissue preserved using high-pressure freezing (**Figure 21E-F**).

There were, nevertheless, some drawbacks to this method. The throughput of the tissue processing protocol was low (possibly due to the complexity of the preparation and lack of expertise in this new technique); therefore, insufficient sample numbers were acquired to perform any formal quantification. Additionally, the tissue preservation quality was not perfect – freeze damage was observed in several samples, and even the best preserved samples had signs of tissue damage (**Figure 21D**). Furthermore, the preservation of some cellular structures was not improved. Some membranes had poorer fixation than others, while the distinctive 'dotted' microtubule structure within axons was often poorly preserved with high-pressure freezing (**Figure 21F**).

The quality of zebrafish spinal cord tissue preservation for electron microscopy can thus be significantly improved by fixation using high-pressure freezing. Yet, this technique requires greater optimisation to further increase the quality of cell ultrastructure preservation for sheath thickness analysis.

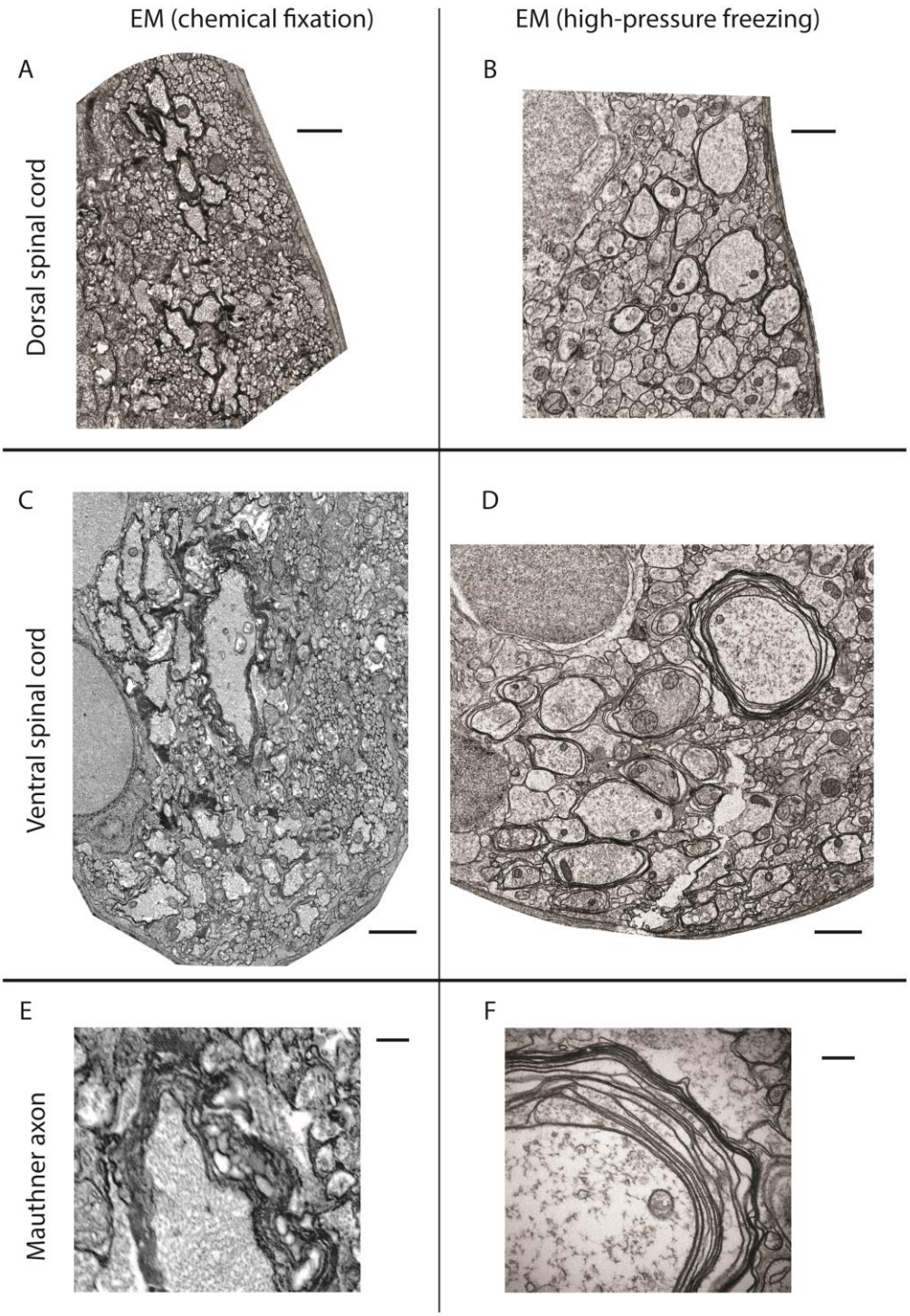

Figure 21 – high-pressure freezing can improve the preservation quality of zebrafish spinal cord tissue for transmission electron microscopy.

A, C and E) Transmission electron micrographs of various regions of the zebrafish spinal cord obtained using conventional chemical fixation techniques. **B, D and F)**

Transmission electron micrographs of the zebrafish spinal cord obtained using high-pressure freezing techniques. Scale bars in A-D = 1 µm; scale bars in E-F = 200 nm.

3.2.14. Conclusion

Here, I have characterised the myelin patterns of two distinct subtypes of myelinated axon in the zebrafish spinal cord. I have found that, for both RS and CoPA axons, the majority of parameters affecting myelin patterns (such as sheath number, sheath length, and nodal gap length) are established within a critical period after the onset of myelination, after which they showed no significant change. Individual myelin sheaths can undergo remodelling (either by growing or shrinking longitudinally, or even being completely retracted from the axon), but the predominance of this remodelling occurs by 7 dpf. Despite using distinct signals to regulate their initial myelination, RS and CoPA axons show remarkable similarities in both the myelin patterns established and the degree of myelin remodelling which occurs within this critical developmental period.

3.3. Discussion

3.3.1. Myelin Patterns are Established within a Defined Developmental Window

Changing myelin sheath parameters such as number, length, and thickness is predicted to adjust conduction speeds within circuits (Waxman, 1980). Establishing a specific myelin pattern may be crucial for circuit function. How and when such myelination patterns are established are important questions concerning the emergence of circuit function. Here, I have found that the myelin patterns along individual axons in the zebrafish spinal cord are established within a defined time window after the onset of myelination. Both RS and CoPA axons begin to be myelinated at approximately 3 dpf (Koudelka et al., 2016; Mensch, 2014); the majority of their myelin sheaths are formed by 5 dpf, and there is some adjustment to sheath number and length by 7 dpf. However, after 7 dpf the sheath number, length, and length variability exhibit very little change. These results confirm previously reported findings that

myelin sheaths become stable several days after initial formation (Auer et al., 2018), and indicate that such stability is consistently established along different axonal subtypes.

Why do these myelin patterns stabilise during this time period? One possibility is that stability reflects establishment of behaviours regulated by the circuits being myelinated. For example, hunting behaviour emerges in larval zebrafish at approximately 4-5 dpf (Muto and Kawakami, 2013), and the prey capture response continues to develop over the following 2-3 days (Budick and O'Malley, 2000). This behaviour is regulated by the MeLr and MeLc RS neurons (Gahtan et al., 2005). It is possible that adjustments to the myelin patterns (and, therefore, conduction properties) along these particular axons occur 5-7 dpf in response to experience as the larvae learns how to hunt. These patterns may subsequently become stable once an optimal hunting strategy has been learned. Alternatively, sheaths may stabilise regardless of experience or learning. Whether the myelin patterns along RS and CoPA axons can be altered by experience after 7 dpf is not clear. It would be fascinating to see whether inducing locomotor behaviours (using visual stimuli such as the optomotor response, or increasing exposure to paramecia prey) or increasing sensory stimulation (such as repeated tactile stimuli) could change the myelin patterns along RS and CoPA axons after 7 dpf. However, live imaging of sheaths in the adult rodent somatosensory cortex demonstrated that myelin sheaths remain highly stable even with increased sensory stimulation (Hughes et al., 2018), suggesting that experience does not significantly alter myelin patterns after their formation.

How do myelin patterns change later in life with continued growth? I have shown that the overall change in sheath length along RS (5-9 dpf) and CoPA (7-9 dpf) axons significantly correlates with change in axon length. Similarly, Auer et al., 2018 demonstrated that stable myelin sheaths continue to grow at the rate of overall body growth for at least three weeks after initial sheath formation. This suggests that the myelin patterns established along axons are simply scaled up with body growth. Given that an organism can increase in size by several-fold throughout development, do myelin sheaths continue to

grow indefinitely with body size? Or is there a threshold after which new myelin sheaths must be added to maintain constant myelin coverage? Imaging individual RS and CoPA axons first at 7 dpf, and then at 1-2 months post-fertilisation, could assess if and how myelin patterns change with significant body growth. However, as zebrafish develop they become progressively less transparent, which makes live imaging at subcellular resolution technically challenging. Pigment mutants, such as the *nacre* line, can increase optical transparency, and imaging techniques such as two-photon or three-photon microscopy (which allows for imaging of deeper tissues) could be used to address these questions.

3.3.2. Individual Myelin Sheaths can be Retracted or Remodelled

I found that, once formed, myelin sheaths along RS and CoPA axons can either be fully retracted or can be remodelled by growing or shrinking in length.

Sheath Retractions

Virtually all of the sheaths which retracted were under 10 µm in length (only one retracted sheath was longer than 10 µm; this sheath was 10.6 µm in length). These results are concurrent with previous observations in the zebrafish spinal cord that retracted sheaths never exceed 10 µm in length (Hines et al., 2015). Between 5 to 7 dpf, sheath length can somewhat predict a sheath's fate – 75% of sheaths under 5 µm in length were retracted, while only 20% of sheaths 5-10 µm in length were retracted, and just one sheath (5.3%) 10-15 µm in length was retracted during the time period analysed. Only two sheaths were retracted after 7 dpf, and both were also under 10 µm in length. These findings suggest that short sheaths are unstable, that sheaths become progressively more stable with longitudinal growth, and are fully stabilised once over 10µm.

What triggers sheath retraction? Bare, unmyelinated axon was never observed after sheath retraction, as the neighbouring sheaths always grew to fill the gap left behind. It is not clear whether sheath retraction occurs before growth of the neighbour sheaths, or whether sheath retraction and neighbouring sheath

growth occur simultaneously. One possibility is that the growth of neighbouring sheaths puts physical pressure on short unstable sheaths to trigger their retraction. Timelapse analysis of sheath dynamics along individual axons could determine whether retraction and neighbouring growth occur in sequence or in parallel.

Alternatively, a signal from the axon itself may initiate sheath retraction. Ca^{2+} imaging in oligodendrocytes has shown that distinct Ca^{2+} events occur in individual myelin sheaths during early growth, and that some of these events are triggered by neuronal activity (Baraban et al., 2018; Krasnow et al., 2018). Interestingly, long-duration high-amplitude Ca^{2+} events seem to predict sheath retraction (Baraban et al., 2018). These sheath retractions are mediated by the Ca^{2+}-dependent protease calpain. This suggests that certain patterns of Ca^{2+} signalling in myelin sheaths can trigger retractions. However, it is not clear if these long-duration high-amplitude Ca^{2+} events occur in response to neuronal activity. Further investigation of sheath retractions along individual axons where activity has been manipulated could elucidate whether activity plays a role in initiating sheath retractions. This will be investigated in Chapter 4.

Sheath Growth and Shrinkage

Individual myelin sheaths along RS and CoPA axons can either grow or shrink in length between 5 to 9 dpf. Sheath growth primarily occurs by 7 dpf, after which the extent of growth significantly declines. This is likely because sheath growth inversely correlates with the amount of myelin along the axon, and by 7 dpf both RS and CoPA axons are well myelinated. However, sheath growth may not be limited to unmyelinated axonal space; sheaths can grow to fill the space left by shrinking or retracted sheaths. Again, it is not clear whether a sheath grows simultaneously or after its neighbouring sheath shrinks or retracts; timelapse analyses are required to address this question.

There is still some sheath growth after 7 dpf, and sheath growth along CoPA axons correlates with change in axon length 7-9 dpf. Again, these findings match the results of Auer et al., 2018, who found that individual sheaths can

grow very rapidly for the first few days after initial formation, and then growth declines to a baseline matching that of overall body growth.

What regulates sheath growth? Neuronal activity is one candidate – the rate of Ca^{2+} transients in myelin sheaths correlates with sheath growth, and global changes in neuronal activity in the zebrafish spinal cord induces a corresponding change in both the rate of Ca^{2+} transients and in sheath growth (Baraban et al., 2018; Krasnow et al., 2018). Whether the activity of an underlying axon directly promotes the growth of its myelin sheaths will be investigated in Chapter 4. However, there are likely to be other signals which also regulate sheath growth. For example, sheath growth may be intrinsically programmed into oligodendrocytes – cortically-derived oligodendrocytes generate shorter myelin sheaths than spinal cord-derived oligodendrocytes in an *in vitro* microfibre myelination system, reflective of the sheath lengths generated *in vivo* (Bechler et al., 2015). This suggests that the growth of cortical myelin sheaths is limited compared to spinal cord sheaths. Oligodendrocytes may have intrinsically programmed myelinating capacities which can also influence sheath growth. The number of myelin sheaths made per oligodendrocyte is largely set within the first few hours after differentiation (Czopka et al., 2013). Oligodendrocytes which form a large number of sheaths during this period may be limited in how much these sheaths can grow; while oligodendrocytes which only form a few myelin sheaths may promote their growth more to produce longer sheaths.

Sheath shrinkage appears to be regulated independently from sheath growth. The extent of sheath shrinkage along RS or CoPA axons does not significantly change between 5 to 9 dpf, and sheath shrinkage does not correlate with the available unmyelinated axonal space nor with change in axon length. It is not clear what regulates sheath shrinkage. One possibility is that a sheath shrinks when it is overcome by the growth forces of its neighbouring sheaths. However, if this was the case then the degree of sheath shrinkage would decline with sheath growth after 7 dpf. Another possibility is that oligodendrocytes have a finite myelinating capacity, and so shrinkage of a sheath occurs when the oligodendrocyte needs to focus its resources on

growing other sheaths. For instance, if an oligodendrocyte myelinates some axons which strongly promote sheath growth, then its other sheaths may shrink as a result. It is not clear whether oligodendrocytes do, indeed, have a finite myelinating capacity. Increasing the axonal surface area causes oligodendrocytes to produce more myelin sheaths than normal, which suggests that an oligodendrocyte's myelinating capacity is flexible (Almeida et al., 2011). The activity of the underlying axon may also regulate sheath shrinkage. As previously discussed, activity can influence the rate of Ca^{2+} transients in myelin sheaths which, in turn, correlates with sheath elongation (Baraban et al., 2018; Krasnow et al., 2018). Sheaths with Ca^{2+} transient rates below approximately 2/hour typically shrank in length; neuronal activity (or lack thereof) may induce such Ca^{2+} transient rates to regulate sheath shrinkage. Whether neuronal activity affects sheath shrinkage will be investigated in more detail in Chapter 4.

3.3.3. Axon Diameter and Nodal Gaps

Axonal parameters such as axon diameter and length of nodes of Ranvier can influence the conduction speed of an axon, and so changes in these parameters will also likely play an important role in regulating circuit function. I found that the diameter of RS axons increases 5-7 dpf, but remained stable thereafter, whereas CoPA axons do not change in diameter 5-9 dpf. These measurements were in accordance with previous data characterising axon diameters during larval development (Mensch, 2014).

It was not possible to measure the length of definitive nodes of Ranvier in this data set, as the axonal marker RFP-Cntn1a does not distinguish between nodes and larger stretches of unmyelinated axon. However, the majority of these gaps shrank to under 2 µm in length by 9 dpf, suggesting that proper nodes form by this time point. Mathematical modelling has suggested that small changes in node length could profoundly affect conduction velocities (Arancibia-Cárcamo et al., 2017). 'Nodal gaps' (gaps between sheaths which were shorter than 5 µm in length) reduce in length 5-9 dpf, but the degree of nodal gap length change significantly declines after 7 dpf. This indicates that,

like myelin sheaths, nodes are refined within a defined time period after the onset of myelination. In order to properly characterise the remodelling of mature nodes of Ranvier, fluorescent reporters such as FP-Caspr and FP-NF186 could be used to label the paranodes and nodes proper along individual axons.

3.3.4. RS and CoPA Axons Show Remarkably Similar Myelin Patterns and Degrees of Myelin Remodelling

RS and CoPA axons belong to locomotor and sensory circuits respectively, and research has shown that only RS axons use synaptic vesicle release to regulate their myelination (Koudelka et al., 2016). If myelin patterns are established based on circuit function, then axons from different circuits should establish their own myelin patterns. Additionally, if myelin can be remodelled by experience, then axons which use neuronal activity to mediate their myelination may exhibit more myelin remodelling than axons which do not. I hypothesised that RS and CoPA axons would establish different myelin patterns, and that RS axons would exhibit a greater degree of myelin sheath remodelling than CoPA axons. However, comparison of myelin patterns (sheath number, length, length variability, unmyelinated gap length, and length variability) and myelin remodelling (sheath retraction, sheath growth, and sheath shrinkage) showed that there were virtually no significant differences between RS and CoPA axons. The only identifiable difference was in sheath shrinkage between 5-7 dpf.

Myelin Patterns

Why do RS axons not exhibit different myelin patterns compared to CoPA axons? There are many different subtypes of RS neurons in the zebrafish mid- and hind-brain, with different RS subtypes involved in distinct locomotor circuits and behaviours. It is possible that more detailed investigation of specific RS subtype axons would identify myelin patterns specific to certain locomotor circuits. For example, MeLr and MeLc RS axons (responsible for prey capture behaviour) may exhibit slightly different myelin patterns compared to RoV3/MiV1/MiV2 RS axons (responsible for changes in

swimming direction). Moreover, each of these sub-groups of RS axons may exhibit subtle myelin pattern differences when individually compared with CoPA axons. The identities of the specific RS subtypes in this chapter's data set are not known; obtaining a sufficient sample size of one particular RS subtype would be difficult to achieve. The RS axons in this chapter were labelled by microinjecting reporter plasmid DNA into Tg(HuC:Gal4) eggs, which then led to random mosaic labelling of neurons with fluorescent reporters. On average, several hundred eggs would have to be injected to obtain between 1 to 5 larvae with isolated fluorescently-labelled RS neurons, and often several of these cells could not be followed through to 9 dpf (insufficient fluorescence signal to image at all time points was the most common problem). Labelling and imaging enough cells of a specific RS subtype using this method is not feasible. An alternative driver line could be used to increase the success rate of mosaic transgenesis; the line Tg(RS:KalTA4) expresses KalTA4 mainly in RS neurons, and so injecting a higher concentration of plasmid DNA into Tg(RS:KalTA4) eggs may be a more efficient method of labelling specific RS neuron subtypes.

RS and CoPA neurons have many similarities; they are born at approximately the same time during development, they have axons of similar diameters, and they are both glutamatergic. CoPA neurons do not use synaptic vesicle release to regulate their initial myelination (Koudelka et al., 2016). However, neurotransmitter signalling may be involved in later remodelling of myelin sheaths after their initial formation, and so may still influence establishment of myelin patterns along CoPA axons. This might explain why RS and CoPA axons have similar myelin patterns. Oligodendrocytes have been shown to detect and respond to neurotransmitters other than glutamate, such as GABA (Berger et al., 1992; von Blankenfeld et al., 1990). GABAergic neurons may signal to oligodendrocytes and myelin sheaths in a different way to glutamate, and so may lead to the formation of different myelin patterns. Many inhibitory axons are myelinated; in the mammalian CNS, myelinated GABAergic axons have been reported in all cortical layers and in underlying white matter, making up almost half of the myelinated axons in layers II/III of the rodent cortex

(Micheva et al., 2016). Tracing single myelinated axons using array tomography revealed that GABAergic axons have shorter nodal gaps and myelin sheaths than non-GABAergic axons – specific myelin patterns may be regulated by specific neurotransmitters (Micheva et al., 2016). Kolmer-Agduhr neurons, dorsal longitudinal ascending (DoLA) neurons, commissural secondary ascending neurons (CoSA), and ventral longitudinal neurons (VeLD) are all present in the zebrafish spinal cord at the same time frame as RS and CoPA axons, and have been shown to express GABA (Bernhardt et al., 1992; Higashijima et al., 2004). It would be interesting to investigate whether these axons are myelinated, and whether they exhibit distinct myelin patterns compared to the glutamatergic RS and CoPA axons. The myelination of these axons could be assessed by microinjecting eGFP and RFP-Cntn1a plasmids into pan-neuronal driver eggs (such as Tg(HuC:Gal4) or Tg(NBT:KalTA4)) and then screening for single cell expression based on previously described morphology and location (Bernhardt et al., 1992, 1990).

Myelin Remodelling

Myelin remodelling along RS axons was generally the same as CoPA axons; the only difference between the two axon subtypes was that RS axons exhibit slightly more sheath shrinkage 5-7 dpf. These findings contradict my hypothesis that axons which use activity-related signals to regulate myelination would exhibit more myelin remodelling. Why do RS axons exhibit a similar degree of myelin remodelling as CoPA axons? Silencing the release of neurotransmitters via expression of TeNT in individual RS axons leads to fewer and shorter myelin sheaths up until 7 dpf (Koudelka et al., 2016). It may be that neurotransmitter signalling plays a role in the formation and very early growth of myelin sheaths, but does not significantly affect the later growth or remodelling of myelin sheaths. In support of this, oligodendrocytes have reduced density of AMPA and NMDA receptors, and exhibit smaller responses than OPCs to glutamate signalling, suggesting a downregulation of neurotransmitter signalling as myelination progresses (De Biase et al., 2010). Restricting the modulation of myelination by activity to a critical developmental period would mean that activity does not constantly change myelin patterns.

Such a result would ensure that circuit function is maintained throughout life. Precisely how and when activity affects the dynamics of myelin sheaths during myelination is in need of investigation. How the activity of an individual neuron affects the early growth, and later growth of myelin sheaths will be investigated in Chapter 4.

3.3.5. Remodelling of Sheath Thickness over Time

One caveat of the live imaging experiments conducted in this chapter is that they do not assess sheath thickness over time. Although sheath number and length are stable after 7 dpf, it is possible that sheaths continue to grow radially. There is a need to accurately measure the thickness of myelin sheaths at multiple time points *in vivo* in order to quantify sheath thickness remodelling. Label-free imaging techniques based on the reflective properties of myelin sheaths have previously been used to measure g-ratios. Lim et al., 2014 used third harmonic generation microscopy to measure the thickness of sheaths made by Schwann cells in co-culture, in teased fibre preparations, and in the sciatic nerve *in vivo*. Alternatively, Kwon et al., 2017 used spectral reflectometry to measure axon diameter changes *in vivo* after traumatic brain injury, and states that this technique can also detect ultrastructural changes to myelin sheaths. Whether these techniques can detect subtle physiological changes in sheath thickness over time needs to be tested. Otherwise, super-resolution microscopy could be used to measure the thickness of fluorescently-labelled myelin sheaths over time. The live imaging data in this chapter were acquired using the super-resolution mode on a Zeiss LSM880 Airyscan confocal microscope. Airyscan microscopy uses an array of 32 detectors and deconvolution processing, which increases lateral resolution to 140 nm (Huff, 2015) (beyond the diffraction limit for conventional fluorescence microscopy of ~200 nm). RS axons are, on average, 1.2 µm in diameter from 7 dpf onwards (**Figure 12A**). Using Airyscan microscopy, the smallest change in g-ratio which could theoretically be detected along an average RS axon with starting g-ratio of 0.8 would be to 0.73. Techniques such as stimulated emission depletion (STED) microscopy could also be used to measure changes in sheath thickness over time. Chéreau et al., 2017 used STED microscopy to measure

changes in the diameter of GFP-labelled axons in brain slices at 50 nm resolution. At this resolution, the smallest change in sheath thickness that STED microscopy could detect along the same RS axon as above would be to g-ratio 0.77. Both of these super-resolution techniques are compatible with live imaging, and so could be used to measure changes in sheath thickness along the same axon over time.

To date, sheath thickness is typically measured by transmission electron microscopy, where ultra-thin sections of fixed tissue are cut, stained, and imaged using an electron microscope. While this technique limits analysis to a single time point, it also provides nanoscale-resolution detail of sheath ultrastructure. Although sheath thickness along the same axon cannot be followed over time, profiling the average sheath thickness of RS or CoPA axons at 5, 7, and 9 dpf could indicate whether sheath thickness is remodelled during these developmental stages. I attempted to address whether sheath thickness changes with age by measuring the g-ratios of myelinated axons in the dorsal and ventral tracts of the zebrafish spinal cord at 5, 7, and 9 dpf. I found that there was no statistically significant difference in sheath thickness between the ages in my dataset.

However, there are several limitations with this experimental approach. Firstly, the current sample size may not be sufficient to identify subtle differences in sheath thickness between groups. For example, the comparison of ventral myelinated axon g-ratios at 5 versus 7 dpf has only 30% power, requiring an n of 16 per group to achieve 80% power. Therefore, this experiment should be repeated to increase the sample size for statistical comparison.

Secondly, the quality of larval zebrafish spinal cord fixation makes measuring sheath thickness difficult. Axons are often distorted in shape and the individual wraps of membrane in myelin sheaths are rarely visible. The poor fixation quality appears to be a stage-specific effect, as the quality of adult zebrafish CNS tissue prepared for transmission electron microscopy is comparable to mammalian tissue. As a result, the sheath thickness measurements made in 5-9 dpf larvae in this chapter may not be accurate. I attempted to improve the

quality of larval spinal cord tissue preservation by testing high-pressure freezing techniques in conjunction with Dr. Joanna Brown (Möbius et al., 2016). Although this technique did improve myelin ultrastructure preservation, the tissue still exhibited fixation issues and freeze damage. Additionally, the protocol was not high-throughput enough to fix and image several samples for formal quantification. High-pressure freezing of zebrafish larvae will need to be further optimised to improve the quality of overall tissue preservation and increase throughput for official analysis of sheath thickness at different ages. For example, tissue preservation could be improved by testing different cryoprotectants. When performing the freezing step, the sample must be enclosed in a cryoprotectant in the specimen carrier. The cryoprotectant prevents air pockets from forming around the sample, transfers heat properly during freezing, and protects the sample from freeze damage. Here, we used 20% BSA in E3 embryo medium as a cryoprotectant, but various others can be used, such as 1-hexadecene, yeast paste, and polyvinylpyrrolidone (PVP) (Möbius et al., 2010). Optimising the cryoprotectant could not only improve the quality of tissue preservation, but could also increase the success rate to improve sample throughput.

Thirdly, it was not possible to identify specific axonal subtypes in spinal cord cross-sections. Combining electron microscopy with cell-specific labelling techniques could help identify and measure g-ratios of RS or CoPA axons. Cell subtype-specific measurements could be undertaken using immunogold staining for cell subtype-driven expression of fluorescent proteins (Viswanathan et al., 2015), or other labels (Lam et al., 2015; Shu et al., 2011). These correlative techniques would be challenging to perform as there are currently no known subtype-specific drivers for RS or CoPA neurons. RS and CoPA neurons are currently labelled using either a pan-neuronal driver (such as the HuC promoter) or partially-specific neuronal drivers (such as the Tg(RS:KalTA4) line, which drives KalTA4 expression mainly in RS neurons but also, occasionally, in other neurons such as CoPA neurons, Rohon-Beard neurons, and neurons in the PNS). A single labelled RS or CoPA neuron would have to be identified by light microscopy with no other cells labelled, to be sure

that any labelled axon(s) identified by electron microscopy were the correct subtype. Ideally a single axon that had been imaged in living animals would then be followed in fixed preparations to correlate live imaging and ultrastructural analyses.

Finally, measuring axonal g-ratios in a single cross-section only tells us the thickness of one myelin sheath along an axon. Serial section electron microscopy and 3D reconstruction of single cells (as performed by Tomassy et al., 2014) could be used to analyse the thickness of several sheaths along an axon at nanoscale resolution.

Alternatively, expansion microscopy can be used to perform nanoscale resolution measurements of structures not normally detectable by light microscopy. The technique involves anchoring chemically fixed tissue to a swellable polymer gel, so that when water is added to the tissue, it uniformly increases in size in all dimensions (Tillberg et al., 2016). This technique can be used in tissue with preserved endogenous fluorescence, or combined with conventional immunostaining, to identify specific proteins or structures of interest. Gao et al., 2019 combined expansion microscopy with lattice light-sheet microscopy to measure myelin sheath thickness along entire fluorescently-labelled axons in the rodent cortex. A similar approach could be used to measure sheath thickness along entire RS or CoPA axons at 5, 7, and 9 dpf in order to assess how sheath thickness changes with age. In preliminary experiments, I have found that expansion microscopy can be used to expand zebrafish larvae and image immunostained axons in the spinal cord (data not shown), indicating that this technique exhibits promise for imaging sheath thickness along individual RS and CoPA axons.

3.3.6. How Do Myelin Patterns Affect Overall Circuit Function?

The data in this chapter show that both RS and CoPA axons have similar myelin patterns (in terms of sheath number, length, length variability, and nodal gap length), which are established within the same time period after onset of myelination. How does establishment of these myelin patterns affect the function of the circuits to which RS and CoPA axons belong? One way to

assess circuit function is by studying behavioural output(s). As discussed in section ‘3.3.4 RS and CoPA Axons Show Remarkably Similar Myelin Patterns and Degrees of Myelin Remodelling’, the myelin patterns for different subsets of RS axons should be further characterised to correlate with specific locomotor behaviours. For instance, the 5-9 dpf myelin pattern parameters along MiD2/3cm RS axons could be correlated with the kinematics of escape responses (such as escape bend angles or escape swim velocity) (Dunn et al., 2016). MeLr and MeLc RS axon myelin patterns could be correlated with hunting efficiency, or with the kinematics of the prey capture response (such as tail angles during orienting swims) (Bianco et al., 2011; Gahtan et al., 2005).

Circuit function can also be assessed by directly measuring the activity of neurons during circuit activity. Electrophysiological recordings could correlate the establishment of myelin patterns with conduction timing and synaptic communication. Electrophysiology is typically done using electrodes to directly record voltage or current in neurons; however, genetically-encoded voltage indicators (GEVIs) are now available to perform entirely optic electrophysiology in single cells *in vivo* (Gong et al., 2015). Indicators such as Ace2N-4AA-mNeon have fast enough kinetics to detect single action potentials when combined with high speed imaging (Bando et al., 2019; Gong et al., 2015). These techniques could be used to record activity in RS neurons and downstream motor and interneurons at 5, 7, and 9 dpf to see how conduction velocity, post-synaptic recruitment and activity changes with myelin pattern establishment. For CoPA neurons, the post-synaptic targets first need to be verified. Combining GEVIs or genetically-encoded Ca^{2+} indicators (GECIs) with optogenetic stimulation of individual CoPA neurons could reveal candidate post-synaptic targets which respond to CoPA stimulation. Once the post-synaptic targets are verified, electrophysiological analysis, as above, could reveal whether myelin pattern establishment between 5-9 dpf affects conduction velocities, or the recruitment or activity of the post-synaptic targets.

It may be that changes in behaviours and electrophysiological properties of circuits do, indeed, correlate with the establishment of myelin patterns along axons *in vivo*. However, this does not mean that myelin pattern establishment

drives changes in circuit function. To determine if there is a causative relationship between myelin patterns and circuit function would require altering the myelin patterns established along RS and CoPA axons and then measuring the circuit's functional output. Manipulating signals known to regulate myelin sheath formation and growth in single neurons might be one way of changing myelin patterns along individual axons. If experience-driven activity does alter myelination patterns, then behavioural paradigms could be used to change the myelin patterns formed along specific axons. Raising larvae with and without live paramecia (to modify hunting behaviour) may alter the patterns specifically along MeLr and MeLc RS axons. Larvae given regular sensory stimulation may have different myelin patterns along CoPA axons compared to larvae without stimulation. Alternatively, the activity of individual neurons could be directly manipulated. There are several transgenic tools which can be used to manipulate synaptic vesicle release or electrical excitability of individual neurons *in vivo* (these will be discussed in more detail in section '4.1 Introduction'). Whether the activity of an individual neuron can permanently alter its myelin pattern will be investigated in Chapter 4. Once the myelin pattern along an axon has been altered, circuit function could be measured using the behavioural and electrophysiological tests described above.

Myelin patterns could be more broadly changed throughout the entire CNS by increasing the number of myelinating oligodendrocytes – research has shown that, when myelinating supply is increased relative to axonal demand, axons have increased sheath number but decreased sheath length (Almeida et al., 2018). Treating larvae with compounds which increase the production of myelinating oligodendrocytes could change the myelin pattern established along all axons rather than a specific axon of interest. Behavioural tests and electrophysiological characterisation described above could then determine whether global changes to myelin patterns affect overall nervous system function. However, it is important to remember that compound treatments may have side effects on cell types other than myelinating oligodendrocytes. Additionally, significant increases in myelinating oligodendrocyte number can

lead to mistargeting of myelin to non-axonal targets such as neuronal cell bodies, the effects of which on circuit function are not currently known (Almeida et al., 2018). Treatments should be carefully selected to ensure that oligodendrocyte number is increased without any adverse effects.

Altering myelin patterns along axons may not significantly affect conduction properties or circuit function. The nervous system can be remarkably plastic; other features such as synapses or axon diameter may be modified to compensate for altered myelin patterns in order to achieve optimal circuit function. It is likely that many different parameters work synergistically to regulate circuit activity. A holistic approach is required to understand if and how the formation and maintenance of myelination patterns influences overall circuit development and function over time.

3.3.7. Disruption to Myelin Patterns

If establishing particular myelin patterns along axons is important for circuit function, then what happens when these myelin patterns are disrupted? Myelin can be lost in response to injury or disease. Spinal cord injury is typically followed by demyelination of nearby spared axons (Kakulas, 1999; Totoiu and Keirstead, 2005). In Multiple Sclerosis (MS), demyelinating lesions can be found throughout grey and white matter of the CNS (Albert et al., 2007; Newcombe et al., 1991). Myelin may also be lost with age. A study of human individuals ranging from 44-77 years old suggests that the microstructure of numerous white matter tracts declines with age (Cox et al., 2016). In rodents, both the number of myelinating oligodendrocytes and myelin coverage in the somatosensory cortex decline at older ages (Hill et al., 2018).

Loss of myelin along axons with age, injury, or disease will disrupt conduction within circuits. For example, toxin-induced demyelination in the cat spinal cord leads to conduction block (Smith et al., 1981). And yet, denuded axons can be remyelinated. In animal models of spinal cord contusion, spared demyelinated axons are remyelinated, with sheaths made during remyelination identified as thinner and shorter than normal healthy sheaths (Lasiene et al., 2008; Totoiu and Keirstead, 2005). Remyelinated axons have also been reported post-

mortem in humans after spinal cord injury (Kakulas, 1999). In MS post-mortem tissue, lesions termed ‘shadow plaques’ have been identified, believed to be sites of previous demyelination that have been repopulated by oligodendrocytes and subsequently remyelinated (Lucchinetti et al., 1999; Prineas et al., 1993; Prineas and Connell, 1979). Like with spinal cord injury, remyelination is not perfect. Studies of both post-mortem MS tissue and demyelinating animal models suggest that sheaths on remyelinated axons are generally shorter and thinner than unaffected healthy myelin sheaths, even several months after the demyelinating episode (Blakemore, 1974; Blakemore and Murray, 1981; Prineas et al., 1993; Prineas and Connell, 1979). Remyelination in injury and disease is believed to restore conduction to demyelinated axons, and has been shown to do so in animal models (Smith et al., 1981). However, remyelination is likely to change the myelin pattern along axons, given that remyelinated sheaths tend to be thinner and shorter than normal. How this disruption to myelin patterns affects circuit function is not clear. Lasiene et al., 2008 performed mathematical modelling based on their measurements of remyelination after spinal cord injury, and found that the shorter sheaths observed after remyelination are predicted to reduce conduction velocities by 21%. How myelin patterns change through de- and remyelination along single axons, and how this affects circuit activity and behaviour warrants further investigation. It would be interesting to see if the myelin patterns along individual axons in the zebrafish spinal cord are changed after demyelination. In a cell-ablation model of demyelination in larval zebrafish (where myelinating cells express the enzyme nitroreductase and can be ablated by treatment with the pro-drug metronidazole), demyelination is followed by robust regeneration of sheaths with normal thickness and length (Karttunen et al., 2017). Further demyelination models could be tested to confirm that robust remyelination is a general feature of demyelination in larval zebrafish. I have generated a novel zebrafish model of demyelination where all myelinating cells express the fusion protein TRPV1-tagRFPt and can be ablated by treatment with high doses of capsaicin (see Appendix 1: A Novel Zebrafish Model of Demyelination – Tg(mbp:TRPV1-RFP)). This model

requires more extensive characterisation to profile the extent of de- and remyelination which occurs. Following characterisation, this model could be compared with other demyelination models to assess how myelination patterns along individual RS and CoPA axons change with de- and remyelination.

Not all myelin sheaths are lost in injury, disease, or old age. Is it possible for surviving myelin sheaths to remodel to compensate for myelin loss in order to maintain conduction speeds? Recent research in zebrafish indicates that myelin sheaths can be induced to remodel when the myelin pattern is disrupted. Auer et al., 2018 ablated individual oligodendrocytes to sparsely remove myelin sheaths along surrounding axons. When a single myelin sheath is lost from a myelinated axon, the adjacent myelin sheaths can reinitiate the rapid growth seen during early sheath formation to cover the exposed portion of the axon. Occasionally, a new myelin sheath is made in this gap and can grow back to restore the original pattern of myelin, even if this requires pushing back against the neighbouring sheaths. This suggests that, although myelin sheaths become stable after initial myelination, they retain the capacity for remodelling. It is not currently known whether mammalian myelin sheaths also retain this remodelling capacity, nor how surviving sheaths along axons remodel in response to more extensive demyelination. It would be intriguing to assess whether surviving myelin sheaths along an axon remodel to maintain conduction properties in response to demyelination and imperfect remyelination. Myelin sheath remodelling should also be characterised in older animals to see if age-associated myelin loss triggers changes in sheath length or thickness, particularly as the declining number of oligodendrocytes suggests that remyelination fails at these stages (Hill et al., 2018).

3.3.8. Summary

In this chapter, I characterised the formation of myelin patterns and remodelling of myelin sheaths along two different subtypes of glutamatergic axon in the zebrafish spinal cord. I found that both RS and CoPA axons exhibit a similar extent of myelin remodelling, and form similar myelin patterns within a defined time period after the onset of myelination. Future work should further

characterise the remodelling of myelin sheath thickness over time; assess which signals contribute to the formation of myelin patterns and myelin remodelling; and investigate the effects of myelin patterns on circuit activity and function in the context of health and disease.

In the next chapter, I will investigate how the activity of individual axons affects the formation and growth of myelin sheaths to mediate myelin pattern establishment.

Chapter 4: Investigating How Neuronal Activity Affects the Formation and Remodelling of Myelinated Axons over Time

4.1. Introduction

There is a growing body of evidence suggesting that experience can shape the myelination in the CNS (see section ‘1.5.3 Experience Affects Myelination’). The primary hypothesis underlying this phenomenon is that the neuronal activity of active circuits can signal to oligodendroglial cells to promote the myelination of these circuits. Much research has shown that neuronal activity can influence OPC proliferation, differentiation, target selection, and myelin sheath formation (as discussed in Chapter 1, section ‘1.6 Neuronal Activity can Influence Myelination’). However, it is not clear how neuronal activity affects the dynamics of myelination along single axons over time, or of existing individual myelin sheaths within a circuit.

One possibility is that existing myelin sheaths continue to detect and respond to neuronal activity after initial formation, and, therefore, can be constantly shaped by circuit activity. Neuronal activity could induce changes to sheath length or thickness to adjust the pattern of myelin along an axon. It is hypothesised that such a mechanism would allow neuronal activity to fine-tune conduction properties within a circuit as and when required to modify the functional output. However, evidence suggests that life-long remodelling of myelin sheaths is limited. To determine whether sheaths are remodelled, Hill et al., 2018 used label-free SCoRe microscopy to live image individual myelin sheaths in the upper layers of the somatosensory cortex of P60 mice. They found that only 19% of sheaths were dynamic in length over an imaging period of 30 days. Hughes et al. 2018 live imaged eGFP-labelled myelin sheaths in the somatosensory cortex of P365 mice for up to 50 days, and found that only 0.97% of sheaths were dynamic over this time period. They also investigated whether circuit activity could influence the remodelling capacity of these stable sheaths by exposing the mice to sensory stimulation for three weeks. This exposure activates sensory circuits and, presumably, increases the activity of the somatosensory cortex. There was no change in the degree of myelin sheath remodelling observed in these stimulated animals. However, there was increased production of oligodendrocytes in the somatosensory cortex of

stimulated animals. It is important to note that this study did not measure the activity of the underlying axons to confirm that sheaths on active axons did not remodel. It, nevertheless, does suggest that, at least in sensory circuits, activity can promote the production of new myelinating oligodendrocytes throughout life, but does not necessarily remodel existing myelin sheaths.

It is, in fact, entirely plausible that remodelling sheaths throughout life would not be beneficial for overall nervous system function. If the myelin patterns of active circuits were always changing, this could lead to constantly fluctuating conduction properties in circuits. Therefore, another possibility is that neuronal activity can remodel myelin sheaths to shape myelin patterns along axons, but only within a critical developmental window. There is some evidence that neuronal activity may influence early sheath growth. Ca^{2+} transients in myelin sheaths have been shown to correlate with early sheath growth (Baraban et al., 2018). Electrical stimulation of the hindbrain increases the frequency of sheath Ca^{2+} transients and sheath growth, while silencing neuronal activity with TTX inhibits the same (Krasnow et al., 2018). It is not clear whether myelin sheaths continue to exhibit these activity-dependent Ca^{2+} transients beyond early stages of growth. Battefeld et al., 2019 found that actively growing myelin sheaths have a high rate of Ca^{2+} transients, which declines with sheath maturation. Electrophysiological recordings of neuro-glial communication show that oligodendrocytes exhibit much smaller responses to neurotransmitter signalling as they differentiate (De Biase et al., 2010; Kukley et al., 2010). This suggests that oligodendrocytes become less responsive to neuronal activity as myelination progresses. Live imaging of myelin sheaths in the zebrafish spinal cord revealed that sheaths exhibit variable rates of sheath growth in the first few days after formation, and then become stable thereafter (Auer et al., 2018). This is concurrent with my findings from Chapter 3 – the growth of myelin sheaths along both reticulospinal and CoPA axons is generally limited to a defined period after the onset of myelination (until 7 dpf). Reticulospinal axons are myelinated in a synaptic vesicular release-dependent manner, which indicates that these neurons are capable of activity-dependent myelination (Koudelka et al., 2016). It is possible that neuronal activity can

regulate the early growth of myelin sheaths to establish a particular myelin pattern, but that, after a critical window of plasticity, these myelin sheaths no longer respond to neuronal activity and remain stable.

Further investigation is required to determine if, how, and when neuronal activity affects the dynamics of myelin sheaths and myelin pattern establishment. Numerous techniques have been employed to study the role of neuronal activity in regulating various aspects of myelination, as summarised in **Table 5**. These techniques include pharmacological treatments to manipulate all neurons or oligodendrocytes, and transgenic tools to manipulate activity in a neuronal subset of choice. If the activity of a single neuron (rather than a whole population of neurons) can locally regulate the myelination of its axon has not been determined. Koudelka et al., 2016 inhibited vesicular release in individual reticulospinal cells in the zebrafish spinal cord and found that this inhibits their myelination. However, they did not assess how local vesicular release affects the dynamics of individual sheaths, or how increasing neuronal activity might affect myelin remodelling. Larval zebrafish are ideally suited for investigating the role of neuronal activity in regulating sheath dynamics and myelin pattern formation due to their optical transparency for live imaging (as shown in Chapter 3).

Investigating how neuronal activity regulates myelination at the single axon level requires a technique to activate or inhibit the activity of individual neurons. Ideally this should be an inducible tool to prevent changes to neuronal activity affecting neuronal development prior to the onset of myelination. Such experiments could be done using optogenetics, where light-gated channelrhodopsins are expressed in a single neuron, and activity can be induced using the relevant wavelength of light (Boyden et al., 2005; Gradinaru et al., 2010). Alternatively, chemogenetics could be used, where ligand-gated ion channels or receptors are expressed in a single neuron, and activity can be induced by application of the appropriate ligand. Chemogenetic techniques are particularly useful in the larval zebrafish given that activating ligands can be easily administered by bath application. Mammalian TRP channels have previously been used in zebrafish to robustly increase neuronal activity (Chen

et al., 2016). TRPV1-tagRFPt (TRPV1-RFP) is a fusion protein between the rat TRPV1 cation channel and tagRFPt. TRPV1 is a non-selective cation channel (although it has a preference for Ca^{2+} over Na^{+} and K^{+} (Munns et al., 2015)), which is expressed in nociceptive sensory neurons. In mammals, the TRPV1 channel is activated by noxious heat, acidity, and capsaicin (a compound found in 'hot' chili peppers) (Caterina et al., 1997); however, due to evolution, the zebrafish orthologue is activated by heat and acidity, but not capsaicin (Gau et al., 2013). Chen et al., 2016 capitalised on this evolutionary difference to generate a chemogenetic tool for stimulating neurons in zebrafish – the rat TRPV1 channel can be expressed in neurons of interest, and then applying the agonist capsaicin will activate these neurons (without affecting endogenous zebrafish TRP channels). They demonstrated that treatment with low-concentrations of capsaicin successfully increases activity of specific neurons, while high-concentration treatments of capsaicin ablates cells (Chen et al., 2016). This is an easy, non-invasive, temporally-regulated system for controlling neuronal activity of single neurons within freely behaving animals. I decided to use this chemogenetic system to investigate the role of neuronal activity in myelin sheath dynamics and myelin pattern establishment.

4.1.1. Aims for this Chapter

In this chapter, I aim to investigate how local neuronal activity affects the dynamics of individual sheaths and the formation of myelin patterns along individual axons in the zebrafish spinal cord. Reticulospinal axons have been shown to be myelinated in a synaptic-vesicle dependent manner. Based on this, I hypothesised that increasing the activity of individual reticulospinal axons would significantly alter sheath dynamics and the myelin patterns established. To test these hypotheses, I stimulated individual reticulospinal axons using the TRPV1-RFP chemogenetic system, coupled with live imaging, during the peak time of myelination (3-7 dpf). I then measured the dynamics of individual sheaths on both stimulated and unstimulated axons during this time period. I also assessed the myelin patterns of stimulated versus unstimulated axons by measuring sheath length, sheath number, and also how nodal gap length and axon diameter were affected by increased neuronal activity.

Table 5 – summary of previous techniques used to investigate role of neuronal activity in myelination.

Technique	Description	Critique	Studies using technique
Tetrodotoxin (TTX)	Voltage-gated Na^+ channel blocker, inhibits action potential propagation. Can be bath applied to cells or animals, or injected to tract or region of interest.	Pharmacological treatments can affect non-neuronal cells as well. Global treatment cannot inhibit just specific neurons of interest, if used *in vivo*.	(Barres and Raff, 1993; Bergles et al., 2000; Demerens et al., 1996; Hines et al., 2015; Káradóttir et al., 2008, 2005; Kukley et al., 2010, 2007; Malone et al., 2013; Wake et al., 2011).
Pentylenetetrazole (PTZ)	GABA receptor antagonist which prevents inhibitory effects of GABA signalling, leading to increased overall excitation.	An indirect method for increasing neuronal activity. May induce seizures (non-physiological levels of activity). Pharmacological treatments can affect non-neuronal cells as well. Global treatment cannot inhibit just specific neurons of interest.	(Mensch et al., 2015).
Electrode stimulation	Electrodes used to directly apply electrical stimulation to region of interest. Can be implanted *in vivo*.	Provides control of firing frequencies in populations of neurons. Cannot stimulate just specific neurons in interest within a region.	(Krasnow et al., 2018; Li et al., 2010; Malone et al., 2013; Nagy et al., 2017; Wake et al., 2011).
$K_{ir}2.1$	Inward-rectifying K^+ channel causing sustained hyperpolarisation and reduced excitability.	Can be expressed in specific neurons of interest. No temporal control of activity.	(Hines et al., 2015; Mitew et al., 2018).

Opsins	Optogenetic system. Light-gated cation channels originally derived from algae. Variety of excitatory and inhibitory opsins available, activated by various wavelengths of light (Boyden et al., 2005; Gradinaru et al., 2010).	Can be expressed in specific neurons of interest. Provides temporal control of activity. May require invasive implantation of optical fibres.	(Geraghty et al., 2019; Gibson et al., 2014).
Designer Receptors Exclusively Activated by Designer Drugs (DREADDs)	Chemogenetic system. Modified muscarinic acetylcholine receptors activated by inert ligand clozapine-N-oxide (Alexander et al., 2009; Armbruster et al., 2007).	Can be expressed in specific neurons of interest. Provides temporal control of activity. DREADDs are actually activated by clozapine, which has endogenous binding targets and could cause side effects (Gomez et al., 2017).	(Mitew et al., 2018).
TeNT	Clostridial neurotoxin which inhibits synaptic vesicle release via cleavage of SNARE protein VAMP-2 (Binz et al., 2010).	Can be expressed globally or in specific neurons of interest. Inhibits specific aspect of neuronal activity (neurotransmitter/BDNF release, not electrical impulses). No temporal control of activity.	(Hines et al., 2015; Mensch et al., 2015; Wake et al., 2015, 2011).
BoNTs	Clostridial neurotoxins which inhibit synaptic vesicle release via cleavage of SNARE proteins (Binz et al., 2010). There are 7 isoforms (A-G).	Can be expressed globally or in specific neurons of interest. Inhibits specific aspect of neuronal activity (neurotransmitter/BDNF release, not electrical impulses). No temporal control of activity.	(Wake et al., 2015, 2011).

Ruthenium Red	Stimulates synaptic vesicle release in Ca^{2+} independent manner (Trudeau et al., 1996).	Increases specific aspect of neuronal activity (neurotransmitter release, not electrical impulses). No temporal control of activity. Has other known targets.	(Kukley et al., 2007; Ziskin et al., 2007).
α-latrotoxin	Stimulates synaptic vesicle release by forming Ca^{2+}-permeable pores to increase Ca^{2+} influx (Henkel and Sankaranarayanan, 1999).	Increases specific aspect of neuronal activity (neurotransmitter release, not electrical impulses). No temporal control of activity.	(Gautier et al., 2015; Kukley et al., 2007; Mangin et al., 2008).
Glutamate receptor antagonists	Antagonists which block glutamatergic receptors. Examples include: CNQX, NBQX, GYKI (AMPA/kainate receptors); AP5, MK-801 (NMDA receptors); DHPG (mGlu receptors).	Inhibits specific aspect of neuronal activity (glutamate signalling to oligodendroglia). Will likely affect cell types other than oligodendroglia.	(Barres et al., 1990; Bergles et al., 2000; De Biase et al., 2010; Káradóttir et al., 2008, 2005; Kukley et al., 2010, 2007; Lundgaard et al., 2013; Luyt et al., 2003; Wang et al., 1996; Wyllie et al., 1991; Žiak et al., 1998; Ziskin et al., 2007)
Glutamate receptor agonists	Agonists which activate glutamatergic receptors. Examples include: glutamate, AMPA, kainate, NMDA, quisqualate (AMPA, kainate and mGlu receptors).	Stimulates specific aspect of neuronal activity (glutamate signalling to oligodendroglia). Will likely affect cell types other than oligodendroglia.	(Barres et al., 1990; Berger et al., 1992; Káradóttir et al., 2005; Spitzer et al., 2019; Wang et al., 1996; Wyllie et al., 1991; Žiak et al., 1998)

4.2. Results

4.2.1. TRPV1-tagRFPt as a Tool to Increase Neuronal Activity without Adversely Affecting Neurodevelopment

To test the suitability of the TRPV1-tagRFPt (TRPV1-RFP) tool for increasing activity during myelination, a transgenic line was generated where TRPV1-RFP is expressed under the UAS promoter sequence (**Figure 22A**). The transgene can then be expressed in neurons of interest by crossing Tg(UAS:TRPV1-RFP) fish with Gal4 or KalTA4 driver fish. Crossing Tg(UAS:TRPV1-RFP) with Tg(Rs:KalTA4) generated progeny where TRPV1-RFP was expressed mosaically in reticulospinal (RS) neurons (**Figure 22B**).

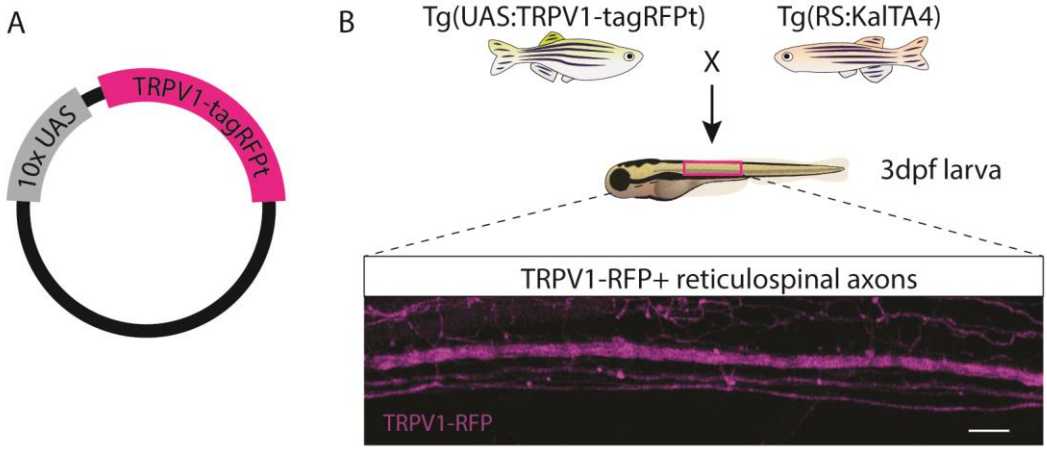

Figure 22 - the TRPV1-tagRFPt tool for chemogenetic stimulation of RS axons.

A) A simplified plasmid map of the 10xUAS:TRPV1-tagRFPt plasmid used to generate the transgenic line Tg(UAS:TRPV1-tagRFPt) (TRPV1-RFP). TRPV1-RFP is under the control of the 10xUAS promoter sequence, so that expression of TRPV1-RFP occurs only in cells where the transcriptional activator Gal4 or KalTA4 is present. **B)** The animal cross used to express TRPV1-RFP specifically in RS axons. Tg(UAS:TRPV1-tagRFPt) is crossed to Tg(RS:KalTA4), a transgenic line where the transcriptional activator KalTA4 is expressed in RS axons. Progeny which are positive for both transgenes will mosaically express TRPV1-RFP in RS axons (example image of RS axons expressing TRPV1-tagRFP is shown in the inset). Scale bar = 10 µm.

Chen et al., 2016 found that different types of neurons had different sensitivities to capsaicin-induced TRPV1-RFP activity. While Rohon-Beard sensory neurons were activated by one hour of 10 µM capsaicin, hypothalamic neurons were ablated by the same treatment. Therefore, several doses of capsaicin were tested to determine which were tolerable for RS axons expressing TRPV1-RFP. Animals aged 3 dpf, containing TRPV1-RFP-expressng RS axons, were treated with either vehicle, 1 µM, or 10 µM capsaicin for one hour. Axons were imaged immediately after this treatment to determine if capsaicin-induced cell ablation occurred (shown by degenerating axons), and found that there was no cell ablation at low capsaicin doses (1 µM) but complete cell ablation at high capsaicin doses (10 µM) (**Figure 23**).

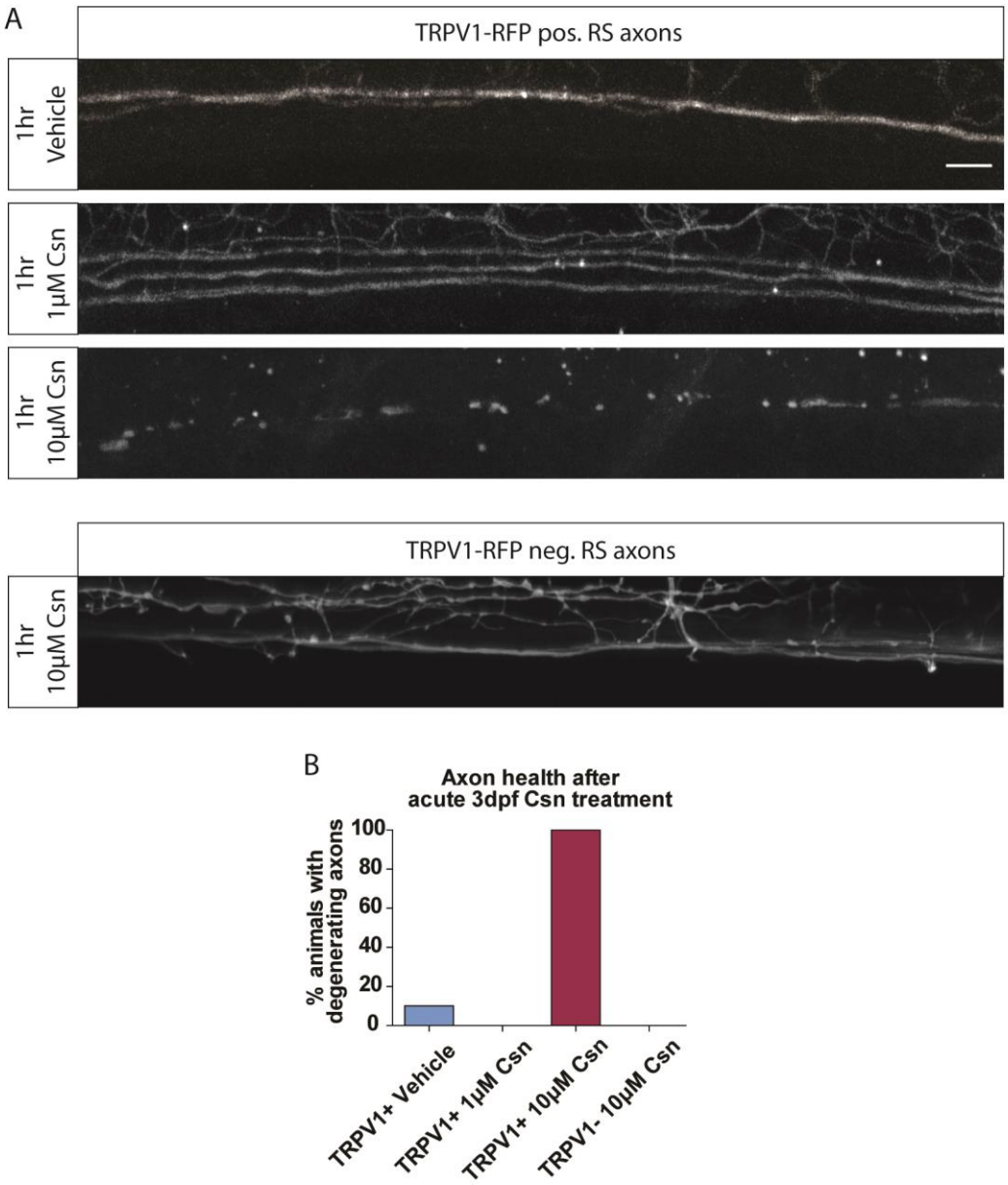

Figure 23 – The effects of acute treatment with low and high doses of capsaicin on RS axon health.

A) Example images of TRPV1-RFP+ RS axons at 3 dpf treated with vehicle, 1 µM capsaicin or 10 µM capsaicin for 1 hour, as well as TRPV1-RFP- axons treated with 10 µM capsaicin. TRPV1-RFP-expressing axons treated with 10 µM capsaicin completely degenerate, as shown by axonal blebbing. **B)** Quantification of % animals with degenerating RS axons in each treatment group. The % of animals with degenerating axons with acute treatment was 10% for vehicle treated TRPV1-RFP+ animals (n = 10), 0% for 1 µM capsaicin treated TRPV1-RFP+ animals (n =

12), 100% for 10 µM capsaicin treated TRPV1-RFP+ animals (n = 9), and 0% for 10 µM capsaicin treated TRPV1-RFP- animals (n = 6). Scale bar = 10 µm.

Next, Ca^{2+} imaging was performed to test that 1 µM capsaicin treatment was sufficient to increase the activity of TRPV1-RFP-expressing RS axons. RS axons were labelled with TRPV1-RFP and an axon-localised form of GCaMP7 cloned by Dr. Rafael Almeida (axon-GCaMP7). GCaMP is a genetically-encoded Ca^{2+} indicator, where an increase in intracellular Ca^{2+} causes a conformational change of the GCaMP protein, and leads to emission of fluorescence (Nakai et al., 2001). When neurons fire action potentials, Ca^{2+} influx occurs and therefore the electrical activity of GCaMP-expressing neurons can be visualised as changes in fluorescence. Short timelapse movies (three to five minutes long) were taken of axon-GCaMP7 fluorescence at distinct regions of RS axons both immediately before and 15 minutes after the application of either vehicle or 1 µM capsaicin (**Figure 24A-C**). The change in activity (calculated as the change in fluorescence, or ΔF/F0) from baseline with treatment was quantified. There was a rapid and significant increase in neuronal activity in TRPV1-RFP-expressing neurons when treated with capsaicin at 3 dpf, with the mean ΔF/F0 for vehicle-treated animals -0.10, and for capsaicin-treated animals 0.42 (unpaired t-test with Welch's Correction for Variance, p = 0.001, **Figure 24C, D**). TRPV1-RFP-expressing cells continued to respond to capsaicin as the larva develops; Ca^{2+} imaging in 5 dpf larvae demonstrated that capsaicin treatment increased the activity of TRPV1-RFP-expressing axons (the mean ΔF/F0 was -0.05 for vehicle treated animals, and 0.18 for 1 µM capsaicin treated animals; unpaired t-test with Welch's Correction for Variance, p = 0.046, **Figure 24E**). These animals had previously received capsaicin or vehicle treatments at both 3 and 4 dpf, showing that cells which received repeated treatments could still respond to capsaicin. Treating with capsaicin had no statistically significant effect on the activity of axons which do not express TRPV1-RFP (the mean ΔF/F0 was -0.07 for vehicle treated animals, and -0.06 for 1 µM capsaicin treated animals; unpaired t-test, p = 0.879, **Figure 24F**).

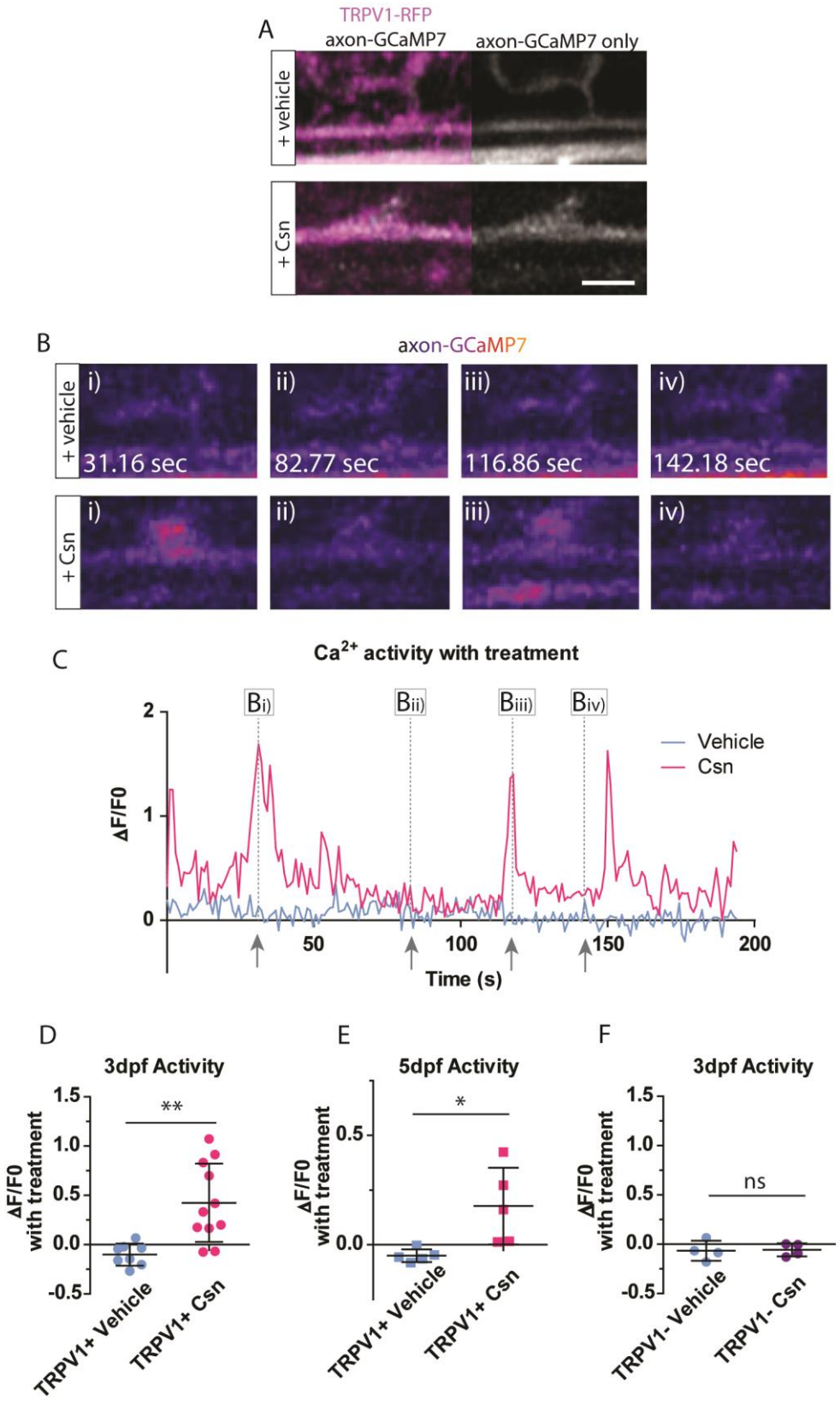

Figure 24 – the effects of capsaicin treatment on neuronal activity of RS axons.

A) Example still images showing RS axons expressing TRPV1-RFP and axon-GCaMP7. **B)** Single timestamped frames from a timelapse movie of GCaMP7 fluorescence in the axons shown in A). **C)** The GCaMP7 fluorescence intensity (plotted as ΔF/F0) trace of the axons shown in A) and B) for a 3 minute timelapse movie. The time points denoted by the grey arrows and dotted lines correspond to the fluorescence values of the frames shown in B). **D)** Quantification of the Ca^{2+} activity of TRPV1-RFP+ RS axons treated with vehicle or 1 µM capsaicin at 3 dpf. The mean ΔF/F0 was -0.10 (SD = 0.11) for vehicle treated animals, and 0.42 (SD = 0.40) for 1 µM capsaicin treated animals. There was a significant increase in the activity of TRPV1-RFP axons with capsaicin treatment (unpaired t-test with Welch's correction for variance, p = 0.001, vehicle n = 8, 1 µM capsaicin n = 11). **E)** Quantification of the Ca^{2+} activity of TRPV1-RFP+ RS axons treated with vehicle or 1 µM capsaicin at 5 dpf. The mean ΔF/F0 was -0.05 (SD = 0.03) for vehicle treated animals, and 0.18 (SD = 0.18) for 1 µM capsaicin treated animals. There was a significant increase in the activity of TRPV1-RFP axons with capsaicin treatment (unpaired t-test with Welch's correction for variance, p = 0.046, vehicle n = 5, 1 µM capsaicin n = 5). **F)** Quantification of the Ca^{2+} activity of TRPV1-RFP- RS axons treated with vehicle or 1 µM capsaicin at 3 dpf. The mean ΔF/F0 was -0.07 (SD = 0.10) for vehicle treated animals, and -0.06 (SD = 0.07) for 1 µM capsaicin treated animals. There is no statistically significant difference between the two groups (unpaired t-test, p = 0.878, vehicle n = 4, 1 µM capsaicin n = 4). Scale bar = 10 µm.

The longer-term effects of repeated capsaicin treatments were then investigated. To do this, animals with TRPV1-RFP-expressing RS axons were treated with either vehicle, or 1 µM capsaicin, daily from 3-7 dpf. Axons were imaged at 3 and 7 dpf to quantify any changes in the number of expressing axons (**Figure 25A**). The treatment time was increased from one hour daily (as tested in previous experiments) to four hours daily to see how more prolonged increases in activity affect axonal health. Capsaicin treatment had no statistically significant effect on long-term survival of TRPV1-RFP-expressing RS axons (the mean % of axons at 7 dpf was 94.1% for vehicle treated animals, and 98.5% for 1 µM capsaicin treated animals; unpaired t-test, p = 0.488, **Figure 25B**).

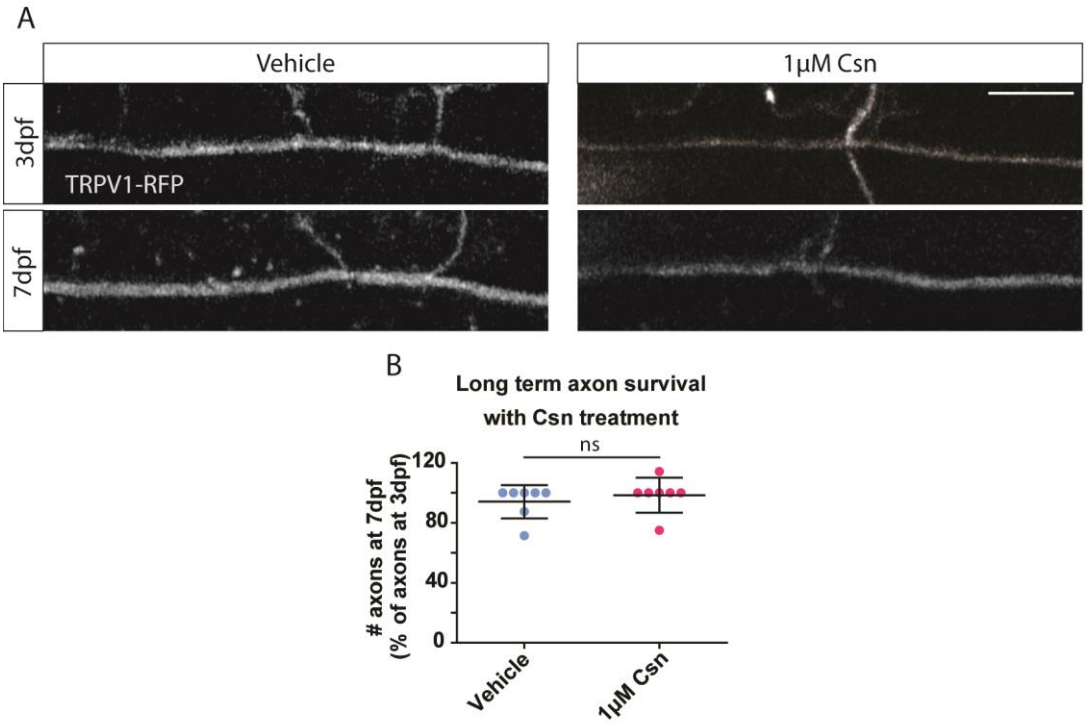

Figure 25 – the effects of long-term treatment with low doses of capsaicin on RS axon health.

A) Example images of RS axons at 3 dpf and 7 dpf, treated with either vehicle or 1 µM capsaicin for 4 hours daily 3-7 dpf. **B)** Quantification of the number of axons at 7 dpf after treatment with vehicle or 1 µM capsaicin daily 3-7 dpf (as % of the number of axons at 3 dpf prior to treatment). The mean % of axons at 7 dpf was 94.1% (SD = 11.0) for vehicle treated animals, and 98.5% (SD = 11.6) for 1 µM capsaicin treated animals. There was no statistically significant difference between the two treatment groups (unpaired t-test, p = 0.488, vehicle n = 7, 1 µM capsaicin n = 7). Scale bar = 10 µm.

Based on these results, I concluded that low doses (1 µM) of capsaicin could selectively increase the activity of TRPV1-RFP-expressing RS axons, and that repeated stimulation of these axons during the time period of myelination (3-7 dpf) had no obvious adverse effects on RS axon development. I decided to use four hour daily treatments of 1 µM capsaicin to stimulate RS neurons and then observe how such stimulation affected their myelination.

4.2.2. Single Axon Activity Does Not Affect Oligodendrogenesis

Research has shown that increased neuronal activity promotes the proliferation of OPCs and their subsequent differentiation into oligodendrocytes (Gibson et al., 2014; Mitew et al., 2018). In both of these studies, a significant population of pyramidal neurons in the rodent cortex was stimulated; it is not clear if the activity of individual axons can affect local oligodendrogenesis. To investigate this, relevant crosses between Tg(UAS:TRPV1-RFP), Tg(RS:KalTA4), and Tg(mbp:nls-eGFP) were performed to obtain larvae that had expression of TRPV1-RFP in RS axons and nuclear-localised eGFP expression in all myelinating cells. In these larvae, single RS axons could be stimulated by treating with capsaicin for four hours daily from 3-7 dpf, and the number of myelinating oligodendrocytes in the surrounding axonal tract could be counted at each age (**Figure 26**). Animals with very sparse expression of TRPV1-RFP were selected for this experiment; between one to five axons expressed TRPV1-RFP per animal, with mean axon number being 1.8 (SD = 1.4) for unstimulated controls and 2.4 (SD = 1.0) for stimulated animals.

The mean number of oligodendrocytes in a 3-somite area of the ventral tract (where RS axons are located) at 3 dpf (prior to any stimulation) was 29.6 for vehicle, and 26.3 for capsaicin (**Figure 26B**). There was no significant difference in oligodendrocyte number between unstimulated and stimulated axons at either 5 or 7 dpf (at 5 dpf the mean oligodendrocyte number was 43.4 for vehicle, and 39.7 for capsaicin; and at 7 dpf it was 49.1 for vehicle, and 47.8 for capsaicin; unpaired t-tests, 5 dpf $p = 0.170$, 7 dpf $p = 0.661$, **Figure 26B**).

The same treatment protocol (four hours daily from 3-7 dpf) was tested in larvae that did not express TRPV1-RFP in order to confirm that long-term capsaicin treatment has no effect on overall oligodendrocyte production independent of neuronal activity. This was done using Tg(mbp:eGFP) larvae, where myelinating cells express cytoplasmic eGFP. Counting the total number of oligodendrocytes at 7 dpf, with either vehicle or capsaicin treatment, showed

that there was no significant effect on oligodendrogenesis (**Figure 27**; number of oligodendrocytes in the dorsal tract was 155.7 for vehicle, and 164.3 for 1 µM capsaicin; unpaired t-test with Welch's Correction for Variance, p = 0.395).

Based on these results, I concluded that neither the activity of individual axons nor treatment with capsaicin has a significant effect on oligodendrogenesis during this initial myelination period. This means that any effects of stimulation on axon myelination are due to activity regulating the formation or growth of the myelin sheaths themselves, rather than sheath formation or growth effects being a by-product of an enlarged oligodendrocyte population.

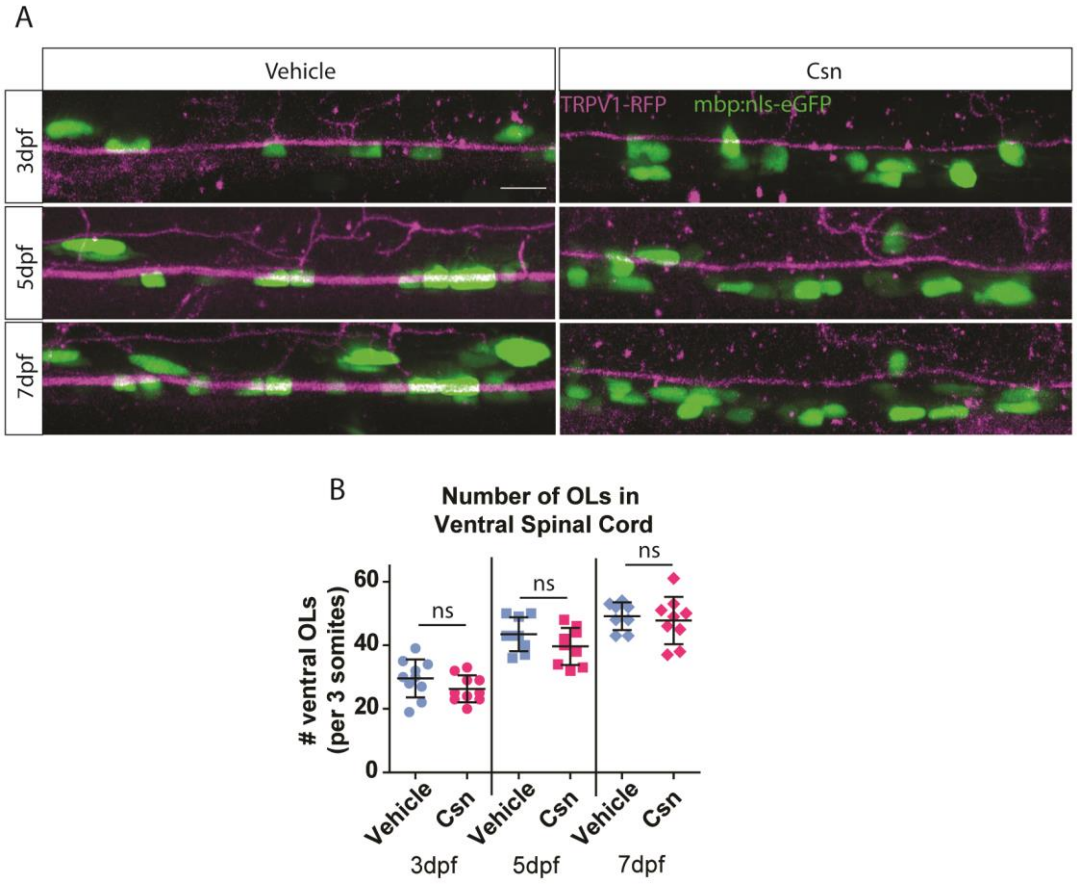

Figure 26 – ventral oligodendrocyte number with chemogenetic stimulation of individual RS axons.

A) Example images of GFP-expressing oligodendrocytes in the ventral spinal cord of animals with individual TRPV1-RFP+ RS axons at 3, 5, and 7 dpf treated with vehicle or 1 µM capsaicin. **B)** Quantification of the number of oligodendrocytes in the ventral spinal cord at 3, 5, and 7 dpf in animals with individual TRPV1-RFP+ RS

axons treated with vehicle or 1 µM capsaicin. The mean number of ventral oligodendrocytes at 3 dpf was 29.6 (SD = 6.0) for vehicle, and 26.3 (SD = 4.2) for capsaicin; at 5 dpf was 43.4 (SD = 5.3) for vehicle, and 39.7 (SD = 5.8) for capsaicin; and at 7 dpf was 49.1 (SD = 4.4) for vehicle, and 47.8 (SD = 7.4) for capsaicin. There was no statistically significant difference between the two groups at any age (unpaired t-tests; 3 dpf p = 0.172, vehicle n = 10, capsaicin n = 10; 5 dpf p = 0.170, vehicle n = 9, capsaicin n = 9; 7 dpf p = 0.661, vehicle n = 8, capsaicin n = 9). Scale bar = 10 µm.

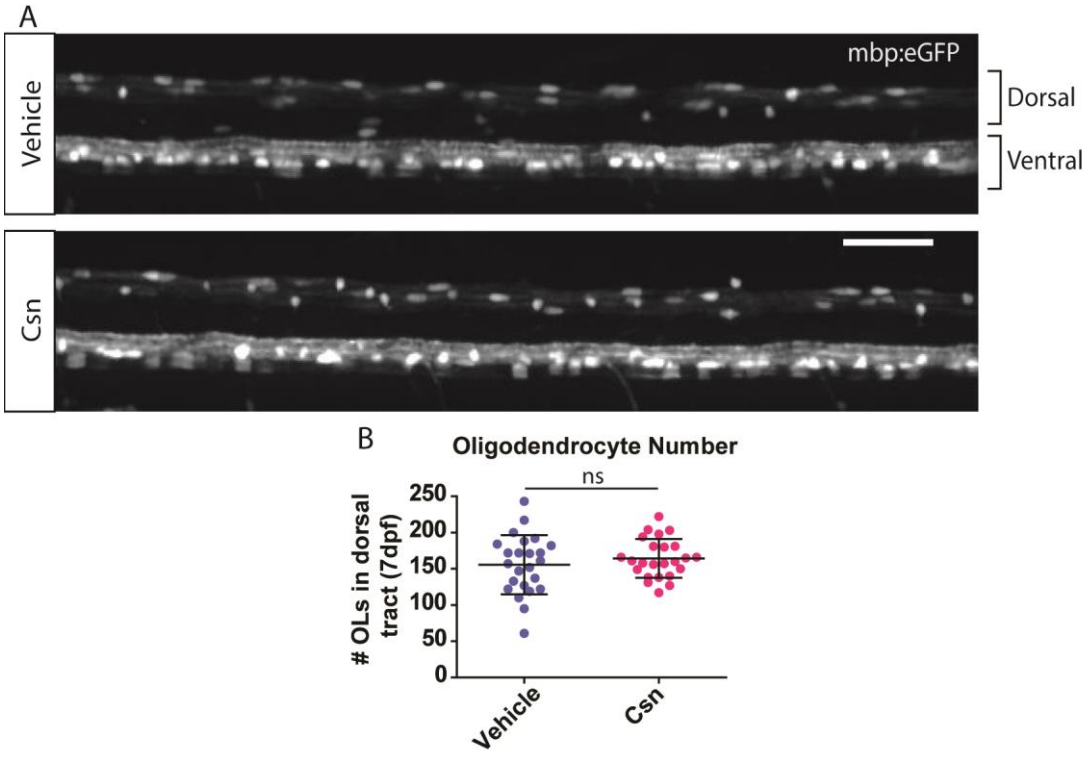

Figure 27 – the effects of capsaicin alone on oligodendrocyte number in the spinal cord.

A) Example images of oligodendrocytes in the spinal cord of 7 dpf larvae, treated with either vehicle or 1 µM capsaicin for 4 hours daily from 3-7 dpf. **B)** Quantification of the number of oligodendrocytes in the dorsal spinal cord at 7 dpf following either vehicle or 1 µM capsaicin treatment. The mean number of oligodendrocytes was 155.7 (SD = 40.9) for vehicle treated animals, and 164.3 (SD = 26.8) for 1 µM capsaicin treated animals. There was no statistically significant difference between the two treatment groups (unpaired t-test with Welch's correction for variance, p = 0.395, vehicle n = 24, 1 µM capsaicin n = 24. Scale bar = 10 µm.

4.2.3. Activity Promotes Early (3-5 dpf) Myelin Sheath Dynamics

FP-Cntn1a fusion proteins act as a marker of myelination along axons by labelling only the unmyelinated regions (Koudelka et al., 2016). A stable transgenic line was generated where GFP-Cntn1a was expressed under the UAS promoter sequence (Tg(UAS:GFP-Cntn1a)), and appropriate crosses were performed with Tg(RS:KalTA4) and Tg(UAS:TRPV1-RFP) fish to generate larvae expressing both TRPV1-RFP and GFP-Cntn1a in single RS axons (**Figure 28**). RS axons were treated with vehicle (unstimulated) or capsaicin (stimulated) for four hours daily 3-7 dpf, and imaged at 3, 5, and 7 dpf to assess how increased activity affected the dynamics of individual myelin sheaths during this period (**Figure 28A**). Only animals with sparse expression of TRPV1-RFP were selected, and only one axon was analysed per animal.

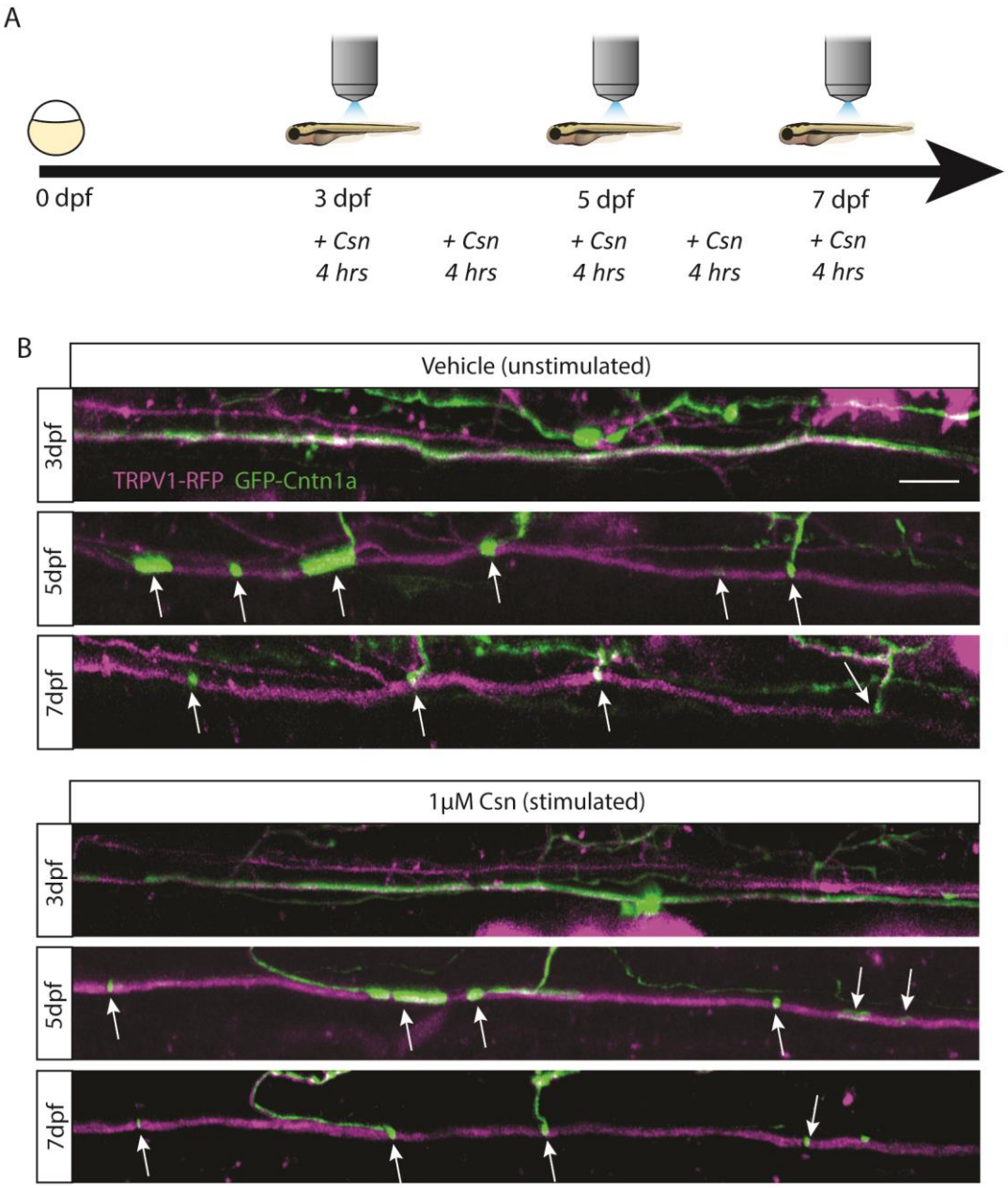

Figure 28 – following the myelination of individual RS axons through chemogenetic stimulation.

A) Experimental timeline; larvae with TRPV1-RFP+ RS axons were imaged at 3, 5, and 7 dpf using reporters for myelination, and treated with either vehicle or 1 µM capsaicin for 4 hours daily from 3-7 dpf. **B)** Example RS axons which were imaged at 3, 5, and 7 dpf with either vehicle or 1 µM capsaicin treatment. Myelination along the axon was assessed using the GFP-Cntn1a reporter (where GFP fluorescence denotes unmyelinated regions, white arrows, and gaps in the GFP fluorescence denote myelin sheaths). Scale bar = 10 µm.

Many axons had not begun myelination by the 3 dpf imaging session; however, some axons did have small myelin sheaths at this time point. To assess early myelin sheath dynamics, analysis was performed on cells where the same area of axon could be followed from 3-5 dpf, measuring the sheaths which were present at both 3 and 5 dpf. The lengths of 'early born' myelin sheaths (sheaths which were present at 3 dpf) were measured at 3 and 5 dpf to see how stimulating axonal activity affected their early growth (**Figure 29A**). Some axons had only one early born sheath, whereas other axons had several. For analysis, the length of early born sheath(s) along an axon were quantified and the mean of these was taken where appropriate to obtain one measurement per axon. At 3 dpf, prior to any stimulation, the mean length of early born sheaths per axon was 8.2 µm for vehicle, and 7.3 µm for capsaicin (**Figure 29B**). By 5 dpf, the mean sheath length of these early born sheaths was significantly longer on stimulated versus unstimulated axons (36.4 µm for vehicle, and 45.4 µm for capsaicin; unpaired t-test, $p = 0.024$, **Figure 29B**). This could also be measured as the change in sheath length, where the difference in length 3-5 dpf was measured for each sheath and the mean value per axon taken where appropriate (**Figure 29C**, mean change in sheath length 3-5 dpf per axon was 27.3 µm for vehicle, and 38.5 µm for capsaicin; unpaired t-test, $p = 0.049$).

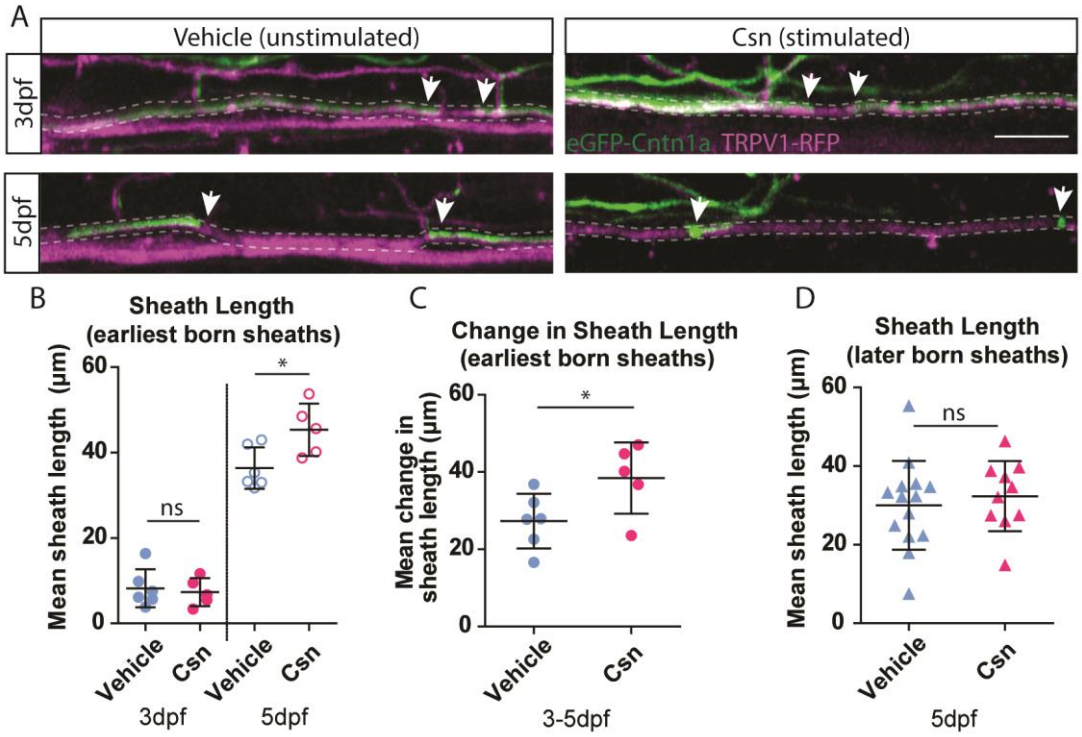

Figure 29 – early sheath dynamics along chemogenetically stimulated individual RS axons.

A) Example images of myelin sheath growth 3-5 dpf on TRPV1-RFP+ RS axons. White arrows = the edges of the myelin sheath. **B)** The mean sheath length of 'earliest born sheaths' on TRPV1-RFP+ RS axons at 3 and 5 dpf treated with either vehicle or 1 µM capsaicin. 'Earliest born sheaths' are defined as sheaths which were formed prior to imaging at 3 dpf. The mean sheath length per axon at 3 dpf was 8.2 µm (SD = 4.5) for vehicle, and 7.3 µm (SD = 3.3) for capsaicin; and at 5 dpf was 36.4 µm (SD = 4.9) for vehicle, and 45.4 µm (SD = 6.1) for capsaicin. There was no statistically significant difference between the two groups at 3 dpf, but there was a significant increase in sheath length with capsaicin treatment at 5 dpf (unpaired t-tests; 3 dpf p = 0.720, vehicle n = 6, capsaicin n = 5; 5 dpf p = 0.024, vehicle n = 6, capsaicin n = 5). **C)** The mean change in sheath length 3-5 dpf of earliest born sheaths along TRPV1-RFP+ RS axons treated with either vehicle or 1 µM capsaicin. The mean change in sheath length 3-5 dpf per axon was 27.3 µm (SD = 7.1) for vehicle, and 38.5 µm (SD = 9.2) for capsaicin. There was a significant increase in the mean change in sheath length with capsaicin treatment (unpaired t-test, p = 0.049, vehicle n = 6, capsaicin n = 5). **D)** The mean sheath length of 'later born sheaths' on TRPV1-RFP+ axons at 5 dpf treated with either vehicle or 1 µM capsaicin. 'Later born sheaths' were defined as sheaths born between the 3 and 5

dpf imaging sessions. The mean sheath length per axon was 30.0 µm (SD = 11.3) for vehicle, and 32.4 µm (SD = 8.9) for capsaicin. There was no statistically significant difference between the two groups (unpaired t-test, p = 0.595, vehicle n = 14, capsaicin n = 10). Scale bar = 10 µm.

Crucially, this effect is specific to stimulated axons and not just a general effect of capsaicin treatment on myelin sheath growth. As a control, the same experiment was performed on larvae with axons which did not express TRPV1-RFP (**Figure 30A**). Analysis showed that capsaicin alone did not significantly affect the early growth of early born myelin sheaths (**Figure 30B, C**; the mean sheath length of early born sheaths per axon at 5 dpf was 34.0 µm for vehicle, and 35.1 µm for capsaicin (unpaired t-test, p = 0.911); the mean change in sheath length 3-5 dpf per axon was 25.3 µm for vehicle, and 24.4 µm for capsaicin (unpaired t-test, p = 0.867)).

Many sheaths were formed along RS axons between 3 to 5 dpf. The mean length of these ‘later born’ myelin sheaths at 5 dpf was calculated for each axon (**Figure 29D**). There was no significant difference in the length of these later born sheaths between unstimulated and stimulated axons at 5 dpf (mean sheath length of later born sheaths per axon was 30.0 µm for vehicle, and 32.4 µm for capsaicin; unpaired t-test, p = 0.595). However, these sheaths could have been formed at any point between imaging at 3 dpf and imaging at 5 dpf. It is not known how long each of these later born sheaths had been exposed to the unstimulated or stimulated conditions, and, therefore, it was impossible to determine whether or not stimulation might have enhanced the initial growth of these later born myelin sheaths.

Based on these results, I concluded that neuronal activity promotes the growth of the early born myelin sheaths along RS axons.

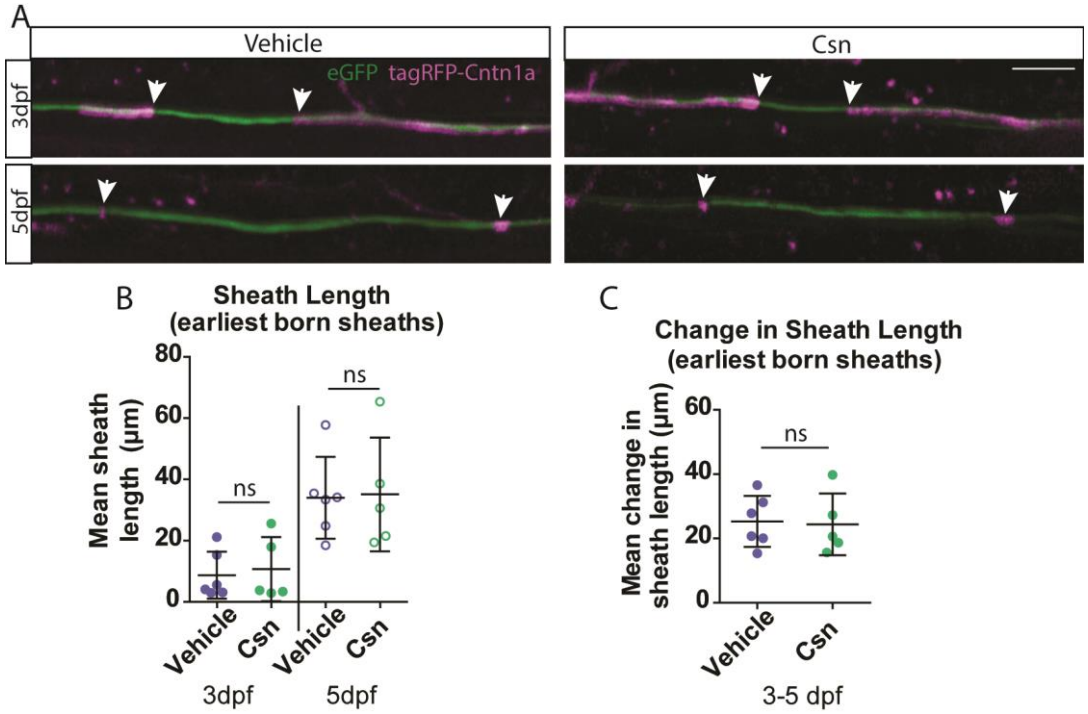

Figure 30 – early sheath dynamics along TRPV1-RFP-negative RS axons treated with capsaicin.

A) Example images of sheath growth 3-5 dpf along TRPV1-RFP-negative RS axons treated with either vehicle or 1 µM capsaicin. Unmyelinated axon is labelled with tagRFPt-Cntn1a. White arrows = the edges of the myelin sheath. **B)** The mean sheath length of "earliest born sheaths" on TRPV1-RFP-negative RS axons at 3 and 5 dpf treated with either vehicle or 1 µM capsaicin. "Earliest born sheaths" are defined as sheaths which were formed prior to imaging at 3 dpf. The mean sheath length per axon at 3 dpf was 8.7 µm (SD = 7.7) for vehicle, and 10.7 µm (SD = 10.5) for capsaicin; and at 5 dpf was 34.0 µm (SD = 13.3) for vehicle, and 35.1 µm (SD = 18.6) for capsaicin. There was no statistically significant difference between the two groups at any age (unpaired t-tests; 3 dpf p = 0.721, vehicle n = 6, capsaicin n = 5; 5 dpf p = 0.911, vehicle n = 6, capsaicin n = 5). **C)** The mean change in sheath length 3-5 dpf of earliest born sheaths along TRPV1-RFP-negative RS axons treated with either vehicle or 1 µM capsaicin. The mean change in sheath length 3-5 dpf per axon was 25.3 µm (SD = 7.9) for vehicle, and 24.4 µm (SD = 9.6) for capsaicin. There was no significant difference between the two groups (unpaired t-test, p = 0.867, vehicle n = 6, capsaicin n = 5). Scale bar = 10 µm.

4.2.4. Activity Does Not Affect Later (5-7 dpf) Myelin Sheath Dynamics

The early born myelin sheaths were then followed 5-7 dpf to see if increased neuronal activity continued to promote their growth (**Figure 31A**). This analysis was performed on cells where the same area of axon could be followed from 3-7 dpf. The mean change in sheath length of early born sheaths 5-7 dpf was calculated per axon. Despite the fact that sheaths on unstimulated axons continued to grow, those on stimulated axons exhibited almost no growth 5-7 dpf (the mean change in sheath length 5-7 dpf per axon was 5.8 µm for vehicle, and 0.1 µm for capsaicin; unpaired t-test, $p = 0.056$, **Figure 31B**). Although this difference was not statistically significant, a power calculation states that this comparison has only 54% power, and that an n of 12 samples per group would be required to reach 80% power. However, the throughput of the experiment meant that increasing the sample size was not feasible (an n of 5-6 per group was obtained after screening several thousand larvae and imaging more than 50 cells over time). It is plausible that the sheaths on stimulated axons ran out of space sooner than the sheaths on unstimulated axons, due to an early stimulation of sheath growth, leading to a reduced change in sheath length compared to unstimulated axons.

The dynamics of later born myelin sheaths were also followed 5-7 dpf. This analysis was performed on cells where the same area of axon could be followed from 3-7 dpf. Unlike the early born sheaths (which exhibited negligible change in length), the later born sheaths along both unstimulated and stimulated axons exhibited significant change in length. However, there was no statistically significant difference in the change in sheath length of later born sheaths between unstimulated and stimulated axons from 5-7 dpf (the mean change in sheath length 5-7 dpf per axon was 11.1 µm for vehicle, and 9.7 µm for capsaicin; unpaired t-test, $p = 0.548$, **Figure 31C**). This further indicates that the dynamics of later born myelin sheaths are not regulated by neuronal activity.

There are two possibilities for a lack of effect of activity on sheath growth between 5 to 7 dpf. One possibility is that sheaths have a finite amount of

space in which to grow by 5-7 dpf; therefore, even if activity were capable of accelerating the growth of sheaths on stimulated axons, they might simply run out of space early on, and so the sheaths on unstimulated axons can catch up by 7 dpf. The other possibility is that myelin sheaths no longer detect or respond to neuronal activity between 5 to 7 dpf, and so sheaths on both unstimulated and stimulated axons would grow at the same rate between 5 to 7 dpf, assuming they had to space to do so. To differentiate between these possibilities, I restricted my analysis to myelin sheaths which still had at least a total of 20 µm adjacent unmyelinated axonal space at 7 dpf, because these sheaths should still have had ample space into which to grow and should, in principle, have had the capacity to respond to activity at the later 5-7 dpf stage. And yet, I found that there was no significant difference in the change in length of these sheaths between unstimulated and stimulated axons (the mean change in sheath length 5-7 dpf per axon was 8.9 µm for vehicle, and 10.8 µm for capsaicin; unpaired t-test, $p = 0.861$, **Figure 31D**). Nevertheless, the sample size was smaller for this analysis ($n = 3$-4 per group), and this calculation may thus be underpowered. A power calculation suggests that, with the variability observed in **Figure 31D**, a sample size of 876 per group would be required to reach 80% power. Therefore, any effect of neuronal activity on sheath dynamics 5-7 dpf is likely to be negligible, even on sheaths with space in which to grow, reflecting the limited remodelling of myelin along these axons at this stage.

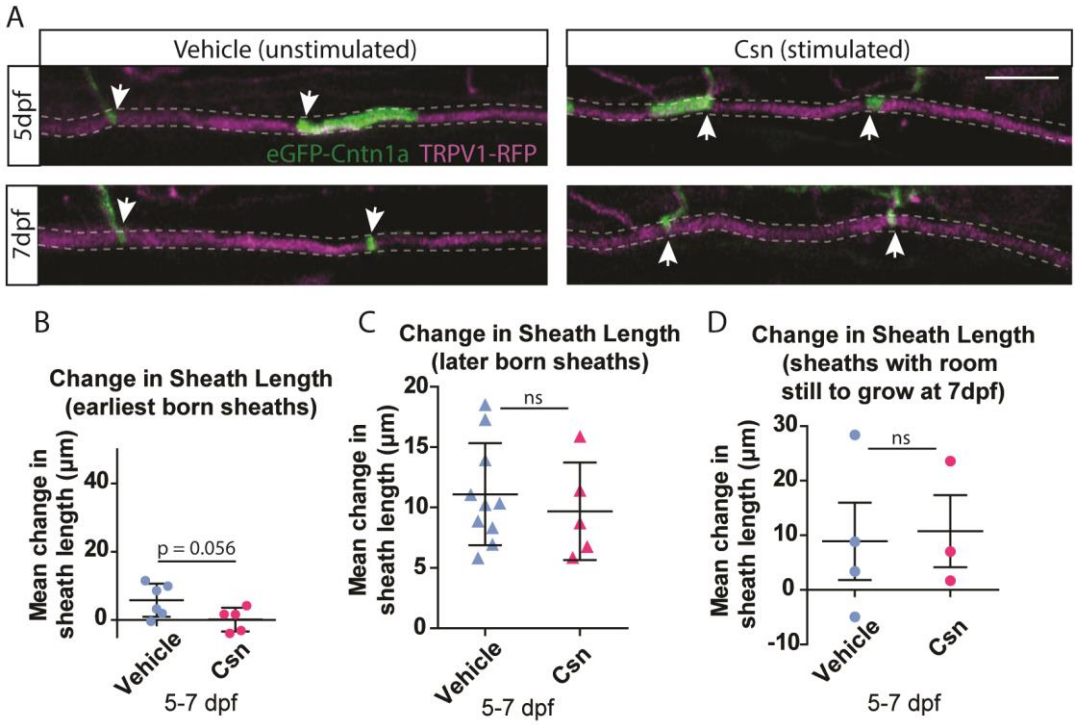

Figure 31 – later sheath dynamics along chemogenetically stimulated individual RS axons.

A) Example images of myelin sheath growth 5-7 dpf on TRPV1-RFP+ RS axons. White arrows = the edges of the myelin sheath. **B)** The mean change in sheath length 5-7 dpf of earliest born sheaths along individual TRPV1-RFP+ RS axons treated with either vehicle or 1 µM capsaicin. 'Earliest born sheaths' were defined as sheaths which were formed prior to imaging at 3 dpf. The mean change in sheath length 5-7 dpf per axon was 5.8 µm (SD = 4.8) for vehicle, and 0.1 µm (SD = 3.5) for capsaicin. There was no statistically significant difference between the two groups (unpaired t-test, p = 0.056, vehicle n = 6, capsaicin n = 5). **C)** The mean change in sheath length 5-7 dpf of later born sheaths along individual TRPV1-RFP+ RS axons treated with either vehicle or 1 µM capsaicin. 'Later born sheaths' were defined as sheaths born between the 3 and 5 dpf imaging sessions. Only sheaths which still had room to grow at 5 dpf were included in this analysis. The mean change in sheath length 5-7 dpf per axon was 11.1 µm (SD = 4.2) for vehicle, and 9.7 µm (SD = 4.0) for capsaicin. There was no statistically significant difference between the two groups (unpaired t-test, p = 0.548; vehicle n = 10, capsaicin n = 5). **D)** The mean change in sheath length 5-7 dpf of sheaths with room still to grow at 7 dpf along individual TRPV1-RFP+ RS axons treated with either vehicle or 1 µM capsaicin. 'Sheaths with room still to grow at 7 dpf' were defined as sheaths which

had at least a total of 20 µm of unmyelinated adjacent axonal space at 7 dpf. The mean change in sheath length 5-7 dpf per axon was 8.9 µm (SD = 14.2) for vehicle, and 10.8 µm (SD = 11.4) for capsaicin. There was no statistically significant difference between the two groups (unpaired t-test, p = 0.861, vehicle n = 4, capsaicin n = 3). Scale bar = 10 µm.

4.2.5. Sheath Growth and Shrinkage

Thus far, I have calculated the mean change in sheath length per axon of early- and later-formed myelin sheaths 3-7 dpf, without discriminating between the growth and shrinkage of the distinct sheaths along those axons. It is possible that neuronal activity may specifically change either the growth or shrinkage of individual sheaths along axons, which would not necessarily be detected by assessing the mean changes in sheath length. However, none of the sheaths which were followed 3-5 dpf shrank in length; therefore, neuronal activity must promote sheath growth between 3 to 5 dpf, rather than inhibit sheath shrinkage.

In Chapter 3, I showed that both sheath growth and shrinkage occur along individual RS axons between 5 to 7 dpf, albeit to a limited extent. I proceeded to quantify sheath growth and shrinkage along unstimulated and stimulated RS axons 5-7 dpf in order to test if neuronal activity affects myelin remodelling at these stages (**Figure 32**). This analysis was performed on cells where the same individual sheaths could be followed between 5 to 7 dpf. I found that, although there was a 46% reduction in the median amount of 5-7 dpf sheath growth along stimulated axons compared to unstimulated (Mann-Whitney effect size r = 0.26), this was not a statistically significant difference (the median sheath growth along vehicle-treated axons was 19.8 µm/100 µm axon, and for capsaicin-treated axons was 10.7 µm/100 µm axon; Mann-Whitney test, p = 0.171, **Figure 32A**). A power calculation confirms that this test has only 18% power, with an n of 86 required to reach 80% power. As noted above in section ‘4.2.4 Activity Does Not Affect Later (5-7 dpf) Myelin Sheath Dynamics’, it is possible that the sheaths along stimulated axons do, indeed,

exhibit less growth than unstimulated axons 5-7 dpf. This could be a result of the transient enhancement of sheath growth between 3 to 5 dpf, which leaves sheaths with less available space into which to grow, or because these sheaths downregulate growth 5-7 dpf to eventually reach the same length as sheaths along unstimulated axons.

Next, I assessed the rates of sheath shrinkage along axons with normal or increased activity. I found that there was no significant effect of neuronal stimulation on sheath shrinkage 5-7 dpf (the median sheath shrinkage along vehicle-treated axons was -3.3 µm/100 µm axon, and for capsaicin-treated axons was -2.8 µm/100 µm axon; Mann-Whitney test, p = 0.835. Vehicle n = 16, capsaicin n = 12; **Figure 32B**).

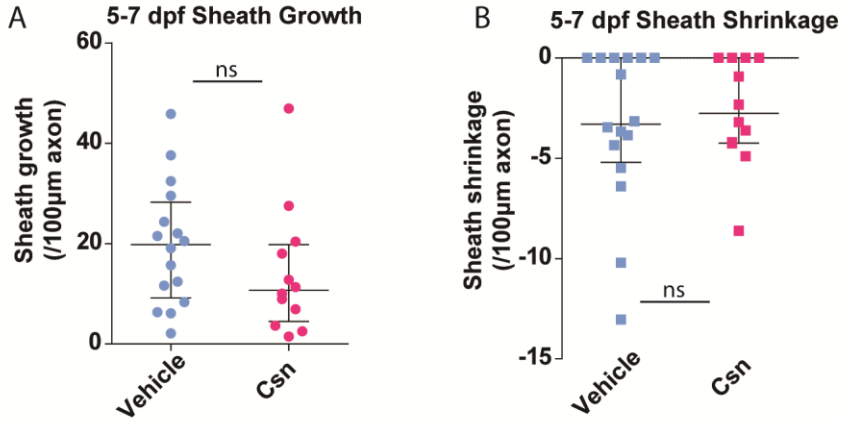

Figure 32 – sheath growth and shrinkage 5-7 dpf along unstimulated and stimulated RS axons.

A) The sheath growth along RS axons 5-7 dpf vehicle or 1 µM capsaicin. The median sheath growth along TRPV1-RFP axons treated with vehicle was 19.8 µm/100 µm axon (IQR = 9.2-28.3), and for capsaicin-treated axons was 10.7 µm/100 µm axon (IQR = 4.4-19.8). There was no statistically significant difference between the two groups (Mann-Whitney test, p = 0.171; vehicle n = 16, capsaicin n = 12). **B)** The sheath shrinkage along RS axons 5-7 dpf vehicle or 1 µM capsaicin. The median sheath shrinkage along TRPV1-RFP axons treated with vehicle was -3.3 µm/100 µm axon (IQR = (-5.2)-(0)), and for capsaicin-treated axons was -2.8 µm/100 µm axon (IQR = (-4.2)-(0)). There was no statistically significant difference

between the two groups (Mann-Whitney test, p = 0.835; vehicle n = 16, capsaicin n = 12).

Based on these results, I concluded that neuronal activity does not affect the dynamics of myelin sheaths 5-7 dpf (although increased n is likely to reveal that growth of myelin sheaths after 5 dpf is downregulated along stimulated axons).

4.2.6. Effects of Single Axon Stimulation on Sheath Retraction

Timelapse and time course analyses of single oligodendrocytes has shown that myelin sheaths can be retracted, typically within a short period after their formation (Baraban et al., 2018; Hines et al., 2015; Mensch et al., 2015). Ca^{2+} imaging in oligodendrocytes identified large-amplitude long-duration Ca^{2+} events in sheaths immediately prior to their retraction, which suggests that sheaths can receive local signals that can induce retraction (Baraban et al., 2018). There is also evidence that inhibiting synaptic vesicle release in axons increases the retraction of short myelin sheaths (Hines et al., 2015).

I have demonstrated that sheath retractions can occur along RS axons after the initial period of myelin sheath formation (see section '3.2.2 Changes in Sheath Number over Time'); however, it is not known how neuronal activity affects sheath retractions. To investigate this, I followed individual myelin sheaths along unstimulated and stimulated axons, and quantified the number of sheath retractions which occurred. Only one out of the 17 sheaths formed before imaging at 3 dpf was retracted by 5 dpf, suggesting that very few sheath retractions occur during early stages of myelination. However, it is likely that a significant amount of sheath dynamics are missed between the imaging sessions on 3 and 5 dpf, and that many small sheaths or contacts form and retract within this time period.

Sheath retractions were also observed between 5 to 7 dpf (**Figure 33A**). I have previously shown that virtually all of the sheaths which are retracted during this time period are under 10 µm long, and that the fate of myelin sheaths appears

to correlate with their length (section '3.2.2 Changes in Sheath Number over Time'). Therefore, I restricted the analysis to axons which had sheaths which were of a size capable of being retracted (that is, axons which had sheaths < 10 µm in length at 5 dpf). There was a 57% reduction in the number of sheaths retracted along stimulated axons compared to controls 5-7 dpf (Cohen's d effect size = 1.13). However, this difference was not statistically significant (the mean number of sheath retractions/100 µm axon 5-7 dpf was 0.7 for vehicle, and 0.3 for capsaicin; unpaired t-test, p = 0.112, **Figure 33B**). A power calculation indicates that this analysis has only 41% power, and that increasing the sample size from six to 16 per group is required to reach 80% power.

These results suggest that activity can likely reduce the rate of sheath retractions along an axon, but further analysis is required to determine whether this phenotype would reach statistical significance.

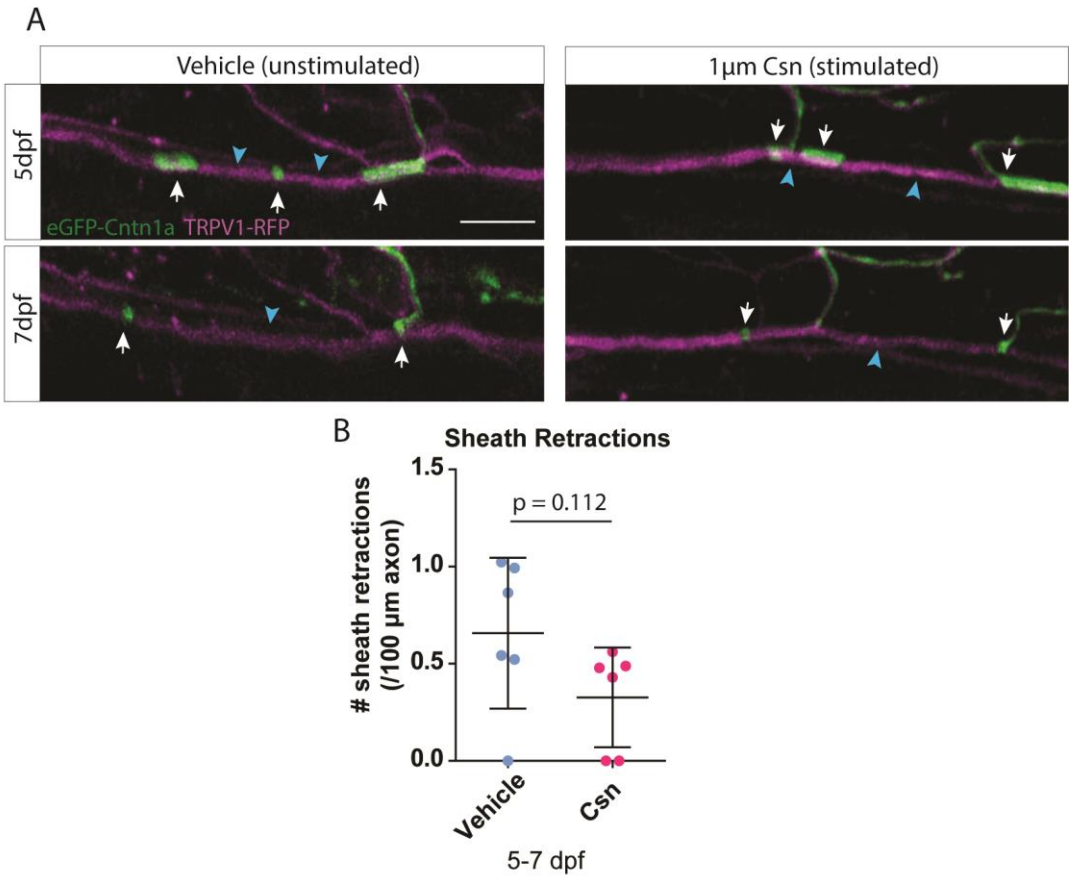

Figure 33 – myelin sheath retractions along chemogenetically stimulated RS axons.

A) Example images of sheath retraction occurring 5-7 dpf on TRPV1-RFP+ RS axons treated with either vehicle or 1 µM capsaicin. White arrows = unmyelinated gaps between myelin sheaths, blue arrow heads = myelin sheaths. In each example one myelin sheath is retracted 5-7 dpf. **B)** Quantification of sheath retractions along vehicle or 1 µM capsaicin treated RS axons. Only axons which had any retractable sheaths (sheaths < 10 µm in length) were analysed. The mean number of sheath retractions/100 µm axon 5-7 dpf was 0.7 (SD = 0.4) for vehicle, and 0.3 (SD = 0.3) for capsaicin. There was no statistically significant difference between the two groups (unpaired t-test, p = 0.112, vehicle n = 6, capsaicin n = 6). Scale bar = 10 µm.

4.2.7. Neuronal Activity Affects the Formation of Myelin Patterns along Individual Axons

Analysis of sheath dynamics along unstimulated and stimulated axons indicates that activity promotes the growth of myelin sheaths during a critical developmental period, after which sheaths no longer respond to neuronal activity. In Chapter 3, I demonstrated that the myelin pattern (the number and length of myelin sheaths) along RS axons is established by 7 dpf. It is not clear whether promoting sheath growth 3-5 dpf permanently alters the myelin patterns established on RS axons by 7 dpf. To investigate this, I characterised the myelin patterns of unstimulated and stimulated axons by measuring the number and length of their myelin sheaths at 3, 5, and 7 dpf.

Myelin Patterns along all RS Axons Imaged

Prior to any manipulation, all of the RS axons imaged were predominantly unmyelinated at 3 dpf (median % axon myelinated at 3 dpf was 3.2% for vehicle, and 3.6% for capsaicin; Mann-Whitney test, p = 0.677, **Figure 34A**). Daily stimulation of neuronal activity did not significantly change the proportion of the axon which was myelinated from a statistical point of view (median % axon myelinated at 5 dpf being 74.3% for vehicle and 81.2% for capsaicin; and at 7 dpf being 91.5% for vehicle and 96.0% for capsaicin (Mann-Whitney tests; 5 dpf p = 0.304, 7 dpf p = 0.531, **Figure 34A**)). It is, nevertheless, interesting

to note the slight increase in % axon myelinated in stimulated axons at both ages.

I have shown that neuronal activity promotes the growth of myelin sheaths 3-5 dpf (**Figure 29**). However, whether this results in permanently longer myelin sheaths along stimulated versus unstimulated RS axons was not clear. The mean sheath length for each axon was calculated at each age; prior to stimulation, the mean sheath length per axon at 3 dpf was 5.7 µm for vehicle, and 4.7 µm for capsaicin. Intriguingly, I found that there was no statistically significant effect of daily activity stimulation on overall mean sheath length at either 5 or 7 dpf (mean sheath length per axon at 5 dpf was 28.9 µm for vehicle, and 31.7 µm for capsaicin; and at 7 dpf was 37.6 µm for vehicle, and 37.2 µm for capsaicin; unpaired t-tests, 5 dpf $p = 0.431$, 7 dpf $p = 0.927$, **Figure 34B**).

Similarly, sheath number (normalised to length of axon analysed) was not significantly changed by daily stimulation at any age (the mean sheath number /100 µm axon at 3 dpf was 0.7 for vehicle, and 0.6 for capsaicin; at 5 dpf was 2.7 for vehicle, and 2.6 for capsaicin; and at 7 dpf was 2.5 for vehicle, and 2.5 for capsaicin; unpaired t-tests, 3 dpf $p = 0.641$, 5 dpf $p = 0.880$, 7 dpf $p = 0.884$, **Figure 34C**).

This data suggests that, although neuronal activity can accelerate the growth of myelin sheaths during a critical period, it does not change the final myelin pattern which is formed along the axon.

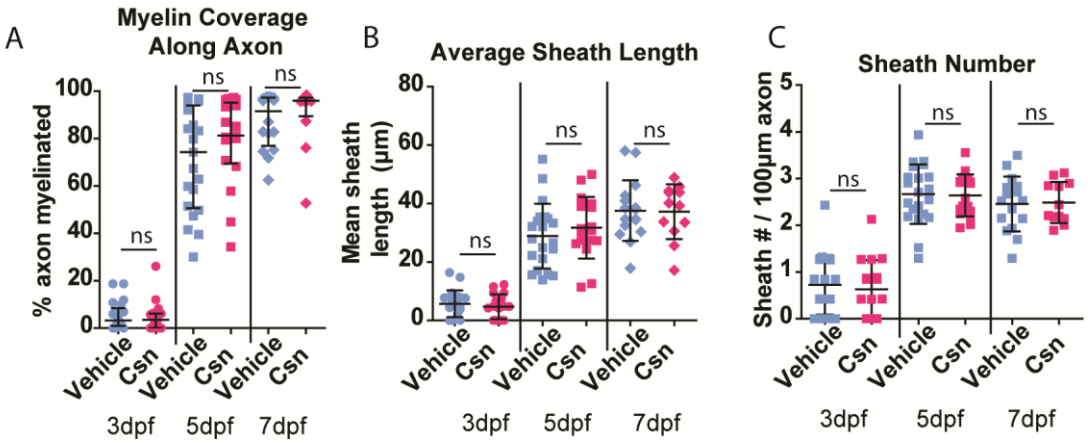

Figure 34 – the myelin pattern of individual chemogenetically stimulated RS axons.

A) The amount of myelin along RS axons at 3, 5, and 7 dpf treated with either vehicle or 1 µM capsaicin. The median % axon myelinated at 3 dpf was 3.2% (IQR = 0.9-8.4) for vehicle, and 3.6% (IQR = 0-6.2) for capsaicin; at 5 dpf was 74.3% (IQR = 50.6-93.9) for vehicle and 81.2% (IQR = 69.5-95.1) for capsaicin; and at 7 dpf was 91.5% (IQR = 76.9-97.3) for vehicle and 96.0% (IQR = 89.4-97.2) for capsaicin. There was no statistically significant difference between the two groups at any age (Mann-Whitney tests; 3 dpf p = 0.677, vehicle n = 21, capsaicin n = 17; 5 dpf p = 0.304, vehicle n = 21, capsaicin n = 17; 7 dpf p = 0.531, vehicle n = 16, capsaicin n = 12). **B)** The average sheath length along RS axons at 3, 5, and 7 dpf treated with either vehicle or 1 µM capsaicin. The mean sheath length per axon at 3 dpf was 5.7 µm (SD = 4.6) for vehicle, and 4.7 µm (SD = 4.3) for capsaicin; at 5 dpf was 28.9 µm (SD = 11.1) for vehicle, and 31.7 µm (SD = 10.6) for capsaicin; and at 7 dpf was 37.6 µm (SD = 10.3) for vehicle, and 37.2 µm (SD = 9.4) for capsaicin. There was no statistically significant difference between the two groups at any age (unpaired t-tests; 3 dpf p = 0.489, vehicle n = 21, capsaicin n =17; 5 dpf p = 0.431, vehicle n = 21, capsaicin n =17; 7 dpf p = 0.927, vehicle n = 16, capsaicin n = 12). **C)** The number of sheaths along RS axons at 3, 5 and 7 dpf treated with either vehicle or 1 µM capsaicin. The mean sheath number at 3 dpf was 0.7 /100 µm axon (SD = 0.6) for vehicle, and 0.6 /100 µm axon (SD = 0.6) for capsaicin; at 5 dpf was 2.7 /100 µm axon (SD = 0.6) for vehicle, and 2.6 /100 µm axon (SD = 0.4) for capsaicin; and at 7 dpf was 2.5 /100 µm axon (SD = 0.6) for vehicle, and 2.5 /100 µm axon (SD = 0.4) for capsaicin. There was no statistically significant difference between the two groups at any age (unpaired t-tests; 3 dpf p = 0.641,

vehicle n = 21, capsaicin n = 17; 5 dpf p = 0.880, vehicle n = 21, capsaicin n = 17; 7 dpf p = 0.884, vehicle n = 16, capsaicin n = 12).

Myelin Patterns of Axons with and without Early born Sheaths

Overall, there was no significant long-lasting change to the myelin patterns of RS axons upon chemogenetic stimulation. However, there was variation in the timescale of myelination within the population of RS axons analysed. As noted above in section '4.2.3 Activity Promotes Early (3-5 dpf) Myelin Sheath Dynamics', on some RS axons myelination began before imaging at 3 dpf, whereas, on other RS axons myelination did not start until between 3 and 5 dpf. My data indicate that neuronal activity only increases the growth of the earliest born sheaths on axons (sheaths formed before 3 dpf) between 3 to 5 dpf, and that activity does not significantly affect the dynamics of any myelin sheaths after 5 dpf (**Figure 29**, **Figure 31**, **Figure 32**). Consequently, neuronal activity might, in principle, selectively affect the myelin patterns of axons where myelination begins before 3 dpf (along axons with early born sheaths) more than axons where myelination begins between 3 and 5 dpf (axons without early born sheaths). I investigated whether activity differentially affected the myelin patterns of RS axons with and without early born sheaths. The myelin patterns were assessed along cells where the same portion of axon could be followed 3-7 dpf.

For axons *with* early born sheaths, chemogenetic stimulation did not significantly change the proportion of axon which was myelinated (the median % axon myelinated at 3 dpf was 8.4% for vehicle-treated axons, 6.2% for capsaicin-treated axons; at 5 dpf was 85.9% for vehicle, 96.4% for capsaicin; and at 7 dpf was 96.7% for vehicle, and 96.7% for capsaicin; Mann-Whitney tests; 3 dpf p = 0.931; 5 dpf p = 0.429; 7 dpf p = 0.662; **Figure 35A**). Neither the number nor the length of myelin sheaths along early myelinated axons were significantly different between unstimulated and stimulated groups at 3 dpf (the mean sheath length per axon at 3 dpf was 9.9 µm for vehicle, 7.6 µm for capsaicin, unpaired t-test p = 0.384; mean sheath number (normalised to

length of axon analysed) at 3 dpf was 1.0 /100 µm axon for vehicle, 1.3 /100 µm axon for capsaicin, unpaired t-test p = 0.362, **Figure 35B, C**). By 5 dpf, the mean sheath length of stimulated axons was 42% longer than controls, in line with the observed increase in growth rate over this period (albeit not quite statistically significant; mean sheath length at 5 dpf was 28.4 µm for vehicle, 40.3 µm for capsaicin, unpaired t-test p = 0.071). There was also a 12% reduction in sheath number along stimulated axons compared to controls (again, not quite statistically significant; mean sheath number at 5 dpf was 2.6 /100 µm axon for vehicle, 2.3 /100 µm axon for capsaicin, unpaired t-test p = 0.098, **Figure 35B, C**). By 7 dpf, there was a statistically significant difference in both sheath length and sheath number between unstimulated and stimulated groups (mean sheath length at 7 dpf was 34.1 µm for vehicle, and 43.7 µm for capsaicin, unpaired t-test p = 0.045; mean sheath number at 7 dpf was 2.7 /100 axon µm for vehicle, and 2.1 /100 µm axon for capsaicin, unpaired t-test p = 0.037, **Figure 35B, C**).

In summary, despite the fact that both stimulated and unstimulated axons were myelinated to the same extent, neuronal activity induced subtle changes in the myelin pattern formed along axons with early born myelin sheaths. These axons had longer myelin sheaths because chemogenetic stimulation promoted the growth of early born myelin sheaths 3-5 dpf. This increase in sheath length likely reduced the available axonal space for new sheaths to form, and so fewer later born myelin sheaths were made along these axons.

Axons *without* early born myelin sheaths also exhibited no significant differences in the proportion of axon which was myelinated upon chemogenetic stimulation (median % axon myelinated at 5 dpf was 75.7% for vehicle, 82.6% for capsaicin; and at 7 dpf was 91.9% for vehicle, and 95.6% for capsaicin; Mann-Whitney tests, 5 dpf p = 0.886; 7 dpf p = 1.000; **Figure 35D**). Unlike the axons which did have early born sheaths, chemogenetic stimulation did not increase sheath length along axons without early born sheaths (mean sheath length at 5 dpf was 32.1 µm for vehicle, and 26.5 µm for capsaicin; and at 7 dpf was 42.0 µm for vehicle, and 33.4 µm for capsaicin; unpaired t-tests, 5 dpf p = 0.603; 7 dpf p = 0.288; **Figure 35E**). There may be

a trend towards a decrease in sheath length, with mean sheath length at 7 dpf being 20% shorter along stimulated axons than controls. There was also no significant change in sheath number (mean sheath number at 5 dpf was 2.6 /100 µm axon for vehicle, 3.0 /100 µm axon for capsaicin; and at 7 dpf was 2.3 /100 µm for vehicle, and 2.8 /100 µm for capsaicin; unpaired t-tests 5 dpf $p = 0.445$; 7 dpf $p = 0.262$; **Figure 35F**). Again, there may be a trend towards an increase in sheath number, with mean sheath number being 22% increased along stimulated axons compared to controls.

In summary, neuronal activity does not significantly alter the extent of myelination along axons without early born sheaths. It is possible that neuronal activity subtly changes the myelin pattern along these axons, where stimulated axons may have more, but shorter, sheaths than controls; however, this is not statistically significant, and requires further investigation to confirm. This potential reduction in sheath length may appear counterintuitive given my previous findings that activity promotes sheath growth during a critical period between 3 to 5 dpf. Nevertheless, a reduction in sheath length and increase in sheath number could be explained by changes to the rate of sheath retraction. Neuronal activity may prevent sheath retractions (as indicated by my data in **Figure 33**). With more sheaths competing for the same amount of axonal space, the mean sheath length may be shorter along stimulated axons than controls. An increased n number is required to determine if changes to sheath number and length could become statistically significant.

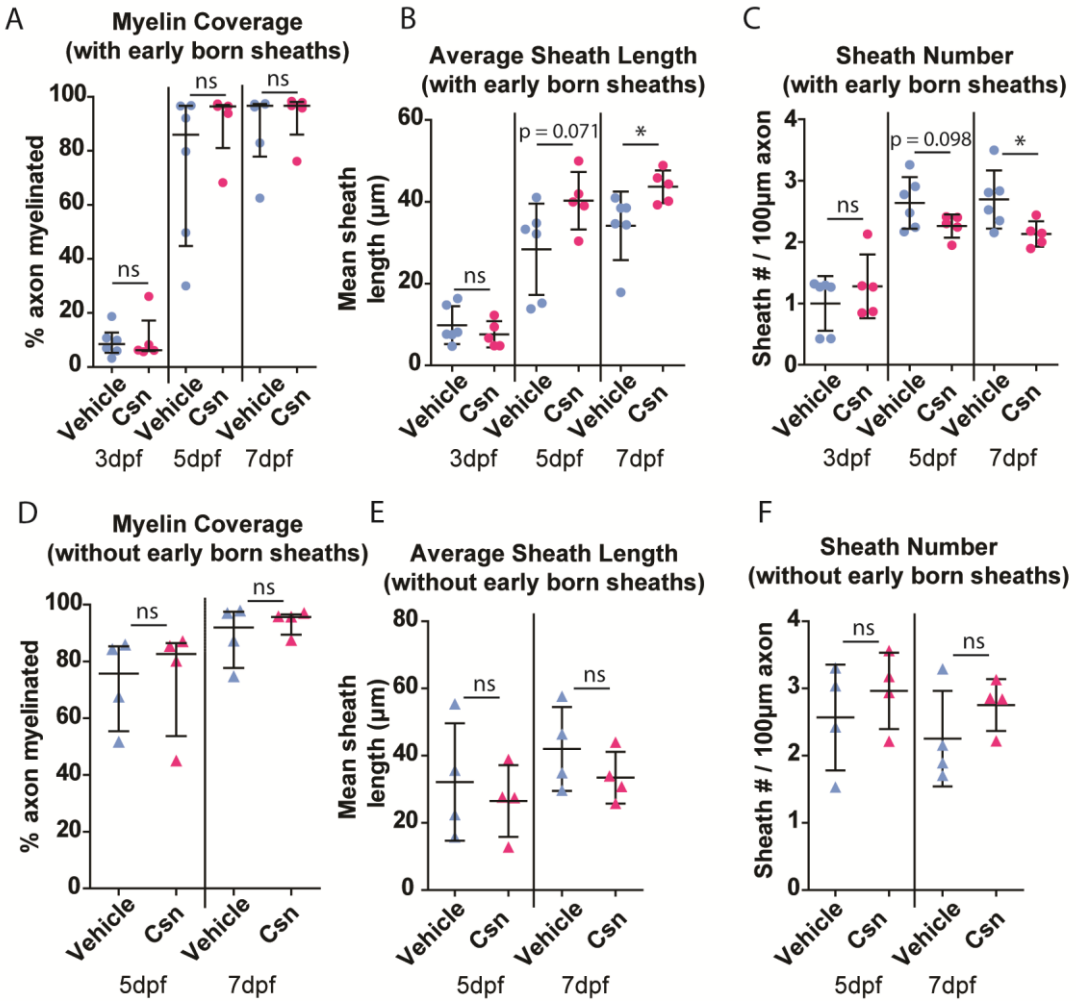

Figure 35 – the myelin patterns of RS axons with and axons without early born sheaths after chemogenetic stimulation.

A) The myelin coverage along RS axons with early born sheaths at 3, 5, and 7 dpf treated with vehicle or 1 µM capsaicin. The median % axon myelinated at 3 dpf was 8.4% (IQR = 5.3-12.7) for vehicle, 6.2% (IQR = 5.9-17.2) for capsaicin; at 5 dpf was 85.9% (IQR = 44.8-96.6) for vehicle, 96.4% (IQR = 81.0-96.9) for capsaicin; and at 7 dpf was 96.7% (IQR = 77.8-97.3) for vehicle, and 96.7 (IQR = 86.0-98.1) for capsaicin. There was no statistically significant difference between the two groups at any age (Mann-Whitney tests; 3 dpf p = 0.931; 5 dpf p = 0.429; 7 dpf p = 0.662; vehicle n = 6, capsaicin n = 5). **B)** The mean sheath length along RS axons with early born sheaths at 3, 5, and 7 dpf treated with vehicle or 1 µM capsaicin. The mean sheath length at 3 dpf was 9.9 µm (SD = 4.6) for vehicle, 7.6 µm (SD = 3.2) for capsaicin; at 5 dpf was 28.4 µm (SD = 11.2) for vehicle, 40.3 µm (SD = 7.0) for capsaicin; and at 7 dpf was 34.1 µm (SD = 8.4) for vehicle, and 43.7 µm (SD = 4.0)

for capsaicin. There was a statistically significant difference between vehicle and capsaicin at 7 dpf (unpaired t-tests; 3 dpf p = 0.384; 5 dpf p = 0.071; 7 dpf p = 0.045; vehicle n = 6, capsaicin n = 5). **C)** The number of sheaths (normalised to length of axon analysed) along RS axons with early born sheaths at 3, 5, and 7 dpf treated with vehicle or 1 µM capsaicin. The mean sheath number at 3 dpf was 1.0 /100 µm axon (SD = 0.4) for vehicle, 1.3 /100 µm axon (SD = 0.5) for capsaicin; at 5 dpf was 2.6 /100 µm axon (SD = 0.4) for vehicle, 2.3 /100 µm axon (SD = 0.2) for capsaicin; and at 7 dpf was 2.7 /100 axon µm (SD = 0.5) for vehicle, and 2.1 /100 µm axon (SD = 0.2) for capsaicin. There was a statistically significant difference between vehicle and capsaicin at 7 dpf (unpaired t-tests; 3 dpf p = 0.362; 5 dpf p = 0.098; 7 dpf p = 0.037; vehicle n = 6, capsaicin n = 5). **D)** The myelin coverage along RS axons without early born sheaths at 5 and 7 dpf treated with vehicle or 1 µM capsaicin. The median % axon myelinated at 5 dpf was 75.7% (IQR = 55.4-85.3) for vehicle, 82.6% (IQR = 53.6-86.5) for capsaicin; and at 7 dpf was 91.9% (IQR = 77.6-97.4) for vehicle, and 95.6% (IQR = 89.4-96.5) for capsaicin. There was no statistically significant difference between the two groups at any age (Mann-Whitney tests; 5 dpf p = 0.886; 7 dpf p = 1.000; vehicle n = 4, capsaicin n = 4). **E)** The mean sheath length along RS axons without early born sheaths at 5 and 7 dpf treated with either vehicle or 1 µM capsaicin. The mean sheath length per axon at 5 dpf was 32.1 µm (SD = 17.5) for vehicle, and 26.5 µm (SD = 10.7) for capsaicin; and at 7 dpf was 42.0 µm (SD = 12.5) for vehicle, and 33.4 µm (SD = 7.7) for capsaicin. There was no statistically significant difference between the two groups at any age (unpaired t-tests; 5 dpf p = 0.603; 7 dpf p = 0.288; vehicle n = 4, capsaicin n = 4). **F)** The number of sheaths (normalised to length of axon analysed) along RS axons without early born sheaths at 5 and 7 dpf treated with either vehicle or 1 µM capsaicin. The mean sheath number at 5 dpf was 2.6 /100 µm axon (SD = 0.8) for vehicle, 3.0 /100 µm axon (SD = 0.6) for capsaicin; and at 7dpf was 2.3 /100 µm (SD = 0.7) for vehicle, and 2.8 /100 µm (SD = 0.4) for capsaicin. There was no statistically significant difference between the two groups at any age (unpaired t-tests; 5 dpf p = 0.445; 7 dpf p = 0.262; vehicle n = 4, capsaicin n = 4).

4.2.8. Increasing Neuronal Activity Using TRPV1 Does Not Affect Node Length or Axon Diameter

As discussed in Chapter 3, node length may also influence conduction properties. It is possible that a subtle difference in sheath length could significantly change the length of nodes, or that activity directly changes nodal architecture itself. I measured the length of nodes at 3, 5, and 7 dpf to see if chemogenetic stimulation affected nodal development during this time period. The reporter FP-Cntn1a labels unmyelinated gaps between myelin sheaths, including nodes of Ranvier. However, it does not specifically label mature nodes of Ranvier. Therefore, I cannot definitively identify which gaps between myelin sheaths are mature nodes of Ranvier, and which are simply larger regions of unmyelinated axon. To exclude larger unmyelinated gaps which were definitely not mature nodes, I only analysed gaps which were under 5 µm in length (these were termed nodal gaps).

At 3 dpf, axons did not have sufficient myelin coverage to have any nodal gaps. There was no significant difference in nodal gap length at either 5 or 7 dpf between the unstimulated and stimulated axons (the median nodal gap length at 5 dpf was 1.23 µm for vehicle, and 1.13 µm for capsaicin; and at 7 dpf was 0.90 µm for vehicle, and 1.08 µm for capsaicin; Mann-Whitney tests, 5 dpf $p = 0.875$, 7 dpf $p = 0.244$, **Figure 36B**).

Sheath growth may have an impact on the size of nodes of Ranvier, and so signals which impact sheath growth may impact node length. I have shown that neuronal activity promotes the growth of early born sheaths 3-5 dpf; this changes the myelin pattern formed along axons which have early born sheaths. It is possible that the enhancement of early born myelin sheath growth alters the length of nodes along axons with early born sheaths. Therefore, nodal gap length analysis was broken down into axons which had early born myelin sheaths and axons which did not have early born myelin sheaths. However, for axons with early born sheaths, there was no significant difference in the average nodal gap length with chemogenetic stimulation (median nodal gap length at 5 dpf was 1.02 µm for vehicle, 1.14 µm for capsaicin; and at 7

dpf was 0.91 µm for vehicle, and 1.07 µm for capsaicin; Mann-Whitney tests, 5 dpf p = 0.905, 7 dpf p = 1.000; **Figure 37B**). For axons without early born sheaths, there was also no significant change in nodal gap length (the median nodal gap length at 5 dpf was 1.58 µm for vehicle, 1.48 µm for capsaicin; and at 7 dpf was 0.93 µm for vehicle, and 1.09 µm for capsaicin; unpaired t-tests, 5 dpf p = 0.582, 7 dpf p = 0.249; **Figure 37D**). It is important to note that, due to limitations in image resolution, it was not possible to measure the nodal gap lengths of some axons at 7 dpf (hence, there are fewer n in **Figure 37** than in **Figure 35**).

Axon diameter is another parameter which may, in principal, be significantly altered by activity, in order to modulate conduction properties. In rodents, reducing activity in the auditory system using ear plugs leads to development of thinner axons in the trapezoid body (Sinclair et al., 2017). To investigate whether increasing the activity along single axons regulates axon size, axon diameter was measured using the same method as described in Chapter 3 (in brief: the area and length of a region of axon was measured and then used to calculate diameter). The diameter of unstimulated versus stimulated axons was not significantly different at any age (the mean axon diameter at 3 dpf was 0.86 µm for vehicle, and 0.89 µm for capsaicin; at 5 dpf was 1.10 µm for vehicle, and 1.15 µm for capsaicin; and at 7 dpf was 1.16 µm for vehicle, and 1.25 µm for capsaicin; unpaired t-tests, 3 dpf p = 0.332, 5 dpf p = 0.315, 7 dpf p = 0.153, **Figure 36A**).

I have shown that axons with early born myelin sheaths have significantly different myelin patterns (fewer but longer myelin sheaths) upon chemogenetic stimulation, whereas axons without early born myelin sheaths did not exhibit these changes to myelin patterns. Axons with specific myelin patterns may exhibit differences in axon diameter growth. To investigate this, I analysed the diameter of axons with and without early born myelin sheaths over time. However, I found that there was no significant change to the diameter of axons with or without early born sheaths upon chemogenetic stimulation (for axons with early born sheaths: the mean axon diameter at 3 dpf was 0.94 µm for vehicle, 0.93 µm for capsaicin; at 5 dpf was 1.09 µm for vehicle, 1.21 µm for

capsaicin; and at 7 dpf was 1.14 µm for vehicle, and 1.28 µm for capsaicin; unpaired t-tests; 3 dpf p = 0.871, 5 dpf p = 0.250, 7 dpf p = 0.243; **Figure 37A**. For axons without early born sheaths: mean axon diameter at 3 dpf was 0.81 µm for vehicle, 0.90 µm for capsaicin; at 5 dpf was 1.10 µm for vehicle, 1.16 µm for capsaicin; and at 7 dpf was 1.14 µm for vehicle, and 1.23 µm for capsaicin; unpaired t-tests, 3 dpf p = 0.202, 5 dpf p = 0.541, 7 dpf p = 0.417; **Figure 37C**). Again, it should be noted that limitations in image resolution meant that axon diameter could not be measured for all axons at 7 dpf (therefore, there are fewer n in **Figure 37** than in **Figure 35**).

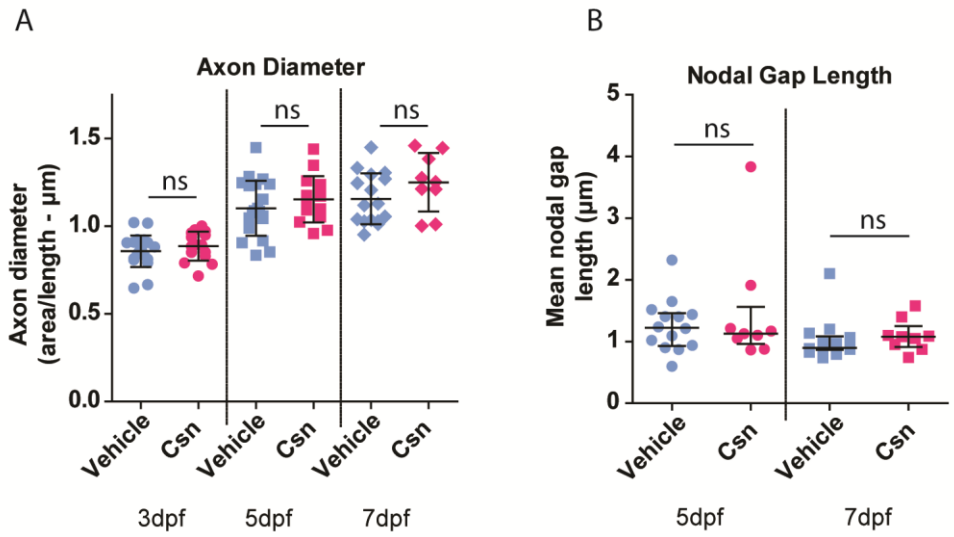

Figure 36 – axon diameter and nodal gap length of individual chemogenetically stimulated RS axons.

A) The diameter of RS axons at 3, 5, and 7 dpf treated with either vehicle or 1 µM capsaicin. The mean axon diameter at 3 dpf was 0.86 µm (SD = 0.09) for vehicle, and 0.89 µm (SD = 0.08) for capsaicin; at 5 dpf was 1.10 µm (SD = 0.16) for vehicle, and 1.15 µm (SD = 0.13) for capsaicin; and at 7 dpf was 1.16 µm (SD = 0.15), and 1.25 µm (SD = 0.17) for capsaicin. There was no statistically significant difference between the two groups at any age (unpaired t-tests; 3 dpf p = 0.332, n = 21, capsaicin n = 17; 5 dpf p = 0.315, n = 21, capsaicin n =17; 7 dpf p = 0.153, vehicle n = 16, capsaicin n = 12). **B)** The mean nodal gap length per RS axon at 3, 5, and 7 dpf treated with either vehicle or 1 µM capsaicin. Nodal gap was defined as unmyelinated gaps between two sheaths which were < 5 µm in length. The median mean nodal gap length at 5 dpf was 1.23 µm (IQR = 0.93-1.46) for vehicle, and 1.13

µm (IQR = 0.96-1.56) for capsaicin; and at 7 dpf was 0.90 µm (IQR = 0.86-1.08) for vehicle, and 1.08 µm (IQR = 0.92-1.25) for capsaicin. There was no statistically significant difference between the two groups at any age (Mann-Whitney tests; 5 dpf, p = 0.875, vehicle n = 14, capsaicin n = 9; 7 dpf p = 0.244, vehicle n = 14, capsaicin n = 9).

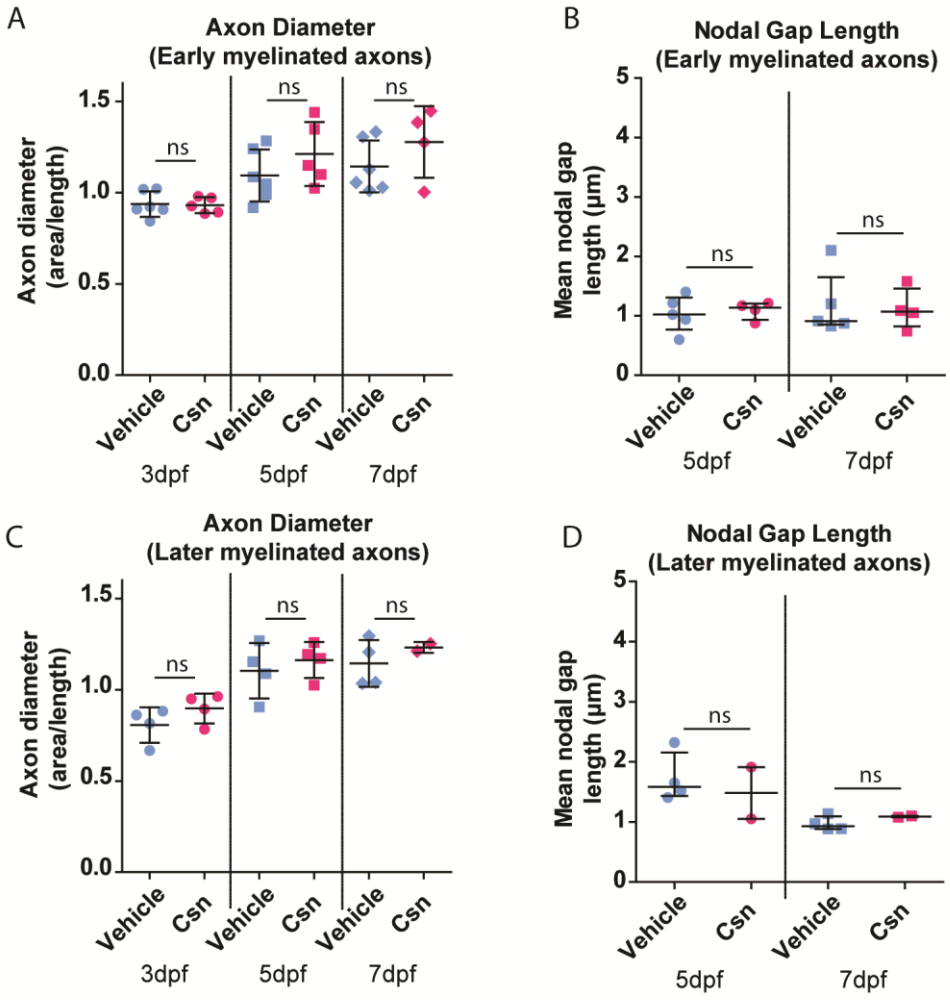

Figure 37 – axon diameter and nodal gap length of chemogenetically stimulated RS axons with and without early born myelin sheaths.

A) The diameter of RS axons with early born myelin sheaths at 3, 5, and 7 dpf treated with either vehicle or 1 µM capsaicin. The mean axon diameter at 3 dpf was 0.94 µm (SD = 0.07) for vehicle, 0.93 µm (SD = 0.04) for capsaicin; at 5 dpf was 1.09 µm (SD = 0.14) for vehicle, 1.21 µm (SD = 0.18) for capsaicin; and at 7 dpf was 1.14 µm (SD = 0.14) for vehicle, and 1.28 µm (SD = 0.20) for capsaicin. There

was no statistically significant differences between the two groups at any age (unpaired t-tests; 3 dpf p = 0.871, vehicle n = 6, capsaicin n = 5; 5 dpf p = 0.250, vehicle n = 6, capsaicin n = 5; 7 dpf p = 0.243, vehicle n = 6, capsaicin n = 4). **B)** The nodal gap length along RS axons with early born myelin sheaths at 5 and 7 dpf treated with either vehicle or 1 µM capsaicin. The median mean nodal gap length at 5 dpf was 1.02 µm (IQR = 0.77-1.31) for vehicle, 1.14 µm (IQR = 0.93-1.20) for capsaicin; and at 7 dpf was 0.91 µm (0.85-1.65) for vehicle, and 1.07 µm (IQR = 0.82-1.46) for capsaicin. There was no statistically significant difference between the two groups at any age (Mann-Whitney tests; 5 dpf p = 0.905; 7 dpf p = 1.000; vehicle n = 5, capsaicin n = 4). **C)** The diameter of RS axons without early born myelin sheaths at 3, 5, and 7 dpf treated with either vehicle or 1 µM capsaicin. The mean axon diameter at 3 dpf was 0.81 µm (SD = 0.10) for vehicle, 0.90 µm (SD = 0.08) for capsaicin; at 5 dpf was 1.10 µm (SD = 0.15) for vehicle, 1.16 µm (SD = 0.10) for capsaicin; and at 7 dpf was 1.14 µm (SD = 0.13) for vehicle, and 1.23 µm (SD = 0.03) for capsaicin. There was no statistically significant differences between the two groups at any age (unpaired t-tests; 3 dpf p = 0.202, vehicle n = 4, capsaicin n = 4; 5 dpf p = 0.541, vehicle n = 4, capsaicin n = 4; 7 dpf p = 0.417, vehicle n = 4, capsaicin n = 2). **D)** The nodal gap length along RS axons with early born myelin sheaths at 5 and 7 dpf treated with either vehicle or 1 µM capsaicin. The median mean nodal gap length at 5 dpf was 1.58 µm (IQR = 1.43-2.15) for vehicle, 1.48 µm (IQR = 1.05-1.91) for capsaicin; and at 7 dpf was 0.93 µm (IQR = 0.88-1.10) for vehicle, and 1.09 µm (IQR = 1.08-1.10) for capsaicin. Non-parametric tests could not be used for statistical comparison due to insufficient sample size. However, there was no statistically significant difference between the two groups at any age using parametric tests (unpaired t-tests; 5 dpf p = 0.582, vehicle n = 4, capsaicin n = 2; 7 dpf p = 0.249, vehicle n = 4, capsaicin n = 2).

4.2.9. Conclusion

Here, I have investigated how increasing the activity of individual RS neurons affects their myelination (**Figure 38A**). I have found that stimulating individual axons did not affect local oligodendrogenesis. Stimulating individual RS axons promoted the growth of early born myelin sheaths 3-5 dpf. After 5 dpf, stimulation had no significant effect on the growth or shrinkage of any myelin sheaths. Very few sheath retractions were observed 3-5 dpf; however, there was a reduction in the number of sheaths retracted from stimulated axons compared to unstimulated controls 5-7 dpf (although, this underpowered analysis did not reach statistical significance).

Based on these phenotypes, chemogenetic stimulation changed the myelin patterns formed along axons, as summarised in **Figure 38B** and **C**.

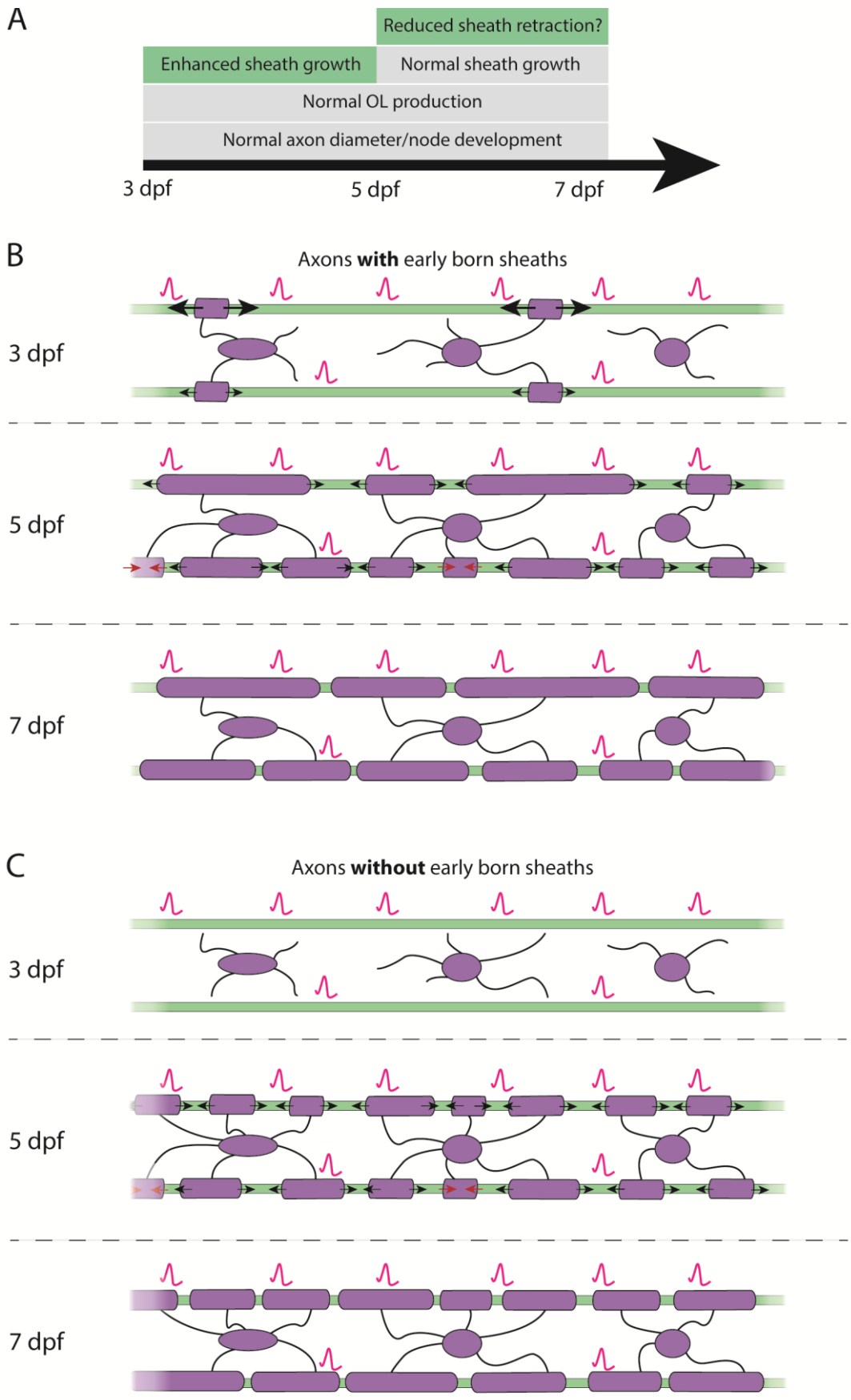
A
Reduced sheath retraction?
Enhanced sheath growth
Normal sheath growth
Normal OL production
Normal axon diameter/node development
3 dpf
5 dpf
7 dpf
B
Axons **with** early born sheaths
3 dpf
5 dpf
7 dpf
C
Axons **without** early born sheaths
3 dpf
5 dpf
7 dpf

Figure 38 – the effects of neuronal activity on myelinated axon development: a summary of this chapter's results.

A) A timeline showing the effects of neuronal activity on RS axon myelination in the zebrafish spinal cord. Increasing activity by chemogenetic stimulation has no effect on oligodendrocyte production, axon diameter growth, or node length 3-7 dpf. Chemogenetic stimulation increases the growth of myelin sheaths 3-5 dpf, but does not affect sheath growth after 5 dpf. Chemogenetic stimulation may reduce the rate of sheath retractions 5-7 dpf. **B)** Myelin pattern formation along axons with early born myelin sheaths, based on the phenotypes described above. Some RS axon begin myelination prior to 3 dpf. At 3 dpf, increased activity promotes the growth of the early born sheaths. By 5 dpf, stimulated axons have fewer myelin sheaths (possibly because there was less space for new sheaths to be formed 3-5 dpf). After 5 dpf, activity does not affect the growth dynamics of sheaths. By 7 dpf, stimulated axons have fewer but longer sheaths than unstimulated axons. **C)** Myelin pattern formation along axons without early born myelin sheaths, based on the phenotypes described above. Some RS axons are completely unmyelinated at 3 dpf. By 5 dpf, there is no noticeable effect of activity on sheath number or sheath length. Activity may inhibit sheath retractions 5-7 dpf. By 7 dpf, stimulated axons may have more sheaths due to fewer sheath retractions, possibly leading to a shorter sheath length on average.

4.3. Discussion

4.3.1. Increasing Neuronal Activity of a Single Axon Promotes Sheath Growth 3-5 dpf

Research has shown that globally manipulating neuronal activity (either by administering TTX to inhibit activity, or using electrodes to increase activity) can affect the early growth of myelin sheaths in the zebrafish spinal cord (Krasnow et al., 2018). Whether the activity of a single axon could locally regulate the growth of its myelin sheaths was not known. Here, I have found that chemogenetically stimulating individual RS axons promotes the growth of their earliest born myelin sheaths 3-5 dpf.

Molecular Mechanism – Glutamate Signalling?

The molecular mechanism by which neuronal activity promotes the growth of early born myelin sheaths along RS axons is not known. One hypothesis is that chemogenetic stimulation of RS axons triggers release of the neurotransmitter glutamate, which then signals to myelin sheaths in order to promote their growth. RS neurons are glutamatergic (Higashijima et al., 2004), and preventing neurotransmitter release in single RS axons inhibits their myelination by reducing both the number and length of myelin sheaths formed, suggesting that glutamate release does, indeed, play a role in myelination (Koudelka et al., 2016). There is significant evidence that oligodendroglial lineage cells express AMPA, NMDA, and mGlu receptors, and exhibit electrophysiological responses to glutamate signalling (as discussed in section ‘1.6.2 Neurotransmitter Signalling from Neurons to Oligodendroglia’). Myelin sheaths may detect glutamate signals from the underlying axon and modulate their growth accordingly.

It is not clear precisely where neurotransmitter release occurs along RS neurons in order to regulate myelination. Neurotransmitter release may occur along the main axon itself (**Figure 39A**), as well as at traditional presynaptic terminals. Both Kukley et al., 2007 and Ziskin et al., 2007 found that OPCs in rodent brain slice appear to form neuro-glial synapses directly with the axonal

membrane, so that axonal stimulation induces OPC current responses. Neurotransmitters may be released either adjacent to or underneath myelin sheaths to influence their growth (**Figure 39A**). Alternatively, neurotransmitter release at presynaptic terminals may signal to myelin sheaths (**Figure 39B**). There may even be some independent signalling mechanism from active synapses which then signals to myelin sheaths to regulate their growth (**Figure 39B**). More detailed characterisation of where and when neurotransmitter vesicles are released is required to properly understand the relationship between neurotransmitter signalling and myelin sheath growth.

The fluorescent reporter SypHy is a fusion of a pH-sensitive GFP (pHluorin) with the protein synaptophysin, which localises to synaptic vesicles (Granseth et al., 2006). Synaptic vesicles have an acidic pH, and so SypHy fluorescence is quenched during vesicle trafficking. However, once the vesicle fuses with the extracellular membrane to release vesicular cargo, the pH rapidly increases to neutral and SypHy fluorescence is emitted. This reporter has been used in RS neurons to quantify synaptic vesicle release from pre-synapses of branching collaterals (Koudelka et al., 2016). SypHy reporter could be expressed in single RS neurons, and coupled with timelapse imaging, to identify sites of synaptic vesicle release along RS axons. By co-expressing the FP-Cntn1a reporter to visualise the location of growing myelin sheaths along an axon, one could correlate the location and rate of vesicular release with myelin sheath dynamics over time. It is possible that vesicular release at a specific developmental time point, at specific axonal sites, or specific rates of vesicular release, correlate with early myelin sheath growth. These questions are currently being investigated by Dr. Rafael Almeida in the Lyons group, University of Edinburgh. Preliminary results indicate that synaptic vesicles are, indeed, released along RS axons, both along unmyelinated regions and underneath myelin sheaths themselves. Interestingly, there is essentially no synaptic vesicular release associated with myelin sheaths which have no space into which to grow (Dr. Rafael Almeida, unpublished). This suggests that an axon can detect the growth dynamics of its myelin sheaths through some feedback signalling mechanism. Consequently, signals, such as

neurotransmitter release, are targeted to myelin sheaths which are still actively growing.

To determine if synaptic vesicle release drives activity-mediated sheath growth, TeNT could be co-expressed with TRPV1-RFP in individual RS axons. Capsaicin treatment should still increase the electrical activity of the RS neuron (which could be assessed by Ca^{2+} imaging, as in **Figure 24**), but release of synaptic vesicles should be reduced (which could be assessed by SypHy imaging). The GFP-Cntn1a reporter could then be used to measure the dynamics of myelin sheaths along individual RS axons; if vesicular release drives activity-mediated sheath growth, then sheaths on TeNT-expressing capsaicin-treated axons should grow at the same rate as sheaths on TeNT-expressing vehicle-treated axons 3-5 dpf.

If synaptic vesicle release does occur along axons, and is required for activity-mediated myelin sheath growth, the next step would be to determine if glutamate is the signalling molecule being released. iGluSnFR is a fusion between a circularly-permuted GFP and a glutamate-binding protein which can be used to live image glutamate levels (Marvin et al., 2013). When the GluSnFR protein binds to glutamate, a conformational change resulting in emission of fluorescence is induced. Different-coloured variants with faster kinetics are now available for detailed characterisation of glutamate transients *in vivo* (Marvin et al., 2018). Membrane-anchored iGluSnFR could be expressed on myelin sheaths; co-expressing this with SypHy in RS axons, and performing timelapse imaging, could identify whether synaptic vesicle release events near or under myelin sheaths corresponds with glutamate release in these regions.

Whether oligodendrocyte expression of glutamate receptors is required for activity-mediated sheath growth could also be investigated. Differentiated oligodendrocytes express both ionotropic and metabotropic glutamate receptors (Berger et al., 1992; Deng et al., 2004; Káradóttir et al., 2005; Luyt et al., 2003; Patneau et al., 1994; Salter and Fern, 2005; Žiak et al., 1998). Studies have shown that oligodendrocyte-specific loss of AMPA or NMDA

receptor sub-units does not appear to affect long-term oligodendrocyte development or myelination (De Biase et al., 2011; Kougioumtzidou et al., 2017; Saab et al., 2016). However, Saab et al., 2016 found that deletion of the NMDA receptor subunit NR1 in mice leads to a transient hypomyelination phenotype which recovers over time. They saw that NR1 knock-out mice have fewer myelinated axons and thinner myelin sheaths in the optic nerve at P18, but that both phenotypes recover by P70. In rodents, myelination begins at approximately P5-10 in the optic nerve, with extensive myelination occurring during the first post-natal month (Gyllensten and Malmfors, 1963). It is also known that experience can influence optic nerve myelination during early post-natal life (Gyllensten and Malmfors, 1963; Tauber et al., 1980). Therefore, it may be that glutamate signalling regulates early myelination of the optic nerve during a critical developmental period, but that other signals can regulate myelination later. This would match my findings that chemogenetic stimulation of RS axons can promote sheath growth within a critical developmental period between 3 to 5 dpf.

NMDA, AMPA, kainate, or mGlu receptors could be disrupted in oligodendrocytes using Crispr/Cas9 technology. Crispr/Cas9 systems allow targeting of random mutations in a gene of choice (Sander and Joung, 2014). They rely on two key components: a Cas9 nuclease enzyme, and a guide RNA. The guide RNA has a 20-nucleotide sequence at the 5’ end, which can be designed to complement the genomic site adjacent to where a mutation is desired. The Cas9 forms a complex with the guide RNA, which then guides the nuclease to the target site in the genome. Cas9 induces a double-stranded break in the DNA, which is then repaired by non-homologous end joining mechanisms; this typically results in random insertions and deletions into the genome, often leading to frame-shifts. Ablain et al., 2015 developed a Crispr/Cas9 system for inducing mutations in specific cells or tissues of interest in zebrafish. They generated a plasmid where a guide RNA is ubiquitously expressed, while Cas9 is expressed under a tissue-specific promoter of interest. This plasmid is then inserted into the genome using the well-established Tol2 system to create a stable transgenic line. Driving Cas9

expression with OPC promoter sequences (such as olig1), or myelinating oligodendrocyte promoter sequences (such as myrf or mbp) would allow cell-specific genetic targeting of the various glutamatergic receptors. Once oligodendrocyte-specific transgenic lines are generated, they could then be combined with the TRPV1-RFP system to see if chemogenetic stimulation of RS axons still promotes sheath growth in these mutants.

Molecular Mechanism – BDNF Signalling?

BDNF is another molecule which can be expressed in a neuronal activity-dependent manner (Castrén et al., 1992), and which can regulate myelination (Vondran et al., 2010). TeNT has been shown to block both the release of BDNF and neurotransmitters (Shimojo et al., 2015), and so BDNF signalling could underlie the hypomyelination phenotype seen in TeNT-expressing RS axons (Koudelka et al., 2016) (**Figure 39A**). Optogenetic stimulation of cortical neurons promotes OPC proliferation (Gibson et al., 2014). Inhibiting activity-regulated BDNF expression, or knocking out the BDNF receptor TrkB specifically in oligodendroglial lineage cells, prevents optogenetic stimulation from increasing OPC proliferation (Geraghty et al., 2019). BDNF induces a switch to activity-dependent myelination *in vitro*; DRG-OPC co-cultures are normally unaffected by NMDA receptor inhibition, but when cultured in the presence of BDNF, myelination is significantly impaired by NMDA receptor inhibition (Lundgaard et al., 2013). Therefore, BDNF is another candidate molecule which may mediate the effects of neuronal activity on myelin sheath growth.

Like synaptic vesicle release, BDNF release can be live imaged. BDNF-pHluorin (a pH-sensitive indicator which fluoresces upon fusion of BDNF vesicles with extracellular membrane) has previously been used to study BDNF release in axons and dendrites (Matsuda et al., 2009; Shimojo et al., 2015). BDNF-pHluorin could be expressed in single RS axons to characterise the location and rate of BDNF release during myelination. These experiments could be combined with the FP-Cntn1a tool to determine whether BDNF release correlates with myelin sheath growth.

If BDNF release does correlate with sheath growth, then BDNF receptors in oligodendrocytes could be targeted using the Crispr/Cas9 strategy above. BDNF is known to bind to two receptors; TrkB and p75 (Park and Poo, 2013). BDNF is initially synthesised as the precursor pro-BDNF, which has high affinity for p75 and contributes to synaptic long-term depression in the hippocampus (Woo et al., 2005). Pro-BDNF is cleaved to generate mature BDNF (mBDNF), which has high affinity for TrkB (Huang and Reichardt, 2001). TrkB is expressed by oligodendrocytes and is activated by BDNF treatment (Veer et al., 2009; Vondran et al., 2010). OPC expression of TrkB is required for activity-mediated OPC proliferation (Geraghty et al., 2019). Oligodendrocyte-specific loss of TrkB signalling in mice leads to hypomyelination in the corpus callosum and spinal cord at P30, but myelination recovers by P60 (Wong et al., 2013). It may be that BDNF-TrkB signalling regulates activity-mediated myelination during a critical developmental period (again, reminiscent of my findings in this chapter: that neuronal activity only promotes sheath growth within a critical period). By disrupting TrkB receptor expression specifically in oligodendrocytes, one could determine whether BDNF-TrkB signalling is required for activity-mediated sheath growth along RS axons 3-5 dpf.

Molecular Mechanism – Another Signal?

The activity-driven signal which regulates sheath growth may be something other than glutamate or BDNF. For example, neuronal stimulation of OPC-DRG neuron co-cultures promotes the formation of myelin sheaths in an adenosine-dependent manner (Stevens et al., 2002).

The signalling mechanism may even be indirect and involve other cell types. Myelination in OPC-DRG neuron co-cultures is significantly enhanced when astrocytes are added to the culture (Ishibashi et al., 2006; Watkins et al., 2008). In such co-cultures, astrocytes detect ATP release by active axons and release LIF which then promotes myelination (Ishibashi et al., 2006). Neuronal activity induces significant transcriptional changes in astrocytes (Hasel et al., 2017),

and, thus, there may be additional signals released by astrocytes in response to activity which could influence myelination (**Figure 39C**).

If neither glutamate nor BDNF signalling regulates sheath growth, then a more unbiased approach could be taken to elucidate the signal responsible. First the receptor(s) which are activated on oligodendrocytes or myelin sheaths need to be identified. Neuronal activity could be robustly increased in a population of neurons (for example, all RS neurons) during early stages of myelination using chemogenetics or optogenetics, followed by isolation of oligodendrocytes and myelin for further analysis. Analysis of purified myelin using large-scale expression or phosphorylation assays could identify changes in the expression or phosphorylation of receptors in myelin sheaths with activity. Analysis of oligodendrocyte transcriptomes by RNA sequencing could identify downstream transcriptional changes in response to activity, which may suggest specific upstream receptors. Both data sets could be combined and coupled with literature searches to identify the most likely candidate signals. These could subsequently be targeted in oligodendrocytes using the cell-type specific Crispr/Cas9 strategy above, in order to confirm which signal is required for activity-mediated sheath growth.

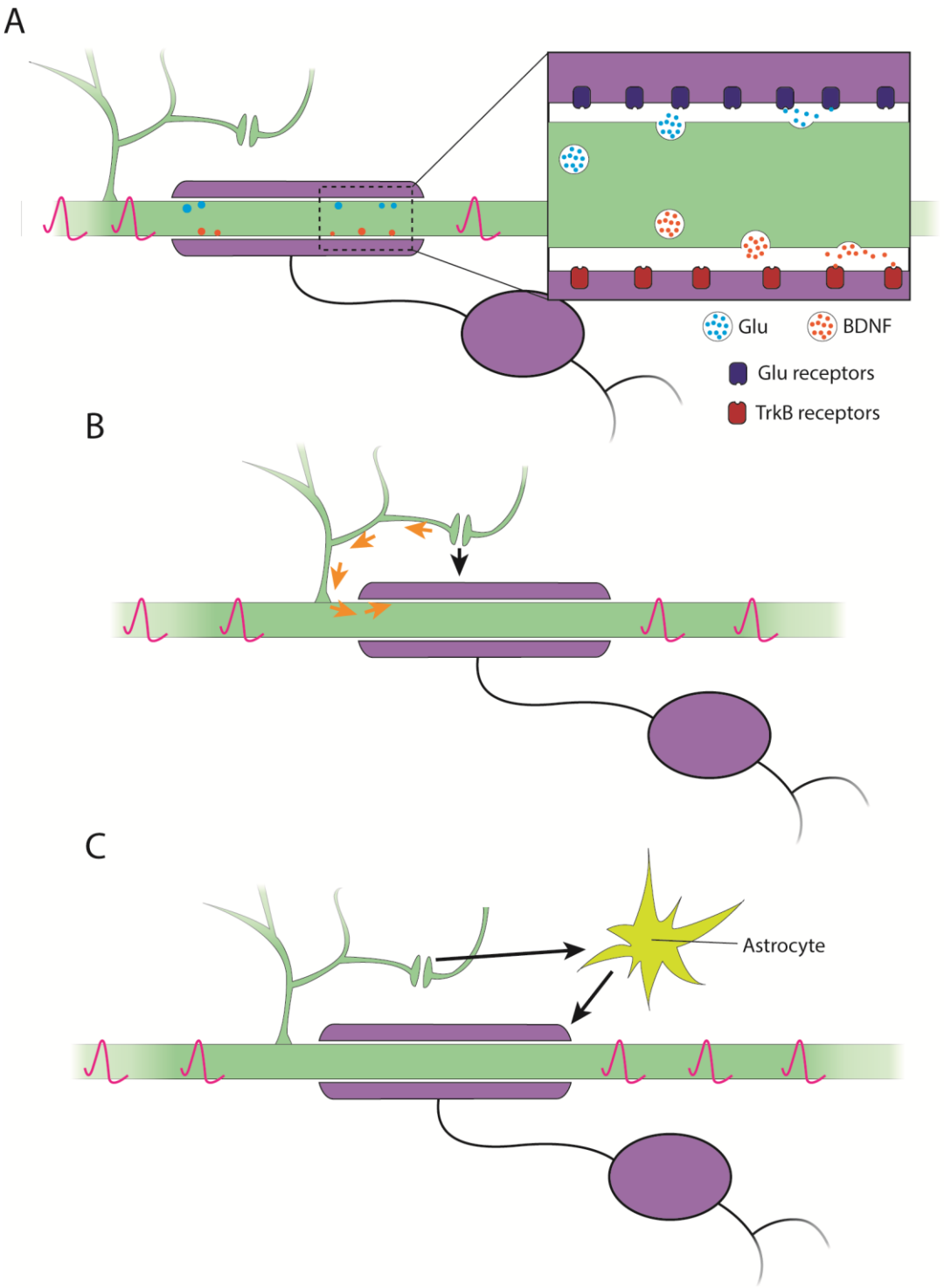

Figure 39 – possible signalling mechanisms for activity mediated sheath growth.

A) Axonal vesicular release to the myelin sheath. Action potentials may trigger the exocytosis of vesicles along the axon, releasing their cargo either under or adjacent to myelin sheaths to activate appropriate receptors and induce sheath growth. For

example, release of neurotransmitters like glutamate (blue) could activate glutamate receptors (dark blue), or release of BDNF (orange) could activate TrkB receptors (red). B) Other signals from active axons to myelin sheaths. Neurotransmitter release at traditional synapses may 'spill over' to activate receptors on neighbouring myelin sheaths and induce sheath growth (black arrow). Alternatively, active synapses may trigger some other signalling mechanism within the presynaptic cell which signals to myelin sheaths to induce sheath growth (orange arrows). C) Indirect signalling from active axon to myelin sheaths via astrocytes. Active neuron may signal to astrocytes (yellow cell), which then signal to myelin sheaths to induce sheath growth.

Ca^{2+} Signalling in Myelin Sheaths

Local Ca^{2+} signalling may play an important role in activity-mediated sheath growth. Ca^{2+} imaging in the zebrafish spinal cord demonstrates that localised Ca^{2+} transients occur within myelin sheaths, with neuronal activity regulating approximately half of these transients (Krasnow et al., 2018). Long-duration high-amplitude events mediate sheath retraction in a calpain-dependent manner (Baraban et al., 2018). Shorter lower-amplitude events may regulate sheath elongation; high Ca^{2+} transient rates correlate with sheath growth, while Ca^{2+} transient rates below 1 transient / 30 mins correlate with sheath shrinkage (Baraban et al., 2018; Krasnow et al., 2018). Particular types and rates of Ca^{2+} signalling in myelin sheaths may act as codes to control whether a sheath grows, shrinks, or retracts.

Precisely how activity of the underlying axon (rather than global neuronal activity) relate to the particular Ca^{2+} codes in sheaths remains unknown. Ca^{2+} imaging in myelin sheaths could be coupled with TRPV1-RFP chemogenetic stimulation of RS axons to study whether stimulating a single axon correlates with Ca^{2+} signalling in its myelin sheaths. The specific firing rate of an underlying axon may, in turn, tune the sheath Ca^{2+} transient rate, and subsequently control sheath growth. Chemogenetic systems such as TRPV1-RFP cannot be used to tightly control neuronal firing rates. Instead, optogenetic systems provide more intricate control of neuronal firing

properties. The activity of individual RS neurons expressing channelrhodopsins could be tightly controlled using different frequencies of light stimulation. Using an optogenetic approach, one could test if specific neuronal firing frequencies correspond to specific sheath Ca^{2+} codes and sheath growth.

The molecular signal which triggers Ca^{2+} transients in myelin sheaths should also be investigated. Expressing TeNT in single RS axons and then assessing sheath Ca^{2+} dynamics would confirm whether activity-mediated vesicular release contributes to sheath Ca^{2+} signalling. If axonal TeNT-expression reduces sheath Ca^{2+} signalling, either neurotransmitter or BDNF release could be responsible. Coupling SypHy or BDNF-pHluorin imaging in RS axons with Ca^{2+} imaging in myelin sheaths could test whether release of either of these molecules correlates with sheath Ca^{2+} dynamics. When the candidate oligodendrocyte receptor(s) responsible for detecting neuronal activity are identified, Ca^{2+} imaging could be performed in oligodendrocyte-specific receptor mutants to determine whether this receptor(s) mediates activity-induced Ca^{2+} transients in myelin sheaths.

4.3.2. Increasing Neuronal Activity of a Single Axon Does Not Affect Myelin Sheath Growth after 5 dpf

Although chemogenetic stimulation promotes sheath growth along RS axons 3-5 dpf, it does not affect the growth of myelin sheaths after 5 dpf. This was regardless of whether the sheath was born early (before 3 dpf) or later (after 3 dpf). The lack of effect on sheath growth was not due to a lack of space, as there was no effect of chemogenetic stimulation on sheath growth even when analysis was restricted to sheaths that still had at least 20µm adjacent unmyelinated axonal space at 7 dpf (**Figure 31**).

One possibility for this lack of phenotype is that the chemogenetic system no longer increases neuronal activity at 5 dpf onwards. However, I showed, using Ca^{2+} imaging, that RS axons expressing TRPV1-RFP continue to respond to capsaicin treatment at 5 dpf (**Figure 24**). Despite my evidence that capsaicin-treated TRPV1 axons had increased activity at 5 dpf, the level of increase may

not be as sustained. Capsaicin was applied for four hours daily, but it is not clear whether activity remains elevated after this treatment period, and for how long. Furthermore, another possibility is that only a particular firing frequency leads to sheath growth. Although RS axons were still stimulated at 5 dpf, the firing frequency upon capsaicin treatment 5-7 dpf may be significantly different compared to the firing frequency upon capsaicin treatment 3-5 dpf. There is a need to investigate how specific neuronal firing frequencies correspond to myelin sheath growth. The precise firing frequencies of TRPV1-RFP-expressing RS axons induced by capsaicin treatment 3-7 dpf could be measured by electrophysiology. If the firing frequency induced by capsaicin treatment significantly changes over time, then daily optogenetic stimulation of RS neurons at the same firing frequency 3-7 dpf could elucidate whether activity-mediated sheath growth is possible after 5 dpf.

Another explanation for sheath growth being affected by activity within a defined period could be that myelin sheaths do not detect or respond to neuronal activity after 5 dpf. The machinery required for oligodendrocytes or myelin sheaths to detect neuronal activity may be downregulated as oligodendrocytes mature. In support of this, the expression levels of AMPA, NMDA, and mGlu receptors (glutamate sensing machinery) are much lower in mature oligodendrocytes than in OPCs (De Biase et al., 2010; Deng et al., 2004; Kukley et al., 2010). First, the receptor(s) in oligodendrocytes which detect neuronal activity and mediate sheath growth 3-5 dpf must be identified, as discussed above in section ‘4.3.1 Increasing Neuronal Activity of a Single Axon Promotes Sheath Growth 3-5 dpf’. Once candidate receptor(s) have been identified, the expression of this receptor(s) in myelin sheaths along RS axons should be assessed via immunohistochemistry or immunogold electron microscopy 3-7 dpf. If expression levels do decline after 5 dpf, then the receptor(s) of interest could be overexpressed in oligodendrocytes (using a myelin-specific promoter sequence such as mbp) to see if this promotes activity-mediated sheath growth along RS axons after 5 dpf.

There is some evidence that oligodendrocytes require multiple signals to detect and respond to neuronal activity. Lundgaard et al., 2013 found that

treating OPC-DRG co-cultures with either BDNF or Nrg1 induces a switch to NMDA receptor-dependent myelination. Therefore, expression of BDNF, Nrg1 or both in RS neurons may control when activity can influence sheath growth. Quantifying BDNF release along RS neurons using BDNF-pHluorin could determine whether BDNF signalling is restricted to 3-5 dpf. Any changes in the expression or localisation of Nrg1 along RS axons could be broadly measured by immunohistochemistry on larvae aged 3-7 dpf. If either BDNF or Nrg1 signalling appears to change after 5 dpf, then they could be inducibly overexpressed from 5 dpf onwards to see if increasing signal levels promotes activity-mediated sheath growth at these time points. Several strategies have been developed for inducible transgene expression in zebrafish. A tamoxifen-inducible form of the transcriptional activator Gal4 has previously been used to activate UAS-driven transgene expression upon tamoxifen or 4-OH-tamoxifen treatment (Akerberg et al., 2014). Similarly, the TetON system relies on activation of a TetActivator by doxycycline treatment; this then drives the expression of Tetracycline responsive element (TRE) driven transgenes (Knopf et al., 2010).

Why would neuronal activity only influence myelin sheath growth within a limited developmental time period? If existing myelin sheaths could be remodelled by neuronal activity throughout life, then the myelin patterns along active axons would be constantly changing. Such changes to myelin patterns would likely lead to constantly changing conduction speeds within circuits. Neuronal activity might only regulate the initial formation of myelin patterns by enhancing production of new oligodendrocytes and promoting early sheath growth. Therefore, activity-mediated myelination may only be important throughout life for axons which are unmyelinated or sparsely myelinated, such as in the cortex (Gao et al., 2019; Hill et al., 2018; Tomassy et al., 2014). However, the responses of myelin sheaths to activity may differ depending on the neuronal subtype. Myelin sheaths along RS axons may only exhibit activity-mediated growth 3-5 dpf, but sheaths on other axon subtypes may continue to respond to activity for a longer period of time or even throughout life. The role of neuronal activity in shaping myelination may vary from circuit

to circuit. Further characterisation of which neuron subtypes use activity to regulate their myelination, and how or when activity affects myelin sheath growth dynamics in different circuits, is required. For example, global reduction of synaptic vesicle release inhibits the myelination of both RS and circumferential descending (CiD) axons in the zebrafish spinal cord (Mensch, 2014). Individual CiD neurons could be chemogenetically stimulated to assess how increasing their activity affects myelin sheath dynamics over time.

4.3.3. Neuronal Activity may Inhibit Sheath Retractions

In Chapter 3, I showed that myelin sheaths can be retracted from RS axons, but that only sheaths under 10 µm can be retracted. Sheath stability appears to correspond with sheath length, as shorter (< 5 µm) sheaths exhibit more instability than longer (5-10 µm) sheaths. Here, I quantified the number of sheath retractions which occurred on stimulated and unstimulated RS axons 5-7 dpf, focusing only on axons which had sheaths under 10 µm (axons which had sheaths that could be retracted). I found that there was a 57% reduction in the number of sheath retractions along stimulated axons compared to control axons (**Figure 33**); however, this was not statistically significant, likely because this statistical analysis is underpowered (41% power, with a sample size of 16 per group required to reach 80% power). Therefore, it is possible that repeating this experiment would show that chemogenetic stimulation does reduce the retraction of myelin sheaths 5-7 dpf.

Furthermore, neuronal activity may regulate sheath retractions prior to 5 dpf. Only one of 17 sheaths present at 3 dpf was retracted by 5 dpf. However, it is possible that many sheaths or contacts were formed and then retracted between 3 and 5 dpf. Timelapse analysis 3-5 dpf should be performed to more rigorously assess whether activity affects the rate of sheath retractions during this time period.

Research has shown that inhibiting synaptic vesicle release increases the number of sheath retractions in the zebrafish spinal cord (Hines et al., 2015); whereas, Mensch et al., 2015 showed that global inhibition of synaptic vesicle release had no effect on the retraction of sheaths over 5 µm. Collectively, this

suggests that neuronal activity may play a specific role in the retraction of shortest unstable sheaths (< 5 µm). Both of these studies used TeNT light chain to globally block vesicular release, which can actually inhibit the release of various signals including neurotransmitter and BDNF release (Shimojo et al., 2015). TeNT may also affect the release of other signals throughout the body; for example, TeNT can inhibit VAMP2-mediated catecholamine release from chromaffin cells of the adrenal medulla (Höne-Zell et al., 1994). More precise manipulations are required to identify the specific signal which may regulate sheath retraction. If chemogenetic stimulation does reduce sheath retraction, then SypHy/BDNF-pHluorin imaging (as described in section 4.3.1) could determine whether neurotransmitter release, or BDNF release, correlates with a sheath's fate. Oligodendrocyte-specific disruption of glutamate or TrkB receptors could confirm whether glutamate or BDNF signalling is involved in sheath stabilisation. An activity-driven signal other than glutamate or BDNF may control sheath stabilisation or retraction; it will be important to follow up on any such candidate signals in the context of sheath retractions if and when they arise.

4.3.4. Increased Activity can Affect Myelin Pattern Formation along RS Axons

My data indicate that neuronal activity can affect the myelination of RS axons by regulating sheath growth and, possibly, sheath retraction at different developmental stages (see **Figure 38A**). How neuronal activity affects the myelin pattern established may, thus, depend on when an axon is myelinated. For example, some RS axons began myelination before 3 dpf (axons with early born sheaths). For these axons, chemogenetic stimulation changed the myelin pattern by increasing sheath length and reducing sheath number by 7 dpf. This change in myelin pattern is likely because increased activity promoted the growth of early born myelin sheaths 3-5 dpf, which, in turn, may have reduced the available axonal space for new sheaths to form (**Figure 38B**).

Other RS axons were still completely unmyelinated at 3 dpf (axons without early born myelin sheaths). Along these axons, chemogenetic stimulation did not change sheath length by 5 dpf; however, it was not possible to properly

assess how activity affects 3-5 dpf sheath growth along these axons because I cannot determine exactly when the sheaths were made. More detailed timelapse analysis may reveal that activity can transiently promote the growth of sheaths born along these axons 3-5 dpf, but not enough to permanently increase sheath length.

By 7 dpf, chemogenetic stimulation may change the myelin pattern formed along axons without early born sheaths by reducing sheath length and increasing sheath number compared to controls. Such a phenotype can be explained if activity inhibits the retraction of short, unstable myelin sheaths between 5 to 7 dpf; stimulated axons would therefore have more sheaths competing for the same axonal space, leading to shorter sheaths overall. Although these changes to the myelin pattern were not statistically significant, the statistical comparisons had a lower n number (4 per group), and so are likely to be underpowered. For example, the comparison between unstimulated and stimulated axons in **Figure 35F** has only 11% power, and would require an n of 63 per group to reach 80% power. Therefore, the sample size should be increased to confirm whether or not chemogenetic stimulation changes the myelin patterns along RS axons without early born sheaths.

Why would the myelin patterns along RS axons with and without early born sheaths be differentially affected by chemogenetic stimulation? There may be a change in all RS axons (such as reduced BDNF release, or reduced Nrg1 expression) which prevents activity from regulating sheath growth after 5 dpf. For axons which did not start myelination until after 3 dpf, there may not be enough time for activity to significantly influence sheath growth before this mechanism is lost at 5 dpf. It may be that oligodendrocytes, or myelin sheaths, only express the appropriate receptors to detect neuronal activity at 3-5 dpf, and so again there is not enough time for activity to affect the growth of myelin sheaths along RS axons without early born sheaths. Alternatively, RS axons without early born sheaths may represent a specific subset of RS neurons which use activity to regulate their myelin pattern in a different way compared to RS axons with early born sheaths. Given that there are many different subtypes of RS neuron, further investigation into these different subtypes is

required. Whether RS axons with and without early born sheaths truly represent distinct populations should be investigated; the specific RS neuron subtypes in these axonal populations should be identified, and signals thought to be involved in activity-mediated myelination characterised in more detail. For example, do RS axons with early born sheaths have consistently different levels of BDNF release or Nrg1 expression than RS axons without early born sheaths? Such analyses could begin to elucidate the properties of circuits which use activity to regulate their myelination.

4.3.5. How Does Activity-mediated Sheath Growth and Pattern Formation Affect Circuit Function?

As discussed in Chapter 1, changing the myelin pattern along an axon will, in theory, change its conduction properties. Does the altered myelin pattern along stimulated RS axons affect conduction? The conduction timings of RS axons, and the recruitment and activity of their post-synaptic neurons, could be assessed by electrophysiology. This could be done either by directly recording the current/voltage properties of individual neurons using electrodes, or using optical techniques such as genetically-encoded voltage indicators, as discussed in section '3.3.6. How Do Myelin Patterns Affect Overall Circuit Function?' (Gong et al., 2015).

There are many different subsets of RS axons in the zebrafish, several of which are known to underlie specific locomotor behaviours. It is not known if the RS axons which have altered myelin patterns in response to chemogenetic stimulation represent a particular set of RS neurons. The identity of these RS axons should be characterised in more detail to determine if they mediate a particular behaviour. For example, MeLr and MeLc RS neurons mediate prey capture behaviour, and RoV3/MiV1/MiV2 RS neurons mediate direction changes in the optomotor response. If these RS neurons mediate a particular behaviour, the success rates and kinematics of that behaviour could be compared between stimulated and unstimulated animals to assess how changing myelin patterns affects behavioural output. However, it would be important to consider that chemogenetic stimulation may have effects on the

circuit other than changing the myelin pattern. Neither the axon diameter nor the length of nodal gaps were significantly changed by chemogenetic stimulation. However, the number or size of synapses along the collaterals of RS axons may have been altered; such synaptic changes would influence post-synaptic recruitment and activity, and behaviours, independently from myelination. The synapses of RS neurons should also be measured and correlated with any effects on circuit function; this could be done by staining for pre-synaptic proteins such as synaptophysin.

4.3.6. Increased Activity of Single Axons Does Not Affect Local Oligodendrogenesis

Research has shown that either experience or experimental neuronal stimulation increases OPC proliferation and differentiation (Gibson et al., 2014; Hughes et al., 2018; Mitew et al., 2018; Xiao et al., 2016). It is not clear whether neuronal activity has separate effects on both OPC proliferation and differentiation, or whether it promotes one process and the other is subsequently upregulated to maintain a balance in the OPC population. Regardless, neuronal activity does seem to promote overall oligodendrocyte production. However, it was not known whether the activity of a single axon can affect local oligodendrogenesis, or whether an entire population or tract needs to be activated to have significant impact on oligodendrocyte production. Here, I have shown that sparse chemogenetic stimulation of RS axons (rather than the entire population) does not affect the local production of oligodendrocytes 3-7 dpf.

BDNF signalling is thought to play a role in activity-mediated OPC proliferation. Optogenetic stimulation of pyramidal cortical neurons increases OPC proliferation, but this effect is lost in animals which do not express BDNF in response to activity or which lack TrkB receptors in oligodendroglial lineage cells (Geraghty et al., 2019; Gibson et al., 2014). This suggests that BDNF release from active axons promotes OPC proliferation, and may subsequently increase oligodendrocyte production. Neurotransmitter signalling may also play a role in oligodendrogenesis, as global inhibition of synaptic vesicle

release reduces the number of oligodendrocytes in the larval zebrafish spinal cord by approximately 10% (Mensch et al., 2015). Individual active neurons may not release enough BDNF or neurotransmitter to affect OPCs, whereas a larger population of neurons may release sufficient levels of BDNF or neurotransmitter to promote OPC proliferation, differentiation, or both. For the experiments in this chapter, only animals where very few RS neurons expressed TRPV1-RFP were selected. However, one could use animals with a larger number of RS neurons labelled with TRPV1-RFP to see if stimulating a larger population of RS axons affects local oligodendrocyte number in the spinal cord. If this did increase the production of oligodendrocytes, then performing the same experiment in oligodendrocyte-specific TrkB or glutamate receptor mutants would confirm whether BDNF or neurotransmitter signalling regulates the oligodendrocyte population.

Alternatively, perhaps only certain patterns of activity promote oligodendrogenesis. Nagy et al., 2017 showed that lower firing frequencies promote OPC differentiation in the mouse corpus callosum, whereas higher firing frequencies promote OPC proliferation. It is possible that chemogenetic stimulation does not induce firing frequencies that promote the production of oligodendrocytes. Optogenetic stimulation of individual RS axons at various firing frequencies could determine whether the activity of a single axon can promote local oligodendrocyte production.

4.3.7. How Does Increased Activity Affect Sheath Thickness?

In this chapter, I have assessed how chemogenetic stimulation of single RS neurons affects the number and length of myelin sheaths along axons. However, research has shown that neuronal stimulation can also increase sheath thickness. Chemogenetic stimulation of pyramidal cortical neurons in both the juvenile and adult mouse leads to increased sheath thickness, specifically on active axons themselves (Mitew et al., 2018). Although chemogenetic stimulation of RS axons does not affect longitudinal growth after 5 dpf, it is still possible that activity promotes radial growth at these time points. Sheath thickness should be assessed along individual TRPV1-RFP

expressing RS axons at 3, 5, and 7 dpf to see how chemogenetic stimulation affects radial growth during these stages. As discussed in section '3.3.5. Remodelling of Sheath Thickness over Time', there are several techniques which may give sufficient resolution to measure sheath thickness of an individually labelled axon. Larvae expressing membrane-tethered GFP in myelin sheaths and TRPV1-RFP in individual RS axons could be live imaged using super-resolution microscopy to assess how individual sheaths change in thickness along a single axon over time. I have preliminarily tested such live imaging approaches using a 63x lens on a Zeiss LSM880 Airyscan confocal microscope, and found that I was able to follow individual sheaths until 7 dpf (data not shown). However, with the maximum resolution possible by Airyscan microscopy, the smallest change in sheath thickness that could be detected is a change of g-ratio from 0.8 to 0.73 (for an axon 1.2 µm in diameter; the average diameter of RS axons at 7 dpf). Measuring smaller changes in sheath thickness would require higher imaging resolution. An alternative approach could be to fix and process larvae for expansion microscopy, which has recently been used to measure sheath thickness along individual axons at a similar resolution as electron microscopy (Gao et al., 2019). Expansion microscopy could be used to measure the average sheath thickness along stimulated RS axons at 3, 5, and 7 dpf. Either of these strategies could help us to understand how and when a single axon's activity affects the dynamics of myelin sheath growth.

4.3.8. How Does Neuronal Activity Affect Sheath Growth and Myelin Patterns after Myelin Disruption?

As discussed in section '3.3.7. Disruption to Myelin Patterns', myelin patterns along axons can be changed by demyelination which occurs in injury, disease, or with age. Myelin loss affects the conduction of the underlying axons (for example, demyelination causes conduction block in the cat spinal cord (Smith et al., 1981)). New myelin sheaths can be made; remyelination has been reported in spinal cord injury (Lasiene et al., 2008; Totoiu and Keirstead, 2005), after toxin-induced demyelination (Blakemore, 1974; Blakemore and Murray, 1981), and in the demyelinating disease Multiple Sclerosis (Prineas et al.,

1993; Prineas and Connell, 1979). However, myelin sheaths made during remyelination are thought to be thinner and shorter than myelin sheaths in the healthy CNS, which could further change myelin patterns.

If de- and remyelination changes myelin patterns and, potentially, conduction speeds and overall circuit function, identifying signals which can promote efficient and complete myelin regeneration could be of significant therapeutic benefit. Given that neuronal activity can increase the production of oligodendrocytes and promote the growth of myelin sheaths, it is possible that neuronal activity could also improve remyelination. Gautier et al., 2015 showed that neuronal activity may already contribute to remyelination in the CNS *in vivo*. Rats with ethidium bromide-induced demyelination in the cerebellum were treated with either vehicle or TTX (voltage-gated Na^+ channel blocker) from three days post-lesion to see how activity within the lesion area affects remyelination (Gautier et al., 2015). The authors found that TTX treatment after demyelination leads to increased OPC proliferation, reduced differentiation into oligodendrocytes, and a slight increase in the death of oligodendroglial lineage cells. There are fewer remyelinated axons in TTX-treated animals by three weeks post-lesion, and those that are myelinated generally have thinner myelin sheaths than saline-treated animals (Gautier et al., 2015). Glutamate signalling may be the molecular mechanism by which neuronal activity promotes remyelination, as OPCs in lesions can detect glutamate via AMPA/kainate receptors, and treating lesions with NBQX (AMPA/kainate receptor antagonist) also impairs remyelination (Gautier et al., 2015).

Enhancing neuronal activity beyond basal levels could improve the endogenous remyelination response to regenerate myelin sheaths of normal length and thickness. Ortiz et al., 2019 attempted to investigate this by optogenetically stimulating axons in the mouse corpus callosum which were demyelinated by lysolecithin. They found that a single bout of stimulation transiently increases OPC proliferation, while daily stimulation for one week increases the production of oligodendrocytes and the number of remyelinated axons in the lesion. In unstimulated animals, they found that sheath thickness within the remyelinated lesion is consistently thinner than in normal appearing

white matter (NAWM). In optogenetically stimulated animals, sheath thickness within the remyelinated lesion is thinner than NAWM for axons under 0.793 µm in diameter. However, axons over 0.793 µm in the remyelinated lesion had myelin sheaths of thickness comparable to NAWM, suggesting that optogenetic stimulation enhances radial sheath growth along larger diameter axons during remyelination. It was suggested that these larger diameter axons were the axons expressing channelrhodopsin, and so increased activity promotes remyelination specifically on the active axons themselves (however, this was not confirmed by immunostaining for channelrhodopsin expression). The authors did investigate whether remyelination specifically targeted active axons by quantifying the proportion of MBP-positive axons which were channelrhodopsin-positive. They found that stimulation does not increase the proportion of channelrhodopsin-positive remyelinated axons. Whether optogenetic stimulation promotes the longitudinal growth of myelin sheaths along channelrhodopsin expressing axons in order to increase remyelinated sheath length is not known. There is a need to investigate how the activity of a single axon affects sheath growth dynamics during remyelination.

Optogenetic or chemogenetic systems could be combined with a demyelination model to assess how a single axon's activity affects its remyelination. In the zebrafish, an individual RS axon could be labelled with TRPV1-RFP or channelrhodopsins and GFP-Cntn1a, and then demyelination could be induced using a model such as the nitroreductase ablation model (Karttunen et al., 2017) or my novel Tg(mbp:TRPV1-RFP) ablation model (see Appendix 1: A Novel Zebrafish Model of Demyelination – Tg(mbp:TRPV1-RFP)). After demyelination, the RS axon could be chemogenetically or optogenetically stimulated and the formation of new myelin sheaths could be followed over time in stimulated and unstimulated animals. Larval zebrafish already exhibit remarkable remyelinating capacity, with new myelin sheaths being of similar length and thickness to normal sheaths in the healthy zebrafish CNS (Karttunen et al., 2017). However, neuronal activity may accelerate the remyelination process. Similar tools could be combined with toxin-induced demyelination in rodents, where two-photon microscopy and cranial windows

could be used to live image myelinated axons in the cortex (Hill et al., 2018; Hughes et al., 2018). Using this set-up, one could determine whether activity promotes the formation of sheaths with normal length and thickness along active axons during remyelination in the mammalian CNS.

Research has shown that, although myelin sheaths are remarkably stable after initial formation, rapid growth and remodelling can be induced by loss of neighbouring myelin sheaths (Auer et al., 2018). Identifying strategies to promote the growth or remodelling of surviving myelin sheaths may also provide therapeutic benefit, especially in the context of old age or later stages of MS, where the production of new myelinating oligodendrocytes seems to fail. The re-initiation of rapid growth in surviving sheaths suggests that these sheaths may detect and respond to growth cues when myelin patterns are disrupted. Chemogenetic or optogenetic stimulation of single RS axons in a zebrafish demyelination model could also be used to determine if neuronal activity promotes the growth or remodelling of surviving myelin sheaths.

If activity does promote the growth of both new and surviving myelin sheaths during remyelination, then identifying the molecular mechanism would be of significant therapeutic interest. Circuit stimulation, or drugs which target the appropriate receptor on oligodendrocytes or myelin sheaths, could promote the recovery of myelin patterns along demyelinated axons in injury or disease. These approaches could even help prevent age-associated cognitive decline by rescuing the loss of myelin with old age. Behaviour-driven treatments, such as cognitive training, task learning, or exercise, have been suggested as potential strategies to enhance remyelination (Jensen and Yong, 2016). In fact, exercise is sufficient to promote oligodendrogenesis and remyelination in a rodent model of demyelination (Jensen et al., 2018). Remyelination could be targeted by engaging in tasks which use specific parts of the CNS (for example, frontal cortex versus motor cortex).

4.3.9. Alternative Roles for Activity-mediated Myelination?

I hypothesise that activity-driven changes to myelin patterns serve to modulate circuit output. However, it is possible that activity-mediated changes to myelin patterns do not significantly affect conduction properties, post-synaptic neuron recruitment and activity, or behaviour. Could there be other functions for activity-driven myelination?

Myelinating oligodendrocytes are known to provide metabolic support to axons. Lactate produced by glycolysis in oligodendrocytes is shuttled to axons through the lactate transporter MCT1 (Fünfschilling et al., 2012; Y. Lee et al., 2012). Stimulation of oligodendrocyte NMDA receptors upregulates their expression of the glucose transporter GLUT1, leading to an increase in both glucose uptake and lactate release by oligodendrocytes (Saab et al., 2016). Oligodendrocyte-specific loss of NMDA receptors reduces the expression of GLUT1 in myelin sheaths and reduces the recovery of axons from oxygen-glucose deprivation, which can be rescued by lactate treatment (Saab et al., 2016). These findings suggest that electrically active axons increase the metabolic support they receive from oligodendrocytes in an activity-dependent manner. From an energetic perspective, increasing the myelin coverage along an axon would boost metabolic reserves required for function and survival. Activity-driven myelin sheath growth may have evolved as a mechanism to accelerate or even enhance the myelination of active axons, and subsequently increase metabolic support for the axons that need it most. In the larval zebrafish, activity-mediated acceleration of myelin sheath growth may provide a slight benefit by ensuring that active axons have sufficient metabolic support to fire optimally as soon as possible. Such optimisation could confer a slight competitive advantage, which, nevertheless, could be the difference between life and death. The altered myelin pattern along RS axons might just be a by-product.

ATP dynamics can now be live imaged to measure cellular metabolism *in vivo*. Imamura et al., 2009 developed a range of fluorescence resonance energy transfer-based (FRET) ATP sensors which can be used to measure ATP levels

in living cells. Trevisiol et al., 2017 used this tool to measure cytosolic ATP levels in axons of the optic nerve, and found that the ATP levels measured correlated with compound action potentials recorded by electrophysiology. ATP sensors could be used to measure metabolism along RS axons throughout myelination, and to determine whether axons with accelerated myelination have increased metabolic support, or reach optimal metabolic support levels sooner than control axons. Performing electrophysiology, or appropriate behavioural tests for the RS subtype being analysed, could determine whether changes in axonal ATP levels with myelination correlates with changes in circuit function.

If there is a correlation between glial metabolic support and circuit function, the next step would be to determine if metabolic support is required for changes in circuit function. It is hypothesised that lactate is shuttled out of oligodendrocytes by MCT1 channels, and then into the axon by neuronal MCT2 channels (Fünfschilling et al., 2012; Y. Lee et al., 2012). Cell-type specific Crispr techniques could be used to delete MCT1 from oligodendrocytes, or MCT2 from RS neurons, to disrupt oligodendroglial metabolic support of axons. These cell-type specific mutants could be tested to see if activity-driven myelination still correlates with changes in axonal metabolism and circuit function. If activity-driven myelination serves to enhance metabolic support then sheath growth should still be enhanced along active axons, but there would be no correlation between myelination and axonal metabolism or circuit function

4.3.10. Testing Other Tools to Investigate the Role of Activity and Activity-related Signals in Myelin Sheath Growth

During my project, I tested several other transgenic tools to look at the role of neuronal activity in regulating the dynamics of sheath growth and maintenance in more detail. I tested several neurotoxins, which either inhibit or enhance synaptic vesicle release (TeNT, BoNT and glycerotoxin). I tested the inward-rectifying K^+ channel tool eGFP-K_{ir}2.1 as a means of inhibiting the overall activity of individual axons. I also tested KalTA4-ERT^2, a zebrafish-optimised

protein which drives the expression of UAS-driven transgenes in a tamoxifen-inducible manner, with the aim of expressing transgenic proteins at specific developmental stages (for example, after sheath formation, after myelin pattern establishment). The results of these tool tests are summarised in **Table 6**.

None of the tools tested were suitable to investigate the role of neuronal activity in regulating myelination along single axons over time according to my stated aims, and further optimisation of these tools is needed. For KalTA4-ERT^2, it may be that a different neuronal promoter sequence leads to lower expression levels in neurons, which could prevent 'leaky' activation of UAS-driven transgene expression. Otherwise, a different inducible system should be used (such as the TetON system (Knopf et al., 2010)). For TeNT and BoNT, different neuronal Gal4/KalTA4 driver lines should be tested to identify which line drives expression at sufficient levels to completely inhibit synaptic vesicle release in single axons. For glycerotoxin and eGFP-K_{ir}2.1, testing different neuronal promoters may identify expression levels which do not affect neuronal development but still affect neuronal activity. Alternatively, these tools may need to be combined with an inducible expression system to prevent adverse effects on early neurodevelopment.

4.3.11. Summary

In this chapter, I have shown that chemogenetic stimulation of individual RS neurons using the TRPV1-RFP system promotes myelin sheath growth within a critical period (3-5 dpf). As a result, chemogenetic stimulation changes the myelin pattern established along some RS axons by increasing sheath length and reducing sheath number. Future work should: determine how and when neuronal activity affects radial sheath growth along an individual axon; identify the molecular mechanism underpinning activity-mediated sheath growth; and assess the impact of activity-mediated sheath growth on circuit function in the context of health and disease.

Table 6 – summary of the other transgenic tools tested to manipulate neuronal activity throughout myelination.

Tool Tested	Description	Summary of Experiment	Results and Evaluation
KalTA4-ERT^2	A tamoxifen-inducible transcriptional activator to temporally control expression of UAS:transgenes. From Dr. Yi Feng.	Generated NBT:KalTA4-ERT^2 transgenic line (pan-neuronal expression of KalTA4-ERT^2). Tested whether UAS:transgene expression could be induced by 4-OH-tamoxifen treatment.	Often led to 'leaky' expression (neuronal expression of UAS:transgenes in the absence of tamoxifen). Not suitable for inducible expression in the nervous system.
TeNT-tdTomato	Inhibits synaptic vesicle release by cleaving the SNARE protein VAMP2.	Attempted to replicate findings from Koudelka et al. 2016 (expressed in single RS axons, assessed their myelination at 5 dpf).	RS axon myelination was unaffected. Struggled to achieve similar levels of expression as Dr. Sigirid Koudelka. After discussion, we hypothesise that epigenetic changes in transgenic lines used prevent sufficient levels of TeNT expression to generate hypomyelination phenotype. The effectiveness of vesicular release inhibition was not quantified.
BoNT-B-eGFP	Zebrafish-optimised version of BoNT-B (Sternberg et al., 2016). Inhibits synaptic vesicle release by cleaving the SNARE protein VAMP2. From Dr. Claire Wyart.	Attempted to verify that this zebrafish-optimised tool was equivalent to TeNT (globally expressed to assess effects on single oligodendrocyte morphology; expressed in single RS axons and assessed their myelination at 5 dpf).	Global expression paralysed zebrafish embryos and reduced myelinating potential per oligodendrocyte (replicating TeNT findings from Mensch et al., 2015). Expression in single axons did not affect myelination at 5 dpf – however, the effectiveness of vesicular release inhibition was not quantified.

Glycerotoxin	Increases synaptic vesicular release by activating $Ca_v2.2$ channels. From Dr. Rafael Almeida.	Globally expressed to assess effects on single oligodendrocyte morphology; expressed in single RS axons and assessed their myelination at 5 dpf.	Global expression increased myelinating potential per oligodendrocyte. Expression in single axons disrupted neuronal development (Dr. Rafael Almeida, unpublished).
eGFP-$K_{ir}2.1$	Inward-rectifying K^+ channel which hyperpolarises neurons by allowing K^+ influx.	Tested various plasmids to express in neurons (NBT: eGFP-$K_{ir}2.1$ and HuC: eGFP-$K_{ir}2.1$ for pan-neuronal expression; UAS:eGFP-$K_{ir}2.1$ combined with RS:KalTA4 for RS neuron expression).	Could not consistently express in single axons (levels of expression may severely disrupt neuron development). Requires further optimisation to determine non-toxic levels of expression, or to induce expression after neurogenesis/axogenesis.

Chapter 5: Discussion

5.1. A Critical Period for the Establishment of Myelin Patterns

In this thesis, I set out to investigate the dynamics myelinated axon formation in the CNS, and how this is regulated by the activity of the underlying axons. Myelin patterns along axons (the number, length, thickness, and distribution of myelin sheaths) vary extensively throughout the CNS (Chong et al., 2012; Gao et al., 2019; Murray and Blakemore, 1980; Remahl and Hildebrand, 1990; Tomassy et al., 2014). Given that changes to sheath parameters are predicted modulate the conduction speed of the underlying axon (Waxman, 1980), it is hypothesised that establishing and refining specific myelin patterns might precisely control conduction timing within circuits. For instance, specific patterns of sheath length are seen in the auditory system of gerbils, which are predicted to facilitate precise sound localisation (Ford et al., 2015).

How and when the myelin patterns are established along individual axons was not fully understood prior to the beginning of this project. Using single cell live imaging in the larval zebrafish spinal cord, I investigated how myelin patterns are formed and remodelled along individual axons *in vivo*. I found that the number and length of myelin sheaths along an axon are generally established within the first few days after the onset of myelination (by 5 dpf for the specific axons that I investigated). After 5 dpf, there is some remodelling (where sheaths can either grow or shrink in length, or be fully retracted from the axon), but very little happens after 7 dpf, with no significant change in overall sheath number, sheath length, sheath length variability, or nodal gap length after 7 dpf.

If myelin patterns are tuned to the function of individual circuits, then it is plausible that axons from different circuits would exhibit different myelin patterns. I characterised the myelin pattern formation and remodelling along two different types of axons, which are known to use different signals to regulate their initial myelination. My hypothesis was that they would exhibit different myelin patterns and extents of myelin remodelling. Surprisingly, I found that both RS and CoPA axons establish remarkably similar myelin patterns and exhibit very little difference in the degree of myelin remodelling.

There is significant evidence to suggest that experience and learning can shape white matter development and myelination throughout life (Bengtsson et al., 2005; Eluvathingal et al., 2006; Hill et al., 2014; Hughes et al., 2018; Makinodan et al., 2012; Sampaio-Baptista et al., 2013; Scholz et al., 2009; Steele et al., 2013; Xiao et al., 2016). Experience-driven neuronal activity may influence the formation of myelin patterns and sheath remodelling to tune conduction timing in circuits. Neuronal activity can influence many aspects of oligodendrocyte development including OPC proliferation, differentiation, and targeting myelination (Barres and Raff, 1993; Demerens et al., 1996; Gibson et al., 2014; Mitew et al., 2018). Here, I investigated how neuronal activity affects the dynamics of myelin sheath growth during the period of myelin pattern establishment. RS neurons have previously been shown to be myelinated in a synaptic vesicle release-dependent manner, suggesting that they use activity-related signals to regulate their myelination (Koudelka et al., 2016). I found that increasing the activity of individual RS axons during myelination promotes the early growth of myelin sheaths 3-5 dpf, but has no effect on sheath dynamics after 5 dpf. Nevertheless, this transient effect on sheath growth was enough to alter the myelin pattern established along the first myelinated RS axons (which had fewer, but longer, myelin sheaths at 7 dpf than unstimulated control axons). My findings suggest that signals like neuronal activity can shape the myelination of axons, but only within a critical developmental window, after which myelin sheaths become stable in number and length irrespective of circuit activity.

Why is activity-driven myelin pattern establishment restricted to a critical period? Critical periods for neuronal plasticity have been well-described throughout CNS development. Columns in the visual cortex are shaped by visual input within a critical period during post-natal development, which is regulated by an excitatory-inhibitory balance (this has been reviewed elsewhere by Hensch, 2005). In the auditory cortex, cortical maps of sound frequencies are established during a critical period (between P11-15 in rodents); this critical period is regulated by adenosine signalling in the auditory thalamus, which increases with age (Blundon et al., 2017). Adult-born neurons

also have critical periods; newly-born dentate granule cells exhibit enhanced synaptic plasticity approximately one month after cell birth, which declines by four months after cell birth (Ge et al., 2007). It is hypothesised that these critical periods exist so that circuit function can be adapted by the external environment and then stably maintained throughout life. Likewise, a critical period for myelin pattern formation would allow conduction properties along an axon to be tuned by a period of learning, and then stabilised thereafter to maintain optimal circuit function throughout life.

What defines the critical period for myelin pattern establishment? It may relate to a specific developmental stage of the animal. Juvenile rodents, which are socially isolated from P21-65, have severe hypomyelination in the medial prefrontal cortex (mPFC) due to fewer sheaths being made per oligodendrocyte (sheath length was not measured in this study) (Makinodan et al., 2012). Isolated animals are antisocial and have impaired working memory. Interestingly, isolation from P21-35 is sufficient to impair myelination and behaviour, while isolation from P35-P65 does not have any effect. Neuronal activity driven by social experience may shape the formation of particular myelin patterns in mPFC circuits within the critical period of P21-35. After P35, the myelin patterns along these circuits may be stabilised, much like how the myelin patterns along RS and CoPA axons in the zebrafish spinal cord are stabilised after 7 dpf. Resocialisation after P35 does not rescue the hypomyelination or behavioural phenotypes (Makinodan et al., 2012). This suggests that circuit activity driven by experience cannot affect the myelination along mPFC circuits after the critical period, similar to how neuronal activity cannot affect the growth of myelin sheaths along RS axons in the zebrafish spinal cord after 5 dpf. Thus, there may be defined developmental windows when activity can influence myelination in the CNS and shape myelin pattern establishment, after which the myelin patterns cannot be changed regardless of experience.

However, there is evidence that experience and activity can alter white matter or myelin development in adulthood. In adult humans (aged 18-33), task learning correlates with structural alterations in the white matter of associated

brain areas detected by DTI (Schlegel et al., 2012; Scholz et al., 2009). Similarly, DTI in adult mice (P120-150) trained in a skilled reaching task shows correlations between learning rate and white matter structure, as well as between learning rate and expression of myelin basic protein (Sampaio-Baptista et al., 2013). Both running on a complex wheel (at P85-115 – Xiao et al., 2016) and sensory stimulation (at P365 – Hughes et al., 2018) increases the production of new oligodendrocytes in relevant cortical areas of adult mice.

How does this fit with the evidence that myelin patterns are stabilised after a critical period? Myelination is a protracted process which continues throughout life (Yakovlev and Lecours, 1967; Yeung et al., 2014). Some circuits are myelinated during early post-natal development, while other circuits continue to be myelinated many years into adulthood. Live imaging in the mouse cortex identifies sparsely myelinated axons where myelin coverage gradually increases over several months during adulthood (between P64-148) (Hill et al., 2018). The critical period for myelin pattern establishment may depend on the timescale over which a specific circuit is myelinated. Additionally, neuronal activity may only signal to oligodendrocytes or myelin sheaths at a certain cellular developmental stage. Expression of glutamatergic receptors significantly declines with oligodendroglial lineage progression (De Biase et al., 2010; Deng et al., 2004; Kukley et al., 2010). Consequently, oligodendrocytes or myelin sheaths may only detect and respond to neuronal activity within a short time period after differentiation, after which they are unaffected by circuit activity. This would be in line with observations that myelin sheaths become remarkably stable in length after initial formation (Auer et al., 2018; Hill et al., 2018; Hughes et al., 2018), even when the underlying circuits are stimulated (Hughes et al., 2018). In circuits which are myelinated during earlier post-natal development, the myelin patterns along axons may be established by activity within this time frame. Whereas, in circuits which exhibit more protracted myelination throughout adulthood, the myelin patterns along axons may be shaped by activity over a longer period of time. Previous studies showing experience-driven oligodendrogenesis in the adult cortex have not then followed these new oligodendrocytes to confirm that they produce myelin

sheaths (Hughes et al., 2018; Xiao et al., 2016). It will be crucial to follow such newly-generated oligodendrocytes in stimulated and unstimulated animals to see if experience affects the initial growth of myelin sheaths formed in adulthood.

The investigation of myelin sheath dynamics over time performed by myself and others (Auer et al., 2018; Hill et al., 2018; Hughes et al., 2018) has focused on sheath length. There is a clear need to characterise how sheath thickness changes over time, as this may be a parameter of myelin patterns which is remodelled beyond the critical period observed for sheath length. For example, Hughes et al., 2018 demonstrated that sensory stimulation does not affect the length of existing myelin sheaths in the sensory cortex. However, Liu et al., 2012 found that eight weeks of social isolation in adult mice (specific age unknown) leads to thinner myelin sheaths in the mPFC. Whether these thin myelin sheaths have been remodelled in thickness, or are simply new sheaths which are thinner than normal, is not clear as the authors assessed sheath thickness at a single time point by transmission electron microscopy. Techniques to repeatedly measure sheath thickness in living animals (see section '3.3.5 Remodelling of Sheath Thickness over Time') are required to fully understand when myelin patterns are established, and whether they can be remodelled. It may be that basal levels of circuit activity are required to maintain a specific myelin pattern long-term, and so prolonged periods of inactivity or deprivation can eventually alter circuit myelin patterns.

Not all types of axon use activity-related signals to regulate their initial myelination (Koudelka et al., 2016); despite this, I found very little difference in the myelin patterns or extent of sheath remodelling between axons that are myelinated in an activity-dependent (RS) and independent (CoPA) manner. However, CoPA axons may still be capable of using experience to shape their myelin patterns; other signals may simply take over when CoPA synaptic vesicle release is inhibited, whereas RS axons may rely more heavily on activity-driven signals to control myelin pattern formation. Whether CoPA axons are capable of using activity to regulate their myelination could be tested

by chemogenetically stimulating TRPV1-RFP-expressing CoPA axons during the period of myelin pattern formation.

Whether some circuits use experience to shape their myelin patterns while other circuits do not requires further investigation. Previous studies have not identified specific neuron subtypes when investigating myelin sheath dynamics (Auer et al., 2018; Hill et al., 2018; Hughes et al., 2018). Future work live imaging myelin sheath dynamics *in vivo* should include the characterisation of specific neuron subtypes and their circuitry to increase our understanding of experience-dependent myelination. For example, two recent studies have shown that different types of experience can increase oligodendrocyte production in the motor (Xiao et al., 2016) and sensory (Hughes et al., 2018) cortices. Characterising the specific neuron subtypes which are then myelinated by these oligodendrocytes, and comparing how experience affects sheath growth dynamics in both motor and sensory cortices, could reveal specifically which neurons and circuits use experience-driven activity to shape their myelination.

5.2. Functional Implications of Experience-driven Myelin Patterns

Activity-dependent sheath growth along RS axons between 3-5 dpf was sufficient to change the myelin patterns established, leading to longer but fewer sheaths per axon. Experience within critical myelination periods could similarly shape the myelin patterns formed along circuits. The functional consequence of such activity-driven myelination is not yet known. Mathematical modelling predicts that changes in sheath length can have a significant impact on conduction speeds along an axon (Brill et al., 1977; Waxman, 1980). For example, for an axon 1 µm in diameter, changing sheath length from 10 µm to 20 µm is predicted to change conduction velocity from 50% of maximum to ~65% of maximum (Waxman, 1980). Smaller changes in sheath length may not yield drastic changes in conduction speeds, but even a small change in conduction timing could significantly affect the synchronisation of signals in a circuit.

In order to dissect the role of myelin patterns in overall circuit function, there is a need to analyse single cells, intact circuits, overall CNS activity, and behavioural outputs within the same model system. Such a multi-level experimental system would allow correlation of experience or neuronal activity with myelin sheath dynamics, conduction speeds, post-synaptic target recruitment and activity, overall circuit activity, and associated behaviour kinematics. Larval zebrafish are already established as a model for correlating cellular resolution imaging of circuit activity with behaviour (Ahrens et al., 2012; Mu et al., 2019; Orger et al., 2008). Whole-brain Ca^{2+} imaging can even be performed in freely-behaving larvae using tracking microscope tools (Cong et al., 2017; Kim et al., 2017; Symvoulidis et al., 2017). Whole circuit Ca^{2+} imaging and behavioural analysis could be combined with single cell activity manipulations, high-resolution cellular imaging of myelin sheath dynamics, and electrophysiology to assess how activity-driven myelin pattern formation affects function on the level of cells, circuits, and behaviour. For instance, MeLr and MeLc RS neurons (the RS neurons responsible for prey capture behaviour) could be selectively stimulated to alter their myelin patterns by 7 dpf. The conduction velocities of stimulated and unstimulated axons, and the activity of post-synaptic motor- and inter-neurons, could be measured during prey capture behaviour, and correlated with success rate and behaviour kinematics such as tail bend angles during orienting swims. Multiscale analyses could be expanded to other neurons and circuits as the specific circuitry underlying particular behaviours are dissected. Hildebrand et al., 2017 performed whole-brain serial-section electron microscopy to reconstruct the connectome (all myelinated axons) in the 5 dpf zebrafish brain; while Kunst et al., 2019 has produced a cellular-resolution neuron atlas of the 6 dpf zebrafish brain, showing the projection morphology of different cells and clustering them into “morphotypes”. These resources could be correlated with brain-wide Ca^{2+} imaging to identify specific neurons and circuits involved in different behaviours; the myelin patterns along identified axons of interest can then be studied in detail to correlate distinct myelin patterns with circuit activity and behaviour.

Studying larval zebrafish can tell us about the role of myelin patterns in circuit function during early development, but may not inform us about the role of myelin pattern formation in a more mature nervous system. Zebrafish become progressively less transparent as they grow in size; once they are several weeks old, high-resolution cellular live imaging is no longer possible. Mammalian models, such as rodents, are more suited for investigation of myelin sheath dynamics and circuit function in the adult CNS. Previous studies have demonstrated that, by making a cranial window in the skull of adult mice, oligodendrocytes and myelin sheaths in the upper cortex can be repeatedly imaged by two-photon microscopy (Hill et al., 2018; Hughes et al., 2018). Miniature two-photon microscopes have been developed to perform CNS live imaging in freely-behaving mice, identifying activity in individual dendritic spines during behavioural paradigms such as tail suspension and social interaction (Zong et al., 2017). Three-photon microscopy shows promise for imaging deeper sub-cortical regions without removing the overlaying cortical tissue (Ouzounov et al., 2017). Live imaging of oligodendrogenesis, myelin sheath formation, and growth should be coupled with assessment of underlying circuit activity and behaviour. A combination of these strategies could elucidate the role of experience-dependent myelination on circuit function in adulthood.

It is important to consider alternative explanations for the role of activity-driven myelination during learning and experience. The metabolic support provided to axons from oligodendroglia can be regulated by NMDA receptor signalling, indicating that neurons can increase energy supply during periods of activity (Saab et al., 2016). Active axons may promote their myelination not to adjust conduction speeds, but simply to ensure that there is sufficient metabolic transfer to support increased activity during learning. This may explain why such sparsely myelinated axons have been reported throughout the CNS (Auer et al., 2018; Gao et al., 2019; Hill et al., 2018; Tomassy et al., 2014). The large unmyelinated gaps between sheaths along these axons are not likely to facilitate saltatory conduction (as this requires clustering of voltage-gated Na^+ channels to short regions separated by insulating myelin sheaths)

and so may not significantly affect conduction velocities. However, these sheaths may provide enough lactate to meet the energetic demands of the underlying axon. Perhaps, on fully myelinated axons, activity-driven myelin sheath growth serves to both increase metabolic support and adjust conduction speeds. Uncoupling the metabolic support role from the insulating role of myelinating cells (see section ‘4.3.9 Alternative Roles for Activity-mediated Myelination?’) could tell us the relative contributions of each in regulating the function of different circuits.

5.3. Investigating the Disruption of Myelin Patterns

Understanding how myelin patterns contribute to circuit function is particularly important in situations where myelin patterns are disrupted. Axons can become demyelinated in CNS injury (Kakulas, 1999; Totoiu and Keirstead, 2005), in diseases such as MS (Albert et al., 2007; Newcombe et al., 1991), and with old age (Hill et al., 2018). Loss of myelin sheaths will disrupt both conduction and metabolic support to axons; it is hypothesised that remyelination is required for long-term axonal survival (Irvine and Blakemore, 2008; Mei et al., 2016). Remyelination does restore conduction along demyelinated axons (Smith et al., 1981), but remyelinated sheaths are believed to be thinner and shorter than sheaths in a healthy CNS (Blakemore, 1974; Blakemore and Murray, 1981; Lasiene et al., 2008; Prineas et al., 1993; Prineas and Connell, 1979; Totoiu and Keirstead, 2005).

How changes to the myelin patterns along axons after remyelination affects conduction and alters circuit function requires further investigation. Remyelination may subtly alter conduction velocities along axons, desynchronising signals in circuits and changing behavioural outputs. If so, then identifying signals which promote the regeneration of sheaths of normal length and thickness would be of significant therapeutic value. Single axon de- and remyelination needs to be characterised in detail to determine whether there is a critical period for the recovery of myelin patterns during remyelination. Characterisation could also reveal whether experience-driven neuronal activity within such a critical period could promote complete

remyelination. Again, the ideal model system would integrate detailed cellular imaging with measurement of circuit activity and behaviour over time. A recently-developed larval zebrafish model of demyelination has shown that zebrafish exhibit efficient remyelination (Karttunen et al., 2017). In this model, myelinating cells express the enzyme nitroreductase, which converts the pro-drug metronidazole into a cytotoxic by-product. Treatment of nitroreductase-expressing larvae with metronidazole kills two thirds of oligodendrocytes and causes demyelination, which recovers by 16 days post-treatment. Other demyelination models could also be used to investigate changes and recovery of myelin patterns. In addition to the work performed in Chapters 3 and 4, I have generated a novel transgenic model of demyelination (see 'Appendix 1: A Novel Zebrafish Model of Demyelination – Tg(mbp:TRPV1-RFP)'), which allows a much more rapid induction of demyelination in the zebrafish CNS. Although this remains to be fully-characterised, it and other model systems of demyelination could be used to investigate how the myelin patterns along specific axon subtypes change through de- and remyelination in zebrafish. Changes to myelin patterns could then be correlated with measurements of circuit activity and behavioural outputs. Neurotoxins or channelrhodopsins could be expressed in single axons to see whether manipulating activity during the de- and remyelination process alters the repair of myelin patterns. Dissecting how remyelination affects single axons, intact circuits, overall CNS activity, and behaviour will test whether specific myelin patterns are required for healthy nervous system function.

5.4. Overall Summary

Investigating the dynamics of myelination along single axons, and determining what signals regulate this process, are crucial steps in understanding the emergence of circuit function at the cellular level. Here, I have characterised the formation of myelin patterns and myelin sheath remodelling along different axon subtypes within a critical period in the larval zebrafish spinal cord. I have shown how the activity of an axon affects the dynamics of its myelination during this critical period. Future work should expand these analyses to different

circuits, and correlate measurement of myelin sheath dynamics with nervous system function on the level of single cells, intact circuits, and overall behaviour. A multiscale approach will inform us how the dynamics of myelination influence the emergence of nervous system function, and may reveal therapeutic avenues to promote complete functional recovery in conditions where myelination is disrupted.

References

Ablain, J., Durand, E.M., Yang, S., Zhou, Y., Zon, L.I., 2015. A CRISPR/Cas9 vector system for tissue-specific gene disruption in zebrafish. Dev. Cell 32, 756–764.

Aggarwal, S., Yurlova, L., Snaidero, N., Reetz, C., Frey, S., Zimmermann, J., Pähler, G., Janshoff, A., Friedrichs, J., Müller, D.J., Goebel, C., Simons, M., 2011. A size barrier limits protein diffusion at the cell surface to generate lipid-rich myelin-membane sheets. Dev. Cell 21, 445–456.

Ahrens, M.B., Li, J.M., Orger, M.B., Robson, D.N., Schier, A.F., Engert, F., Portugues, R., 2012. Brain-wide neuronal dynamics during motor adaptation in zebrafish. Nature 485, 471–477.

Akerberg, A.A., Stewart, S., Stankunas, K., 2014. Spatial and temporal control of transgene expression in zebrafish. PLoS One 9, e92217.

Albert, M., Antel, J., Brück, W., Stadelmann, C., 2007. Extensive cortical remyelination in patients with chronic multiple sclerosis. Brain Pathol. 17, 129–138.

Alexander, G.M., Rogan, S.C., Abbas, A.I., Armbruster, B.N., Pei, Y., Allen, J.A., Nonneman, R.J., Hartmann, J., Moy, S.S., Nicolelis, M.A., Mcnamara, J.O., Roth, B.L., 2009. Remote control of neuronal activity in transgenic mice expressing evolved G Protein-Coupled Receptors. Neuron 63, 27–39.

Almeida, R.G., 2018. The rules of attraction in central nervous system myelination. Front. Cell. Neurosci. 12.

Almeida, R.G., Czopka, T., Ffrench-Constant, C., Lyons, D.A., 2011. Individual axons regulate the myelinating potential of single oligodendrocytes in vivo. Development 138, 4443–4450.

Almeida, R.G., Pan, S., Cole, K.L.H., Williamson, J.M., Early, J.J., Czopka, T., Klingseisen, A., Chan, J.R., Lyons, D.A., 2018. Myelination of neuronal cell bodies when myelin supply exceeds axonal demand. Curr. Biol. 28, 1296–1305.

Arancibia-Cárcamo, I.L., Ford, M.C., Cossell, L., Ishida, K., Tohyama, K., Attwell, D., 2017. Node of Ranvier length as a potential regulator of myelinated axon conduction speed. Elife 6, e23329.

Armbruster, B.N., Li, X., Pausch, M.H., Herlitze, S., Roth, B.L., 2007. Evolving the lock to fit the key to create a family of G protein-coupled receptors potently activated by an inert

ligand. PNAS 104, 5163–5168.

Auer, F., Vagionitis, S., Czopka, T., 2018. Evidence for myelin sheath remodeling in the CNS revealed by in vivo imaging. Curr. Biol. 28, 549–559.

Baecher-Allan, C., Kaskow, B.J., Weiner, H.L., 2018. Multiple Sclerosis: mechanisms and immunotherapy. Neuron 97, 742–768.

Bando, Y., Sakamoto, M., Kim, S., Ayzenshtat, I., Yuste, R., 2019. Comparative evaluation of genetically encode voltage indicators. Cell Rep. 26, 802–813.

Baraban, M., Koudelka, S., Lyons, D.A., 2018. Ca2+ activity signatures of myelin sheath formation and growth in vivo. Nat. Neurosci. 21, 19–23.

Barbazuk, W.B., Korf, I., Kadavi, C., Heyen, J., Tate, S., Wun, E., Bedell, J.A., Mcpherson, J.D., Johnson, S.L., 2000. The syntenic relationship of the zebrafish and human genomes. Genome Res. 10, 1351–1358.

Barres, B.A., Hart, I.K., Coles, H.S.R., Burne, J.F., Voyvodic, J.T., Richardson, W.D., Raff, M.C., 1992. Cell death and control of cell survival in the oligodendrocyte lineage. Cell 70, 31–46.

Barres, B.A., Koroshetz, W.J., Swartz, K.J., Chun, L.Y., Corey, D.P., 1990. Ion channel expression by white matter glia: The O-2A glial progenitor cell. Neuron 4, 507–524.

Barres, B.A., Raff, M., 1993. Proliferation of oligodendrocyte precursor cells depends on electrical activity in axons. Nature 361, 258–260.

Battefeld, A., Popovic, M.A., de Vries, S.I., Kole, M.H.P., 2019. High-frequency microdomain Ca2+ transients and waves during early myelin internode remodeling. Cell Rep. 26, 182–191.

Baumann, N., Pham-Dinh, D., 2001. Biology of oligodendrocyte and myelin in the mammalian central nervous system. Physiol Rev 81, 871–927.

Beaulieu, C., 2002. The basis of anisotropic water diffusion in the nervous system - a technical review. NMR Biomed. 15, 435–455.

Bechler, M.E., Byrne, L., Ffrench-Constant, C., 2015. CNS myelin sheath lengths are an intrinsic property of oligodendrocytes. Curr. Biol. 25, 2411–2416.

Bengtsson, S.L., Nagy, Z., Skare, S., Forsman, L., Forssberg, H., Ullén, F., 2005. Extensive piano practicing has regionally specific effects on white matter development. Nat.

Neurosci. 8, 1148–1150.

Berger, T., Walz, W., Schnitzer, J., Kettenmann, H., 1992. GABA- and glutamate-activated currents in glial cells of the mouse corpus callosum slice. J. Neurosci. Res. 31, 21–27.

Bergles, D.E., Richardson, W.D., 2016. Oligodendrocyte development and plasticity. Cold Spring Harb. Perspect. Biol. 8, a020453.

Bergles, D.E., Roberts, J.D.B., Somogyi, P., Jahr, C.E., 2000. Glutamatergic synapses on OPCs in the hippocampus. Nature 405, 187–191.

Bernhardt, R.R., Chitnis, A.B., Lindamer, L., Kuwada, J.Y., 1990. Identification of spinal neurons in the embryonic and larval zebrafish. J. Comp. Neurol. 302, 603–616.

Bernhardt, R.R., Patel, C.K., Wilson, S.W., Kuwada, J.Y., 1992. Axonal trajectories and distribution of GABAergic spinal neurons in wildtype and mutant zebrafish lacking floor plate cells. J. Comp. Neurol. 326, 263–272.

Bianco, I.H., Kampff, A.R., Engert, F., 2011. Prey capture behavior evoked by simple visual stimuli in larval zebrafish. Front. Syst. Neurosci. 5.

Binz, T., Sikorra, S., Mahrhold, S., 2010. Clostridial neurotoxins: mechanism of SNARE cleavage and outlook on potential substrate specificity reengineering. Toxins (Basel). 2, 665–682.

Blakemore, W.F., 1974. Pattern of remyelination in the CNS. Nature 249, 577–578.

Blakemore, W.F., Murray, J.A., 1981. Quantitative examination of internodal length of remyelinated nerve fibres in the CNS. J. Neurol. Sci. 49, 273–284.

Bliss, T., Collingridge, G., 1993. A synaptic model of memory: long-term potentiation in the hippocampus. Nature 361, 31–39.

Blundon, J.A., Roy, N.C., Teubner, B.J.W., Yu, J., Eom, T.-Y., Sample, K.J., Pani, A., Smeyne, R.J., Han, S.B., Kerekes, R.A., Rose, D.C., Hackett, T.A., Vuppala, P.K., Freeman, B.B., Zakharenko, S.S., 2017. Restoring auditory cortex plasticity in adult mice by restricting thalamic adenosine signaling. Science . 356, 1352–1356.

Bonkowsky, J.L., Nelson, C., Kingston, J.L., Filloux, F.M., Mondorff, M.B., Srivastava, R., 2010. The burden of inherited leukodystrophies in children. Neurology 75, 718–725.

Boyden, E.S., Zhang, F., Bamberg, E., Nagel, G., Deisseroth, K., 2005. Millisecond-timescale, genetically targeted optical control of neural activity. Nat. Neurosci. 8, 1263–1268.

Brill, M., Waxman, S.G., Moore, J., Joyner, R.W., 1977. Conduction velocity and spike configuration in myelinated fibres: computed dependence on internode distance. J. Neurol. Neurosurg. Psychiatry 40, 769–774.

Brinkmann, B.G., Agarwal, A., Sereda, M.W., Garratt, A.N., Müller, T., Wende, H., Stassart, R.M., Nawaz, S., Humml, C., Velanac, V., Radyushkin, K., Goebbels, S., Fischer, T.M., Franklin, R.J., Lai, C., Ehrenreich, H., Birchmeier, C., Schwab, M.H., Nave, K.A., 2008. Neuregulin-1/ErbB signaling serves distinct functions in myelination of the peripheral and central nervous aystem. Neuron 59, 581–595.

Brody, B.A., Kinney, H.C., Kloman, A.B., Gilles, F.H., 1987. Sequence of central nervous system myelination in human infancy. I. An autopsy study of myelination. J. Neuropathol. Exp. Neurol. 46, 283–301.

Brösamle, C., Halpern, M.E., 2002. Characterization of myelination in the developing zebrafish. Glia 39, 47–57.

Buckley, C.E., Marguerie, A., Alderton, W.K., Franklin, R.J.M., 2010. Temporal dynamics of myelination in the zebrafish spinal cord. Glia 58, 802–812.

Budick, S.A., O'Malley, D.M.O., 2000. Locomotor repertoire of the larval zebrafish: swimming, turning and prey capture. J. Exp. Biol. 203, 2565–2579.

Bullock, T.H., 1984. Comparative neuroethology of startle, rapid escape, and giant fiber-medated responses. In: Neural Mechanisms of Startle Behaviour. Springer Science, pp. 1–11.

Bullock, T.H., Moore, J.K., Fields, R.D., 1984. Evolution of myelin sheaths: Both lamprey and hagfish lack myelin. Neurosci. Lett. 48, 145–148.

Bunge, R.P., Bunge, M.B., Bates, M., 1989. Movements of the Schwann cell nucleus implicate progression of the inner (axon-related) Schwann cell process during myelination. J. Cell Biol. 109, 273–284.

Castrén, E., Zafra, F., Thoenen, H., Lindholm, D., 1992. Light regulates expression of brain-derived neurotrophic factor mRNA in rat visual cortex. PNAS 89, 9444–9448.

Caterina, M.J., Schumacher, M.A., Tominaga, M., Rosen, T.A., Levine, J.D., Julius, D., 1997. The capsaicin receptor: a heat-activated ion channel in the pain pathway. Nature 389, 816–824.

Chang, A., Nishiyama, A., Peterson, J., Prineas, J., Trapp, B.D., 2000. NG2-positive

oligodendrocyte progenitor cells in adult human brain and multiple sclerosis lesions. J Neurosci 20, 6404–6412.

Charles, P., Hernandez, M.P., Stankoff, B., Aigrot, M.S., Colin, C., Rougon, G., Zalc, B., Lubetzki, C., 2000. Negative regulation of central nervous system myelination by polysialylated-neural cell adhesion molecule. PNAS 97, 7585–7590.

Chen, S., Chiu, C.N., McArthur, K.L., Fetcho, J.R., Prober, D.A., 2016. TRP channel mediated neuronal activation and ablation in freely behaving zebrafish. Nat. Methods 13, 147–150.

Chen, T.-J., Kula, B., Nagy, B., Barzan, R., Gall, A., Ehrlich, I., Kukley, M., 2018. In vivo regulation of oligodendrocyte precursor cell proliferation and differentiation by the AMPA-receptor subunit GluA2. Cell Rep. 25, 852–861.

Chéreau, R., Saraceno, G.E., Angibaud, J., Cattaert, D., Nägerl, U.V., 2017. Superresolution imaging reveals activity-dependent plasticity of axon morphology linked to changes in action potential conduction velocity. PNAS 114, 1401–1406.

Chong, S.Y.C., Rosenberg, S.S., Fancy, S.P.J., Zhao, C., Shen, Y.-A.A., Hahn, A.T., McGee, A.W., Xu, X., Zheng, B., Zhang, L.I., Rowitch, D.H., Franklin, R.J.M., Lu, Q.R., Chan, J.R., 2012. Neurite outgrowth inhibitor Nogo-A establishes spatial segregation and extent of oligodendrocyte myelination. PNAS 109, 1299–1304.

Cole, K.L.H., Early, J.J., Lyons, D.A., 2017. Drug discovery for remyelination and treatment of MS. Glia 65, 1565–1589.

Colman, D.R., Kreibich, G., Frey, A.B., Sabatini, D.D., 1982. Synthesis and incorporation of myelin polypeptides into CNS myelin. J. Cell Biol. 95, 598–608.

Cong, L., Wang, Z., Chai, Y., Hang, W., Shang, C., Yang, W., Bai, L., Du, J., Wang, K., Wen, Q., 2017. Rapid whole brain imaging of neural activity in freely behaving larval zebrafish (Danio rerio). Elife 6, e28158.

Cox, S.R., Ritchie, S.J., Tucker-Drob, E.M., Liewald, D.C., Hagenaars, S.P., Davies, G., Wardlaw, J.M., Gale, C.R., Bastin, M.E., Deary, I.J., 2016. Ageing and brain white matter structure in 3,513 UK Biobank participants. Nat. Commun. 7.

Czopka, T., Ffrench-Constant, C., Lyons, D.A., 2013. Individual oligodendrocytes have only a few hours in which to generate new myelin sheaths in vivo. Dev. Cell 25, 599–609.

Czopka, T., Lyons, D.A., 2011. Dissecting mechanisms of myelinated axon formation usng zebrafish. In: Methods in Cell Biology. Elsevier Inc., pp. 26–62.

De Biase, L.M., Kang, S.H., Baxi, E.G., Fukaya, M., Pucak, M.L., Mishina, M., Calabresi, P.A., Bergles, D.E., 2011. NMDA receptor signaling in oligodendrocyte progenitors is not required for oligodendrogenesis and myelination. J Neurosci 31, 12650–12662.

De Biase, L.M., Nishiyama, A., Bergles, D.E., 2010. Excitability and Synaptic Communication within the Oligodendrocyte Lineage. J Neurosci 30, 3600–3611.

Demerens, C., Stankoff, B., Logak, M., Anglade, P., Allinquant, B., Couraud, F., Zalc, B., Lubetzki, C., 1996. Induction of myelination in the central nervous system by electrical activity. Neurobiology 93, 9887–9892.

Deng, W., Wang, H., Rosenberg, P.A., Volpe, J.J., Jensen, F.E., 2004. Role of metabotropic glutamate receptors in oligodendrocyte excitotoxicity and oxidative stress. PNAS 101, 7751–7756.

Driever, W., Solnica-Krezel, L., Schier, A.F., Neuhauss, S.C.F., Malicki, J., Stemple, D.L., Stainier, D.Y.R., Zwartkruis, F., Abdelilah, S., Rangini, Z., Belak, J., Boggs, C., 1996. A genetic screen for mutations affecting embryogenesis in zebrafish. Development 123, 37–46.

Dunn, T.W., Gebhardt, C., Naumann, E.A., Riegler, C., Ahrens, M.B., Engert, F., Del Bene, F., 2016. Neural circuits underlying visually evoked escapes in larval zebrafish. Neuron 89, 613–628.

Early, J.J., Cole, K.L.H., Williamson, J.M., Swire, M., Kamadurai, H., Muskavitch, M., Lyons, D.A., 2018. An automated high-resolution in vivo screen in Zebrafish to identify chemical regulators of myelination. Elife 7, e35136.

Easley-Neal, C., Fierro, J., Buchanan, J., Washbourne, P., 2013. Late recruitment of synapsin to nascent synapses is regulated by Cdk5. Cell Rep. 3, 1199–1212.

Eaton, R.C., Farley, R.D., Kimmel, C.B., Schabtach, E., 1977. Functional development in the Mauthner cell system of embryos and larvae of the zebrafish. J. Neurobiol. 8, 151–172.

Eluvathingal, T.J., Chugani, H.T., Behen, M.E., Juhász, C., Muzik, O., Maqbool, M., Chugani, D.C., Makki, M., 2006. Abnormal brain connectivity in children after early severe socioemotional deprivation: a diffusion tensor imaging study. Pediatrics 117, 2093–2100.

Emery, B., Lu, Q.R., 2015. Transcriptional and epigenetic regulation of oligodendrocyte development and myelination in the central nervous system. Cold Spring Harb. Perspect. Biol. 7, a020461.

Faber, D., Fetcho, J.R., Korn, H., 1989. Neuronal networks underlying the escape response in goldfish: General mplications for motor control. Ann. New York Acad. Sci. 563, 11–33.

Fard, M.K., Van der Meer, F., Sánchez, P., Cantuti-Castelvetri, L., Mandad, S., Jäkel, S., Fornasiero, E.F., Schmitt, S., Ehrlich, M., Starost, L., Kuhlmann, T., Sergiou, C., Schultz, V., Wrzos, C., Brück, W., Urlaub, H., Dimou, L., Stadelmann, C., Simons, M., 2017. BCAS1 expression defines a population of early myelinating oligodendrocytes in multiple sclerosis lesions. Sci. Transl. Med. 9, eaam7816.

Fernandez, P.-A., Tang, D.G., Cheng, L., Prochiantz, A., Mudge, A.W., Raff, M.C., 2000. Evidence that axon-derived neuregulin promotes oligodendrocyte survival in the developing rat optic nerve. Neuron 28, 81–90.

Fetcho, J.R., Faber, D.S., 1988. Identification of motoneurons and interneurons in the spinal network for escapes initiated by the Mauthner cell in goldfish. J Neurosci 8, 4192–4213.

Fetcho, J.R., Higashijima, S., Mclean, D.L., 2008. Zebrafish and motor control over the last decade. Brain Res. Rev. 57, 86–93.

Foran, D.R., Peterson, A.C., 1992. Myelin acquisition in the central nervous system of the mouse revealed by an MBP-Lac Z transgene. J Neurosci 12, 4890–4897.

Ford, M.C., Alexandrova, O., Cossell, L., Stange-Marten, A., Sinclair, J., Kopp-Scheinpflug, C., Pecka, M., Attwell, D., Grothe, B., 2015. Tuning of Ranvier node and internode properties in myelinated axons to adjust action potential timing. Nat. Commun. 6.

Friede, R., Samorajski, T., 1967. Relation between the number of myelin lamellae and axon circumference in fibers of vagus and sciatic nerves of mice. J Comp Neur 130, 223–231.

Fünfschilling, U., Supplie, L.M., Mahad, D., Boretius, S., Saab, A.S., Edgar, J., Brinkmann, B.G., Kassmann, C.M., Tzvetanova, I.D., Möbius, W., Diaz, F., Meijer, D., Suter, U., Hamprecht, B., Sereda, M.W., Moraes, C.T., Frahm, J., Goebbels, S., Nave, K.-A., 2012. Glycolytic oligodendrocytes maintain myelin and long-term axonal integrity. Nature 485, 515–521.

Gahtan, E., O'Malley, D.M.O., 2003. Visually guided injection of identified reticulospinal neurons in zebrafish: a survey of spinal arborization patterns. J. Comp. Neurol. 200, 186–200.

Gahtan, E., Sankrithi, N., Campos, J.B., O'Malley, D.M.O., 2002. Evidence for a widespread brain stem escape network in larval zebrafish. J Neurophysiol 87, 608–614.

Gahtan, E., Tanger, P., Baier, H., 2005. Visual prey capture in larval zebrafish is controlled by identified reticulospinal neurons downstream of the tectum. J Neurosci 25, 9294–9303.

Gao, R., Asano, S.M., Upadhyayula, S., Pisarev, I., Milkie, D.E., Liu, T.-L., Singh, V., Graves, A., Huynh, G.H., Zhao, Y., Bogovic, J., Colonell, J., Ott, C.M., Zugates, C., Tappan, S., Rodriguez, A., Mosaliganti, K.R., Sheu, S.-H., Pasolli, H.A., Pang, S., Xu, S., Megason, S.G., Hess, H., Lippincott-Schwartz, J., Hantman, A., Rubin, G.M., Kirchhausen, T., Saalfeld, S., Aso, Y., Boyden, E.S., Betzig, E., 2019. Cortical column and whole-brain imaging with molecular contrast and nanoscale resolution. Science . 363, eaau8302.

Gau, P., Poon, J., Ufret-Vincenty, C., Snelson, C.D., Gordon, S.E., Raible, D.W., Dhaka, A., 2013. The zebrafish ortholog of TRPV1 is required for heat-induced locomotion. J Neurosci 33, 5249–5260.

Gautier, H.O.B., Evans, K.A., Volbracht, K., James, R., Sitnikov, S., Lundgaard, I., James, F., Lao-Peregrin, C., Reynolds, R., Franklin, R.J.M., Káradóttir, R.T., 2015. Neuronal activity regulates remyelination via glutamate signalling to oligodendrocyte progenitors. Nat. Commun. 6.

Ge, S., Yang, C., Hsu, K., Ming, G., Song, H., 2007. A critical period for enhanced synaptic plasticity in newly generated neurons of the adult brain. Neuron 54, 559–566.

Ge, W.-P., Yang, X.-J., Zhang, Z., Wang, H.-K., Shen, W., Deng, Q.-D., Duan, S., 2006. Long-term potentiation of neuron-glia synapses mediated by Ca-permeable AMPA receptors. Science . 312, 1533–1537.

Geraghty, A.C., Gibson, E.M., Ghanem, R.A., Greene, J.J., Ocampo, A., Goldstein, A.K., Ni, L., Yang, T., Marton, R.M., Pasca, S.P., Greenberg, M.E., Longo, F.M., Monje, M., 2019. Loss of adaptive myelination contributes to Methotrexate chemotherapy-related cognitive impairment. Neuron 103, 1–16.

Gibson, E.M., Purger, D., Mount, C.W., Goldstein, A.K., Lin, G.L., Wood, L.S., Inema, I., Miller, S.E., Bieri, G., Zuchero, J.B., Barres, B.A., Woo, P.J., Vogel, H., Monje, M., 2014. Neuronal activity promotes oligodendrogenesis and adaptive myelination in the mammalian brain. Science . 344, 1252304.

Gimnopoulos, D., Becker, C.G., Ostendorff, H.P., Bach, I., Schachner, M., Becker, T., 2002. Expression of the zebrafish recognition molecule F3/F11/contactin in a subset of differentiating neurons is regulated by cofactors associated with LIM domains. Mech. Dev. 119S, S135–S141.

Givogri, M.I., Costa, R.M., Schonmann, V., Silva, A.J., Campagnoni, A.T., Bongarzone, E.R.,

2002. Central nervous system myelination in mice with deficient expression of Notch1 receptor. J. Neurosci. Res. 67, 309–320.

Goldman, S.A., Kuypers, N.J., 2015. How to make an oligodendrocyte. Development 142, 3983–3995.

Gomez, J.L., Bonaventura, J., Lesniak, W., Mathews, W.B., Sysa-Shah, P., Rodriguez, L.A., Ellis, R.J., Richie, C.T., Harvey, B.K., Dannals, R.F., Pomper, M.G., Bonci, A., Michaelides, M., 2017. Chemogenetics revealed: DREADD occupancy and activation via converted clozapine. Science . 357, 503–507.

Gong, Y., Huang, C., Li, J.Z., Grewe, B.F., Zhang, Y., Eismann, S., Schnitzer, M.J., 2015. High-speed recording of neural spikes in awake mice and flies with a fluorescent voltage sensor. Science . 350, 1361–1366.

Gradinaru, V., Zhang, F., Ramakrishnan, C., Mattis, J., Prakash, R., Diester, I., Goshen, I., Thompson, K.R., Deisseroth, K., 2010. Molecular and cellular approaches for diversifying and extending optogenetics. Cell 141, 154–165.

Granseth, B., Odermatt, B., Royle, S.J., Lagnado, L., 2006. Clathrin-mediated endocytosis is the dominant mechanism of vesicle retrieval at hippocampal synapses. Neuron 51, 773–786.

Gyllensten, L., Malmfors, T., 1963. Myelinization of the optic nerve and its dependence on visual function — a quantitative investigation in mice. J. Embryol. exp. Morph. 11, 255–266.

Haenisch, C., Diekmann, H., Klinger, M., Gennarini, G., Kuwada, J.Y., Stuermer, C.A.O., 2005. The neuronal growth and regeneration associated Cntn1 (F3/F11/Contactin) gene is duplicated in fish: expression during development and retinal axon regeneration. Mol. Cell. Neurosci. 28, 361–374.

Haffter, P., Granato, M., Brand, M., Mullins, M.C., Hammerschmidt, M., Kane, D.A., Odenthal, J., Eeden, F.J.M. Van, Jiang, Y.-J., Heisenberg, C.-P., Kelsh, R.N., Furutani-Seiki, M., Vogelsang, E., Beuchle, D., Schach, U., Fabian, C., Nüsslein-Volhard, C., 1996. The identification of genes with unique and essential functions in the development of the zebrafish , Danio rerio. Development 123, 1–36.

Hale, M.E., Ritter, D.A., Fetcho, J.R., 2001. A confocal study of spinal interneurons in living larval zebrafish. J. Comp. Neurol. 437, 1–16.

Hamilton, N.B., Clarke, L.E., Arancibia-Carcamo, I.L., Kougioumtzidou, E., Matthey, M.,

Káradóttir, R.T., Whiteley, L., Bergersen, L.H., Richardson, W.D., Attwell, D., 2016. Endogenous GABA controls oligodendrocyte lineage cell number, myelination, and CNS Internode Length. Glia 65, 309–321.

Hartline, D.K., Colman, D.R., 2007. Rapid Conduction and the Evolution of Giant Axons and Myelinated Fibers. Curr. Biol. 17, 29–35.

Hasel, P., Dando, O., Jiwaji, Z., Baxter, P., Todd, A.C., Heron, S., Márkus, N.M., McQueen, J., Hampton, D.W., Torvell, M., Tiwari, S.S., McKay, S., Eraso-Pichot, A., Zorzano, A., Masgrau, R., Galea, E., Chandran, S., Wyllie, D.J.A., Simpson, T.I., Hardingham, G.E., 2017. Neurons and neuronal activity control gene expression in astrocytes to regulate their development and metabolism. Nat. Commun. 8, 15132.

Henkel, A.W., Sankaranarayanan, S., 1999. Mechanisms of α-latrotoxin action. Cell Tissue Res. 296, 229–233.

Hensch, T.K., 2005. Critical period plasticity in local cortical circuits. Nat. Rev. Neurosci. 6, 877–888.

Higashijima, S.-I., Schaefer, M., Fetcho, J.R., 2004. Neurotransmitter properties of spinal interneurons in embryonic and larval zebrafish. J. Comp. Neurol. 480, 19–37.

Hildebrand, C., Bowe, C.M., Remahl, I.N., 1994. Myelination and myelin sheath remodelling in normal and pathlogical PNS nerve fibres. Prog. Neurobiol. 43, 85–141.

Hildebrand, C., Hahn, R., 1978. Relation between myelin sheath thickness and axon size in spinal cord white matter of some vertebrate species. J. Neurol. Sci. 38, 421–434.

Hildebrand, C., Remahl, S., Persson, H., Bjartmar, C., 1993. Myelinated nerve fibres in the CNS. Prog. Neurobiol. 40, 319–384.

Hildebrand, D.G.C., Cicconet, M., Torres, R.M., Choi, W., Quan, T.M., Moon, J., Wetzel, A.W., Champion, A.S., Graham, B.J., Randlett, O., Plummer, G.S., Portugues, R., Bianco, I.H., Saalfeld, S., Baden, A.D., Lillaney, K., Burns, R., Vogelstein, J.T., Schier, A.F., Lee, W.-C.A., Jeong, W.-K., Lichtman, J.W., Engert, F., 2017. Whole-brain serial-section electron microscopy in larval zebrafish. Nature 545, 345–349.

Hill, R.A., Li, A.M., Grutzendler, J., 2018. Lifelong cortical myelin plasticity and age-related degeneration in the live mammalian brain. Nat. Neurosci. 21, 683–695.

Hill, R.A., Patel, K.D., Goncalves, C.M., Grutzendler, J., Nishiyama, A., 2014. Modulation of oligodendrocyte generation during a critical temporal window after NG2 cell division. Nat.

Neurosci. 17, 1518–1527.

Hines, J.H., Ravanelli, A.M., Schwindt, R., Scott, E.K., Appel, B., 2015. Neuronal activity biases axon selection for myelination in vivo. Nat. Neurosci. 18, 683–689.

Höne-Zell, B., Ecker, A., Weller, U., Gratzl, M., 1994. Synaptobrevin cleavage by the tetanus toxin light chain is linked to the inhibition of exocytosis in chromaffin cells. FEBS Lett. 355, 131–134.

Huang, B., Wei, W., Wang, G., Gaertig, M.A., Feng, Y., Wang, W., Li, X.-J., Li, S., 2015. Mutant huntingtin downregulates myelin regulatory factor-mediated myelin gene expression and affects mature oligodendrocytes. Neuron 85, 1212–1226.

Huang, E.J., Reichardt, L.F., 2001. Neurotrophins: roles in neuronal development and function. Annu. Rev. Neurosci. 24, 677–736.

Hubbard, J.M., Böhm, U.L., Prendergast, A., Tseng, P.-E.B., Newman, M., Stokes, C., Wyart, C., 2016. Intraspinal sensory neurons provide powerful inhibition to motor circuits ensuring postural control during locomotion. Curr. Biol. 26, 2841–2853.

Huff, J., 2015. The Airyscan detector from ZEISS: confocal imaging with improved signal-to-noise ratio and super-resolution. Nat. Methods 12, i–ii.

Hughes, E.G., Kang, S.H., Fukaya, M., Bergles, D.E., 2013. Oligodendrocyte progenitors balance growth with self-repulsion to achieve homeostasis in the adult brain. Nat. Neurosci. 16, 668–676.

Hughes, E.G., Orthmann-Murphy, J.L., Langseth, A.J., Bergles, D.E., 2018. Myelin remodeling through experience-dependent oligodendrogenesis in the adult somatosensory cortex. Nat. Neurosci. 21, 696–706.

Ibrahim, M., Butt, A.M., Berry, M., 1995. Relationship between myelin sheath diameter and internodal length in axons of the anterior medullary velum of the adult rat. J. Neurol. Sci. 119–127.

Imamura, H., Huynh Nhat, K.P., Togawa, H., Saito, K., Iino, R., Kato-Yamada, Y., Nagai, T., Noji, H., 2009. Visualization of ATP levels inside single living cells with fluorescence resonance energy transfer-based. PNAS 106, 15651–15656.

Ioannidou, K., Anderson, K.I., Strachan, D., Edgar, J.M., Barnett, S.C., 2012. Time-lapse imaging of the dynamics of CNS glial-axonal interactions in vitro and ex vivo. PLoS One 7, e30775.

Irvine, K.A., Blakemore, W.F., 2008. Remyelination protects axons from demyelination-associated axon degeneration. Brain 131, 1464–1477.

Ishibashi, T., Dakin, K.A., Stevens, B., Lee, P.R., Kozlov, S. V., Stewart, C.L., Fields, R.D., 2006. Astrocytes promote myelination in response to electrical impulses. Neuron 49, 823–832.

Jäkel, S., Agirre, E., Falcão, A.M., Bruggen, D. Van, Lee, K.W., Knuesel, I., Malhotra, D., Ffrench-Constant, C., Williams, A., Castelo-Branco, G., 2019. Altered human oligodendrocyte heterogeneity in multiple sclerosis. Nature 566, 543–547.

Jensen, S.K., Michaels, N.J., Ilyntskyy, S., Keough, M.B., Kovalchuk, O., Yong, V.W., 2018. Multimodal enhancement of remyelination by exercise with a pivotal role for oligodendroglial PGC1α. Cell Rep. 24, 3167–3179.

Jensen, S.K., Yong, V.W., 2016. Activity-dependent and experience-driven myelination provide new directions for the management of Multiple Sclerosis. Trends Neurosci. 39, 356–365.

Jontes, J.D., Buchanan, J., Smith, S.J., 2000. Growth cone and dendrite dynamics in zebrafish embryos: early events in synaptogenesis imaged in vivo. Nat. Neurosci. 3, 231–237.

Kakulas, B.A., 1999. A review of the neuropathology of human spinal cord injury with emphasis on special features. J. Spinal Cord Med. 22, 119–124.

Kang, S.H., Li, Y., Fukaya, M., Lorenzini, I., Cleveland, D.W., Ostrow, L.W., Rothstein, J.D., Bergles, D.E., 2013. Degeneration and impaired regeneration of gray matter oligodendrocytes in amyotrophic lateral sclerosis. Nat. Neurosci. 16, 571–579.

Káradóttir, R., Cavelier, P., Bergersen, L.H., Attwell, D., 2005. NMDA receptors are expressed in oligodendrocytes and activated in ischaemia. Nature 438, 1162–1166.

Káradóttir, R., Hamilton, N.B., Bakiri, Y., Attwell, D., 2008. Spiking and nonspiking classes of oligodendrocyte precursor glia in CNS white matter. Nat. Neurosci. 11, 450–456.

Karttunen, M.J., Czopka, T., Goedhart, M., Early, J.J., Lyons, D.A., 2017. Regeneration of myelin sheaths of normal length and thickness in the zebrafish CNS correlates with growth of axons in caliber. PLoS One 12, 1–27.

Kim, D.H., Kim, J., Marques, J.C., Grama, A., Hildebrand, D.G.C., Gu, W., Li, J.M., Robson, D.N., 2017. Pan-neuronal calcium imaging with cellular resolution in freely swimming zebrafish. Nat. Methods 14, 1107–1114.

Kimmel, C.B., 1989. Genetics and early development of zebrafish. Trends Genet. 5, 283–288.

Kimmel, C.B., Powell, S.L., Metcalfe, W.K., 1982. Brain neurons which project to the spinal cord in young larvae of the zebrafish. J. Comp. Neurol. 127, 112–127.

Kirby, B.B., Takada, N., Latimer, A.J., Shin, J., Carney, T.J., Kelsh, R.N., Appel, B., 2006. In vivo time-lapse imaging shows dynamic oligodendrocyte progenitor behavior during zebrafish development. Nat. Neurosci. 9, 1506–1511.

Knobler, R.L., Stempak, J.G., Laurencin, M., 1974. Oligodendroglial ensheathment of axons during myelination in the developing rat central nervous system. A serial section electron microscopical study. J. Ultrastruct. Res. 49, 34–49.

Knogler, L.D., Drapeau, P., 2014. Sensory gating of an embryonic zebrafish interneuron during spontaneous motor behaviors. Front. Neural Circuits 8, 1–16.

Knopf, F., Schnabel, K., Haase, C., Pfeifer, K., Anastassiadis, K., Weidinger, G., 2010. Dually inducible TetON systems for tissue-specific conditional gene expression in zebrafish. PNAS 107, 19933–19938.

Koudelka, S., Voas, M.G., Almeida, R.G., Baraban, M., Soetaert, J., Meyer, M.P., Talbot, W.S., Lyons, D.A., 2016. Individual neuronal subtypes exhibit diversity in CNS myelination mediated by synaptic vesicle release. Curr. Biol. 26, 1447–1455.

Kougioumtzidou, E., Shimizu, T., Hamilton, N.B., Tohyama, K., Sprengel, R., Monyer, H., Attwell, D., Richardson, W.D., 2017. Signalling through AMPA receptors on oligodendrocyte precursors promotes myelination by enhancing oligodendrocyte survival. Elife 6, e28080.

Krasnow, A.M., Ford, M.C., Valdivia, L.E., Wilson, S.W., Attwell, D., 2018. Regulation of developing myelin sheath elongation by oligodendrocyte calcium transients in vivo. Nat. Neurosci. 21, 24–28.

Kucenas, S., Snell, H., Appel, B., 2008. Nkx2.2a promotes specification and differentiation of a myelinating subset of oligodendrocyte lineage cells in zebrafish. Neuron Glia Biol. 4, 71–81.

Kukley, M., Capetillo-Zarate, E., Dietrich, D., 2007. Vesicular glutamate release from axons in white matter. Nat. Neurosci. 10, 311–320.

Kukley, M., Nishiyama, A., Dietrich, D., 2010. The fate of synaptic input to NG2 glial cells: neurons specifically downregulate transmitter release onto differentiating

oligodendroglial cells. J Neurosci 30, 8320–8331.

Kunst, M., Laurell, E., Mokayes, N., Kramer, A., Kubo, F., Fernandes, A.M., Förster, D., Maschio, M.D., Baier, H., 2019. A cellular-resolution atlas of the larval zebrafish brain. Neuron 103, 21–38.

Kwan, K.M., Fujimoto, E., Grabher, C., Mangum, B.D., Hardy, M.E., Campbell, D.S., Parant, J.M., Yost, H.J., Kanki, J.P., Chien, C.-B., 2007. The Tol2kit: A multisite gateway-based construction kit for Tol2 transposon transgenesis constructs. Dev. Dyn. 236, 3088–3099.

Kwon, J., Kim, M., Park, H., Kang, B.-M., Jo, Y., Kim, J.-H., James, O., Yun, S.-H., Kim, S.-G., Suh, M., Choi, M., 2017. Label-free nanoscale optical metrology on myelinated axons in vivo. Nat. Commun. 8.

Lam, S.S., Martell, J.D., Kamer, K.J., Deerinck, T.J., Ellisman, M.H., Mootha, V.K., Ting, A.Y., 2015. Directed evolution of APEX2 for electron microscopy and proximity labeling. Nat. Methods 12, 51–54.

Lappe-Siefke, C., Goebbels, S., Gravel, M., Nicksch, E., Lee, J., Braun, P.E., Griffiths, I.R., Nave, K.-A., 2003. Disruption of Cnp1 uncouples oligodendroglial functions in axonal support and myelination. Nat. Genet. 33, 366–374.

Larson, V.A., Mironova, Y., Vanderpool, K.G., Waisman, A., Rash, J.E., Agarwal, A., Bergles, D.E., 2018. Oligodendrocytes control potassium accumulation in white matter and seizure susceptibility. Elife 7.

Lasiene, J., Shupe, L., Perlmutter, S., Horner, P., 2008. No evidence for chronic demyelination in spared axons after spinal cord injury in a mouse. J Neurosci 28, 3887–3896.

Lebel, C., Beaulieu, C., 2011. Longitudinal development of human brain wiring continues from childhood into adulthood. J Neurosci 31, 10937–10947.

Lee, S., Leach, M.K., Redmond, S.A., Chong, S.Y.C., Mellon, S.H., Tuck, S.J., Feng, Z.-Q., Corey, J.M., Chan, J.R., 2012. A culture system to study oligodendrocyte myelination processes using engineered nanofibers. Nat. Methods 9, 917–922.

Lee, X., Yang, Z., Shao, Z., Rosenberg, S.S., Levesque, M., Pepinsky, R.B., Qiu, M., Miller, R.H., Chan, J.R., Mi, S., 2007. NGF regulates the expression of axonal LINGO-1 to inhibit oligodendrocyte differentiation and myelination. J Neurosci 27, 220–225.

Lee, Y., Morrison, B.M., Li, Y., Lengacher, S., Farah, M.H., Hoffman, P.N., Liu, Y., Tsingalia, A., Jin, L., Zhang, P.-W., Pellerin, L., Magistretti, P.J., Rothstein, J.D., 2012.

Oligodendroglia metabolically support axons and contribute to neurodegeneration. Nature 487, 443–448.

Li, Q., Brus-Ramer, M., Martin, J.H., Mcdonald, J.W., 2010. Electrical stimulation of the medullary pyramid promotes proliferation and differentiation of oligodendrocyte progenitor cells in the corticospinal tract of the adult rat. Neurosci. Lett. 479, 128–133.

Ligon, K.L., Fancy, S.P.J., Franklin, R.J.M., Rowitch, D.H., 2006. Olig gene function in CNS development and disease. Glia 54, 1–10.

Lim, H., Sharoukhov, D., Kassim, I., Zhang, Y., Salzer, J.L., Melendez-Vasquez, C. V, 2014. Label-free imaging of Schwann cell myelination by third harmonic generation microscopy. PNAS 111, 18025–18030.

Lin, S., Bergles, D.E., 2004. Synaptic signaling between GABAergic interneurons and oligodendrocyte precursor cells in the hippocampus. Nat. Neurosci. 7, 24–32.

Linneberg, C., Harboe, M., Laursen, L.S., 2015. Axo-glia interaction preceding CNS myelination is regulated by bidirectional Eph-Ephrin signalling. ASN Neuro 1–17.

Lister, J.A., Robertson, C.P., Lepage, T., Johnson, S.L., Raible, D.W., 1999. Nacre encodes a zebrafish microphthalmia-related protein that regulates neural-crest-derived pigment cell fate. Development 126, 3757–67.

Liu, J., Dietz, K., DeLoyht, J.M., Pedre, X., Kelkar, D., Kaur, J., Vialou, V., Lobo, M.K., Dietz, D.M., Nestler, E.J., Dupree, J., Casaccia, P., 2012. Impaired adult myelination in the prefrontal cortex of socially isolated mice. Nat. Neurosci. 15, 1621–1623.

Liu, J., Dupree, J.L., Gacias, M., Frawley, R., Sikder, T., Naik, P., Casaccia, P., 2016. Clemastine enhances myelination in the prefrontal cortex and rescues behavioral changes in socially isolated mice. J. Neurosci. 36, 957–962.

Liu, K.S., Fetcho, J.R., 1999. Laser ablations reveal functional relationships of segmental hindbrain neurons in zebrafish. Neuron 23, 325–335.

Lu, Q.R., Yuk, D., Alberta, J.A., Zhu, Z., Pawlitzky, I., Chan, J., McMahon, A.P., Stiles, C.D., Rowitch, D.H., 2000. Sonic Hedgehog–regulated oligodendrocyte lineage genes encoding bHLH proteins in the mammalian central nervous system. Neuron 25, 317–329.

Lucchinetti, C., Brück, W., Parisi, J., Scheithauer, B., Rodriguez, M., Lassmann, H., 1999. A quantitative analysis of oligodendrocytes in multiple sclerosis lesions: A study of 113

cases. Brain 122, 2279–2295.

Lundgaard, I., Luzhynskaya, A., Stockley, J.H., Wang, Z., Evans, K.A., Swire, M., Volbracht, K., Gautier, H.O.B., Franklin, R.J.M., Ffrench-Constant, C., Attwell, D., Káradóttir, R.T., 2013. Neuregulin and BDNF induce a switch to NMDA receptor-dependent myelination by oligodendrocytes. PLoS Biol. 11, e1001743.

Luyt, K., Varadi, A., Molnar, E., 2003. Functional metabotropic glutamate receptors are expressed in oligodendrocyte progenitor cells. J. Neurochem. 84, 1452–1464.

Lyons, D.A., Pogoda, H.-M., Voas, M.G., Woods, I.G., Diamond, B., Nix, R., Arana, N., Jacobs, J., Talbot, W.S., 2005. erbb3 and erbb2 are essential for Schwann cell migration and myelination in zebrafish. Curr. Biol. 15, 513–524.

Mabbott, D.J., Noseworthy, M., Bouffet, E., Laughlin, S., Rockel, C., 2006. White matter growth as a mechanism of cognitive development in children. Neuroimage 33, 936–946.

Makinodan, M., Rosen, K.M., Ito, S., Corfas, G., 2012. A critical period for social experience–dependent oligodendrocyte maturation and myelination. Science . 337, 1357–1360.

Malone, M., Gary, D., Yang, I.H., Miglioretti, A., Houdayer, T., Thakor, N., Mcdonald, J., 2013. Neuronal activity promotes myelination via a cAMP pathway. Glia 61, 843–854.

Mangin, J.-M., Kunze, A., Chittajallu, R., Gallo, V., 2008. Satellite NG2 progenitor cells share common glutamatergic inputs with associated interneurons in the mouse dentate gyrus. J Neurosci 28, 7610–7623.

Marques, S., Zeisel, A., Codeluppi, S., Bruggen, D. Van, Falcão, A.M., Xiao, L., Li, H., Häring, M., Hochgerner, H., Romanov, R.A., Gyllborg, D., Muñoz-Manchado, A.B., Manno, G. La, Lönnerberg, P., Floriddia, E.M., Rezayee, F., Ernfors, P., Arenas, E., Hjerling-Leffler, J., Harkany, T., Richardson, W.D., Linnarsson, S., Castelo-Branco, G., 2016. Oligodendrocyte heterogeneity in the mouse juvenile and adult central nervous system. Science . 352, 1326–1329.

Marvin, J.S., Borghuis, B.G., Tian, L., Cichon, J., Harnett, M.T., Akerboom, J., Gordus, A., Renninger, S.L., Chen, T.-W., Bargmann, C.I., Orger, M.B., Schreiter, E.R., Demb, J.B., Gan, W.-B., Hires, S.A., Looger, L.L., 2013. An optimized fluorescent probe for visualizing glutamate neurotransmission. Nat. Methods 10, 162–170.

Marvin, J.S., Scholl, B., Wilson, D.E., Podgorski, K., Kazemipour, A., Müller, J.A., Schoch, S., Quiroz, F.J.U., Rebola, N., Bao, H., Little, J.P., Tkachuk, A.N., Cai, E., Hantman, A.W., Wang, S.S., DePiero, V.J., Borghuis, B.G., Chapman, E.R., Dietrich, D., DiGregorio,

D.A., Fitzpatrick, D., Looger, L.L., 2018. Stability, affinity, and chromatic variants of the glutamate sensor iGluSnFR. Nat. Methods 15, 936–939.

Matsuda, N., Lu, H., Fukata, Y., Noritake, J., Gao, H., Mukherjee, S., Nemoto, T., Fukata, M., Poo, M., 2009. Differential activity-dependent secretion of brain-derived neurotrophic factor from axon and dendrite. J Neurosci 29, 14185–14198.

McKenzie, I.A., Ohayon, D., Li, H., Paes de Faria, J., Emery, B., Tohyama, K., Richardson, W.D., 2014. Motor skill learning requires active central myelination. Science . 346, 318–322.

Mei, F., Fancy, S.P.J., Shen, Y.-A.A., Niu, J., Zhao, C., Presley, B., Miao, E., Lee, S., Mayoral, S.R., Redmond, S.A., Etxeberria, A., Xiao, L., Franklin, R.J.M., Green, A., Hauser, S.L., Chan, J.R., 2014. Micropillar arrays as a high-throughput screening platform for therapeutics in multiple sclerosis. Nat. Med. 20, 954–60.

Mei, F., Lehmann-Horn, K., Shen, Y.-A.A., Rankin, K.A., Stebbins, K.J., Lorrain, D.S., Pekarek, K., Sagan, S.A., Xiao, L., Teuscher, C., von Büdingen, H.-C., Wess, J., Lawrence, J.J., Green, A.J., Fancy, S.P., Zamvil, S.S., Chan, J.R., 2016. Accelerated remyelination during inflammatory demyelination prevents axonal loss and improves functional recovery. Elife 5, 1–21.

Mendelson, B., 1986a. Development of reticulospinal neurons of the zebrafish. I. time of origin. J. Comp. Neurol. 251, 160–171.

Mendelson, B., 1986b. Development of reticulospinal neurons of the zebrafish. II. early axonal outgrowth and cell body position. J. Comp. Neurol. 251, 172–184.

Mensch, S., 2014. Investigating axon-oligodendrocyte interactions during myelinated axon formation in vivo. University of Edinburgh.

Mensch, S., Baraban, M., Almeida, R., Czopka, T., Ausborn, J., El Manira, A., Lyons, D.A., 2015. Synaptic vesicle release regulates myelin sheath number of individual oligodendrocytes in vivo. Nat. Neurosci. 18, 628–630.

Metcalfe, W.K., Mendelson, B., Kimmel, C.B., 1986. Segmental homologies among reticulospinal neurons in the hindbrain of the zebrafish larva. J. Comp. Neurol. 251, 147–159.

Michailov, G. V, Sereda, M.W., Brinkmann, B.G., Fischer, T.M., Haug, B., Birchmeier, C., Role, L., Lai, C., Schwab, M.H., Nave, K.-A., 2004. Axonal neuregulin-1 regulates myelin sheath thickness. Science . 304, 700–704.

Micheva, K.D., Wolman, D., Mensh, B.D., Pax, E., Buchanan, J., Smith, S.J., Bock, D.D., 2016. A large fraction of neocortical myelin ensheathes axons of local inhibitory neurons. Elife 5, e15784.

Mitew, S., Gobius, I., Fenlon, L.R., McDougall, S.J., Hawkes, D., Xing, Y.L., Bujalka, H., Gundlach, A.L., Richards, L.J., Kilpatrick, T.J., Merson, T.D., Emery, B., 2018. Pharmacogenetic stimulation of neuronal activity increases myelination in an axon-specific manner. Nat. Commun. 9.

Möbius, W., Cooper, B., Kaufmann, W.A., Imig, C., Ruhwedel, T., Snaidero, N., Saab, A.S., Varoqueax, F., 2010. Electron microscopy of the mouse central nervous system. In: Methods in Cell Biology. pp. 475–512.

Möbius, W., Nave, K.-A., Werner, H.B., 2016. Electron microscopy of myelin: Structure preservation by high-pressure freezing. Brain Res. 1641, 92–100.

Monk, K.R., Oshima, K., Jörs, S., Heller, S., Talbot, W.S., 2011. Gpr126 is essential for peripheral nerve development and myelination in mammals. Development 138, 2673–2680.

Monk, K.R., Talbot, W.S., 2009. Genetic dissection of myelinated axons in zebrafish. Curr. Opin. Neurobiol. 19, 486–490.

Mount, C.W., Monje, M., 2017. Wrapped to adapt: experience-dependent myelination. Neuron 95, 743–756.

Mu, Y., Bennett, D. V, Rubinov, M., Narayan, S., Yang, C.-T., Tanimoto, M., Mensh, B.D., Looger, L.L., Ahrens, M.B., 2019. Glia accumulate evidence that actions are futile and suppress unsuccessful behavior. Cell 178, 27–43.

Munns, C.H., Chung, M.-K., Sanchez, Y.E., Amzel, L.M., Caterina, M.J., 2015. Role of the outer pore domain in transient receptor potential vanilloid 1 dynamic permeability to large cations. J. Biol. Chem. 290, 5707–5724.

Murray, J.A., Blakemore, W.F., 1980. The relationship between internodal length and fibre diameter in the spinal cord of the cat. J. Neurol. Sci. 45, 29–41.

Muto, A., Kawakami, K., 2013. Prey capture in zebrafish larvae serves as a model to study cognitive functions. Front. Neural Circuits 7.

Nagy, B., Hovhannisyan, A., Barzan, R., Chen, T.-J., Kukley, M., 2017. Different patterns of neuronal activity trigger distinct responses of oligodendrocyte precursor cells in the

corpus callosum. PLoS Biol. 15.

Nagy, Z., Westerberg, H., Klingberg, T., 2004. Maturation of white matter is associated with the development of cognitive functions during childhood. J. Cogn. Neurosci. 16, 1227–1233.

Nakai, J., Ohkura, M., Imoto, K., 2001. A high signal-to-noise Ca2+ probe composed of a single green fluorescent protein. Nat. Biotechnol. 3, 137–141.

Narahashi, T., Scott, W.R., 1964. Tetrodotoxin blockage of sodium conductance increase in lobster giant axons. J. Gen. Physiol. 47, 965–974.

Nasrabady, S.E., Rizvi, B., Goldman, J.E., Brickman, A.M., 2018. White matter changes in Alzheimer's disease: a focus on myelin and oligodendrocytes. Acta Neuropathol. Commun. 6, 1–10.

Nawaz, S., Sánchez, P., Schmitt, S., Snaidero, N., Mitkovski, M., Velte, C., Brückner, B.R., Alexopoulos, I., Czopka, T., Jung, S.Y., Rhee, J.S., Janshoff, A., Witke, W., Schaap, I.A.T., Lyons, D.A., Simons, M., 2015. Actin filament turnover drives leading edge growth during myelin sheath formation in the Central Nervous System. Dev. Cell 34, 1–13.

Newcombe, J., Hawkins, C.P., Henderson, C.L., Patel, H.A., Woodroofe, M.N., Hayes, G.M., Cuzner, M.L., MacManus, D., Du Boulay, E.P.G.H., Mcdonald, W.I., 1991. Histopathology of Multiple Sclerosis lesions detected by magnetic resonance imaging in unfixed post-mortem central nervous system tissue. Brain 114, 1013–1023.

O'Malley, D.M., Kao, Y.-H., Fetcho, J.R., 1996. Imaging the functional organization of zebrafish hindbrain segments during escape behaviors. Neuron 17, 1145–1155.

Orentas, D.M., Hayes, J.E., Dyer, K.L., Miller, R.H., 1999. Sonic hedgehog signaling is required during the appearance of spinal cord oligodendrocyte precursors. Development 126, 2419–2429.

Orger, M.B., Kampff, A.R., Severi, K.E., Bollmann, J.H., Engert, F., 2008. Control of visually guided behavior by distinct populations of spinal projection neurons. Nat. Neurosci. 11, 327–333.

Ortega, M.C., Bribián, A., Peregrín, S., Gil, M.T., Marín, O., de Castro, F., 2012. Neuregulin-1/ErbB4 signaling controls the migration of oligodendrocyte precursor cells during development. Exp. Neurol. 235, 610–620.

Ortiz, F.C., Habermacher, C., Graciarena, M., Houry, P.-Y., Nishiyama, A., Oumesmar, B.N.,

Angulo, M.C., 2019. Neuronal activity in vivo enhances functional myelin repair. JCI Insight 4, e123434.

Ouzounov, D.G., Wang, T., Wang, M., Feng, D.D., Horton, N.G., Cruz-Hernández, J.C., Cheng, Y.-T., Reimer, J., Tolias, A.S., Nishimura, N., Xu, C., 2017. In vivo three-photon imaging of activity of GCaMP6-labeled neurons deep in intact mouse brain. Nat. Methods 14, 388–390.

Pajevic, S., Basser, P.J., Fields, R.D., 2014. Role of myelin plasticity in oscillations and synchrony of neuronal activity. Neuroscience 276, 135–147.

Park, H.-C., Mehta, A., Richardson, J.S., Appel, B., 2002. olig2 is required for zebrafish primary motor neuron and oligodendrocyte development. Dev. Biol. 248, 356–368.

Park, H.-C., Shin, J., Appel, B., 2004. Spatial and temporal regulation of ventral spinal cord precursor specification by Hedgehog signaling. Development 131, 5959–5969.

Park, H., Poo, M.-M., 2013. Neurotrophin regulation of neural circuit development and function. Nat. Rev. Neurosci. 14, 7–23.

Patneau, D.K., Wright, P.W., Winters, C., Mayer, M.L., Gallo, V., 1994. Glial cells of the oligodendrocyte lineage express both kainate- and AMPA-preferring subtypes of glutamate receptor. Neuron 12, 357–371.

Philips, T., Bento-Abreu, A., Nonneman, A., Haeck, W., Staats, K., Geelen, V., Hersmus, N., Küsters, B., Van Den Bosch, L., Van Damme, P., Richardson, W.D., Robberecht, W., 2013. Oligodendrocyte dysfunction in the pathogenesis of amyotrophic lateral sclerosis. Brain 136, 471–482.

Pietri, T., Manalo, E., Ryan, J., Saint-Amant, L., Washbourne, P., 2009. Glutamate drives the touch response through a rostral loop in the spinal cord of zebrafish embryos. Dev. Neurobiol. 69, 780–795.

Pogoda, H.-M., Sternheim, N., Lyons, D.A., Diamond, B., Hawkins, T.A., Woods, I.G., Bhatt, D.H., Franzini-Armstrong, C., Dominguez, C., Arana, N., Jacobs, J., Nix, R., Fetcho, J.R., Talbot, W.S., 2006. A genetic screen identifies genes essential for development of myelinated axons in zebrafish. Dev. Biol. 298, 118–131.

Postlethwait, J.H., Woods, I.G., Ngo-Hazelett, P., Yan, Y.-L., Kelly, P.D., Chu, F., Huang, H., Hill-Force, A., Talbot, W.S., 2000. Zebrafish comparative genomics and the origins of vertebrate chromosomes. Genome Res. 10, 1890–1902.

Prineas, J.W., Barnard, R.O., Kwon, E.E., Sharer, L.R., Cho, E.S., 1993. Multiple Sclerosis: remyelination of nascent lesions. Ann. Neurol. 33, 137–151.

Prineas, J.W., Connell, F., 1979. Remyelination in Multiple Sclerosis. Ann. Neurol. 5, 22–31.

Pujol, J., Ortiz, H., Sebastián-Gallés, N., Losilla, J.M., Dues, J., 2006. Myelination of language-related areas in the developing brain. Neurology 66, 339–343.

Rasband, M.N., Peles, E., 2016. The nodes of Ranvier: molecular assembly and maintenance. Cold Spring Harb. Perspect. Biol. 8, a020495.

Redmond, S.A., Mei, F., Eshed-Eisenbach, Y., Osso, L.A., Leshkowitz, D., Shen, Y.-A.A., Kay, J.N., Aurrand-Lions, M., Lyons, D.A., Peles, E., Chan, J.R., 2016. Somatodendritic expression of JAM2 inhibits oligodendrocyte myelination. Neuron 91, 824–836.

Remahl, S., Hildebrand, C., 1990. Relations between axons and oligodendroglial cells during initial myelination. II . The individual axon. J. Neurocytol. 19, 883–898.

Richardson, W.D., Kessaris, N., Pringle, N., 2006. Oligodendrocyte wars. Nat. Rev. Neurosci. 7, 11–18.

Ritchie, S.J., Bastin, M.E., Tucker-Drob, E.M., Maniega, S.M., Engelhardt, L.E., Cox, S.R., Royle, N.A., Gow, A.J., Corley, J., Pattie, A., Taylor, A.M., del C Valdés Hernández, M., Starr, J.M., Wardlaw, J.M., Deary, I.J., 2015. Coupled changes in brain white matter microstructure and fluid intelligence in later life. J Neurosci 35, 8672–8682.

Rivers, L.E., Young, K.M., Rizzi, M., Jamen, F., Psachoulia, K., Wade, A., Kessaris, N., Richardson, W.D., 2008. PDGFRA/NG2 glia generate myelinating oligodendrocytes and piriform projection neurons in adult mice. Nat. Neurosci. 11, 1392–1401.

Roberts, M.T., Seeman, S.C., Golding, N.L., 2013. A mechanistic understanding of the role of feedforward inhibition in the mammalian sound localization circuitry. Neuron 78, 923–935.

Rossi, A., Kontarakis, Z., Gerri, C., Nolte, H., Hölper, S., Krüger, M., Stainier, D.Y.R., 2015. Genetic compensation induced by deleterious mutations but not gene knockdowns. Nature 524, 230–233.

Rowitch, D.H., 2004. Glial specification in the vertebrate neural tube. Nat. Rev. Neurosci. 5, 409–419.

Roy, K., Murtie, J.C., El-Khodor, B.F., Edgar, N., Sardi, S.P., Hooks, B.M., Benoit-Marand, M.,

Chen, C., Moore, H., O'Donnell, P., Brunner, D., Corfas, G., 2007. Loss of erbB signaling in oligodendrocytes alters myelin and dopaminergic function, a potential mechanism for neuropsychiatric disorders. PNAS 104, 8131–8136.

Saab, A.S., Tzvetavona, I.D., Trevisiol, A., Baltan, S., Dibaj, P., Kusch, K., Möbius, W., Goetze, B., Jahn, H.M., Huang, W., Steffens, H., Schomburg, E.D., Pérez-Samartín, A., Pérez-Cerdá, F., Bakhtiari, D., Matute, C., Löwel, S., Griesinger, C., Hirrlinger, J., Kirchhoff, F., Nave, K.-A., 2016. Oligodendroglial NMDA receptors regulate glucose import and axonal energy metabolism. Neuron 91, 119–132.

Sachdev, P.S., Zhuang, L., Braidy, N., Wen, W., 2013. Is Alzheimer's a disease of the white matter? Curr. Opin. Psychiatry 26, 244–251.

Salter, M.G., Fern, R., 2005. NMDA receptors are expressed in developing oligodendrocyte processes and mediate injury. Nature 438, 1167–1171.

Salzer, J.L., 2003. Polarised domains of myelinated axons. Neuron 40, 297–318.

Sampaio-Baptista, C., Khrapitchev, A.A., Foxley, S., Schlagheck, T., Scholz, J., Jbabdi, S., DeLuca, G.C., Miller, K.L., Taylor, A., Thomas, N., Kleim, J., Sibson, N.R., Bannerman, D., Johansen-Berg, H., 2013. Motor skill learning induces changes in white matter microstructure and myelination. J Neurosci 33, 19499–19503.

Sander, J.D., Joung, J.K., 2014. CRISPR-Cas systems for editing, regulating and targeting genomes. Nat. Biotechnol. 32, 347–355.

Schain, A.J., Hill, R.A., Grutzendler, J., 2014. Label-free in vivo imaging of myelinated axons in health and disease with spectral confocal reflectance microscopy. Nat. Med. 20, 443–449.

Scheer, N., Campos-Ortega, J.A., 1999. Use of the Gal4-UAS technique for targeted gene expression in the zebrafish. Mech. Dev. 80, 153–158.

Schiffmann, R., Knaap, M.S. Van Der, 2004. The latest on leukodystrophies. Curr. Opin. Neurol. 17, 187–192.

Schirmer, L., Möbius, W., Zhao, C., Cruz-Herranz, A., Haim, L. Ben, Cordano, C., Shiow, L.R., Kelley, K.W., Sadowski, B., Timmons, G., Probstel, A.-K., Wright, J.N., Sin, J.H., Devereux, M., Morrison, D.E., Chang, S.M., Sabeur, K., Green, A.J., Nave, K.-A., Franklin, R.J.M., Rowitch, D.H., 2018. Oligodendrocyte-encoded Kir4.1 function is required for axonal integrity. Elife 7, e36428.

Schlegel, A.A., Rudelson, J.J., Tse, P.U., 2012. White matter structure changes as adults learn a second language. J. Cogn. Neurosci. 24, 1664–1670.

Scholz, J., Klein, M.C., Behrens, T.E.J., Johansen-Berg, H., 2009. Training induces changes in white-matter architecture. Nat. Neurosci. 12, 1370–1371.

Schweitzer, J., Becker, T., Schachner, M., Nave, K.-A., Werner, H., 2006. Evolution of myelin proteolipid proteins: gene duplication in teleosts and expression pattern divergence. Mol. Cell. Neurosci. 31, 161–177.

Seidl, A.H., Rubel, E.W., Barria, A., 2014. Differential conduction velocity regulation in ipsilateral and contralateral collaterals innervating brainstem coincidence detector neurons. J Neurosci 34, 4914–4919.

Seidl, A.H., Rubel, E.W., Harris, D.M., 2010. Mechanisms for adjusting interaural time differences to achieve binaural coincidence detection. J Neurosci 30, 70–80.

Shimojo, M., Courchet, J., Pieraut, S., Torabi-Rander, N., Sando, R., Polleux, F., Maximov, A., 2015. SNAREs controlling vesicular release of BDNF and development of callosal axons. Cell Rep. 11, 1054–1066.

Shu, X., Lev-Ram, V., Deerinck, T.J., Qi, Y., Ramko, E.B., Davidson, M.W., Jin, Y., Ellisman, M.H., Tsien, R.Y., 2011. A genetically encoded tag for correlated light and electron microscopy of intact cells, tissues, and organisms. PLoS Biol. 9, e1001041.

Silva, N.A., Sousa, N., Reis, R.L., Salgado, A.J., 2014. From basics to clinical: A comprehensive review on spinal cord injury. Prog. Neurobiol. 114, 25–57.

Simpson, A.H., Gillingwater, T.H., Anderson, H., Cottrell, D., Sherman, D.L., Ribchester, R.R., Brophy, P.J., 2013. Effect of limb lengthening on internodal length and conduction velocity of peripheral nerve. J Neurosci 33, 4536–4539.

Sinclair, J.L., Fischl, M.J., Alexandrova, O., Heb, M., Grothe, B., Leibold, C., Kopp-Scheinpflug, C., 2017. Sound-evoked activity influences myelination of brainstem axons in the trapezoid body. J Neurosci 37, 8239–8255.

Smith, K.J., Blakemore, W.F., Mcdonald, W.I., 1981. The restoration of conduction by central remyelination. Brain 104, 383–404.

Snaidero, N., Möbius, W., Czopka, T., Hekking, L.H.P., Mathisen, C., Verkleij, D., Goebbels, S., Edgar, J., Merkler, D., Lyons, D.A., Nave, K.-A., Simons, M., 2014. Myelin membrane wrapping of CNS axons by PI(3,4,5)P3-dependent polarized growth at the inner tongue.

Cell 156, 277–290.

Snaidero, N., Simons, M., 2014. Myelination at a glance. J. Cell Sci. 127, 2999–3004.

Snaidero, N., Simons, M., 2017. The Logistics of Myelin Biogenesis in the Central Nervous System. Glia 65, 1021–1031.

Snaidero, N., Velte, C., Myllykoski, M., Raasakka, A., Ignatev, A., Werner, H.B., Erwig, M.S., Möbius, W., Kursula, P., Nave, K.-A., Simons, M., 2017. Antagonistic functions of MBP and CNP establish cytosolic channels in CNS myelin. Cell Rep. 18, 314–323.

Sobottka, B., Ziegler, U.R.S., Kaech, A., Becher, B., Goebels, N., 2011. CNS live imaging reveals a new mechanism of myelination: the liquid croissant model. Glia 59, 1841–1849.

Spalding, K.L., Bhardwaj, R.D., Buchholz, B.A., Druid, H., Frisén, J., 2005. Retrospective birth dating of cells in humans. Cell 122, 133–143.

Spitzer, S.O., Sitnikov, S., Kamen, Y., Evans, K.A., Kronenberg-Versteeg, D., Dietmann, S., Faria, O. de, Agathou, S., Káradóttir, R.T., 2019. Oligodendrocyte progenitor cells become regionally diverse and heterogeneous with age. Neuron 101, 1–13.

Steele, C.J., Bailey, J.A., Zatorre, R.J., Penhune, V.B., 2013. Early musical training and white matter plasticity in the corpus callosum: evidence for a sensitive period. J Neurosci 33, 1282–1290.

Sternberg, J.R., Severi, K.E., Fidelin, K., Gomez, J., Ihara, H., Alcheikh, Y., Hubbard, J.M., Kawakami, K., Suster, M., Wyart, C., 2016. Optimization of a neurotoxin to investigate the contribution of excitatory interneurons to speed modulation in vivo. Curr. Biol. 26, 2319–2328.

Stevens, B., Porta, S., Haak, L.L., Gallo, V., Fields, R.D., 2002. Adenosine: a neuron-glial transmitter promoting myelination in the CNS in response to action potentials. Neuron 36, 855–868.

Sun, L.O., Mulinyawe, S.B., Collins, H.Y., Ibrahim, A., Li, Q., Simon, D.J., Tessier-Lavigne, M., Barres, B.A., 2018. Spatiotemporal Control of CNS Myelination by Oligodendrocyte Programmed Cell Death through the TFEB-PUMA Axis. Cell 175, 1–16.

Svoboda, K.R., Linares, A.E., Ribera, A.B., 2001. Activity regulates programmed cell death of zebrafish Rohon-Beard neurons. Development 128, 3511–3520.

Symvoulidis, P., Lauri, A., Stefanoiu, A., Cappetta, M., Schneider, S., Jia, H., Stelzl, A., Koch,

M., Perez, C.C., Myklatun, A., Renninger, S., Chmyrov, A., Lasser, T., Wurst, W., Ntziachristos, V., Westmeyer, G.G., 2017. NeuBtracker — imaging neurobehavioral dynamics in freely behaving fish. Nat. Methods 14, 1079–1082.

Takahashi, N., Sakurai, T., Davis, K.L., Buxbaum, J.D., 2011. Linking oligodendrocyte and myelin dysfunction to neurocircuitry abnormalities in schizophrenia. Prog. Neurobiol. 93, 13–24.

Tauber, H., Waehneldt, T. V, Neuhoff, V., 1980. Myelination in rabbit optic nerves is accelerated by artificial eye opening. Neurosci. Lett. 16, 235–238.

Taveggia, C., Feltri, M.L., Wrabetz, L., 2010. Signals to promote myelin formation and repair. Nat. Rev. Neurol. 6, 276–287.

Taveggia, C., Thaker, P., Petrylak, A., Caporaso, G.L., Toews, A., Falls, D.L., Einheber, S., Salzer, J.L., 2008. Type III neuregulin-1 promotes oligodendrocyte myelination. Glia 56, 284–293.

Taveggia, C., Zanazzi, G., Petrylak, A., Yano, H., Rosenbluth, J., Einheber, S., Xu, X., Esper, R.M., Loeb, J.A., Shrager, P., Chao, M. V., Falls, D.L., Role, L., Salzer, J.L., 2005. Neuregulin-1 type III determines the ensheathment fate of axons. Neuron 47, 681–694.

Tillberg, P.W., Chen, F., Piatkevich, K.D., Zhao, Y., Yu, C.C., English, B.P., Gao, L., Martorell, A., Suk, H., Yoshida, F., Degennaro, E.M., Roossien, D.H., Gong, G., Seneviratne, U., Tannenbaum, S.R., Desimone, R., Cai, D., Boyden, E.S., 2016. Protein-retention expansion microscopy of cells and tissues labeled using standard fluorescent proteins and antibodies. Nat. Biotechnol. 34, 987–992.

Tomassy, G.S., Berger, D.R., Chen, H.-H., Kasthuri, N., Hayworth, K.J., Vercelli, A., Seung, H.S., Lichtman, J.W., Arlotta, P., 2014. Distinct profiles of myelin distribution along single axons of pyramidal neurons in the neocortex. Science . 344, 319–324.

Totoiu, M.O., Keirstead, H.S., 2005. Spinal cord injury is accompanied by chronic progressive demyelination. J. Comp. Neurol. 486, 373–383.

Trapp, B.D., Nishiyama, A., Cheng, D., Macklin, W., 1997. Differentiation and death of premyelinating oligodendrocytes in developing rodent brain. J. Cell Biol. 137, 459–468.

Trevisiol, A., Saab, A.S., Winkler, U., Marx, G., Imamura, H., Möbius, W., Kusch, K., Nave, K.-A., Hirrlinger, J., 2017. Monitoring ATP dynamics in electrically active white matter tracts. Elife 6, e24241.

Tripathi, R.B., Clarke, L.E., Burzomato, V., Kessaris, N., Anderson, P.N., Attwell, D., Richardson, W.D., 2011. Dorsally and ventrally derived oligodendrocytes have similar electrical properties but myelinate preferred tracts. J. Neurosci. 31, 6809–6819.

Tripathi, R.B., Jackiewicz, M., Mckenzie, I.A., Kougioumtzidou, E., Grist, M., Richardson, W.D., 2017. Remarkable stability of myelinating oligodendrocytes in mice. Cell Rep. 21, 316–323.

Trudeau, L.-E., Doyle, R.T., Emery, D.G., Haydon, P.G., 1996. Calcium-independent activation of the secretory apparatus by Ruthenium Red in hippocampal neurons: a new tool to assess modulation of presynaptic function. J Neurosci 16, 46–54.

Tsai, H.-H., Niu, J., Munji, R., Davalos, D., Chang, J., Zhang, H., Tien, A.-C., Kuo, C.J., Chan, J.R., Daneman, R., Fancy, S.P.J., 2016. Oligodendrocyte precursors migrate along vasculature in the developing nervous system 351, 379–384.

Veer, A.V., Du, Y., Fischer, T.Z., Boetig, D.R., Wood, M.R., Dreyfus, C.F., 2009. Brain-Derived Neurotrophic Factor Effects on Oligodendrocyte Progenitors of the Basal Forebrain Are Mediated Through TrkB and the MAP Kinase Pathway. J. Neurosci. Res. 87, 69–78.

Venkatesh, H.S., Johung, T.B., Caretti, V., Noll, A., Tang, Y., Nagaraja, S., Gibson, E.M., Mount, C.W., Polepalli, J., Mitra, S.S., Woo, P.J., Malenka, R.C., Vogel, H., Bredel, M., Mallick, P., Monje, M., 2015. Neuronal activity promotes glioma growth through neuroligin-3 secretion. Cell.

Viganò, F., Möbius, W., Götz, M., Dimou, L., 2013. Transplantation reveals regional differences in oligodendrocyte differentiation in the adult brain. Nat. Neurosci. 16, 1370–1372.

Viswanathan, S., Williams, M.E., Bloss, E.B., Stasevich, T.J., Speer, C.M., Nern, A., Pfeiffer, B.D., Hooks, B.M., Li, W.-P., English, B.P., Tian, T., Henry, G.L., Macklin, J.J., Patel, R., Gerfen, C.R., Zhuang, X., Wang, Y., Rubin, G.M., Looger, L.L., 2015. High-performance probes for light and electron microscopy. Nat. Methods 12, 568–576.

von Blankenfeld, G., Trotter, J., Kettenmann, H., 1990. Expression and developmental regulation of GABAA receptor in cultured murine cells of the oligodendrocyte lineage. Eur.J.Neurosci. 3, 310–316.

Vondran, M.W., Clinton-Luke, P., Honeywell, J.Z., Dreyfus, C.F., 2010. BDNF+/- mice exhibit deficits in oligodendrocyte lineage cells of the basal forebrain. Glia 58, 848–856.

Voyvodic, J.T., 1989. Target size regulates calibre and myelination of sympathetic axons.

Nature 342, 430–433.

Waehneldt, T., Matthieu, J., Jeserich, G., 1986. Appearance of myelin proteins during evolution. Neurochem. Int. 9, 463–474.

Wake, H., Lee, P.R., Fields, R.D., 2011. Control of local protein synthesis and initial events in myelination by action potentials. Science . 333, 1647–1651.

Wake, H., Ortiz, F.C., Woo, D.H., Lee, P.R., Angulo, M.C., Fields, R.D., 2015. Nonsynaptic junctions on myelinating glia promote preferential myelination of electrically active axons. Nat. Commun. 6.

Walhovd, K.B., Fjell, A.M., 2007. White matter volume predicts reaction time instability. Neuropsychologia 45, 2277–2284.

Wang, C., Pralong, W.-F., Schulz, M.-F., Rougon, G., Aubry, J.-M., Pagliusi, S., Robert, A., Kiss, J.Z., 1996. Functional N-Methyl-D-Aspartate receptors in O-2A glial precursor cells: a critical role in regulating polysialic acid-neural cell adhesion molecule expression and cell migration. J. Cell Biol. 135, 1565–1581.

Watkins, T.A., Emery, B., Mulinyawe, S., Barres, B.A., 2008. Distinct stages of myelination regulated by gamma-secretase and astrocytes in a rapidly myelinating CNS coculture system. Neuron 60, 555–569.

Waxman, S.G., 1980. Determinants of conduction velocity in myelinated nerve fibers. Muscle Nerve 3, 141–150.

Williams, J.A., Barrios, A., Gatchalian, C., Rubin, L., Wilson, S.W., Holder, N., 2000. Programmed cell death in zebrafish Rohon Beard neurons is influenced by TrkC1/NT-3 Signaling. Dev. Biol. 226, 220–230.

Williamson, J.M., Lyons, D.A., Almeida, R.G., 2019. Manipulating neuronal activity in the developing zebrafish spinal cord to investigate adaptive myelination. In: Lyons, D.A., Kegel, L. (Eds.), Oligodendrocytes: Methods and Protocols. Springer New York, New York, NY, pp. 211–225.

Williamson, A. V., Mellor, J.R., Grant, A.L., Randall, A.D., 1998. Properties of GABA(A) receptors in cultured rat oligodendrocyte progenitor cells. Neuropharmacology 37, 859–873.

Wong, A.W., Xiao, J., Kemper, D., Kilpatrick, T.J., Murray, S.S., 2013. Oligodendroglial expression of TrkB independently regulates myelination and progenitor cell proliferation.

J Neurosci 33, 4947–4957.

Woo, N.H., Teng, H.K., Siao, C.-J., Chiaruttini, C., Pang, P.T., Milner, T.A., Hempstead, B.L., Lu, B., 2005. Activation of p75 NTR by proBDNF facilitates hippocampal long-term depression. Nat. Neurosci. 8, 1069–1077.

Wyllie, D.J., Mathie, A., Symonds, C.J., Cull-Candy, S.G., 1991. Activation of glutamate receptors and glutamate uptake in identified macroglial cells in rat cerebellar cultures. J. Physiol. 432, 235–258.

Xiao, L., Ohayon, D., Mckenzie, I.A., Sinclair-Wilson, A., Wright, J.L., Fudge, A.D., Emery, B., Li, H., Richardson, W.D., 2016. Rapid production of new oligodendrocytes is required in the earliest stages of motor-skill learning. Nat. Neurosci. 19, 1210–1217.

Yakovlev, P.I., Lecours, A.-R., 1967. The myelogenetic cycles of regional maturation of the brain. In: Regional Development of the Brain in Early Life: A Symposium. Blackwell Scientific Publications, pp. 3–70.

Yeung, M.S.Y., Zdunek, S., Bergmann, O., Bernard, S., Salehpour, M., Alkass, K., Perl, S., Tisdale, J., Possnert, G., Brundin, L., Druid, H., Frisén, J., 2014. Dynamics of oligodendrocyte generation and myelination in the human brain. Cell 159, 766–774.

Yoshida, M., Colman, D.R., 1996. Parallel evolution and coexpression of the proteolipid proteins and protein zero in vertebrate myelin. Neuron 16, 1115–1126.

Young, K.M., Psachoulia, K., Tripathi, R.B., Dunn, S.-J., Cossell, L., Attwell, D., Tohyama, K., Richardson, W.D., 2013. Oligodendrocyte dynamics in the healthy adult CNS: evidence for myelin remodeling. Neuron 77, 873–885.

Zeisel, A., Muñoz-Manchado, A.B., Codeluppi, S., Lönnerberg, P., Manno, G. La, Juréus, A., Marques, S., Munguba, H., He, L., Betsholtz, C., Rolny, C., Castelo-Branco, G., Hjerling-Leffler, J., Linnarsson, S., 2015. Cell types in the mouse cortex and hippocampus revealed by single-cell RNA-seq. Science . 347, 1138–1142.

Žiak, D., Chvátal, A., Syková, E., 1998. Glutamate-, kainate- and NMDA-evoked membrane currents in identified glial cells in rat spinal cord slice. Physiol. Res. 47, 365–375.

Ziskin, J.L., Nishiyama, A., Rubio, M., Fukaya, M., Bergles, D.E., 2007. Vesicular release of glutamate from unmyelinated axons in white matter. Nat. Neurosci. 10, 321–330.

Zong, W., Wu, R., Li, M., Hu, Y., Li, Y., Li, J., Rong, H., Wu, H., Xu, Y., Lu, Y., Jia, H., Fan, M., Zhou, Z., Zhang, Y., Wang, A., Chen, L., Cheng, H., 2017. Fast high-resolution

miniature two-photon microscopy for brain imaging in freely behaving mice. Nat. Methods 14, 713–719.

Appendices

Appendix 1: A Novel Zebrafish Model of Demyelination – Tg(mbp:TRPV1-RFP)

As discussed in Chapter 1, the formation of particular myelin patterns (the number, length, thickness, and distribution of myelin sheaths) along axons may be critical for circuit function through the precise regulation of conduction timing. Demyelination in injury, disease, or old age will likely change the myelin patterns along axons and could potentially impact circuit function. Although axons can be remyelinated, it is thought that the myelin sheaths generated during remyelination are shorter and thinner than sheaths in a healthy CNS (Blakemore, 1974; Blakemore and Murray, 1981; Lasiene et al., 2008; Prineas et al., 1993; Prineas and Connell, 1979; Totoiu and Keirstead, 2005). Therefore, even repair after demyelination could change myelin patterns, conduction properties, and subsequently impact circuit function. To understand precisely how de- and remyelination impacts circuit function, one must investigate de- and remyelination along single axons in intact circuits over time.

The larval zebrafish is an ideal model for following the myelination of single axons in identified circuits over time (as discussed in Chapter 3). A recent study described a transgenic larval zebrafish model of demyelination where myelinating cells express the enzyme nitroreductase and are ablated by treatment with the pro-drug metronidazole (Karttunen et al., 2017). Metronidazole treatment kills two thirds of oligodendrocytes and causes wide-spread demyelination. Efficient remyelination occurs by 16 days post-treatment, with the new sheaths being of similar length and thickness to sheaths in a healthy CNS. Whether zebrafish always exhibit such efficient remyelination, of if this efficient remyelination is a characteristic of this particular demyelination model, remains unknown. There is a need to test additional models of demyelination in larval zebrafish, not only to confirm the efficiency of remyelination, but to see whether different extents of demyelination can be induced. Additionally, a more rapid model of demyelination would be practically beneficial as it could reduce the time

duration of experiments and allow for higher resolution imaging (as larvae age, their increase in size impedes the quality of live imaging).

In addition to the experiments shown in Chapters 3 and 4, I generated a novel zebrafish transgenic model of demyelination where myelinating cells express the fusion protein TRPV1-tagRFPt. As noted in Chapter 4, mammalian TRPV1 is a cation channel which is activated by the ligand capsaicin to allow cation influx (with a strong preference for Ca^{2+} (Caterina et al., 1997; Munns et al., 2015)). Zebrafish TRPV1 channels are insensitive to capsaicin (Gau et al., 2013). Chen et al., 2016 showed that, in larval zebrafish, cells which express mammalian TRPV1-RFP can be ablated by treatments with high concentrations of capsaicin (discussed in more detail in section '4.1 Introduction'). By expressing TRPV1-RFP in myelinating cells (oligodendrocytes and Schwann cells), I reasoned that I could ablate these myelinating cells and damage myelin sheaths by bath application of high doses of capsaicin.

First I cloned a plasmid where TRPV1-RFP is expressed under the myelin basic protein (MBP) promoter (**Figure 40A**), to induce expression of TRPV1-RFP in oligodendrocytes and Schwann cells. I then used this plasmid to generate a stable transgenic zebrafish line where all myelinating cells express TRPV1-RFP – Tg(mbp:TRPV1-RFP) (**Figure 40B**).

TRPV1-RFP-expressing cells are ablated when treated with high concentrations of capsaicin, as demonstrated by Chen et al., 2016 and by myself (**Figure 23**). Indeed, treating Tg(mbp:TRPV1-RFP) larvae with 10 µM capsaicin for just two hours was sufficient to induce significant demyelination in the spinal cord (**Figure 40C, D**). Neuronal RFP-Cntn1a expression labels unmyelinated regions along the axon; however, it was unclear whether this could be used to observe demyelination along an individual axon over time (**Figure 40D**). Along a fully myelinated axon, RFP-Cntn1a is localised to the gaps between myelin sheaths (nodes of Ranvier). When myelin sheaths are lost during demyelination, RFP-Cntn1a does indeed become more diffusely localised along the axon. Therefore, this tool could be used to see how the

number and length of myelin sheaths along an individual axon changes throughout the de- and remyelination process.

More robust characterisation is required to determine whether changing concentrations or durations of capsaicin treatment can alter the extent of demyelination in the CNS. For example, some oligodendrocytes and myelin sheaths appear to survive two hours of 10 µM capsaicin, particularly in the ventral spinal cord (**Figure 40C)**. De- and remyelination should be characterised in more detail. This should include: the severity of demyelination; the dynamics of the immune response; the timing of remyelination; and the morphology of sheaths generated during remyelination. The model is currently being characterised by PhD student Ms. Sarah Neely.

Once characterised, the Tg(mbp:TRPV1-RFP) demyelination model could be used to investigate how myelin patterns change along individual neuronal subtypes through de- and remyelination, and determine if and how surviving myelin sheaths along different axons remodel in response to loss of their neighbours. Demyelination models could also be combined with manipulations of neuronal activity (using neurotoxins or optogenetics) to see how individual axon activity affects the remyelination of specific axonal subtypes *in vivo*.

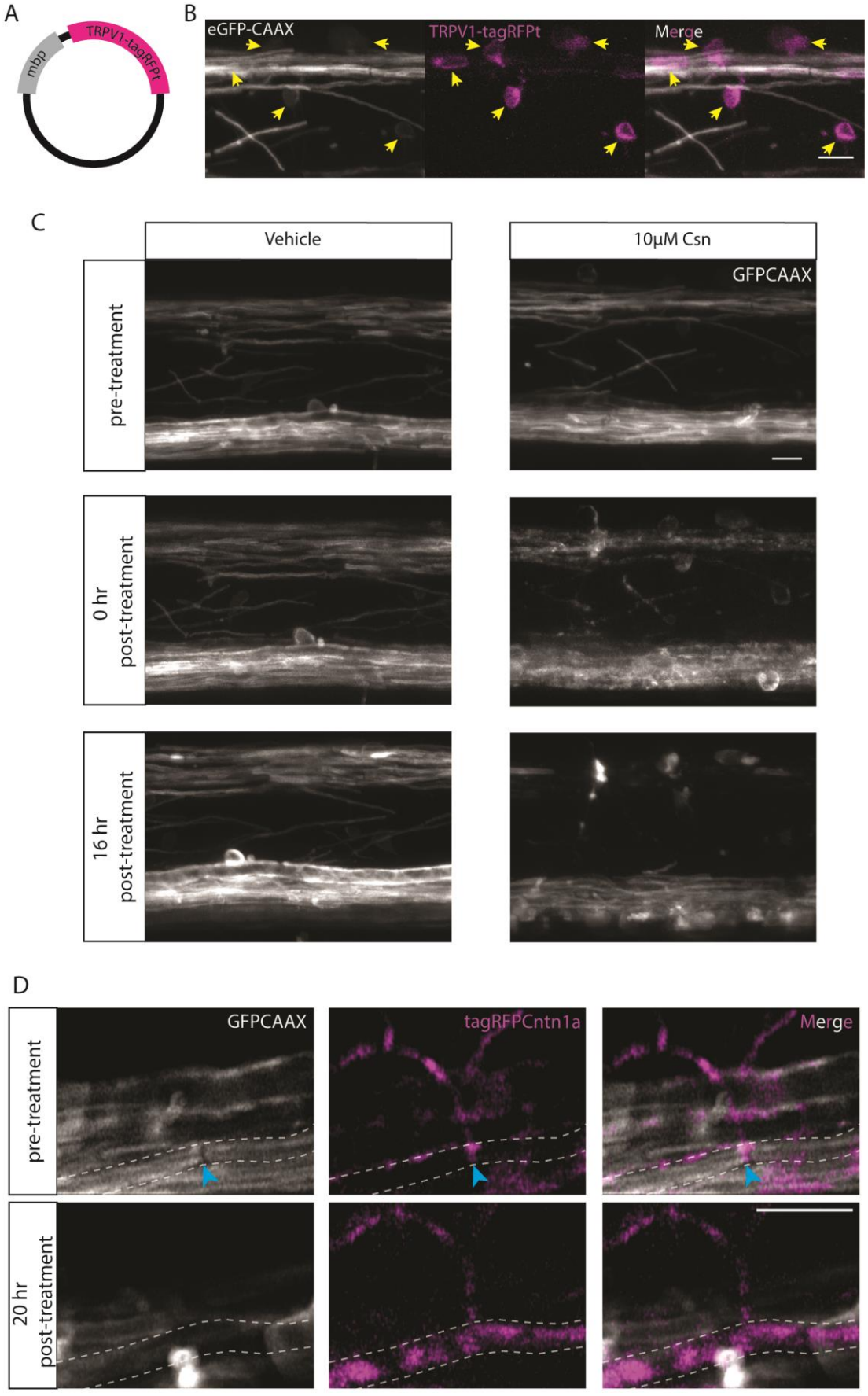
A
mbp
TRPV1-tagRFPt
B
eGFP-CAAX
TRPV1-tagRFPt
Merge
C
Vehicle
10μM Csn
GFPCAAX
pre-treatment
0 hr post-treatment
16 hr post-treatment
D
GFPCAAX
tagRFPCntn1a
Merge
pre-treatment
20 hr post-treatment

Figure 40 – the Tg(mbp:TRPV1-RFP) demyelination model to investigate the disruption and remodelling of myelin patterns along individual axons *in vivo*.

A) A simplified plasmid map of the mbp:TRPV1-tagRFPt plasmid used to generate the transgenic line Tg(mbp:TRPV1-tagRFPt) (TRPV1-RFP). TRPV1-RFP is under the control of the myelin basic protein (MBP) promoter sequence, so that expression of TRPV1-RFP occurs only in myelinating cells. **B)** TRPV1-RFP is expressed in myelinating cells. Crossing Tg(mbp:TRPV1-RFP) with Tg(mbp:eGFP-CAAX), a transgenic line which labels all myelinating cells with membrane-tethered eGFP, shows that oligodendrocytes in the spinal cord co-express both markers (shown by the yellow arrows). **C)** Capsaicin treatment induces rapid demyelination in Tg(mbp:TRPV1-RFP); Tg(mbp:eGFP-CAAX) larvae. Before treatment, Tg(mbp:TRPV1-RFP) larvae have myelinated axons in the dorsal and ventral spinal cord tracts, as labelled by eGFP-CAAX. After a 2 hour treatment with vehicle (1% DMSO), there is no significant change to myelin in the spinal cord up to 16 hours post-treatment. After a 2 hour treatment with 10 µM capsaicin, there is significant disruption to oligodendrocytes and myelin sheaths. 16 hours post-treatment, there is significant demyelination in both the dorsal and ventral tracts. However, some oligodendrocytes and myelin sheaths appear to survive the demyelination. **D)** Following single axons through demyelination. An individual RS neuron was labelled with RFP-Cntn1a to measure the myelination pattern along the axon (outlined by dotted lines). Prior to any treatment, RFP-Cntn1a is localised to the node (blue arrow) between eGFP-CAAX expressing myelin sheaths. 20 hours post-treatment (10 µM capsaicin), RFP-Cntn1a expression along the axon shows that there has been demyelination (which is confirmed by loss of eGFP-CAAX expressing sheaths along the axon). Scale bars = 10 µm.

Appendix 2: List of Relevant Authored Publications

Williamson, J. M., and Lyons, D. A. (2018). Myelin dynamics throughout life: an ever-changing landscape? *Front. Cell. Neurosci.* 12. doi:10.3389/fncel.2018.00424.
Published online on 19.11.2018.

Manuscript was conceptualised by DAL and JMW. Manuscript was written by JMW, and edited by DAL.

Williamson, J. M., Lyons, D. A., and Almeida, R. G. (2019). “Manipulating neuronal activity in the developing zebrafish spinal cord to investigate adaptive myelination,” in *Oligodendrocytes: Methods and Protocols*, eds D. A. Lyons and L. Kegel (New York, NY: Springer New York), 211-225. doi:10.1007/978-1-4939-9072-6_12.
Published online on 01.03.2019.

Manuscript was conceptualised by DAL. Manuscript was co-written by JMW and RGA, and edited by DAL.